The conformation of the β-ionone ring region of the chromophore of rhodopsin, in the dark and meta-I photostates

Jonathan M. Sharples

Submitted in partial fulfilment of the requirements for the

degree of Doctor of Philosophy

Corpus Christi College, Oxford

Hilary, 2003

Abstract

The conformation of the β-ionone ring region of the chromophore of rhodopsin, in the dark and meta-I photostates

Jonathan M. Sharples   D.Phil
                                                               Thesis

Corpus Christi College   Hilary
2003

Rhodopsin is the light-sensitive GPCR that triggers the signal transduction cascade that results in a visual response. It serves as a paradigm for the superfamily of transmembrane G-protein coupled receptors (GPCR), which are responsible for many cell signal transduction pathways and are a major family of drug targets. Upon excitation with light, photo-isomerization of the 11-*Z*-retinylidene chromophore to 11-*E*-retinylidene activates rhodopsin, through a series of transient photointermediates. Defining the detailed structure of retinal within its binding site in rhodopsin is essential for a functional understanding of rhodopsin activation and an understanding of the general mechanism of GPCR activation.

Here, solid state NMR has been applied to deduce the conformation of the β-ionone ring of the chromophore of rhodopsin, in non-perturbing $[8,18-^{13}C_2]$ 11-*Z* retinal and $[8,16/17-^{13}C_2]$ 11-*Z* retinal, regenerated into rhodopsin in rod outer segments (ROS). The rotational resonance NMR technique was used to measure the internuclear distance between a ^{13}C labelled nucleus on the polyene chain (C8) and three ^{13}C labelled methyl groups (C16, C17 and C18) on the β-ionone ring of the chromophore. The distance constraints, C8 to C16 and C17 (4.05 ± 0.25 Å) and C8 to C18 (2.95 ± 0.15 Å) showed that the major portion of retinal in rhodopsin adopts a modestly twisted 6-*s-cis* conformation (C5-C6-C7-C8 torsion angle = -28±7°), with the C17 and C16 methyl groups in respective, axial and equatorial conformations. A minor proportion of the retinylidene (25-30%) was observed in a 6-*s-trans* conformation, indicating conformational flexibility within the binding pocket. However, by using the distinct chemical shift separation of the bound C16 and C17 methyls as an indicator of a 6-*s-cis* ring conformation (~4.5ppm), it was shown that the ring adopts exclusively a 6-*s-cis* conformation in the native 11-*Z*-retinylidene chromophore.

Upon excitation with light, photo-isomerization of the 11-*Z*-retinylidene chromophore to 11-*E*-retinylidene activates rhodopsin, through a series of transient photointermediates. Methods for trapping frozen NMR samples in the meta-I photointermediate were investigated by using the C8 and C20 ^{13}C nuclei as probes for the proportion of rhodopsin trapped in the meta-I photostate. Photoregeneration of 9-Z-retinal and 7-Z-retinal that occurs upon prolonged illumination of rhodopsin, hampers the direct generation of the meta-I photointermediate. Trapping the bathorhodopsin intermediate at -190°C, then warming to   -20°C, was found to be the optimum method for accumulating the meta-I photointermediate.

Rotational resonance NMR measurements between the C8 and C18 nuclei in $[8,18-^{13}C_2]$ retinylidene meta-I rhodopsin indicated that the β-ionone ring adopted a 6-*s-cis*

conformation in the meta-I photointermediate. The C16 and C17 methyl groups were observed in a similar axial/equatorial conformation in $[8,16/17\text{-}^{13}C_2]$retinylidene meta-I rhodopsin and $[16,17\text{-}^{13}C_2]$retinylidene meta-I rhodopsin as observed in dark state retinylidene, suggesting that the binding sites for the β-ionone ring were similar in both dark and meta-I photostates. This was in contrast to recent evidence that suggests that the β-ionone ring is repositioned prior to the formation of the meta-I photointermediate. The implications of this result for the activation mechanism of rhodopsin and for GPCRs in general are discussed.

Publications

Spooner, P. J. R., Sharples, J. M., Verhoeven, M. A., Lugtenburg, J., Glaubitz, C., Watts, A. (2002) Relative orientation of the β-ionone ring and the polyene chain for the chromophore of rhodopsin in native membranes. *Biochemistry* **41**: 7549-7555

*Spooner P. J. R., *Sharples J. M., Goodall S., Seedorf H., Verhoeven M. A., Lugtenburg J., Bovee-Geurts P.H.M., deGrip W.J., Watts A. (2003) Conformational similarities in the β-ionone ring region of the rhodopsin chromophore in its ground and on photoactivation to the meta-I rhodopsin intermediate (in preparation) *Contributed equally to the work

Spooner, P.J.R., Sharples, J.M., Goodall, S., Watts, A. Verhoeven M. A., Lugtenburg J., Bovee-Geurts P.H.M., deGrip W.J. (2003) The rhodopsin chromophore remains in the binding pocket through the signalling state (in preparation)

Acknowledgements

I would sincerely like to thank Dr. Paul Spooner for all his help and advice throughout the course of this project. His unwillingness to let me take the easy option has taught me the benefit of working with integrity, for which I am grateful. It has been a privilege to work with such a knowledgeable and imaginative scientist.

I would like to thank Prof. Anthony Watts for providing me with the opportunity and resources to do this work, his overall supervision and for critically reading the manuscript.

I am grateful to Prof. Wim deGrip (Nijmegen, The Netherlands) for showing enthusiasm for my work, the many stimulating discussion and showing such patience when I would ring up armed with a barrage of questions. Many thanks to Petra Bovee-Geurts, for her expert assistance in preparing and characterising rhodopsin samples. She makes things look very easy and has an uncanny ability to work very fast, in complete darkness!

Many thanks to Prof. Johan Lugtenburg (Leiden, The Netherlands) for providing me with the labelled retinals for this study and to Michiel Verhoeven for his assistance in purifying and characterising retinals.

Thank you to the group of Prof. Arlene Albert (Conneticutt, U.S.A.) for teaching me the fundamentals of rhodopsin regeneration and for providing unlabelled retinal.

I am grateful to all the members of the "Watts" group over the last few years for their general help and support, and particularly these people: Peter Fisher for collecting and dissecting cow's eyes, Prof. Clemens Glaubitz for proving rotational resonance software, Dr. Ian Burnett for synthesizing retinals, Liz Mitchell for administrative help and Dr. Scott Goodall for all the help in the "computing" aspects of the work and for proof-reading the manuscript.

Contents

Chapter 3 Determining the β-ionone ring conformation of retinal in rhodopsin   using   RR NMR……………………………………Error! Bookmark not defined.

Abbreviations and Symbols

$7TM_A$	family A GPCR
$7TM_B$	family B GPCR
$7TM_C$	family C GPCR
bR	bacteriorhodopsin
BSA	bovine serum albumin
BSI	blue-shifted intermediate
cAMP	adenosine 3',5'-cyclic monophosphate
CD	circular dichroism
cGMP	guanosine 3',5'-cyclic monophosphate
CNGC	cGMP-gated cation channels
CP	cross-polarization
CSA	chemical shift anisotropy
CTAB	cetyltrimethylammonium bromide
DMF	dimethyl formamide
DMPC	1,2-dimyristol-*sn*-glycerol-3-phosphocholine
DQF	double-quantum filtering
FWHM	full width half maximum
FTIR	fourier transform infra red

GDP	guanosine diphosphate
GPCR	G protein-coupled receptor
GTP	guanosine triphosphate
HPLC	high performance liquid chromatography
MAS	magic angle spinning
NADPH	nicotinamide adenine dinucleotide phosphate
NMS	N-methyl scopolamine
OR	olfactory receptor
PDB	protein data bank
R^*	active meta-II rhodopsin
PDE	phosphodiesterase
PSB	protonated Schiff base
RK	rhodopsin kinase
RMSD	root mean squared deviation
ROS	rod outer segments
RPE	retinal pigment epithelium
RR	rotational resonance
SDS PAGE	SDS- polyacrylamide gel electrophoresis
SS NMR	solid state nuclear magnetic resonance
T	transducin

TM	transmembrane
TMS	tetra methylsilane
UV-VIS	ultraviolet-visible
T_2^{ZQ}	zero-quantum relaxation time constant
b_{IS}	dipolar coupling constant
μ_o	permeability of free space
γ_I	gyromagnetic ratio of spin I
γ_S	gyromagnetic ratio of spin S
η	Planck's constant divided by 2π
r_{IS}	distance between nuclear spins I and S

Chapter 1   Introduction

1.1   Biological membranes

1.1.1   Structure of cell membranes

The biological membranes of cells play an essential role in the life cycle of all organisms. They are not simply barriers for partitioning the cell from its surrounding environment but are intimately involved in biological processes occurring in the cell, enabling complex interactions with the surrounding environment.

The membranes of living cells have an intricate molecular composition. On the extracellular face of the membrane there is a macromolecular layer of oligosaccharides called the glycocalyx. Inside this is a liquid crystalline bilayer composed of amphipathic phospholipids, arranged so the hydrophilic headgroups are exposed to the aqueous exterior or interior of the cell and the hydrophobic chains are oriented towards the membrane core (Figure 1.1). The bilayer forms a relatively impermeable barrier to solutes, enabling the compartmentalization of cell function that is crucial to cell survival. Restoration of the permeability across the bilayer is controlled through proteins embedded in the membrane.

The intracellular side of the plasma membrane in many cells is lined with a macromolecular

cytoskeleton.

Figure 1.1 – Schematic representation of a lipid bilayer. The circles represent the polar headgroups of the lipids and the lines connected to the circle represent the hydrophobic hydrocarbon chains of the lipids. These amphipathic phospholipids orient to limit the exposure of the hydrophobic lipid chains to the aqueous phase that is found on both sides of the membrane. From [1].

Figure 1.2 – Schematic representation of a biological membrane based on the fluid mosaic model. Adapted from [2].
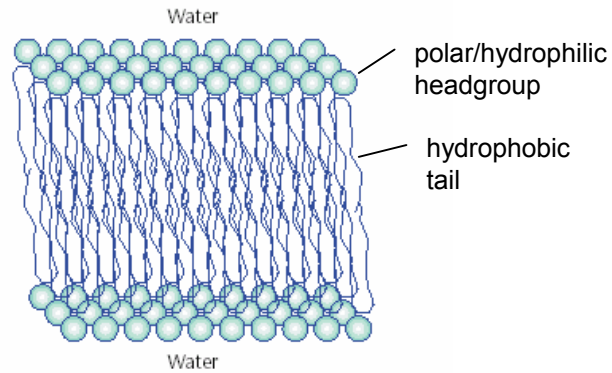
In 1972 Singer and Nicolson suggested the "fluid-mosaic-model" which describes biological membranes as a fluid two-dimensional matrix of lipids in which are embedded integral and peripheral globular proteins [3]. Integral proteins have one or more domains that span the entire lipid bilayer and are made up of both hydrophobic and hydrophilic regions of amino acids that interact with the hydrophobic interior of the membrane and aqueous exterior, respectively. Peripheral proteins associate with the membrane through interactions with lipid headgroups or integral membrane proteins or by covalent attachment through anchors. Although components can partially diffuse within the plane of the membrane, the interactions between the proteins and the bilayer anchors them in the membrane, preventing
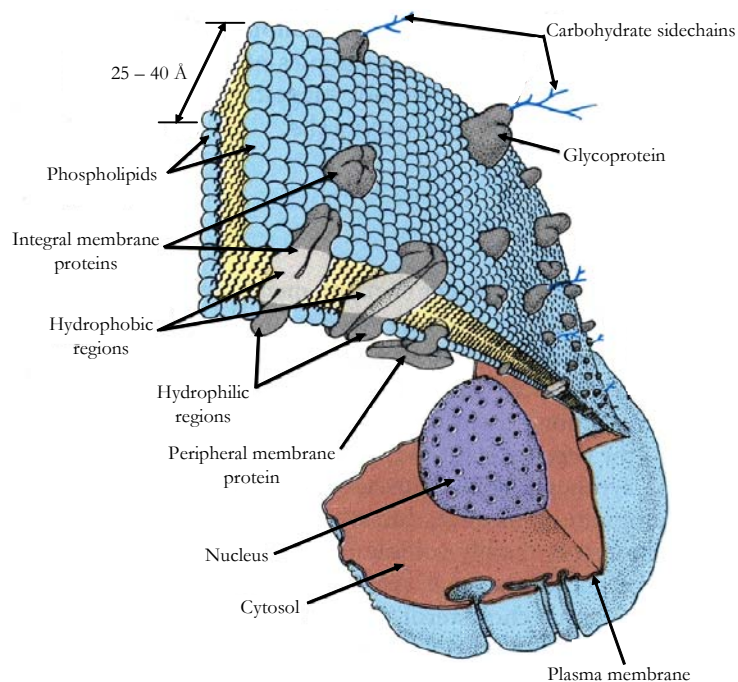
"flip-flop". This results in an asymmetric structure to the membrane with different protein and lipid compositions on each face of the bilayer.

Recent research has suggested a modified version of the "fluid-mosaic-model" with the presence of lateral heterogeneities known as rafts that may form rigid domains within the membrane, based on the dynamic clustering of protein, sphingolipids and cholesterol [4].

The plasma membrane plays many roles, which can be summarised in four points:

1. *Compartmentalization*: Forms an electrically isolated barrier that enables different compositions inside and out of the cell. Essential in maintaining ion gradients required for action potentials.

2. *Transport*: Forms a diffusion barrier, which controls composition of the cell interior through highly organised transport processes.

3. *Signal transduction and enzymatic activity*: Forms a dynamic matrix for enzymatic activity, receptors for signal transduction and recognition for immune responses.

4. *Cellular form*: Forms a mechanical structure which influences shape and motion of cells or organelles.

To perform these roles the many different proteins in the membrane have to act as pumps, channels, receptors, energy transducers and enzymes. It is estimated that approximately 80% of all cellular signals are triggered through membrane-bound proteins including receptors, transporters and channels [5]. It is the receptor function of membrane proteins, involved in signal transduction that is of particular interest in this study.

For all functions of the membrane the reduction of a three-dimensional reaction space to two-dimensions allows the membrane to localize the reacting machinery and thus act as a

concentration zone for metabolism and cell signalling [6, 7].

The evolution of multicellular organisms has greatly depended on the capacity of their cells to communicate with each other and with their environment. It has recently been recognized that membrane-bound receptors devised to recognize sensory messages from the environment and intercellular messages are very similar and derive from common ancestral genes [8]. These receptors belong to a small number of protein families which can be classified based on their structure and their function: (1) channel receptors, (2) tyrosine kinase receptors, (3) guanylate cyclase receptors, (4) serine/threonine kinase receptors, (5) cytokine receptors, (6) receptors coupled to guanosine triphosphate (GTP)-binding proteins (G protein-coupled receptors: GPCRs). The most common family is the GPCR family that represent approximately 1-2% of the genome in vertebrates and over 5% of the genome in *Caenorhabditis elegans* [9].

1.1.2 GPCRs

G-protein-coupled receptors (GPCRs) are located at the cell surface and are responsible for the transduction of an endogenous signal into an intracellular response. Structurally, GPCRs share a conserved structure of seven transmembrane (TM) helices connected by three extracellular loops and three intracellular loops. The superfamily of GPCRs regulate an extremely diverse range of physiological processes by transmitting signals to cells in response to stimuli such as light, peptide and protein hormones (for example, angiotensin, endothelin, melanocortin), biogenic amines (such as adrenaline, dopamine, serotonin), nucleotides (adenosine, ADP, UTP, ADP), lipids and eicosanoids (cannabinoids, prostaglandins) and others (such as glutamate, Ca^{2+}). Binding of these specific ligands to the extracellular or transmembrane regions of GPCRs causes conformational changes of the receptor that act as

a switch, transferring the signal to the trimeric guanine nucleotide binding regulatory proteins (G proteins), thus inhibiting or stimulating the production of intracellular secondary messengers (for example, cyclic adenosine monophosphate (cAMP), Ca^{2+} ions)(Figure 1.3).

Based on structural differences, mammalian GPCRs are grouped into three major families: family A (rhodopsin-like or adrenergic-receptor-like family), family B (glucagon-like receptor family) and family C (metabotropic glutamate receptors). Family A is by far the largest and will be focused on predominately in this study. These proteins have short amino tails and have highly conserved amino acid residues within each transmembrane helix. Family B receptors display longer amino-terminal tails with a set of six conserved cysteine residues whilst family C receptors have long (500-600 residues) amino tails that are folded as separate ligand binding domains.
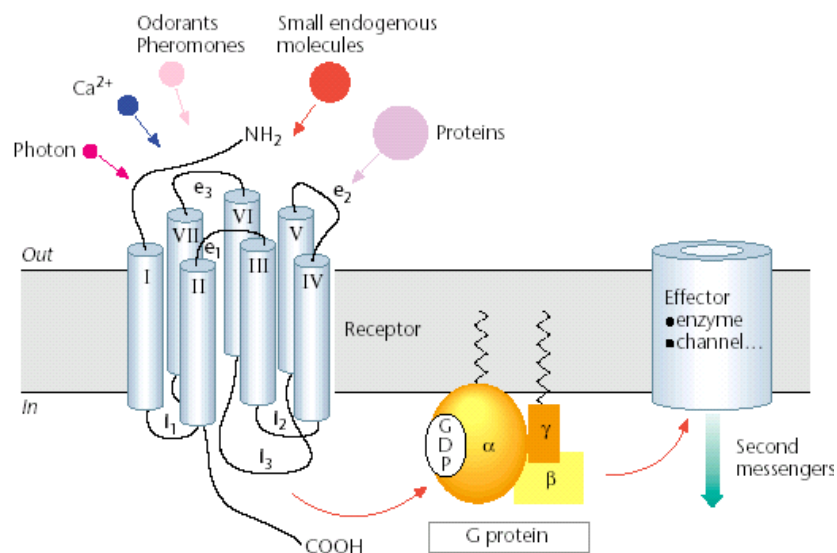
Figure 1.3 – The three-partner model of G-protein-coupled receptor (GPCR) signal transduction. GPCRs have seven transmembrane domains and three extracellular and intracellular domains. Heteromeric G proteins have three subunits: α, β, γ. βγ are always associated in physiological conditions, with both α and βγ covalently bound to lipids enabling association with the membrane. Upon activation of the receptor the exchange of GTP for GDP bound to the Gα subunit is induced, followed by the dissociation of the Gα-GTP unit from Gβγ and coupling to effector enzymes. Thus the production of

The discovery of drugs acting on GPCRs has been extremely successful. Over 50% of all the drugs recently launched were targeted against GPCRs with annual worldwide sales exceeding $30 billion [10, 11]. Among the 100 top-selling drugs 25% are targeted at GPCRs. Preliminary analysis of the human genome has revealed approximately 1000 members of the GPCR family [12-14] (including 500 olfactory receptors), of which only 30 represent targets for currently marketed drugs. Approximately 200 of the remaining endogenous ligand receptors have known natural ligands, however about 150 identified novel GPCRs, so called "orphan receptors" have been identified within the genome whose ligand and physiological function is unknown. The scope for developing new pharmaceuticals is therefore excellent, if a functional understanding of GPCRs and the interaction with their ligands can be used to aid the design of novel drugs.

By far the most extensively studied signal transduction system involving GPCRs is the visual cascade, which uses the light-sensitive GPCR rhodopsin to convert light into a biological signal.

1.2 Vision

Vertebrates have two kinds of photoreceptor cells, called rods and cones, because of their distinctive shape. The rod cells initiate dim light vision and but do not perceive colour whilst the cones function in bright light and trigger the process of colour vision. A human retina contains about three million cones and a hundred million rods, which form synapses with bipolar cells (Figure 1.4).

Vision begins in the outer segments of rod and cone photoreceptor cells when the light sensitive rhodopsin and cone visual pigments absorb photons and become activated. A signal transduction cascade is triggered that eventually results in an electrical signal that is

processed by the brain.
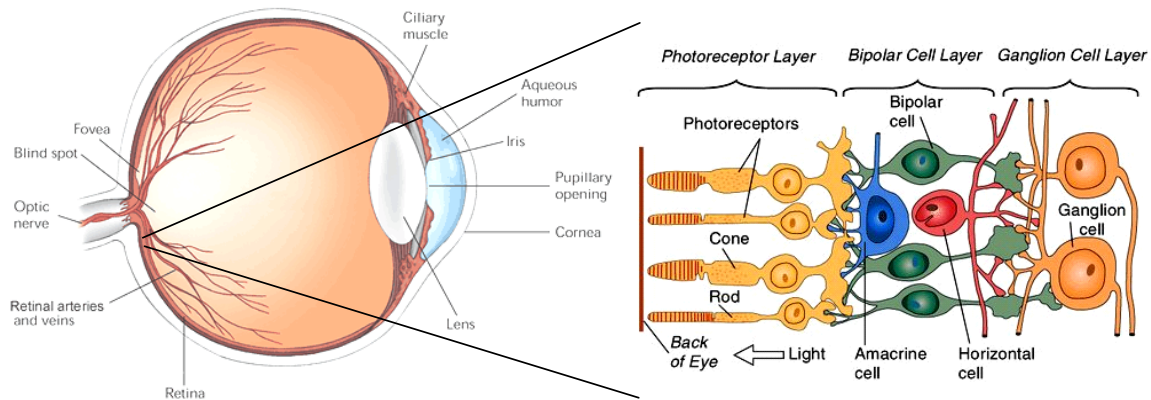
Figure 1.4 – Diagram of the eye showing the composition of the retina. Light is detected in the rod and cone cells and converted to an electrical signal at the synapse with the bipolar cells. From [15]

In the dark, sodium ions rapidly flow into the outer segment of rod cells through cation-specific channels, down a gradient maintained by Na^+/K^+ ATPase pumps located in the inner segment (Figure 1.5). Absorbance of a single photon of light triggers a signal transduction cascade that closes hundreds of cation-specific channels in the outer segment of photoreceptor cells, resulting in hyperpolarization (~1mV) of the plasma membrane and a nerve impulse to other neurons of the retina.

The electrical signals generated by the photoreceptors are processed by an intricate array of secondary neurons within the retina and then transmitted to the brain by the fibres of the optic nerve. The retina has a dual function: to transform light into nerve impulses and to integrate visual information. The outer segment of the rod cell is specialised for photoreception. It contains about 1000 discs, which are membranous structures densely packed with photoreceptor proteins, called rhodopsins. Vertebrate rhodopsins are composed of an approximately 40kDa protein, opsin, linked covalently to an 11-Z retinylidene chromophore (called 11-Z-retinal in its unbound conformation). The retinal occupies a

binding pocket in the interior of the protein where it is attached to a specific lysine side

chain by a protonated Schiff base linkage (i.e. Lys-296 in bovine rhodopsin).
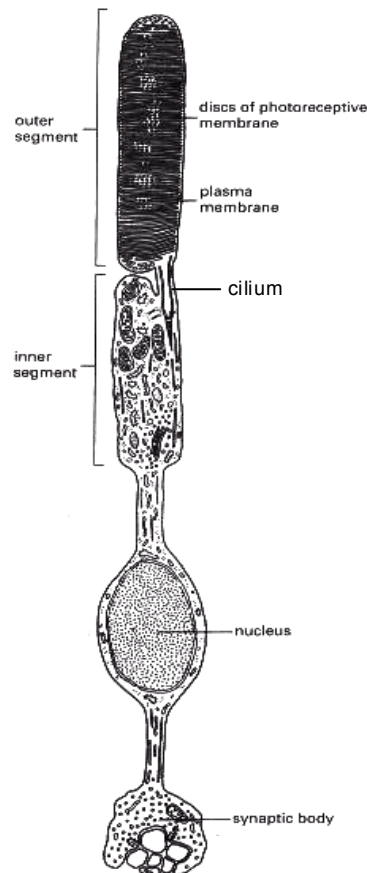
Figure 1.5 – Drawing of a rod photoreceptor cell. The rod cell is a highly specialised neuron whose outer segment consists primarily of a plasma membrane enveloping a stack of disc membranes. Rhodopsin is situated in the disc membranes of the rod outer segments

1.2.1 Visual cascade

1.2.1.1 The signal transduction cascade

In darkness, the cytoplasm of the rod cell contains a high level of cGMP, which by binding

to cGMP-gated cation channels (CNGC) keeps them in an open state. The open channels

allow an inward flow of cations (primarily Na^+ and Ca^{2+}), termed the "dark current", across the plasma membrane. Visual transduction is initiated by a photochemical reaction where 11-Z retinal, bound to opsin, undergoes isomerization to all-E retinal. The protein undergoes a series of conformational changes that can be identified by a series of precise colour changes in the molecule, eventually establishing the catalytically active meta-II form of the receptor (R^*). Activated rhodopsin (R^*) promotes exchange of GDP by GTP on the α-subunit of the heterotrimeric G-protein transducin (T), which leads to the dissociation of T^*-GTP from $T\beta\gamma$. T^*-GTP is an activator of a cGMP-specific phosphodiesterase (PDE) which regulates the levels of cGMP in the cytoplasm of photoreceptors. In the dark, the two catalytic subunits (α and β) of PDE are held in check by a pair of inhibitory subunits (PDEγ). T^*-GTP forms a complex with PDE, prying away its inhibitory subunit to form the highly active PDE^*, which hydrolyses cGMP at a turnover rate close to its diffusion-controlled limit [16]. The drop in the concentration of cGMP reduces the amount of cGMP that bind to and maintain the CNGCs in their open state, resulting in closure of hundreds of CNGCs, which terminates the influx of cations and produces a hyperpolarizing electrical change

within the rod. The affinity of cGMP for the channel may also be modulated by

Ca^{2+}/calmodulin, which plays a role in recovery of the dark state rhodopsin. A direct consequence of this light-triggered hyperpolarization is a reduction in the rate of release of neurotransmitter, L-glutamate, at the rod's synaptic terminal, and thus communication of a visual signal from the rod cell to adjacent neurons of the retina.

1.2.1.2 Amplification

The transient photoactivation of rhodopsin is especially remarkable because the absorption of a single photon can result in the flow of more than a *million* sodium ions being blocked. Amplification is characteristic of a G-protein signal transduction cascade although vision is especially efficient in this aspect, able to detect a brief flash that produces a single photoisomerisation in each of just a few rod photoreceptors [17]. The first stage of amplification is at the transducin stage. One activated rhodopsin molecule results in the activation of $\sim 10^2$-10^3 transducin molecules with extraordinary reproducibility, whereas dark state rhodopsin has virtually no transducin stimulating activity [18, 19]. The second stage of

Figure 1.6 – The light induced signal transduction cascade responsible for vision. See text for details. From [16].
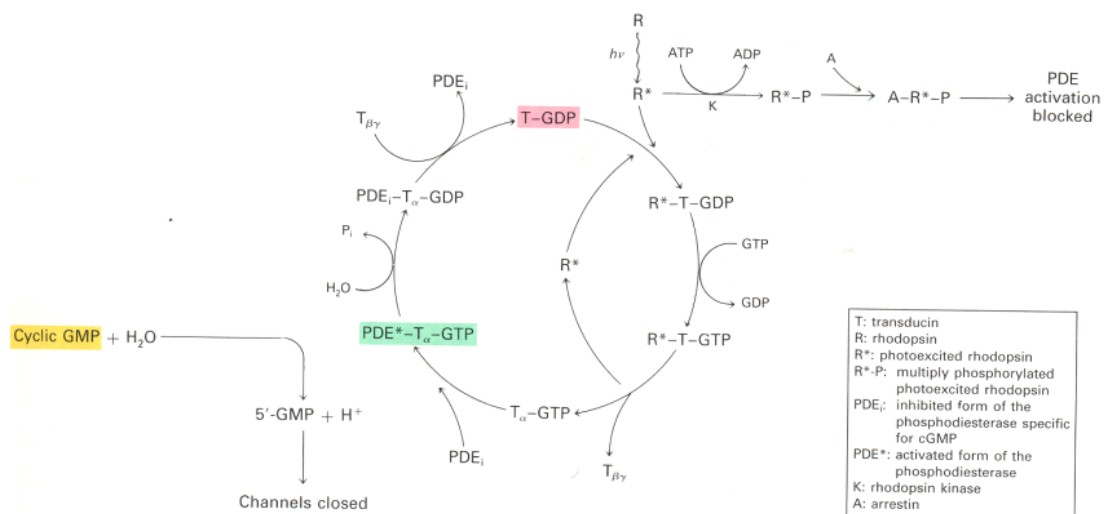
amplification is in the hydrolysis of cGMP by PDE*. At high cGMP concentrations this

enzyme has a turnover rate of approximately $4000s^{-1}$, and as at least three cGMP are required for the opening of a single CNGC the amplification effect is enhanced [20].

1.2.1.3 Recovery of the system to the dark state

For recovery to the dark state a series of shut-off mechanisms are required. PDE is deactivated when the α-subunit of transducin hydrolyzes bound GTP to GDP (Figure 1.6). To prevent reactivation of transducin, R^* must also be deactivated. Rhodopsin kinase (RK) phosphorylates multiple serine and threonine residues in rhodopsin's C terminal and promotes the binding of an inhibitory protein, arrestin, to the surface of the meta-II receptor. Arrestin blocks the binding of transducin until it dissociates together with all-E retinal, upon the decay of meta-II. Restoration of the dark state also requires regeneration of the levels of cGMP that re-open the cation channels. The synthesis of cGMP from GTP is catalysed by guanylate cyclase that is regulated by the concentration of Ca^{2+} ions. Following hyperpolarization the level of Ca^{2+} drops so serving as a feedback messenger for the recovery mechanism.

Full recovery of rhodopsin also requires regeneration of opsin with 11-Z retinal. This requires the formation of 11-Z retinal from an all-E precursor, via a pathway of enzymatic reactions called the retinoid pathway [21] involving reduction, esterification and isomerization of the retinal in the ROS and the retinal pigment epithelium cells (RPE). Full recovery of the dark state for a rhodopsin molecule occurs within humans with a time constant of ~400s for rhodopsin and ~100s for cone pigments [22, 23].

1.3   Rhodopsin

Rhodopsin is the highly specialized GPCR that detects photons in the rod photoreceptor cell. It defines the family A GPCRs, with which it shares primary structural homology. Bovine rhodopsin was the first GPCR to be sequenced by amino acid sequencing [24], the first to be cloned [25, 26], the first to be crystallized [27] and the first to yield a crystal structure [28]. The visual pigment rhodopsin was originally extracted from bovine retina using bile salt as a detergent [29], and since then, its plentiful supply (0.5-1.0 mg/retina) and stability in a variety of detergents [30] have enabled significant numbers of studies into this protein for its role in the visual process and more recently, as a paradigm for GPCR mechanism in general.
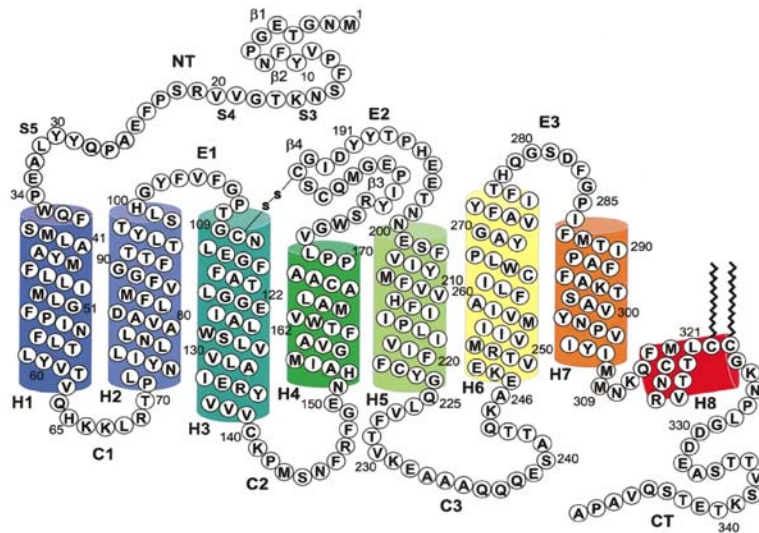
Figure 1.7 – A secondary structure diagram of bovine rhodopsin. Amino acid residues are depicted in single-letter code. The amino-terminal tail and extracellular domain is towards the top and the carboxy-terminal tail and cytoplasmic domain is towards the bottom. Transmembrane α-helical segments (H1 to H7) and the cationic amphipathic helix H8 are shown as coloured cylinders. An essential disulpide bond links Cys-110 and

The reddish colour of rhodopsin results from the formation of a protonated Schiff base of the 11-Z retinal chromophore within the binding pocket of rhodopsin, giving a characteristic absorption maximum at 498nm [31]. 11-Z retinal has favourable chromophoric properties because it is a polyene. Its six alternating double and single bonds result in a conjugated π-electron network that gives a visible absorption band upon excitation (Figure 1.8) [32]. Upon formation of a protonated Schiff base linkage the absorption maximum (λ_{max}) of retinal red-shifts from 380nm to 440nm. However, it is the environmental perturbations provided by the interaction between the 11-Z retinylidene chromophore and the opsin binding pocket that tune the absorption maximum of the retinal chromophore over a wide range – from 360nm to 635nm [33].
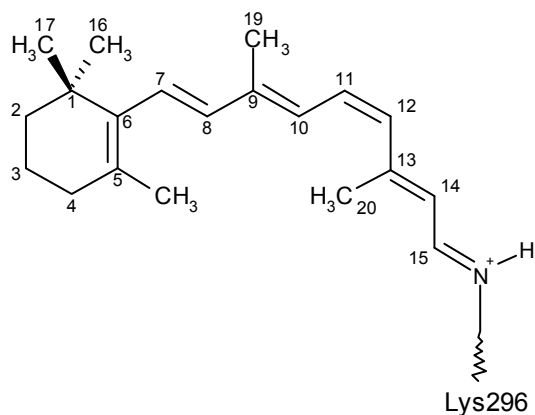
Figure 1.8 – The 11-Z retinylidene chromophore of bovine rhodopsin with International Union of Pure and Applied Chemistry (IUPAC) numbering shown for the carbon atoms. 11-Z retinal is covalently bound to Lys-296 of opsin by a protonated Schiff base.

This shift in wavelength of maximum absorbance is called the opsin shift and spectral tuning in this way permits colour vision. There are three different types of cone cells (red ~560 nm, green ~530nm and blue ~425nm) based upon the maximum wavelength absorbance of their particular opsin-retinal visual pigments, whose differential responses enable colour vision.

Since the instigation of this project there have been huge advances in our structural

knowledge of rhodopsin, largely through the determination of the crystal structure of bovine rhodopsin at 2.8Å resolution [28, 34]. The publication of the dark state rhodopsin structure provided a major breakthrough in structural studies, not only for the GPCR superfamily, but also for membrane proteins in general. It is the only member of the GPCRs for which structural data at atomic level is available and it has enabled the validation and re-interpretation of hundreds of previous biochemical and biophysical studies. Cryo-electron microscopic studies of frog rhodopsin had previously revealed the structure of this receptor at low-resolution (7.5Å x 16.5Å), predicting correctly the location of seven tilted transmembrane (TM) helices. The exhaustive analysis of Baldwin *et al* [35] turned out to be correct, and the molecular graphics models of the transmembrane core of the rhodopsin, based on many biochemical and spectroscopic studies were reasonably accurate [36].

A diagram of rhodopsin, based on a refined crystal structure (PDB entry: 1HZX), is shown in Figure 1.9. As an integral membrane protein, rhodopsin comprises three domains: an extracellular domain (sometimes termed intradiscal), a membrane-embedded domain and a cytoplasmic domain. Seven transmembrane segments (H1-H7) are linked sequentially by extracellular (E1, E2 and E3) and cytoplasmic (C1, C2 and C3) loops. The amino-terminal tail is extracellular and the carboxy-terminal tail is cytoplasmic. The retinylidene is situated more towards the extracellular boundary of the membrane bilayer.

In addition to 11-Z retinylidene, rhodopsin is post-translationally modified by two carbohydrate moieties at Asn-2 and Asn-15 [37], two palmitoyl groups at Cys-322 and Cys-323 [38], a Cys-110-Cys-187 disulphide bond [39] and by functional phosphorylation at multiple Ser and Thr residues [40]. These sites are analogous to phosphorylation sites found on the carboxy tails of other GPCRs [41]. The carbohydrate chains and the disulphide linkage are oriented towards the extracellular face of rhodopsin and the C-terminal domain is

cytoplasmic.
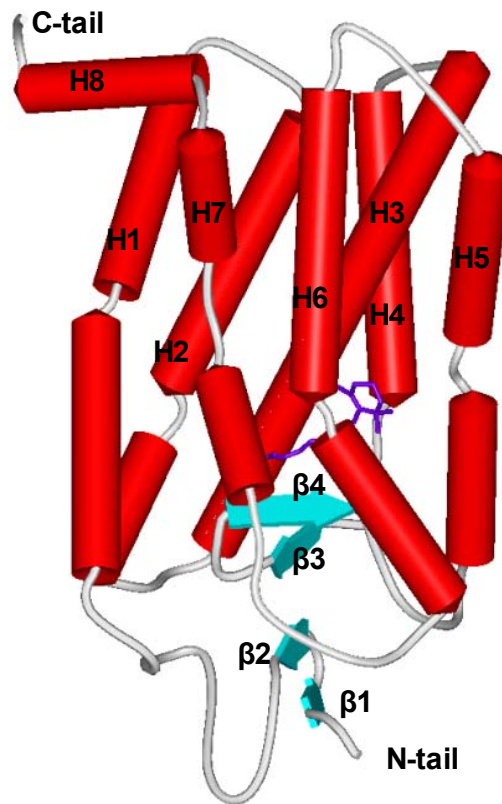
Figure 1.9 – Crystal structure of bovine rhodopsin prepared from the 2.8Å crystal structure coordinates (PDB entry: 1HZX). The intracellular cytoplasmic surface encompasses loops C1 to C3 and the   C-terminal tail. The extracellular region includes the N-terminal tail (N-tail) and the E1 to E3 loops. Helical portions of the protein, including the transmembrane helices (H1 to H7), are shown as red rods and the β-strands are shown as grey arrows (β1 to β4). A short helix (H8) corresponding to

The crystal structure has been reviewed a number of times in detail [28, 34, 42-44]. Some of

the key features are summarized below:

Transmembrane domain – Tilted kinked helices.

As predicted, the polypeptide passed through the membrane in seven helical segments (H1 to H7). The helices are irregular in length (20-33 residues) and orientation, varying in their degree of bending around Gly/Pro residues and in their tilt angle. A strong distortion is imposed in H6 by Pro-267, one of the most conserved residues amongst GPCRs, yet the presence of a Pro residue does not cause bending of H5 nor does a Gly-Gly tandem lead to significant distortion of H3, the longest and most tilted of the helices (33° to the membrane normal). Other helical bends are observed in H2 (Gly-89-Gly-90), H4 (Pro-170) and H7 (Pro-303), which shows considerable elongation in the region around the retinal attachment site (Lys-296) and contains the highly conserved Asn-Pro-X-X-Tyr motif. A Glu(Asp)/Arg/Tyr(Trp) tripeptide sequence if found at the cytoplasmic border of H3 that is conserved in family A GPCRs and has been shown to be involved in interaction with the transducin G protein [45, 46].

Cytoplasmic and extracellular domains

One of the most striking features was the presence of a short amphipathic helix (H8) lying almost parallel to the membrane normal on the cytoplasmic side of the membrane, anchored by palmitoyl residues attached to a pair of Cys residues. This region of rhodopsin plays a role in the regulation of transducin binding and is possibly a binding site for the transducin α-subunit [47]. It has also been implicated in an interaction with a phospholipid molecule in the disc membrane, which may be linked to a specific lipid-protein interaction that changes upon receptor activation [48]. High conservation of Phe-313 and Arg-314 suggests that the amphipathic character of H8 may be functionally important.

Whereas the cytoplasmic loops were poorly resolved, indicating flexibility, the extracellular domain showed significant secondary structure. An unexpected finding was the positioning of an anti-parallel β-sheet (β4) which forms a roof for the retinal binding pocket. A highly

conserved disulphide bridge (Cys-110-Cys-187) holds the β-sheet close to the retinal so it runs parallel from C9 of retinylidene to the Schiff base. Glu-181 from the β3 sheet is brought into the vicinity of the polyene chain where it has recently been implicated in an interaction with the C11-C12 isomerization site, in a complex with a water molecule [49]. Several neuropeptide and peptide hormone receptors have also been shown to use extracellular loops to bind their ligands [50, 51]. The β4 strand is highly conserved amongst vertebrate opsins however, in family A GPCRs that do not bind retinal, for example, adrenergic receptors, this region does not seem to be highly conserved, except for the Cys-187 residue, indicating that the β4 strand might serve specifically to define the retinal ligand-binding pocket in vertebrates [52, 53].

Interhelical interactions

Besides interacting with the chromophore, numerous other structural modules that stabilise the ground state structure are found in the crystal structure. Stabilising the inactive ground state structure prevents untriggered activation of the protein and results in a very low basal level of activity for the receptor, required for sensitive light detection. The stabilising modules include several distinct hydrogen-bonded networks between helices, as well as hydrophobic interactions that are mediated by residues that are highly conserved in GPCRs. Multiple hydrogen bonding contacts are observed between most of the helices. For example, H3 makes contacts with H2, H4, H5 and H7. Such a network has been suggested between the conserved Arg-135 residue on H3 and Glu-247 and Thr-251 on H6 [28, 54, 55], although
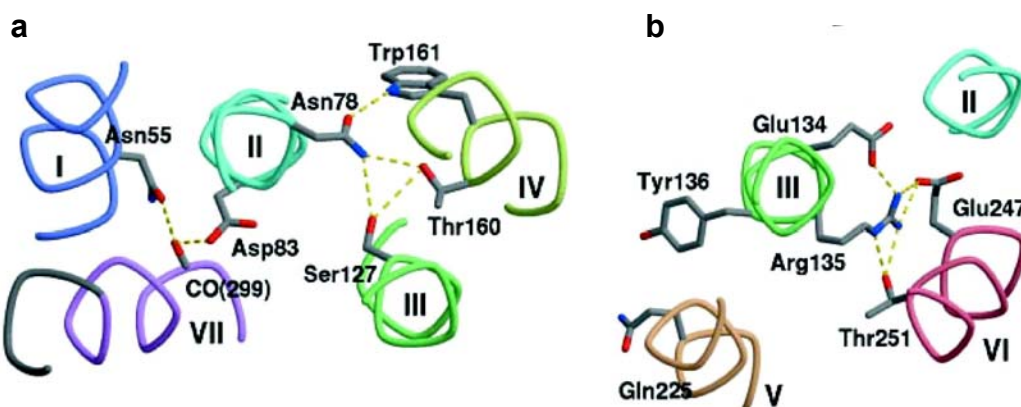
the refined crystal structure suggests that Arg-135 interacts solely with its neighbour, Glu-134 [34]. An additional H-bonding network includes the highly conserved Asn/Pro/X/X/Tyr motif (H7) that is thought to mediate several core-stabilizing interactions with residues on H2 and H6.

Chromophore binding pocket

Rhodopsin's chromophore, 11-*Z* retinylidene, is located between the transmembrane helices, offset from the centre of the membrane towards the extracellular side of the molecule as suggested previously. Many detailed descriptions of the retinal environment have been provided previously, including discussions of relevant noncrystallographic information [28, 34, 53]. The chromophore binding pocket is made up from a mixture of hydrophobic and polar/charged groups. Helix 3 provides many of the amino acid side chains that form the retinal binding pocket, almost running parallel to the polyene chain from C11 to the β-ionone ring. The polar side chains from Thr-118, in addition to Tyr-268, are located near the centre of polyene chain and appear to determine the position of the C9 methyl group of the chromophore. On the extracellular face, the polyene chain is capped by the amino acids from the β4 sheet (Ser-186 to Ile-189) of the E2 loop as described above. A counter-ion for the protonated Schiff base is provided by Glu-113 in a complex with a water molecule [56]. This interaction raises the pKa of the Schiff base, preventing spontaneous hydrolysis of the chromophore [57] and is one of the critical determinants of activity. Residues from H1 (Tyr-

Figure 1.10 – Interhelical H-bond interactions mediated by the highly conserved Asn-55 residues, connecting H1, H2 and H7 and by Asn-78 for H2, H3 and H4 (a). The tripeptide motif at the cytoplasmic face of H3 contains the conserved (Asp/Glu)/Arg/Tyr motif that may form interhelical contacts with H6 (b). From [28].

43, Met-44 and Leu-47), H2 (Thr-93 and Thr-94) and H7 (Ala-292, Phe-293) form most of the retinal contacts in this region. The position of the Schiff base counterion is one helix

turn away from the position of an Asp residue, conserved in biogenic amine receptors, that serves as the counterion to the cationic amine ligands.

The binding site of the β-ionone ring of the chromophore is largely described by hydrophobic residues from helices 3, 5 and 6 (H3, H5 and H6) of the protein. The position of the β-ionone ring is largely constrained on the cytoplasmic side of the chromophore (C4-C6) by four residues: Gly-121 (H3), Glu-122 (H3), Phe-261 (H6) and Trp-265 (H6). The residues around the C1-C3 region of the chromophore, including the C16 and C17 methyls are predominantly hydrophobic and aromatic: Met-207, His-211, Phe-208 and Phe-212 on H5 and Phe-261, Trp-265, Tyr-268 and Ala-269 on H6 (shortest internuclear distance <5Å with the chromophore between C1 and C3). The binding pocket for the β-ionone ring of the chromophore is illustrated in Figure 1.11.
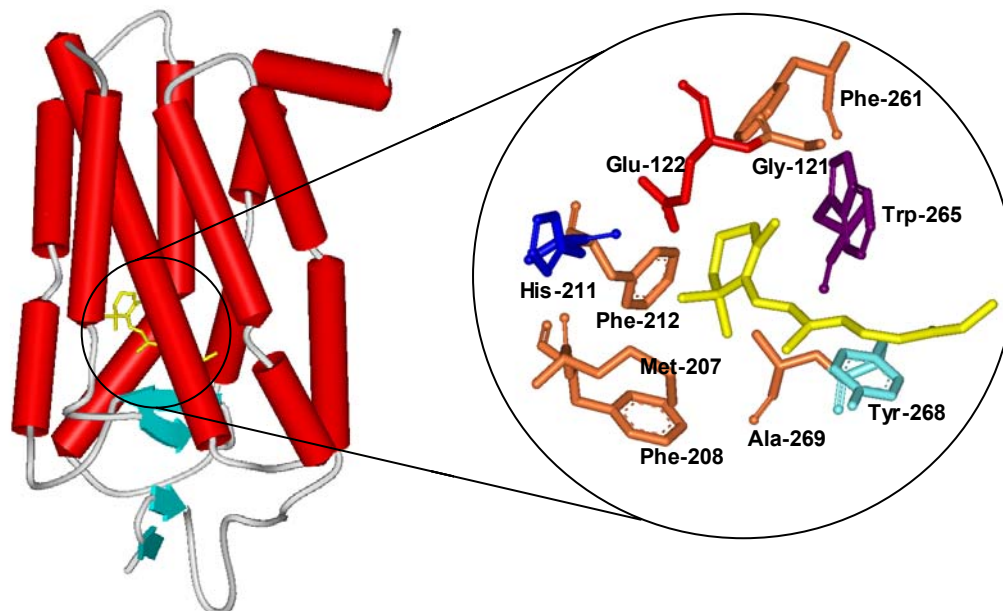
Figure 1.11 – Crystal structure of bovine rhodopsin at 2.8Å showing the chromophore binding site around the β-ionone ring (with internuclear carbon-carbon distances <5Å with the chromophore). The colours of the side chains are: red for acidic, blue for basic, light blue for polar, orange for hydrophobic and purple for Trp residues. The retinylidene chromophore is shown in yellow.

1.4 Rhodopsin activation

Although rhodopsin activation is a dynamic process that takes place over a few milliseconds, the complexity of visual transduction means that a reductionist approach is useful for understanding the transduction mechanism. The mechanism of rhodopsin activtation is more easily understood in terms of intermediates, along with the dynamic processes which link the intermediates. The goals of research into rhodopsin activation are therefore to obtain structural knowledge of the intermediates and elucidation of the driving forces responsible for change from one intermediate to the next. Because activation energy barriers typically separate the intermediate states, intermediates that are highly unstable at physiological temperatures can be thermally trapped at extremely low temperatures [31, 58, 59].

The ability to trap intermediates allowed preliminary characterisation of visual pigment intermediates to begin even before structural methods with fast time resolution were available. Starting in the early 1940's, the basic intermediates of the rhodopsin activation pathway were identified using this method in combination with UV-VIS spectrophotometry. Over the next 25 years this led to the detailed description of rhodopsin intermediates (Figure 1.13)[59].

λ max (nm)	Formation time scale	Temperature of transition to next intermediate	
498			Rhodopsin $\xleftarrow{}$
	~ 200 fs		$\downarrow$ hυ
542			Bathorhodopsin
	~ 30 ns	-140 °C	$\downarrow$
497			Lumirhodopsin
	~ 50 μs	-50 °C	$\downarrow$
478			Metarhodopsin I
	~ 20 ms	-20 °C	$\updownarrow$
380			Metarhodopsin II
		-5 °C	$\downarrow$
460			Metarhodopsin III
			$\downarrow$
387			Opsin + free all-E-retinal

11-Z-retinal (*in vivo*)
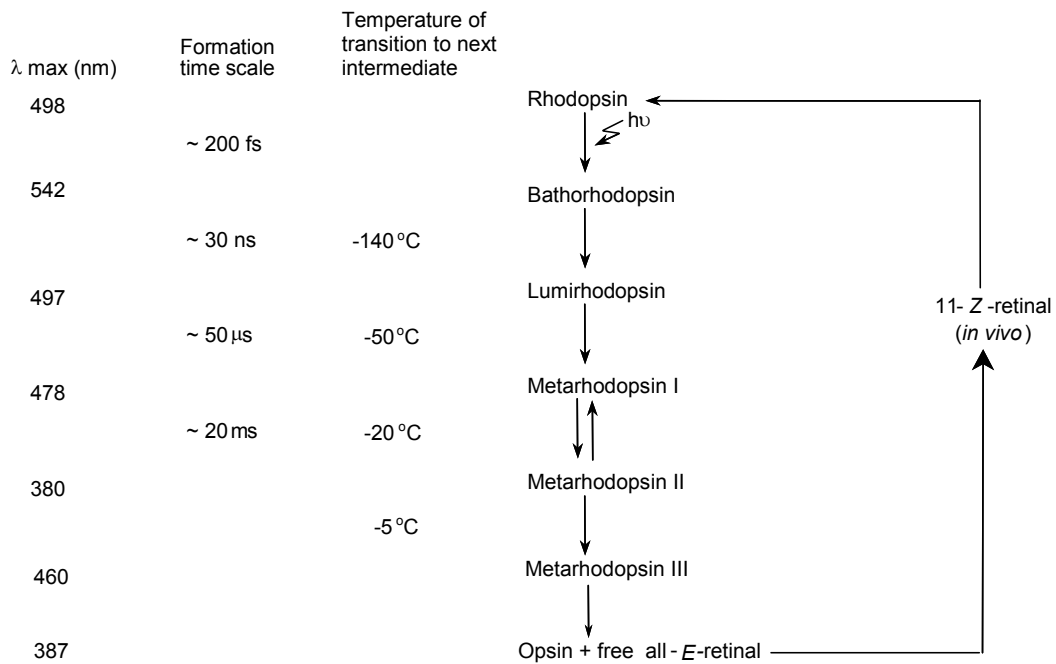
Whilst thermal trapping provided clear evidence for the existence of intermediates in rhodopsin, it was limited to trapping intermediates with successively higher thermal barriers and therefore not so successful at characterizing the less stable intermediates in entropy driven processes, such as the Blue-Shifted Intermediate (BSI) which lies between the bathorhodopsin and lumirhodopsin states. Kinetic measurements using more recently developed time-resolved optical methods have been used to identify additional intermediates within the activation pathway and at more physiologically relevant temperatures [60-63].

The description of the current model for the activation mechanism represents only a summary of the key steps in the activation of transducin following activation of rhodopsin

Figure 1.13 - The photocascade of bovine rhodopsin deduced from trapping methods. The maximum wavelengths (λ_{max}) of the absorption spectra of each photointermediate is shown. The transition to the next intermediate takes place spontaneously above the indicated temperatures in ROS membranes. Subsequent time-resolved measurements led to identification of the BSI intermediate following bathorhodopsin, which cannot be trapped at low temperatures and appears transiently.

with light. Comprehensive reviews of the activation mechanism are provided elsewhere [59, 64-67].

Activation of rhodopsin begins with the absorption of a photon, that results in isomerizaton of the retinylidene C11-C12 bond from 11-*Z* to 11-*E* and formation of the primary photoproduct photorhodopsin (Figure 1.14). The isomerization is complete in less than 200fs and is very efficient, with a quantum yield of 0.67 [68]. The first high-energy intermediate that can be stabilized at low-temperatures is bathorhodopsin, which stores 60% of the incident photon energy (~35kcal mol^{-1}) [69].

C11-C12 bond in
11-*Z* configuration

11-*Z* retinal

light
(ROS)

re-isomerisation
(ROS and RPE)
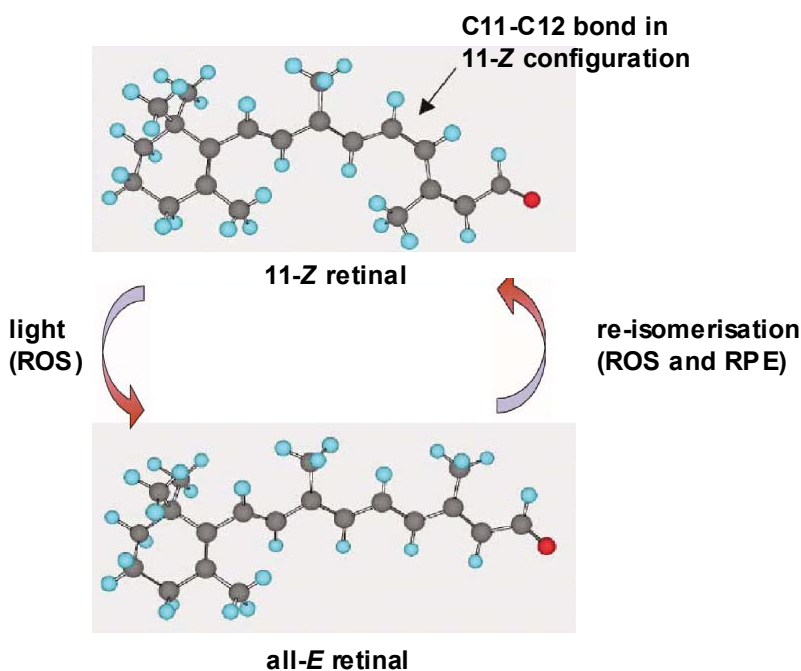
all-*E* retinal

Figure 1.14 – A model of the photo- and enzymatic isomerization of the 11-*Z* retinylidene chromophore. Absorption of light causes the isomerization of the C11-C12 bind of 11-*Z* retinal, covalently bound to opsin in rod outer segments (ROS), to all-*E* retinal. A similar process takes place in cone photoreceptors. Re-isomerization of the all-*E* retinal back to the 11-*Z* isomer takes place via the "retinoid cycle", initially in the ROS, then later in the retinal pigment epithelial cells (RPE).

The 180° rotation of the C11=C12 bond resulting from *cis/trans* isomerization is converted into smaller torsions that are distributed over the bonds in the middle of the polyene chain, as neither the position of the β-ionone ring nor the environment of the Schiff base changes upon formation of bathorhodopsin [59, 70-74]. This twisted all-*E* conformation state is

thought to be stabilized by steric hindrance between the C8 proton and the C18 methyl, which forms a barrier to motion in bathorhodopsin and prevents release of the torsion [75, 76]. It is well established that the formation of the primary photointermediate, bathorhodopsin, and its successive BSI intermediate, is primarily restricted to changes in the chromophore structure. Thermal relaxation leads through a blue-shifted intermediate (BSI), which is thought to involve an increase in the twist around the C6-C7 bond from the dark state and bathorhodopsin forms, contributing to BSI's blue shift [76]. This is consistent with the observation that increased flexibility introduced in the ring by removing the C5-C6 double bond results in an increase in BSI formation [59, 70] and that restricted C6-C7 rotation, introduced by locking the 6-*s-cis* linkage, results in the formation of the batho but not the lumi intermediate [77].

In lumirhodopsin, which can be stabilized at -50°C, most of the twist in the polyene chain has relaxed and this relaxation is subsequently increased in the meta-I intermediate state, as shown by FTIR, NMR [78-80] and Resonance Raman studies [81, 82]. Cross-linking studies indicate that a large movement of the β-ionone ring accompanies the batho→ lumi transition in which the ring moves from cross-linking to Trp-265 on H6 to Ala-169 on H4 [83, 84]. The extended conformation of the photoisomerized chromophore is predicted to cause reorganization of transmembrane helix H3, and subsequently H6 moves away from H3, yielding the lumi and meta-I states respectively [21, 85]. In its re-positioned environment the β-ionone ring initiates, in turn, a sequence of conformational changes that produces the active meta-II conformation of the receptor, R[*]. These changes cause deprotonation of the chromophore Schiff base and concurrent protonation of Glu-113, resulting in a large shift in the absorption maximum of from 480nm in meta-I to 380nm in meta-II (see Section 1.3: "opsin shift"). By cross-linking helices with Cys-Cys disulphide bridges and Zn^{2+} ions it has

been shown that rigid-body movement of H3 and H6 are required for receptor activation, most likely a separation at their cytoplasmic ends [86, 87]. The movement of H3 and H6 is thought to disrupt interhelical H-bonding and Van der Waals interactions between H3, H6 and H7 that results in formation of R*. Disruption of the interactions between Arg-135 and Glu-134 on H3, as a result of movement of Glu-247 on H6 are thought to result in reorientation of Arg-135 so it may interact with transducin [34].

It was found that Schiff base deprotonation is followed by proton uptake at the cytoplasmic surface at Glu-134, which was shown to be protonated in the complex between rhodopsin and transducin [88]. The two events were found to be separated by a 20ms time interval, indicating the existence of two meta-II forms, meta-II$_a$ and meta-II$_b$, corresponding to low (meta-II$_a$) and high-affinity (meta-II$_b$) forms of the receptor for transducin [64].

The mechanism for interaction of R* with transducin is less clear, although mutagenesis and peptide competition studies point to the interaction of cytoplasmic loops 2 (C2; helix 3-4 loop) and 3 (C3; helix 5-6 loop) with transducin [45, 46, 89, 90]. This was supported by a recent study in which the loops of other GPCRs were substituted for rhodopsin. G-protein activation experiments showed that C2 and C3 might have distinct roles in transducin activation and G-protein specificity [91]. Structural rearrangements of the cytoplasmic end of H7 have also been implemented in formation of the active R* receptor [92] and are consistent with the observation of an interaction between H8 and the $\beta\gamma$-subunit of transducin [93].

1.5   Rhodopsin as a paradigm for GPCR function

1.5.1.1   Family A GPCRs

The high-resolution structure of rhodopsin has provided an improved template for

interpreting the extensive body of activity, mutagenesis and affinity labelling data available for related 7TM receptors. It has also provided the first opportunity to use a real GPCR as a template to generate 3D models of other GPCRs, particularly the cationic amine receptors that are members of the family A GPCRs (7TM$_A$), of which rhodopsin is a member. These include the β_1-adrenergic receptor [94], M$_1$ muscarinic acetylcholine receptor [66], and dopamine D$_2$ receptor [95] for which structure-function data have been carefully interpreted using the rhodopsin template. Homology modelling has also been extended to the cholecystokinin CCK$_1$ receptor, which is also a member of the Family A class GPCRs but has a small peptide ligand [96].

The sequence identity between bovine rhodopsin and other 7TM$_A$ receptors is not high (~20% homology) although the presence of a number of highly conserved residues makes it possible to align the TM residues in this class of receptor [95]. Many of the key structural features highlighted in rhodopsin appear to be replicated in 7TM$_A$ receptors. To simplify the identification of aligned residues in different GPCRs the most conserved residues within each helix are assigned the position index "50" and other residues are numbered based on the relative position within that TM helix e.g. Pro-303 is Pro-6.50 and therefore Asn-302 is Asn-6.49 and Val-304 is Val-6.51.

Within the helices Pro residues in helices 5 (Pro-3.50), 6 (Pro-6.50) and 7 (Pro-7.50) are highly conserved, providing kinks that are thought to play an essential role in receptor activation. Additional Pro residues showed more divergence between receptors, such as the Pro in H2, where they may bend differently. Intramolecular interactions, such as the disulphide bond between H3 and the E2 loop in the extracellular region (Cys-110-Cys-187 in rhodopsin), the tripeptide Asp(Glu)/Arg/Tyr motif at the cytoplasmic border of H3 and the common Asn/Pro/X/X/Tyr motif in H7 are all highly conserved, suggesting these

receptors have evolved to maintain a common overall fold.

1.5.1.2 Family B and C GPCRs

The similarities described are relevant largely to $7TM_A$ receptors. Family B ($7TM_B$) are thought to employ multiple extracellular contacts to bind ligands, whilst the large amino-terminal tail (500-600 residues) binds the ligand in family C receptors ($7TM_C$). Each class of GPCR has conserved residues although they are not the same as those conserved in $7TM_A$ receptors. A common structural element might be the Cys-Cys disulphide bond that links H3 with loop E2 [54]. The relevance of the rhodopsin crystal structure and continuing structure-function relationships appears therefore to be more relevant for the $7TM_A$ receptors at present.

Figure 1.15 - The most conserved residues amongst family A GPCRs illustrated for rhodopsin, including the tripeptide Asp(Glu)/Arg/Tyr motif in H3 (E-134/R-135/Y-136 in rhodopsin), the Asn/Pro/X/X/Tyr motif in H7 (N-302/P-303/X/X/Y-306 and the disulphide bridge between Cys-110 and Cys-187. From [67].
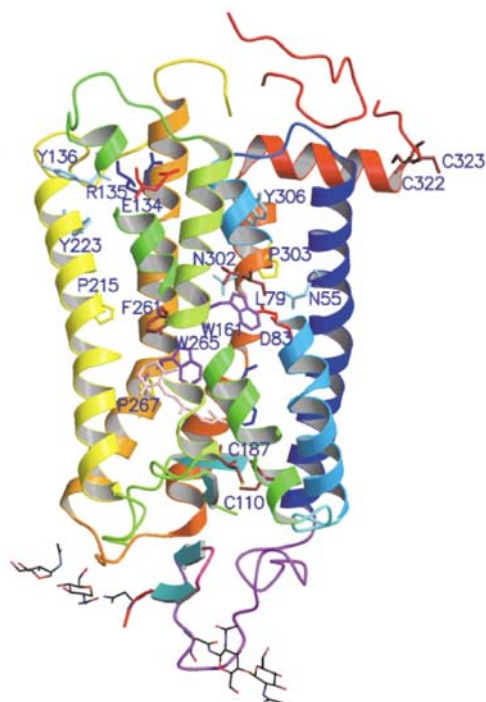
Biochemical experiments have suggested some common functional properties exist between rhodopsin and family A GPCRs and are discussed later in the study (Section **Error! Reference source not found.**). The apparent structural similarity between these proteins alone suggests this may be true, hence gaining a detailed understanding of the activation mechanism of rhodopsin should be a key factor in elucidating activation mechanisms for $7TM_A$ GPCR receptors in general.

1.6 The 11-*Z* retinylidene chromophore

As with the protein the resolution for the 11-Z retinylidene chromophore in the crystal structure of rhodopsin is moderate (2.8 Å), meaning it cannot be used to define torsion angles or bond lengths accurately at present. Consequently, a range of other techniques are required to study the chromophore in detail and determine its role in the activation mechanism. Atomic resolution structural details are essential in order to uncover:

1. The details of the chromophore-protein interactions that stabilize the dark state conformation of the protein.

2. The mechanism by which the chromophore so efficiently captures the light energy immediately following *cis/trans* isomerization around the C11-C12 bond.

3. How the chromophore communicates the isomerization signal into structural changes in the protein that result in formation of the active receptor, R^*.

The structure of the chromophore in its dark state conformation has been studied extensively by a large number of different techniques, in the native membrane or in detergent solubilized form. UV-VIS [59, 97-99], Fourier Transform Infra Red (FTIR) [74, 100], Resonance Raman [72], Circular dichroism (CD) [101-104] and Nuclear Magnetic Resonance (NMR) [32, 78, 80, 105-108] spectrometry have been used on rhodopsin pigments regenerated with native and modified retinal analogues. Modelling studies have also been used to predict the structure of the bound chromophore, which have been aided by the crystal structure [109-111]. These have, in general, resulted in a 6-*s-cis*, 11-*s-cis*, 12-*s-trans* conformation for the chromophore. A similar conformation for the retinylidene was derived in the crystal structure based on the approximate positions of the methyl groups in the electron density [28].

Interactions between the chromophore and the protein have been investigated through the use of side-directed mutagenesis [112-114], cross-linking studies [115, 116] and NMR chemical shift measurements [107, 117] that correctly determined the position of the retinal within the protein, and deduced some of the key interactions between the chromophore and the protein.

Solid-state NMR has been used extensively to study the chromophore in rhodopsin.

Although good progress has been made in the development of methods for complete structure determination of small proteins by solid state NMR (<20kDa), it is more suited at present to answering specific structural questions for which very high resolution is required, such as the study of ligands bound to their receptors [118, 119]. Unlike mutagenesis, chemical labelling or retinal analogue studies the unperturbed chromophore and protein are studied by solid state NMR, which are crucial when investigating the precise structure and binding mechanism of the chromophore. As proteins can be studied in the natural membrane environment with solid-state NMR they are normally functional, enabling dynamic and functional information to be obtained. Unfortunately, the preparation of samples for solid state NMR experiments is expensive and NMR experiments are generally long, meaning relevant questions must be asked. To date, solid state NMR has been used to study the dark state chromophore in rhodopsin using predominantly the following techniques:

- *Chemical shift measurements* – ^{13}C chemical shift data for the retinylidene carbons of bovine rhodopsin has been used to investigate the orientation of the C6-C7 bond [32, 105, 120] and the environment around the Schiff base region [106, 108, 117] of the chromophore, revealing the partial penetration of the PSB positive charge into the retinal polyene chain. Complete ^{13}C chemical shift data is available for the retinylidene chromophore [106, 107], although it is difficult to interpret this data in terms of precise structural constraints for the chromophore, as additional factors such as the protein environment influence the data. However, this can been used advantageously to investigate chromophore-opsin interactions, as was shown in a ^{15}N and ^{13}C NMR study that correctly determined the water-mediated environment of the Schiff base in the absence of a crystal structure [117].

- *Torsional angles* – Double-quantum heteronuclear local field ^{13}C NMR was used to determine directly the torsional angle of the C10-C11 bond, observing a twist away from planarity (160 ± 10º) [121].

- *Orientational constraints* – Using ^{2}H NMR methods on oriented systems, the orientations of the three methyl groups C18, C19 and C20 were determined with respect to the membrane normal [80, 122]. A model of the retinal was produced that exhibited the recognized twist in the polyene chain, although the ring was shown to adopt a twisted 6-*s-trans* conformation, in contrast to previous studies.

- *Internuclear distance measurements* – Solid-state ^{13}C NMR is able to measure selective carbon-carbon distances by reintroducing the dipolar coupling using homonuclear recoupling techniques. In this way internuclear distances in the bound chromophore around the isomerization region were determined to enable the degree of twist of the C10-C13 region to be estimated (~44º) [78] and in a recent study, the bond-lengths from C10 to C15 were determined to picometre-resolution [49], identifying perturbations in the bond lengths that were attributed to a proximal glutamate residue (Glu-181 from the E2 loop).

1.6.1 The β-ionone region of retinylidene

The majority of direct high-resolution NMR data has been obtained for the polyene chain region of retinylidene, examining the C11-C12 isomerization region [49, 121] and the Schiff base region of the chromophore [106, 108, 117]. In a recent ^{2}H NMR study Grobner *et al* determined the orientation of the C18 ring methyl directly with respect to the membrane normal using the MAOSS NMR technique [80]. Based on the relative orientation between this methyl and the C19 and C20 methyls on the polyene chain, a conformation of the β-

ionone ring was proposed. Ambiguities existed in the absolute conformation around the C6-C7 bond compared with previous solid state NMR chemical shift and CD measurements. The detailed atomic structure of the β-ionone ring region of the retinylidene chromophore has yet to be determined.

The original aims of this project were to use solid state NMR techniques to determine the high-resolution structure of the β-ionone ring region of the bound retinylidene chromophore in bovine rhodopsin. The wild-type 11-Z retinylidene chromophore in rhodopsin would be replaced with 11-Z retinal that is synthetically ^{13}C labelled in the β-ionone ring region, enabling resonances from individual nuclei within the β-ionone ring and polyene chain to be observed. Rotational resonance NMR would then be used to measure the interatomic distances between the introduced ^{13}C spin pairs, enabling the geometry of the β-ionone region to be defined. The details of this procedure are discussed in Chapter 3.

UV-VIS studies using modified retinal analogues have suggested the β-ionone ring forms an essential binding interaction with the protein binding pocket [98], and is the primary interaction between the chromophore and opsin [123] (see Chapter 3). Chemical shifts of the ^{13}C labelled nuclei in the β-ionone ring region could reveal perturbations in the ring structure that occur on binding of the retinal ligand, highlighting chromophore-protein interactions from the chromophore's perspective. As the ^{13}C labelled retinals are non-perturbing and the spectroscopy is non-evasive any interactions that are detected would accurately reflect the binding characteristics of the wild-type chromophore. With the recent advance of the crystal structure the approximate positions of the residues forming the chromophore binding pocket are now known. Thus, a more specific interpretation of any observed perturbations in the   β-ionone ring structure should be possible.

1.6.2 The activated 11-*E*-retinylidene chromophore

Until recently, a paucity of direct structural information existed for retinylidene in the photointermediate states. The structure and role of the chromophore in the photointermediates of rhodopsin has been mainly investigated by Raman [72, 81, 82, 124], optical (UV-VIS) [70, 71, 76, 125-129] and FTIR spectroscopy [100, 130-132] on a variety of visual pigments with site-specific mutations and/or chemically modified retinal chromophores. These techniques have yielded useful insights into chromophore structure and chromophore-opsin interactions throughout the photocycle and have led to the current model of rhodopsin activation. However, the methods used do not observe the chromophore directly and care must be taken interpreting data using perturbing artificial chromophores.

Solid state NMR spectroscopy has recently provided direct atomic resolution structural information on the chromophore in rhodopsin photointermediates by low-temperature trapping of the activated protein in the required photointermediate state [73, 78-80, 133]. Most of this work has focused on the meta-I photointermediate, which is the precursor to the transducin activating meta-II state and the latest photointermediate that can be stably trapped for solid state NMR measurements at present. Low-temperature trapping of a photointermediate results in a mixed population of retinal isomers being generated, hence only partial conversion to the meta-I photostate can be achieved. The trapping of the meta-I photointermediate has not been properly characterized and is investigated in this study, using solid state NMR to quantify the conversion rate to the meta-I intermediate (Chapter 4).

With the advance of the crystal structure of rhodopsin a structural template of the protein has been provided through which more specific functional questions can now be asked. The high-resolution structural detail available from solid-state NMR spectroscopy and the

functionality of the rhodopsin NMR samples lends itself to this role. Although rhodopsin crystals have been shown to be functionally active [56], it is unlikely that diffraction data from photointermediates will be obtained, due to the heterogeneous populations of activation states in any of the trapped photointermediate states. A novel technique where the structures of individual segments of rhodopsin were determined using 2-D solution NMR and then assembled using long-range distance constraints has been used to model the meta-II receptor [55]. Although this is useful in investigating the protein structure in meta-II the detailed structure of the retinylidene chromophore in the activated protein cannot be determined by this method. In the absence of crystallographic data for the photointermediates states, the role of solid state NMR in investigating the role of the chromophore in the activation mechanism of rhodopsin is pertinent.

The β-ionone ring has been shown to be an essential requirement in forming the active meta-II (R^{*}) receptor. Modifications to both the C1-C4 segment of the ring [85] and to the methyl moieties on the ring significantly influence the meta-I/meta-II equilibrium [125], indicating the ring plays an important role in transmitting the changes that occur in the retinal structure upon photoisomerisation into conformational changes in the protein structure that activate the receptor. Recent cross-linking evidence predicted the ring is repositioned as early as the batho→ lumi phototransition and from this new position it controls the formation of the later photointermediates [84]. Additionally, the β-ionone ring has been suggested to adopt a planar 6-s-*trans* conformation in the meta-I photointermediate, requiring a movement of the β-ionone with respect to the polyene chain from the twisted 6-s-*trans* conformation of dark state [80].

Following the dark state NMR measurements on the β-ionone ring it was intended to trap the β-ionone ring ^{13}C labelled rhodopsin samples in their meta-I photointermediate states

and determine the absolute conformation around the C6-C7 bond using rotational resonance NMR. By observing changes in the chemical shift observations from the dark state, changes in the binding of the β-ionone ring could hopefully be detected. By characterizing the structural changes that occur within this region of the chromophore upon activation, a detailed functional understanding of the role of the β-ionone ring in the activation mechanism would be gained.

1.7   Solid state NMR

NMR spectra result from the interaction of nuclear spins with a large external static magnetic field and many small internal fields, originating from neighbouring spins. The resonances, visible in the spectrum, are modulated by a number of spin interactions, like chemical shift anisotropy (CSA), *J* coupling, dipolar interactions and quadrupolar interactions. Because of rapid molecular tumbling in solutions, the interactions that have an angular dependence (CSA, dipolar interactions) are averaged to give narrow lines. To study this protein in its natural environment, solid state NMR has to be applied. Long correlation times or restricted motions of proteins in solids lead to incomplete averaging of the spin interactions described. In this case, spectra are dominated by broadening from the anisotropic interactions and specific resonances are difficult to resolve individually. A number of techniques can be utilised to increase the sensitivity and resolution of solid state NMR, enabling the investigation of the structural and dynamic properties of proteins and their ligands in the natural membrane environment.

1.7.1   Magic angle spinning

In a MAS NMR experiment the chemical shift anisotropy broadening is averaged by macroscopic sample rotation around an axis aligned to 54.7° to the applied magnetic field,

the "magic angle". The inhomogeneous anisotropic terms with a dependency upon $[1-(3 \cos^2 \theta)]$ are effectively removed when the spinning speed (ω_r) exceeds the magnitude of the interaction. The reduced linewidth enables resonances to be resolved and also produces an increase in signal to noise levels. When the spinning speed is less than the magnitude of the CSA interaction a number of spinning side-bands are observed at integral multiples, with respect to the isotropic shift σ_i, which is the average chemical shift experienced by every molecule in the rotating sample. The effect of MAS on the NMR spectrum is illustrated in Figure 1.16. In the static spectrum only two resonances are clearly visible. Sample spinning causes the spectrum to separate into isotropic components, which are masked at slow spinning speeds by their spinning sidebands. At higher speeds a large proportion of the magnetization is focused into the isotropic peaks and the sideband pattern becomes clearer. At the highest spinning speeds only two resonances with the greatest CSA still have associated sidebands.
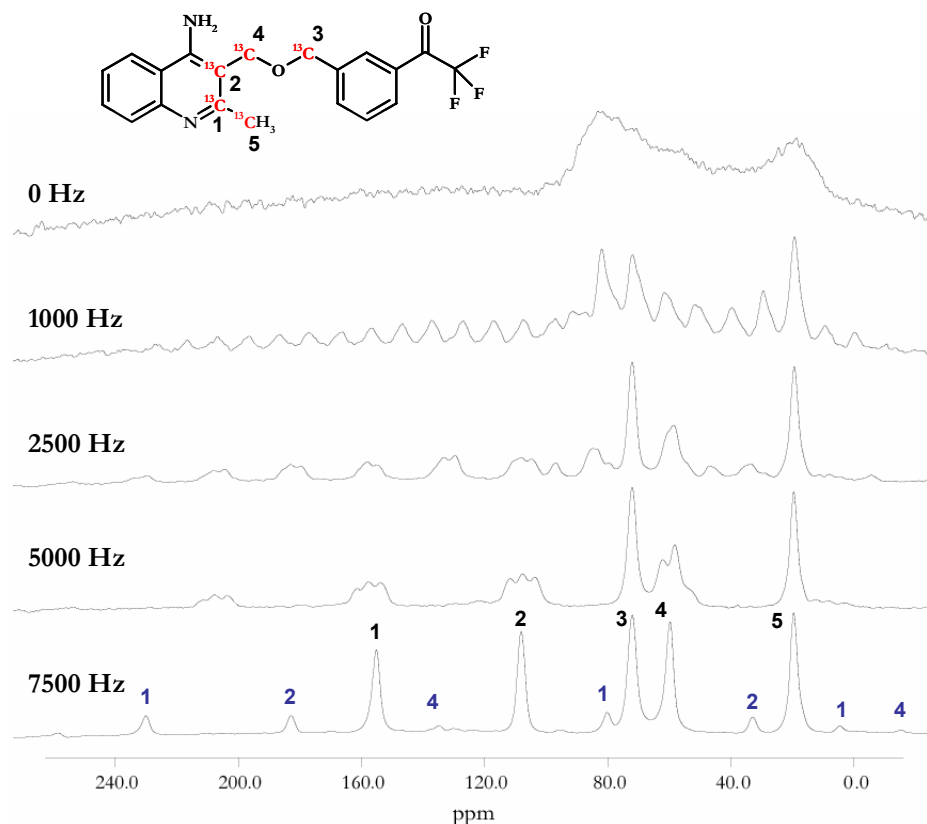
Figure 1.16 – ^{13}C CP-MAS NMR spectra of a selectively labelled solid compound shown above illustrating the effect of magic angle sample spinning (MAS). Isotropic chemical shift resonances are numbered in black, assigned to the ^{13}C nuclei numbering scheme shown above. Spinning sidebands corresponding to the relavant isotropic resonances are numbered in blue. All spectra were recorded on a 400MHz NMR spectrometer, at a ^{13}C frequency of 100MHz. Spectra normalized to spectral scale.

Dipolar interactions between nuclei are key to determining interatomic distances and molecular orientations. This through-space coupling has an r^{-3} dependence and is the source of distance constraints in both solution and solid state NMR. Since this interaction is also anisotropic it is also averaged to zero by the applied magic angle spinning. Several techniques have been developed to reintroduce this dipolar interaction into the solid state NMR experiment whilst still retaining high resolution through MAS [134]. In this study the rotational resonance technique is used, developed by Levitt *et al* [135]. It enables the measurement of the distance between two homonuclear spins that have a large (>3 kHz) resonance frequency difference. This technique is discussed in more detail in Chapter 3.

1.7.2 Cross polarization

The sensitivity of a particular nucleus to NMR experiments may be related to it gyromagnetic ratio (γ). Unfortunately, many nuclei of interest in biological NMR have relatively low γ values. Cross-polarization (CP) involves the creation of transverse magnetization on the abundant high γ protons, before transfer to low γ spins and subsequent observation [136]. Magnetization transfer is achieved by the simultaneous application of a spin-lock on both the proton and low γ channels, such that the Hartmann-Hahn condition is met [137].

$$\gamma_I \, B_{1I} = \gamma_S B_{1S}$$ Equation 1.1

where B_1 = applied field strength

The sensitivity gained compared to direct generation of transverse magnetisation depends on the ratio of γ values; in the case of proton/carbon transfer a four-fold increase in signal to noise is possible [138]. Additionally, the delay between acquisitions may be reduced since magnetisation is dependent upon proton relaxation rates (which is typically faster than carbon relaxation rates), thus increasing the number of acquisitions which may be complete within a given time period.

Precise selection of applied field strengths for the Hartman-Hahn match condition is important for efficient CP, in particular under MAS where the match condition breaks down into a series of sharp peaks separated by sample spinning frequency [139]. A number of schemes have been developed to reduce the dependency of magnetisation transfer on an exact match, such as ramped CP [140] and variable amplitude CP [141].

1.7.3 Isotropic enrichment

For biological systems, like membrane proteins that are rich in carbon, hydrogen and oxygen, generally the ^{13}C isotope is investigated. Since the abundancy of the ^{13}C nuclei in nature is only 1.1%, the NMR sensitivity for carbon is rather small. The ^{13}C NMR spectrum of a 41kDa membrane protein, such as rhodopsin, comprises resonances from all ^{13}C nuclei, present in the protein backbone and amino acid side groups, as well as the chromophore. Hence, the spectrum is a superposition of numerous ^{13}C resonances and the signal of an *individual* nucleus cannot be discerned. The low natural abundance of ^{13}C can be used advantageously to obtain atomic resolution, through specific ^{13}C labelling at a predetermined site. A 90-fold increase in NMR signal can be observed for a single nucleus with 99% [13]C labelling, and hence this signal is clearly visible in the spectrum. With multiple ^{13}C labels, distance measurements can be achieved by measuring the dipolar coupling between spin pairs. In rhodopsin research, specific ^{13}C labelling has been used extensively to study the structure of the chromophore, and its interaction with the protein binding pocket [32, 78, 106, 107, 120, 121, 142]. Incorporation of ^{2}H and ^{19}F labels into the chromophore has also used successfully to study the structure of the chromophore [80, 122, 143], whilst chromophore-protein interactions have been probed using ^{15}N and ^{13}C labelling of the protein, expressed in mammalian cell lines [117].

In order to obtain an NMR signal from the labelled nuclei, a spectral subtraction of the protein and lipid background is required. An unlabelled sample is prepared under identical conditions to the labelled sample, yielding an NMR spectrum that can be subtracted from that of the labelled rhodopsin sample to give signal that is derived only from the labelled sites. In this study spectral subtraction gives rise to clean difference spectra with few artefacts, although this technique results in long NMR experiments, as an NMR spectrum

from the control sample has to be acquired after every labelled rhodopsin NMR experiment to give an accurate subtraction. The signals from the introduced ^{13}C labels may also be separated by using recoupling sequences to excite double-quantum coherences between coupled ^{13}C spin pairs, whilst suppressing signals from the natural abundance background that do not pass through double-quantum coherence [144-146]. Unfortunately the efficiency of DQF is limited in practical circumstances, especially over the longer through-space distances under investigation in this study. The method is more suited to directly carbon-carbon distance and torsional measurements, as shown for the bound retinylidene chromophore in the C10-C15 segment of the chromophore [49, 79, 121].

1.8   Overview of the project

The overall aim of this study is to use solid state NMR techniques to obtain direct distance constraints for the β-ionone region of the retinylidene chromophore and observe the effect of chromophore-protein interactions on the chromophore, in the dark and meta-I photoactivated states.

Chapter 2 describes the characterization of the ^{13}C labelled 11-Z retinals, the regeneration of these retinals into rhodopsin in ROS membranes and the characterization of the generated rhodopsin pigments.

Chapter 3 describes the use of rotational resonance NMR to measure the internuclear distances between C8 on the polyene chain and the three methyl carbons attached to the β-ionone ring (C16, C17 and C18), to determine the geometry of this region of the chromophore at atomic resolution. Chemical shift measurements are used to observe any perturbations in the retinylidene structure that occur on chromophore binding.

To study the meta-I intermediate accurately, the proportion of rhodopsin converted to meta-

I phototransition must be known. In Chapter 4, solid state NMR is used to investigate different methods of trapping the meta-I intermediate, using chemical shift changes that occur for a polyene chain ^{13}C labelled retinylidene upon the rhodopsin→ meta-I phototransition to quantify the proportion of trapped meta-I rhodopsin.

Using the optimised method for trapping the meta-I photointermediate the β-ionone ring ^{13}C labelled rhodopsin pigments are converted into their respective meta-I photostates. Chapter 5 considers the conformation of the β-ionone ring in the meta-I photoactivated state. Rotational resonance NMR experiments are repeated to determine the conformation of the β-ionone ring and chemical shift measurements are used as a probe for the environment of the β-ionone ring at this point in the photocycle. The implications for the activation mechanism of rhodopsin and GPCRs in general are discussed in Chapter 6.

Chapter 2   Preparation of ^{13}C labelled rhodopsin samples in ROS membranes

2.1 Introduction

The study of the retinylidene chromophore in rhodopsin by solid state NMR requires replacing the native 11-Z retinylidene chromophore of rhodopsin in the natural Rod Outer Segment (ROS) membrane with a ^{13}C labelled 11-Z retinal ligand. This requires synthesising ^{13}C labelled retinals by organic synthesis then purification to obtain 11-Z retinal with ^{13}C labels at the required positions. The ^{13}C labelled retinal is then regenerated into ROS isolated from bovine eyes, which have had the native 11-Z retinylidene chromophore removed through bleaching. Excess retinal is then removed from the system and the sample characterised by UV-VIS spectrophotometry. The procedure is summarised in Figure 2.1.

2.2 Purification and characterization of 11-Z retinal

2.2.1 Introduction

Table 2.1 illustrates the four different ^{13}C labelled retinals that were available for use in this

study, previously synthesised in the laboratory of Professor J. Lugtenberg (Leiden, The Netherlands) for solid state NMR studies on bacteriorhodopsin and rhodopsin.

Synthesis of ^{13}C labelled retinal using organic synthesis

↓

Purification and characterization 11-*Z* retinal isomer

↓

Isolation of opsin in Rod Outer Segments (ROS) from bovine eyes

↓

Regeneration of ROS with ^{13}C labelled 11-*Z* isomer

↓

Removal of excess labelled retinal

↓

Characterisation of rhodopsin samples using UV-VIS spectrophotometry

↓

Packing of rhodopsin samples for NMR analysis

Figure 2.1 – Summary of the stages required for the preparation of ^{13}C labelled rhodopsin in ROS membranes, for study by solid state NMR

Table 2.1 – Summary of ^{13}C labelled retinals regenerated into rhodopsin in this study.

[13]C labelleing scheme	chemical structure	mols of 11-*Z* isomer (nmol)
$[8,18-^{13}C_2]$		260
$[8,16/17-^{13}C_2]$		500
$[10,20-^{13}C_2]$		11260
$[16,17-^{13}C_2]$		3870

The synthetic pathways and characterization details for each of the ^{13}C labelled retinals have been extensively described [133, 147, 148]. Characterization of the correct synthesis of the retinals was performed by ^{1}H and ^{13}C NMR and mass spectrometry. ^{1}H and ^{13}C solution state NMR of the retinals in deuterated chloroform confirmed that all the ^{13}C labels were present at their predetermined position and the degree of incorporation was >95% in all cases [133, 147, 148]. Mass spectrometry showed that the experimentally found masses of the synthesized compounds were all according to expectations, with >95% incorporation of the ^{13}C labels [133, 147, 148].

2.2.2 Purification of 11-*Z* retinal

Incorporation of retinal into rhodopsin requires the native 11-*Z* retinal isomer. Each ^{13}C labelled retinal was supplied in an isomeric mixture, therefore, purification was necessary to isolate the 11-Z isomer. The purification procedure involved three stages: flash chromatography over a silica gel column to remove degradation products, illumination of the all-*E* retinal in polar solvent to obtain a mixture of isomers and High Performance Liquid Chromatography (HPLC) to isolate the 11-Z isomer. UV-VIS spectrometry was then used to characterize the isomerization state of the retinal and detect any contamination with other isomers.

Following their synthesis, each labelled retinal had been stored in hexane at -80°C. During this period some oxidation of the retinal could have occurred, yielding degraded retinoid fragments that had to be removed from the intact *Z* and all-*E* retinal isomers. Flash chromatography over a silica column (eluent of 10% diethyl ether/90% petroleum ether) was used to separate crudely the *Z* and all-*E* isomers from the degraded retinoid fragments [149]. The exact nature of oxidised retinal compounds is not known, but as they bind to a

polar silica column it is expected they contain extra hydroxyl groups. The slowest running

all-*E* isomer was collected from the column and dissolved in HPLC grade acetonitrile and

illuminated over night (15 hrs; 100W tungsten lamp), generating a photostationary mixture

of isomers (Figure 2.2(a)) [150]. The major isomeric components following illumination are

11-*Z*, 13-*Z*, 9-*Z*, 7-*Z* and all-*E* retinal although additional di-*Z* and tri-*Z* isomers are also

generated in small amounts (<5%) [150-152]. Purification of the 11-*Z* isomer was

accomplished by straight-phase preparative HPLC using a silica gel column and a mixture of

diethyl ether/petroleum ether (1/4 v/v) for the eluent. The resolution achieved by this
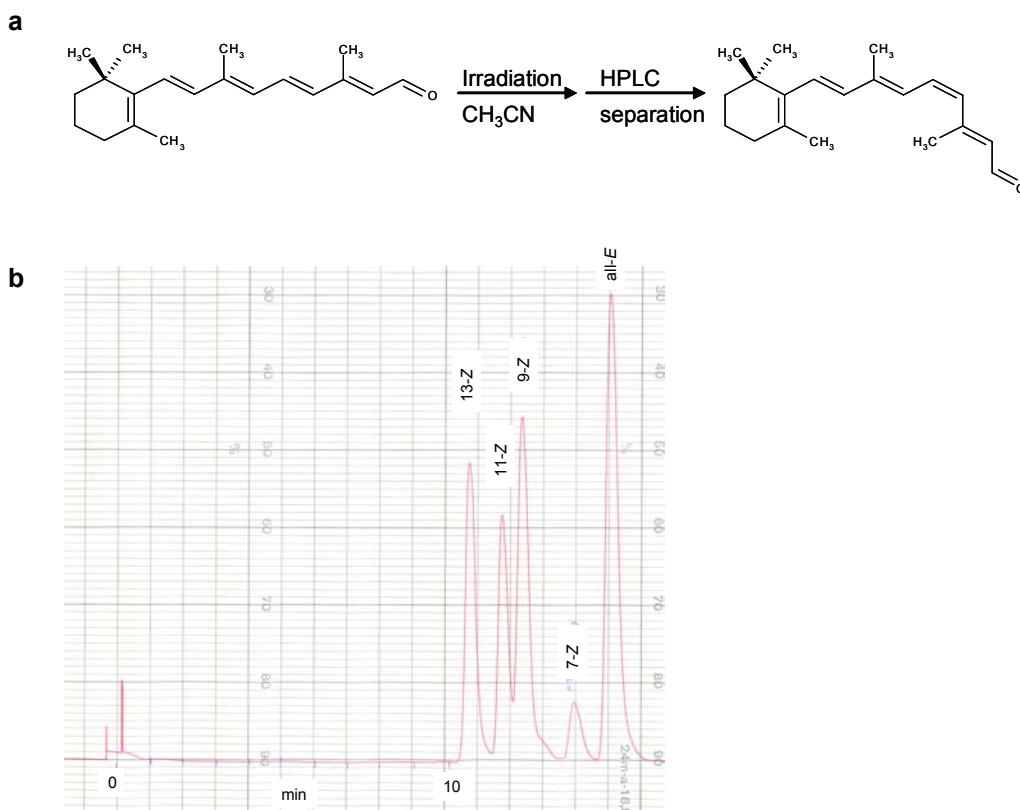
Figure 2.2 – Overview of the synthesis scheme of 11-*Z* retinal from all-*E* retinal (a).
HPLC trace of the photostationary mixture after 15 hours irradiation of the all-*E* isomer
in acetonitrile. The separation was performed using elution with a diethyl
ether/petroleum ether (1/4 v/v) as eluent and a flow rate of 15ml/min. Detection was

method enabled separation of the 11-Z isomer, which was collected in the dark to prevent reisomerization. An HPLC trace of the photostationary mixture of retinal is shown in Figure 2.2(b).

2.2.3 UV-VIS spectroscopic characterisation of 11-Z retinal

The five double bonds in conjugation with the aldehyde moiety in the polyene chain results in the bright colours and connected maximal absorption wavelengths (λ_{max}) of retinoids that are situated in the visible region of the electromagnetic spectrum [153]. As a general rule, the introduction of double bonds in a conjugated system of a chromophore results in a blue-shift in the absorption maximum, whilst the presence of strain and torsional twists in an unsaturated chromophore results in a decrease in conjugation and a red-shift [105]. Consequently different isomers of retinals have different absorption properties and can be characterized by UV-VIS spectroscopy.

Figure 2.3 shows the UV-VIS spectra of the 11-Z (red) and all-E (black) isomeric forms of [16,17-^{13}C$_2$] retinal, recorded in *n*-hexane. The spectrum of the 11-Z form is comprised of three broad bell-shaped features without fine structure: one strong band at λ=363nm and two weaker bands at λ=280 and λ=250nm [154, 155]. Each of the isolated 11-Z isomers of the ^{13}C labelled and unlabelled retinals showed these characteristic features for 11-Z retinal. Small deviations in the λ_{max} values were observed ($\pm$2nm), resulting from minor
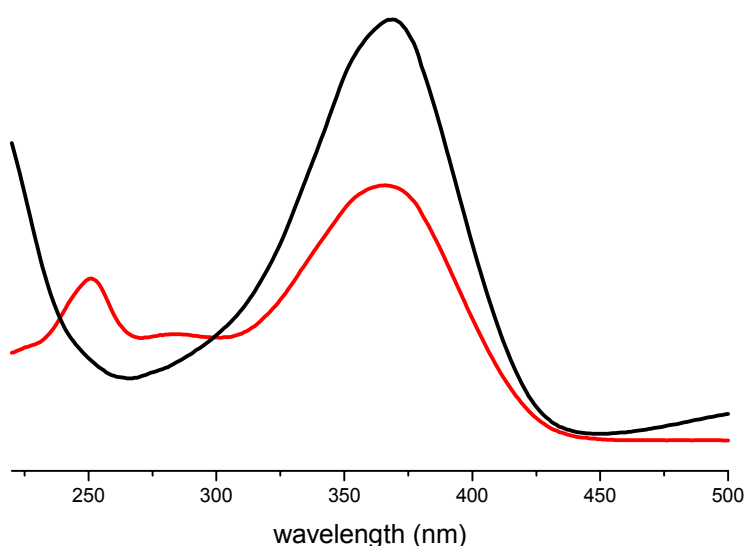
Figure 2.3 – UV-VIS spectra of 11-Z retinal (λ_{max}= 363nm) before (red) and after isomerization (black) from illumination (5min; 100W) in the presence of iodine as a catalyst. Following illumination the mixture was predominantly all-E retinal (λ_{max}=

contamination with other retinal isomers (<5%, [150-152]), although this was not considered significant enough to prevent regeneration (see Table 2.2).

Illumination (5min, 100W tungsten lamp) of 11-Z retinal in the presence of an iodine catalyst (1µg/ml in *n*-hexane) results in isomerization to predominantly all-E retinal, observed as a small bathochromatic shift (λ_{max}=368nm) and an increase in absorption in the UV-VIS spectrum. By measuring the ratio of values before and after illumination ($\lambda_{cis}/\lambda_{trans}$) an estimate of the purity of the 11-Z isomer can be made, as contaminating isomers (13-Z, 9-Z,

7-Z etc) have greater molar extinction coefficients than 11-Z retinal (26360 M^{-1} cm^{-1} for 11-Z, 35000-48000 M^{-1} cm^{-1} for other Z isomers and all-E retinal) and will reduce the ratio if present. A maximal $\lambda_{cis}/\lambda_{trans}$ ratio of 1.66 indicates pure 11-Z retinal, however, some slight contamination from other Z–isomers is inevitable from the HPLC procedure (<5%). $\lambda_{cis}/\lambda_{trans}$ ratios over 1.6, as recorded for each isolated 11-Z isomer, are considered acceptable for regeneration (Table 2.2)[156]. The opsin binding site exhibits a strong preference for the 11-Z-retinal in the binding pocket of rhodopsin [157] so when an excess of 11-Z retinal to opsin is used in the regeneration procedure the binding of any contaminating isomers is minimal.

Table 2.2 – UV-VIS characteristics of 11-Z retinals isolated for regeneration into opsin.

Retinal	11-Z isomer λ_{max} (nm)	$\lambda_{cis}/\lambda_{trans}$ ratio	Amount of 11-Z retinal available (nmol)
[8,18-^{13}C$_2$]	362	1.60	260
[8,16/17-^{13}C$_2$]	362	1.61	500
[10,20-^{13}C$_2$]	364	1.64	11260
[16,17-^{13}C$_2$]	364	1.63	3870
Unlabelled	363	1.61	24600

Following purification, the 11-Z retinal isomers were kept under argon at -80°C before regeneration into opsin.

2.3 Isolation of ROS from bovine eyes

2.3.1 Introduction – Properties of rhodopsin used in ROS isolation protocols

Rhodopsin is the predominant protein of the photoreceptor membrane, accounting for 80-

90% of the total membrane protein content so these membranes are an almost ideal preparation for most types of studies on rhodopsin [158-160]. As the photoreceptor membranes form almost all of the ROS (>70% dry weight), isolation of the photoreceptor membranes is most easily accomplished by isolating the rod outer segments. This is facilitated by two essential properties of the ROS: firstly, the rod outer segments are connected to the main body of the rod cell by a thin cilium [161] (see **Error! Reference source not found.**5), which can be easily broken with mild homogenisation of the retina, releasing the ROS from the rest of the cell; secondly, the high membrane content of ROS added to the high lipid content of the photoreceptor membrane means they have a relatively low density ($\sim$1.11-1.12 g/cm^3) which means that once separated from the rest of the cell they can easily be isolated by means of density centrifugation.

2.3.2 UV-VIS assay for rhodopsin

The isolation of ROS and regeneration procedures are generally monitored using UV-VIS spectrophotometry, making use of the characteristic absorption properties of the protein. Three absorption bands are observed for rhodopsin, one band in the ultra-violet region from the protein backbone at 280nm (γ-band) and two bands in the visible region derived from the bound 11-Z-retinal chromophore at 350nm (β-band) and 498nm (α-band) [162] (Figure 2.4). A crude indication of the purity of rhodopsin preparations can be made from the A_{280}/A_{500} and A_{400}/A_{500} ratios, however, these ratios should not be overemphasised since they are affected by scattering phenomena in micellar solution. Ratios of purified solubilized rhodopsin preparations are in the region of 1.65-1.80 for A_{280}/A_{500} and 0.16-0.19 for A_{400}/A_{500} while solubilized ROS preparations have A_{280}/A_{500} ratios in the region of 2.1-2.2 and A_{400}/A_{500} of 0.25 at best [162]. Upon absorption of light, 11-Z retinal is isomerised to all-

E retinal, which is eventually released from the protein. Subsequently, the two visible bands disappear (α and β) and a new absorption band appears at 380nm resulting from the free all-*E* retinal [31].
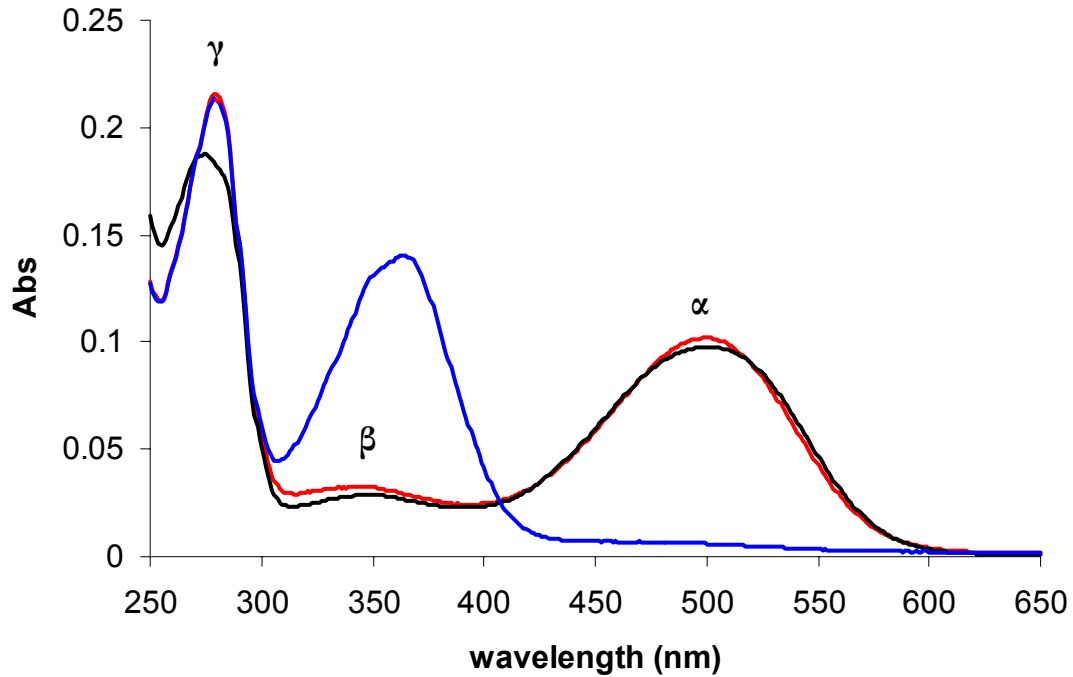
Figure 2.4 – UV-VIS spectra of solubilized rhodopsin samples. Isolated ROS membranes before illumination (red) and after illumination (blue) (5min; 300W tungsten lamp; Schott KG1 heat filter in the presence of 25mM hydroxylamine). Purified rhodopsin shown in black.

The concentration of rhodopsin is commonly determined by measuring the change in absorbance at 498nm upon illumination and applying the Beer-Lambert law ($\varepsilon = 40,500$ M^{-1} cm^{-1} for rhodopsin).

$$A = \varepsilon l C \qquad \text{Equation 2.1}$$

where: A   = absorbance

ε = molar extinction coefficient (M^{-1} cm^{-1})

l   = light path (cm)

C   = concentration (mol L^{-1})

The assay can be performed on suspensions of ROS membranes, but scattering artefacts interfere with the detection. Most accurate results are obtained after solubilization of the membrane in an appropriate detergent. 1.3% cetyltrimethylammonium bromide (CTAB) solution was initially used to solubilze ROS suspensions, however in later experiments 1% Ammonyx-LO was used, as it has the same high solubilizing power of CTAB but has very low absorbance at 280nm. As some of the photoproducts can also absorb at 498nm, hydroxylamine was added to the assay, converting free all-E retinal into all-E retinal-oxime (λ_{max}=365nm) which has virtually no absorbance beyond 450nm.

Typically, a ROS suspension was diluted to a final concentration of 10-20µM with buffer A (Table 2.3), 1% Ammonyx-LO and 25mM hydroxylamine hydrochloride, resulting in an A_{500} of 0.4-0.8 (1cm light path) and a UV-VIS spectrum was recorded between 250nm and 650nm. The cuvette was illuminated (5min; 300W tungsten lamp through a Schott KG1 heat filter that cuts off >500nm) and rescanned. The rhodopsin concentration was calculated from applying Equation 2.2.

$$[\text{rhodopsin}] = \text{dilution factor} \times [(A_{500 \text{ before bleaching}} - A_{500 \text{ after bleaching}})/\varepsilon] \qquad \text{Equation 2.2}$$

where: $\qquad \varepsilon = 40{,}500 \text{ M}^{-1}\text{cm}^{-1}$

When using UV-VIS to monitor rhodopsin photointermediates it was necessary to measure suspensions of ROS membranes without detergent, as the membrane is required to stabilize the intermediates states. To minimise the scattering effects resulting from ROS suspensions a modified spectrophotometer (Perkin Elmer 19, Nijmegen) was used with the photomultiplier close (~2mm) to the cuvette.

2.3.3 Improvements to the ROS isolation protocol

Optimising the ROS isolation protocol was necessary to produce reliable, high yields of ROS membranes with low contamination from other cell components ($A_{280}/A_{500} \sim 2.2$). The isolation of ROS from retina can be separated into four stages:

1. dissection of the retina from the eye

1. homogenization of the retinas to break the cilium and release the ROS

2. separation of the ROS fragments from larger cell fragments

3. purification of ROS from contaminating cell organelles and membrane material using density centrifugation.

The protocol previously used in the laboratory was changed at each of the four preparation stages, following the methods of Prof. W. de Grip (Nijmegen) [162]. Although the original method sometimes yielded ROS of acceptable purity ($A_{280}/A_{500} \sim 2.5$) the preparation was unreliable, sometimes giving low quality ($A_{280}/A_{500} > 3$) and low yields of ROS (<10nmol of rhodopsin per retina). Following the updated method, ROS could be prepared consistently with good purity ($A_{280}/A_{500} = 2.3 \pm 0.2$, $A_{400}/A_{500} = 0.25 \pm 0.02$) and good yields (up to 20nmol of rhodopsin per retina). The modifications to the protocol are discussed below, followed by a detailed description of the updated protocol.

2.3.3.1   Dissection of retina

In previous dissections the vitreous was removed after cutting away the lens and the cornea. The eyecup was inverted and the retina carefully scraped together and cut at the beginning of the optic nerve [163]. In the modified procedure part of the vitreous was left in the eyecup and the connection between the retina and the pigment epithelium loosened at the edges

with a spatula. The retina, still sticking to the vitreous could be carefully guided out in one piece and cut loose from the optic nerve [162]. This procedure gives less contamination from pigment epithelium material and a greater yield of rhodopsin from each eye.

2.3.3.2 Homogenization

Homogenization was previously performed by forceful shaking of the dissected retina in 33% w/w sucrose solution [164]. A more uniform method was later employed, using ten strokes of a loosely fitting Teflon on glass Potter-Elvehjem homogeniser (2-3mm clearance) [162].

2.3.3.3 Separation of crude ROS fraction from debris

Isolation of crude ROS fragments was previously performed by twice repeated centrifugation in 33% w/w sucrose solution to remove large and dense material [164]. This was replaced by a step in which the homogenized material was filtered through a Teflon gauze (100-125 mesh). As well as being quicker, this step does not involve packing and resuspending the crude ROS, which has been reported to hamper purification and fragment the ROS [165].

2.3.3.4 Purification

For the final purification step density centrifugation in various media is employed. In the original method this involved floatation of the ROS on a sucrose cushion of specific density (1.13g/cm^3) [164]. This method was unreliable and yielded ROS with more contamination than using a continuous sucrose gradient (23-36%) [162].

2.3.4 Isolation of ROS using continuous sucrose density gradients

Table 2.3 – Composition of isotonic Buffer A (pH 7.2 at 4°C) used for the isolation of ROS from bovine eyes. Buffer degassed and saturated with argon.

Solute	Concentration (mM)	Mass/unit volume (g/l)
MOPS	20	4.9
NaCl	130	7.6
KCl	10	0.746
$MgCl_2$ ($6H_2O$)	3	0.610
$CaCl_2$ ($2H_2O$)	2	0.299
EDTA-Na_2	0.1	0.037
DTE (add fresh)	1	0.154

Sucrose density gradients were made up from:

23% sucrose (w/w)

150g sucrose in 500ml Buffer A (diluted 1:2 in water), with 0.1mM NADPH added fresh

36% sucrose (w/w)

281g sucrose in 500ml Buffer A (diluted 1:2 in water), with 0.1mM NADPH added fresh

All procedures performed on rhodopsin were carried out under dim red light and at 4 °C.

Bovine eyes were collected from the abattoir and transported to the lab in a light-tight container to be processed within 4 hours of animal death. The retina were dissected from the eyes by making an incision in the sclera, cutting away the cornea and the lens and part of the vitreous removed. If the rhodopsin was to be used for regeneration the opsin was bleached (see Section 2.5.1.1) by illuminating the eyecups from above (30min; 300W tungsten lamp). Using a spatula the retina was loosened from the pigment epithelium and using tweezers, the retina was pinched. The eye was inverted and the retina "flowed" in one piece out of the eye so it hanged from the optic nerve once the vitreous had dropped off.

The retina were cut at the optic nerve and suspended in 25ml of ice-cold 23% (w/w) sucrose Buffer A under argon in a measuring cylinder. The retina were homogenised with ten strokes of a loosely fitting Teflon pestle (clearance 2-3mm) and filtered through a Teflon gauze (125 mesh) stirring with a plastic spoon to push the filtrate through. About 30-40ml of filtrate was collected from 50 eyes with a yield of 25-50nmol of rhodopsin per adult cattle retina. The A_{280}/A_{500} ratio of the filtrate lies between 10 and 15.

Continuous sucrose gradients were prepared from ice-cold sucrose (23% and 36% w/w, 16ml of each in Buffer A) in a two-leg, plexiglas gradient mixer at 4°C. The gradients could be stored overnight without appreciable loss in separation efficiency. Using a syringe fitted with a soft polypropylene tube the filtrate was carefully loaded onto the top of the gradient. Following centrifugation (80000g; 9°C; 1.5hrs; SW-28 rotor and swinging buckets) the components of the cell were separated according to density, as shown in Figure 2.5. The low density components, consisting mainly of small membrane fragments and vesicles are situated in the upper part of the gradient. The second, heavy band represents almost pure ROS which are morphologically reasonably intact [162]. A small band below the ROS contains material of uncertain origin, possibly Golgi or lysosomes. The sediment contains all the larger organelles, such as the mitochondria, endoplasmic reticulum and red blood cells.

The ROS bands were removed with a pipette and placed in a measuring cylinder, diluted 1:1 with isotonic MOPS Buffer A and centrifuged (3000g; 10mins; 4°C). The ROS were lysed by resuspending in doubly distilled water and centrifuged (100000g; 30mins; 4°C) to remove any soluble material.

filtrate

small vesicles

sucrose
gradient

ROS

golgi and lysosomes

sediment: ER,
mitochondria, red blood
cells etc
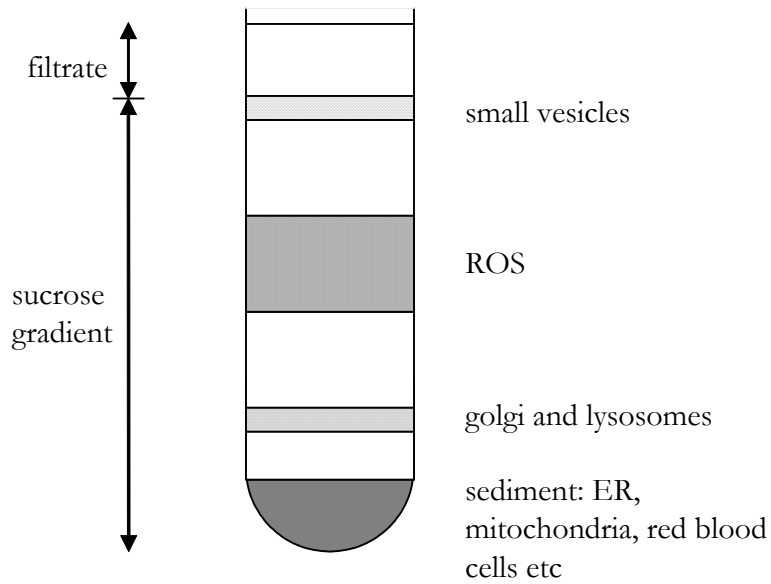
Figure 2.5 – Band distribution following centrifugation of retinal filtrate on a continuous sucrose (23-36% w/w) gradient (80000g; 9°C; 1.5hrs; SW-28 rotor and swinging

2.4 UV-VIS and gel analysis

To illustrate the purification procedure a SDS-PAGE gel is shown for a sample of retina homogenate and purified ROS in Figure 2.6. Isolated ROS can be clearly observed at 36kDa (a), purified from the mixture of proteins observed in the retina homogenate (b). In addition to the main rhodopsin band (36kDa), other proteins can be observed from the photoreceptor membrane, however rhodopsin is the predominant protein of the ROS (70%).
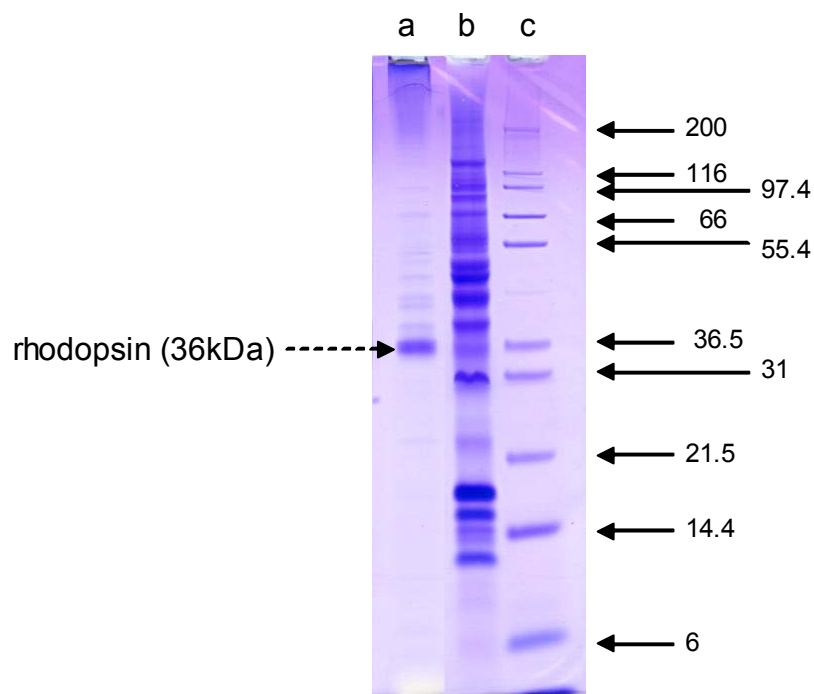
Figure 2.6 – SDS PAGE gel of purified ROS (a), retina homogenate (b) and the calibration gel showing molecular weights x 10^3 (c).

2.5   Regeneration of opsin in ROS with 11-*Z*-retinal

2.5.1 Introduction – Improvements to the regeneration protocol

The aim of regeneration is to replace the native retinylidene chromophore with the ^{13}C labelled retinal for study by NMR. The procedure can be divided into three steps:

1. removal of the unlabelled retinal through bleaching with light

2. regeneration of opsin with the ^{13}C labelled retinylidene chromophore

3. removal of the excess ^{13}C labelled retinal as retinal-oxime.

An optimised regeneration procedure results in >90% replacement of unlabelled retinal with the labelled chromophore and >90% removal of excess labelled retinal.

The regeneration procedure in this study was optimised from the previous protocol used in

this laboratory [122]. The objectives for each step in the regeneration pathway are discussed, along with the necessary improvements that were made to the procedure.

2.5.1.1 Bleaching

The aim of bleaching rhodopsin is to remove the native 11-Z retinal from the binding site of rhodopsin through illumination, then wash the retinal from the system so it is unable to regenerate back with the opsin. In previous procedures bleaching of the protein was performed following isolation of the ROS [122]. Hydroxylamine was added to a high concentration (200mM) and the ROS were illuminated with bright white light (15min; 500W; 0°C). The native retinal was removed as all-E retinal-oxime by repeated washing with buffer. Following the methods of de Grip *et al*, the rhodopsin is bleached whilst in the posterior part of the eye, the so called eye cup [162]. The bleached retina are dissected and the all-E retinal is removed as the ROS are collected on the sucrose gradient, in the presence of NADPH. NADPH is the cofactor for the enzyme retinal dehydrogenase which catalyses the conversion of retinal to retinol, which migrates more easily from the membrane than retinal [156]. This procedure results in more efficient removal of native retinal and minimises the risk of hydroxylamine remaining in the sample, which can bind to the ^{13}C labelled 11-Z retinal being added to the opsin in the "regeneration" step.

2.5.1.2 Regeneration

Successful regeneration of opsin with 11-Z retinal gives almost complete replacement of the native retinal with labelled chromophore as a result of the high binding affinity of the opsin binding pocket for the 11-Z chromophore [157]. The process is spontaneous and the resulting level of regeneration relies on the purity of opsin and the 11-Z retinal. Contamination of either of these components will lead to incomplete regeneration.

The regeneration procedure was unchanged: incubating opsin with 11-*Z* retinal initially at room temperature (1.5hr) then at 4°C (overnight). The solvent for handling the 11-*Z* retinal was altered, from ethanol (which can oxidise the 11-*Z* retinal) to dimethylformamide (DMF) which is very soluble in water and harmless towards the protein.

2.5.1.3 Removal of excess ^{13}C labelled 11-*Z* retinal

To ensure complete regeneration of opsin a 2x excess of retinal was generally used. The additional 11-Z-retinal that does not bind to opsin can bind to lysine residues and phospholipids outside the binding pocket [156]. Since this retinal can be ^{13}C labelled, it will also give rise to a signal in the NMR experiment, so must be effectively removed from the system. Addition of hydroxylamine following regeneration converts all unbound 11-*Z* retinal to aqueous retinal-oxime, enabling easier removal from the preparation. In previous regeneration protocols excess retinal was removed by washing with 4% bovine serum albumin (BSA). Washing of the BSA-retinal oxime complex can result in up to 80% removal of retinal, although this was rarely achieved in practice [166]. Following a novel procedure, exclusion of excess retinal in the new protocol was done with a solution of heptakis-2,6-di-O-methyl-β-cyclodextrin [166]. This glycoside has a circular structure that forms a cavity, producing a soluble inclusion complex upon binding to retinal and retinal-oximes [167]. Repeated washing with high concentrations (50mM) of cyclodextrin solution can result in over 95% removal of excess retinal [166]. The procedure also reduces the lipid content of the phospholipids bilayers, restricting the meta-I to meta-II transition, but having no effect on the formation of earlier photointermediates [156].

To illustrate the improvements to the regeneration protocol using 50mM β-cyclodextrin compared to 4% BSA a parallel extraction was performed on the same regenerated

rhodopsin sample and the removal of excess 11-Z-retinal monitored using UV-VIS spectroscopy.

50mM opsin was regenerated with 2x excess of unlabelled 11-*Z* retinal following the procedure described in Section 2.5.2. Hydroxylamine (0.1M in Buffer B) was added to a final concentration of 10mM, incubated (25°C; 20min) and the sample split into two aliquots. The excess 11-*Z* retinal in one sample was removed by washing with 4% BSA solution and in the other using 50mM cyclodextrin, following the procedure described (Section 2.5.2). The UV-VIS spectra of the solubilized ROS samples prior to washing (blue), after washing with 4% BSA (red) and after washing with 50mM β-cyclodextrin (black) are shown in Figure 2.7. The excess retinal-oxime is much more effectively removed following washing with β-cyclodextrin as observed by a lower absorbance at 365nm. The BSA is also less efficiently washed out of the membrane than β-cyclodextrin, shown in the elevated 280nm absorbance.
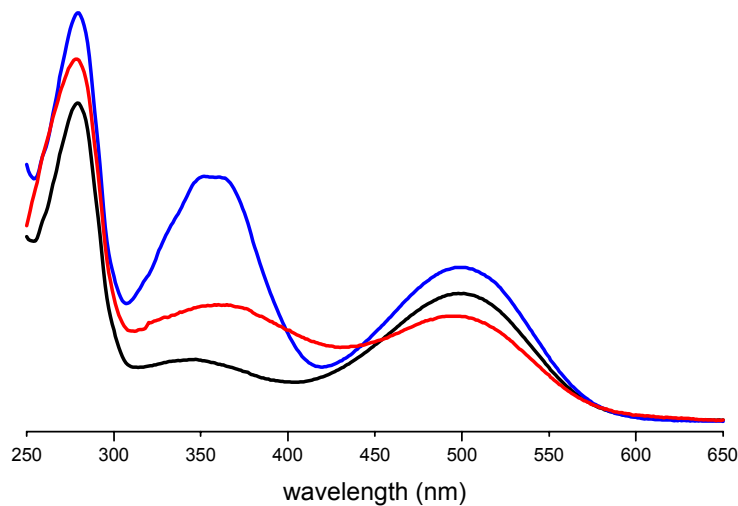
Figure 2.7 – UV-VIS spectra of opsin regenerated with 2x excess 11-*Z* retinal prior to washing (blue), after washing with 4% BSA solution (red) and 50mM β-cyclodextrin (black).

2.5.2 Regeneration of opsin in ROS with 11-Z retinal using β-cyclodextrin

Opsin in ROS disc membranes from the ROS preparation step (Section 2.3.4) were resuspended in Buffer B (Table 2.4) to a concentration of 25-50μm (~1-2mg/ml) in JA-20 centrifuge tubes. A 2x excess of 11-Z retinal was removed from the stock solution in hexane and the hexane evaporated off in a stream of nitrogen. The retinal was resusupended in dimethylformamide (maximal concentration 2%), added to the opsin suspension and incubated at room temperature for 1.5hrs with mixing. The sample was incubated overnight (4°C with stirring) and a UV-VIS spectrum taken to show regeneration was successful (Section 2.3.2). Using this procedure 90-95% of the opsin could be regenerated. The amounts of $[8,18\text{-}^{13}C_2]$ and $[8,16/17\text{-}^{13}C_2]$ 11-Z retinal obtained from the purification steps were very small (260nmol and 500nmol, respectively), so to obtain maximum ^{13}C retinal labelled rhodopsin for NMR analysis these retinals were regenerated in a 1:1 ratio with opsin.

Table 2.4 – Composition of Buffer B (pH6.5 at 4°C) used for the regeneration of opsin with 11-Z retinal. Buffer degassed and saturated with argon.

Solute	Concentration (mM)	Mass/unit volume (g/l)
PIPES	20	6.048
NaCl	130	7.600
KCl	5	0.380
CaCl$_2$ (2H$_2$0)	2	0.294
MgCl$_2$ (6H$_2$0)	3	0.610
EDTA	0.1	0.040

Hydroxylamine (0.2M hydroxylamine hydrochloride in Buffer B, pH 6.5) was added to the suspension to a final concentration of 10mM and incubated (20min; 25°C), converting excess 11-Z retinal to retinal-oxime. The suspension was centrifuged (90000g; 20min; 4°C) and resuspended in

50mM heptakis-2,6-di-O-methyl-β-cyclodextrin in Buffer B [168]. The mixtures were vortexed (10min) and centrifuged at lower speed (50000g; 20min; 4°C). The supernatant was removed and checked by UV-VIS spectrophotometry for the presence of solubilized retinal-oxime at 365nm. This procedure was repeated twice, until the supernatant no longer showed absorbance at 365nm. The regenerated rhodopsin samples were washed with double distilled water (90000g; 20min; 4°C) and resuspended in Buffer B. Aliquots of approximately 10mg (280nmol) were separated and centrifuged in a swing-out rotor (SW-40; 150000g; 20min; 4°C), creating a fast pellet that was frozen rapidly in liquid nitrogen. Regenerated rhodopsin samples were kept at -80°C in the dark before packing into NMR rotors.

Figure 2.8 shows UV-VIS spectra from various points throughout the regeneration process of [16,17-^{13}C$_2$]retinylidene rhodopsin, which showed similar UV-VIS characteristics to all regenerated rhodopsin samples. The complete removal of 11-Z retinal during isolation of the ROS samples could be observed by an absence of absorbance at 498nm (green). Incubation with excess 11-Z retinal resulted in regeneration of chromophore binding, yielding rhodopsin (λ_{max}=498nm) with excess 11-Z retinal (red) that was associated with the membrane. Excess retinal which was removed as retinal-oxime, in a soluble inclusion complex with β-cyclodextrin, could be observed in the supernatants following centrifugation (black)(λ_{max}~365nm). Treatment with β-cyclodextrin removed the majority of the excess retinal-oxime, yielding a regenerated rhodopsin sample in ROS (blue).

The amount of regenerated rhodopsin could be deduced from subtracting the UV-VIS spectrum of fully bleached rhodopsin (yellow) from the dark state rhodopsin spectrum (Figure 2.9)(see Section 2.3.2).
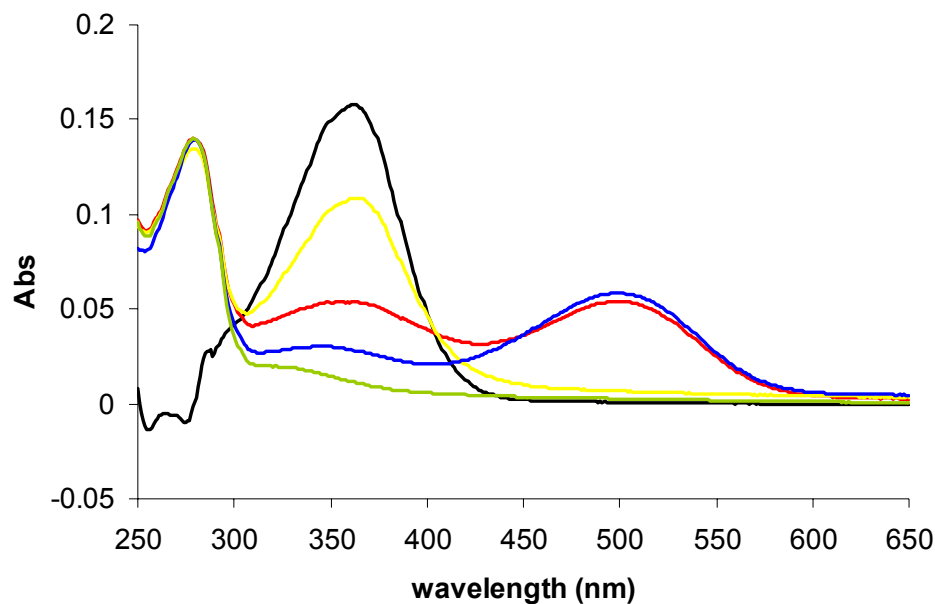
Figure 2.8 – UV-VIS spectra of solubilized showing various stages from the regeneration procedure. Opsin (green) was regenerated with 11-*Z* retinal, to give regenerated rhodopsin (λ_{max}=498nm) with an excess of retinal (red). Excess retinal was removed as retinal-oxime (black) yielding a regenerated rhodopsin sample (blue). Bleaching of the sample by illumination (5mins; 100W tungsten lamp through a Schott KG1 heat filter) removes the all-*E* retinal from the binding pocket (yellow).
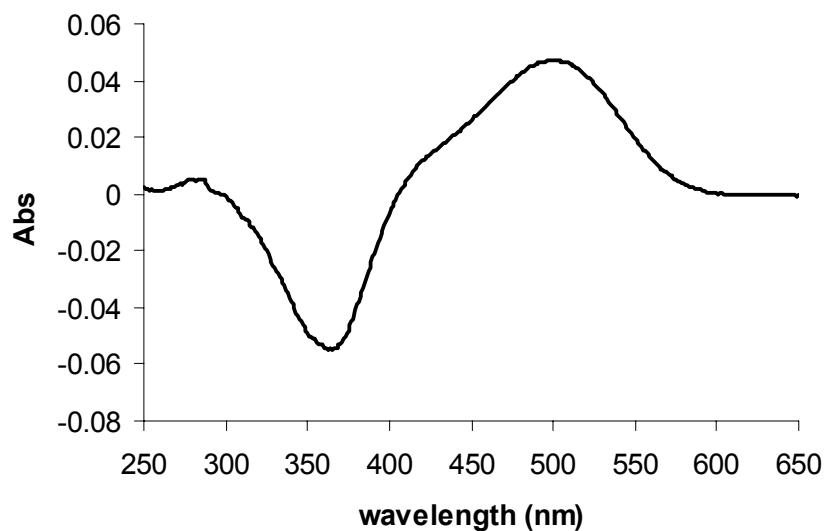
Figure 2.9 – Difference UV-VIS spectrum of the solubilized rhodopsin pigment (1% Ammonyx-LO with 25mM hydroxylamine) formed from regenerating opsin in ROS with [16,17-^{13}C$_2$] 11-*Z* retinal. Illumination by a 100W tungsten lamp through a Schott KG1 heat filter for 5mins. The λ_{max}=498nm, indicating the presence of rhodopsin.

2.6 UV-VIS analysis of regenerated rhodopsin samples

Following the described procedures, rhodopsin in ROS membranes were regenerated with each of the ^{13}C labelled retinals shown in Table 2.5. The ^{13}C labelled samples for use in the rotational resonance NMR experiments ($[8,18-^{13}C_2]$retinylidene rhodopsin and $[8,16/17-^{13}C_2]$ retinylidene rhodopsin) were prepared concurrently, in parallel with an unlabelled rhodopsin sample, using the same batch of ROS. By preparing the samples in this manner, the lipid and protein composition of the membranes were equivalent, illustrated by the similar Abs_{280}/Abs_{500} ratios between the labelled and the control sample (control[1]; Table 2.5). This was essential in providing a clean difference NMR spectrum, with ^{13}C resonance derived only from the labelled nuclei (see Figure 3.8 and Figure 3.9). The same preparation method was used for the $[16,17-^{13}C_2]$retinylidene rhodopsin and $[10,20-^{13}C_2]$retinylidene rhodopsin samples, prepared in parallel with an unlabelled control for subtraction (control[2]).

Table 2.5 – UV-VIS spectrophotometry characterisation of unlabelled and ^{13}C labelled retinylidene rhodopsin samples in ROS membranes.

Sample	λ_{max} (nm)	Abs_{280}/Abs_{500} ratio	Abs_{365}/Abs_{500} ratio	Abs_{400}/Abs_{500} ratio	Rhodopsin mass(mg)	Rhodopsin (nmol)
ROS	498	2.3±0.2	0.21±0.02	0.25±0.02	-	-
1. $[8,18-^{13}C_2]$	496	2.36	0.43	0.32	7.2	200
2. $[8,16/17-^{13}C_2]$	496	2.34	0.40	0.32	12.0	333
3. control[1]	498	2.34	0.31	0.26	19.4	539
4. $[16,17-^{13}C_2]$	498	2.38	0.44	0.30	15.1	419
5. $[10,20-^{13}C_2]$	498	2.40	0.46	0.30	111.0	3080
6. control[2]	498	2.44	0.36	0.28	12.9	358

Removal of all of the excess 11-Z retinal with β-cyclodextrin is impossible and hence some contamination with unbound retinal-oxime is inevitable. An estimate of the removal of

excess retinal can be made from the Abs_{365}/Abs_{500} and Abs_{400}/Abs_{500} ratios. A good quality ROS sample will typically have UV-VIS characteristics of Abs_{365}/Abs_{500}= 0.21±0.02 and Abs_{400}/Abs_{500}= 0.25±0.02, lower than the ratios observed for the regenerated samples [162] (Abs_{365}/Abs_{500}= 0.34±0.02 and Abs_{400}/Abs_{500}= 0.28±0.02). This represents less than 5% contamination with unbound retinal-oxime [156, 166]. The Abs_{365}/Abs_{500} and Abs_{400}/Abs_{500} ratios of the ^{13}C labelled samples were slightly higher than normal levels and greater than those observed for the unlabelled regenerated control samples, possibly indicating some additional retinal-oxime in the system. This was surprising considering both sets of labelled and unlabelled samples were prepared in parallel. It is difficult to assess the contribution of retinal-oxime to the overall UV-VIS spectra as the contribution of non-specifically bound retinal-oxime associated with the membrane is unknown and rhodopsin has absorbance at 365nm and 400nm itself. Interpreting the small differences in Abs_{365}/Abs_{500} and Abs_{400}/Abs_{500} ratios in terms of the levels of non-bound retinal-oxime is therefore difficult.

The UV-VIS data showed that all the regenerated rhodopsin samples consisted predominately of rhodopsin in ROS membranes, with the required 11-*Z* retinylidene chromophore fully regenerated and were suitable for study by solid-state NMR.

2.7   Preparation of rhodopsin samples for NMR analysis

For NMR analysis the ^{13}C labelled and unlabelled rhodopsin samples were packed into Chemagnetics zirconium 4mm MAS rotors.

Following regeneration the frozen rhodopsin samples were removed from SW-40 centrifuge tubes and placed in the mouth of the packing apparatus (Figure 2.8) without any loss of sample. The apparatus was centrifuged (10000g; SW-28; 4°C), spinning the sample into the rotor. The rotor was closed with a PTFE insert and spun slowly in a Chemagnetics Apex

MAS probe to distribute the sample evenly within the rotor ($\omega_r=3$kHz). The samples were

frozen rapidly in liquid nitrogen and stored in a light-tight container at -80°C.
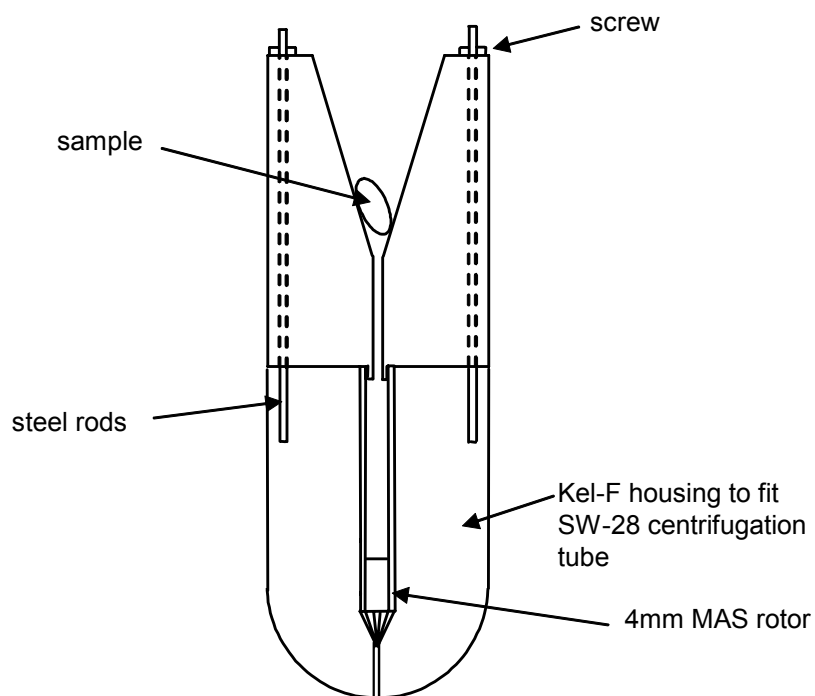
Figure 2.8 – Packing apparatus used to fill Chemagnetics 4mm MAS rotors with rhodopsin samples. Not drawn to scale.

Chapter 3   Determining the β-ionone ring conformation of retinal in rhodopsin using RR NMR

3.1 Introduction

When 11-*Z* retinal binds to opsin under formation of rhodopsin a large red-shift occurs in its absorption spectrum (378 to 498nm), the so called "opsin shift" [169]. The ~60nm shift observed on formation of a protonated Schiff base (380→ 440nm) [105] is not sufficient to explain the further red-shifted absorption maxima of rhodopsin (500nm), green (~530nm) and red (~560nm) visual pigments. The red-shift is thought be a result of delocalizisation of the conjugated π-electron system in the retinal polyene chain. Several mechanisms by which chromophore-protein interactions might cause this opsin shift might include (1) charge separation between the protonated Schiff base and its protein counterion [170] (2) electrostatic interactions between the chromophore and charged amino acid groups [171] (3) planarization of the chromophore caused by the protein environment [172].

To relieve the steric interaction between the 18-methyl/8-H and 20-methyl/10-H the retinal

chromophore is twisted around the C6-C7 single bond and over the C10-C13 region so the retinal can be described roughly in three planes A, B and C [121] (Figure 3.3.1). Conformational distortion of the retinal chromophore around these bonds could influence the opsin shift. For example, the C6-C7 bond is in the *s-cis* conformation and twisted 40-70° out of the plane of the polyene chain in most retinal model compounds [173-175]. However, UV-VIS studies on *6-s-cis* and *6-s-trans* [176] and electronic calculations [171] indicated that a 25-35nm red-shift occurs when the *twisted 6-s-cis* isomer converts to the *planar 6-s-trans*
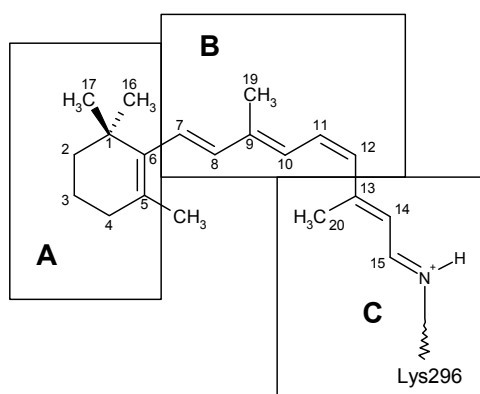
conformation. A ~30nm red shift due to the protein induced *6-s-cis* → *6-s-trans* isomerization would represent a significant fraction of the total opsin shift observed in rhodopsin.

Determining the conformation around the C6-C7 bond has therefore been the focus of numerous studies in both bacteriorhodopsin and rhodopsin. Solid-state ^{13}C NMR measurements detected a perturbed *6-s-trans* chromophore in bacteriorhodopsin, based on the isotropic chemical shifts of C5 and C8 positions that are sensitive to the conformation around the C6-C7 bond [177]. Corresponding chemical shift NMR measurements on ^{13}C

Figure 3.3.1 – 11-Z retinal chromophore of rhodopsin showing the three planes that arise due to the steric interaction between C18 methyl and 8-H (A/B plane) and the C20 methyl and 10-H (B/C plane).

labelled retinal in lyophilized [120] and solubilized rhodopsin [32, 105] indicated the bound chromophore in rhodopsin adopted a 6-*s-cis* conformation, by observing chemical shifts close to those for the unbound protonated Schiff base of 11-Z retinal with a 6-*s-cis* conformation. Two retinal analogue binding studies showed rhodopsin formed with a 6-*s-cis*-locked retinal analogue (11-Z-8,18-ethanoretinal) had almost identical UV-VIS and CD characteristics to wild-type rhodopsin, providing further evidence to support the 6-*s-cis* conformation [102, 103].

A contrasting conformation was proposed by Grobner *et al* [80]. They applied solid state NMR to determine the orientation of the deuterium quadrupole coupling tensor of rhodopsin samples regenerated with retinals carrying trideuterated methyl groups (CD_3) at positions C18, C19 and C20 oriented on glass plates within the NMR rotor. The orientation of the methyl groups best fit with a twisted 6-*s-trans* conformation. They argued that the former determination of the 6-*s-cis* conformation by ^{13}C NMR had to rely on indirect evidence in which the NMR data from labelled retinal in rhodopsin were compared with model compounds in organic solvents, and the chemical shifts "were found at the upper end of the region for 6-*s-cis* model compounds, close to the range for the 6-*s-trans* derivatives". A 6-*s-trans* locked retinal has been shown to form a rhodopsin pigment, showing this conformation of the retinal can be accommodated within the binding pocket and a modelling study predicted that the 6-*s-trans* conformer represented the lowest energy state of the bound chromophore [178].

Based on the approximate position of the methyl electron densities, the recent crystal structure predicts a 6-*s-cis* conformation for the bound retinal, however the resolution achieved does not allow an unambiguous assignment [34]. In view of the controversial nature of the orientation of the β-ionone region, defining the spatial arrangement of the β-

ionone ring and C6-C7 region of the chromophore in rhodopsin was important. The torsion angle around the C6-C7 bond had not been determined directly, so the influence of opsin on the geometry of the retinylidene around the β-ionone ring and its consequence on the "opsin shift" remained uncertain.

Through the binding of modified retinal analogues it was shown that the length of the polyene chain of an 11-*Z* analogue was a decisive factor in coupling with opsin, as retinals with extended or contracted polyene chains do not bind to opsin, indicating there is an interaction between the protein and a moiety on the β-ionone ring. A modelling study based on the binding of the different geometric isomers of retinal has also suggested the β-ionone ring provided a "point of anchor" within the binding pocket [179].

The interaction between the β-ionone ring and the protein was also suggested to be the *primary* interaction between the chromophore and the binding pocket. Matsumoto and Yoshizawa found that β-ionone fully competitively inhibits the binding of 11-*Z*-retinal, so that β-ionone occupies the retinal-binding site so exclusively that the β-ionone-opsin complex is completely inactive in the regeneration of 11-*Z* retinal [123]. Taking into account that only retinals with the "correct" length of polyene chain will bind to opsin, they concluded that only when the aldehyde group of an analogue, already bound to opsin through the β-ionone ring, comes sterically near to the ε-amino group of Lys-296 in the opsin binding site can the Schiff base be formed. Investigating the interaction between the β-ionone ring and the opsin binding pocket was therefore of interest.

3.2   Aims

The rotational resonance (RR) NMR method had been previously used to measure the internuclear distance between C8 and the methyl groups C16, C17 and C18 in the membrane

bound protein pump bacteriorhodopsin (bR) regenerated with $[8,16/17-^{13}C_2]$ all-*E*-retinal and $[8,18-^{13}C_2]$ all-*E* retinal [148, 180]. By comparison with 6-*s-trans* retinal and 6-*s-trans* retinoic acid model compounds it was deduced that the retinal adopted a planar 6-*s-trans* conformation within the binding pocket of bR, confirming conclusions made from chemical shift observations.

The initial aim of this study was to conduct rotational resonance NMR experiments on $[8,16/17-^{13}C_2]$11-*Z*-retinal and $[8,18-^{13}C_2]$11-*Z*-retinal regenerated into rhodopsin in ROS membranes. Measuring the intermolecular distances between C8 on the polyene chain and the C16, C17 and C18 methyl groups on the ring would determine not only the absolute configuration around the C6-C7 bond but also the torsion angle between the β-ionone ring and the polyene chain.
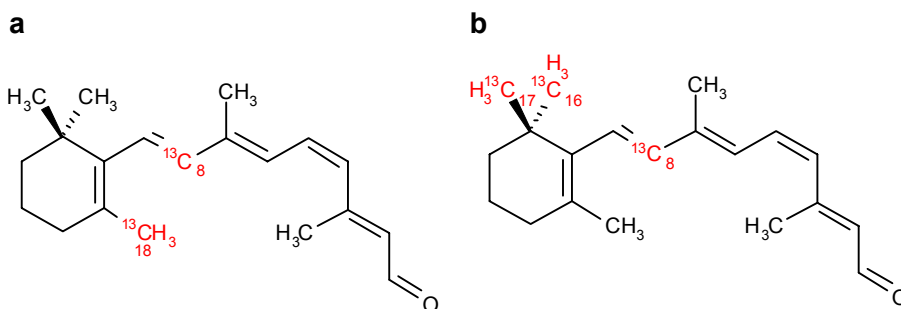
Figure 3.2 – Schematic respresentation of $[8,18-^{13}C_2]$ 11-*Z* retinal and $[8,16/17-^{13}C_2]$ 11-*Z* retinal regenerated into rhodopsin in ROS membranes to determine the geometry of the β-ionone ring in the bound retinylidene chromophore.

Although not the immediate aim of the study it was possible that chromophore-protein interactions could be detected through ^{13}C chemical shift measurements. No ^{13}C chemical shift information was available for the ring methyls of the β-ionone ring of the bound retinylidene chromophore prior to this study. Variations in chemical shift measurements from those derived from protonated Schiff base (PSB) retinal compounds have been used to investigate protein-chromophore interactions in bR [181, 182] and in rhodopsin, where they

were used to identify perturbations in the retinal structure resulting from the Glu-113 counterion [106, 117]. By observing changes in ^{13}C isotropic chemical shifts from the chromophore in its unbound state protein-chromophore interactions could possibly be detected.

3.3 Materials and Methods

3.3.1 Rotational Resonance (RR) ^{13}C NMR

In solution NMR, NOE data are used to determine ^{1}H-^{1}H distance constraints. However, in solids, ^{1}H studies in membranes are hampered by the strongly coupled proton spins meaning alternative approaches have had to be developed that measure ^{13}C-^{15}N and ^{13}C-^{13}C distances through the measurement of dipolar couplings (b_{IS}). The dipolar coupling between nuclei in specific sites in solids is an important structural parameter due to its r^{-3} dependence. The dipolar coupling can be related to the distance between the two spins using the following expression:

$$ b_{IS} = \left(\frac{\mu_o}{4\pi} \right) \frac{\gamma_I \gamma_S \eta}{r_{IS}^3} \qquad \text{Equation 3.1} $$

where: b_{IS} =   dipolar coupling between nuclear spins I and S

μ_o =   permeability of free space

γ_I =   gyromagnetic ratio of spin I

γ_S =   gyromagnetic ratio of spin S

η =   Planck's constant divided by 2π

r_{IS} =   distance between nuclear spins I and S

Which, for a ^{13}C homonuclear spin pair can be simplified to:

$$r_{IS} = \sqrt[3]{\frac{7.59382 \times 10^3}{b_{IS}}}$$
Equation 3.2

where: b_{IS} is specified in Hz and r_{IS} is in Å.

Magic angle spinning, which is necessary to obtain well resolved spectra, averages the anisotropic dipolar coupling to zero so to obtain distance information it must be reintroduced. In the early 1960s Andrew and co-workers studied ^{31}P T_1 rates in solid phosphorous pentachloride using MAS NMR. They observed two resonances in the phosphorous spectrum that corresponded to distinct PCl_4^+ and PCl_6^- resonances in the crystal lattice, with different T_1 relaxation rates. They noted that the relaxation rates became equal if the sample spinning speed was set equal to the frequency difference between the two resonances i.e. the chemical shift difference [183]. This T_1 effect, as well as significant line broadening was also observed when the MAS rate was set at 1/2 or 1/3 the chemical shift difference between the ^{31}P nuclei, enabling fast cross-relaxation between the two crystal lattice sites [184]. The matching of an integral multiple of the MAS frequency (ω_r) with the chemical shift difference between the two spins ($\Delta\omega = n\omega_r$) is now referred to as rotational resonance. Raleigh found similar effects in dilute homonuclear dipolar coupled spin pairs, this time observing a splitting of isotropic resonances and exchange of Zeeman magnetization between the recoupled spins [185].

The RR experiment targets homonuclear spin pairs in which the two dipolar coupled spins have different isotropic chemical shifts. The sample is set spinning under the rotational resonance condition, reintroducing the dipolar coupling. This leads to two important effects: broadening and splitting of usually well resolved MAS resonance lines (illustrated for [1,2-$^{13}C_2$] glycine in Figure 3.4) and an enhancement of Zeeman magnetization exchange between

the dipolar coupled spins [185].

The reintroduced dipolar coupling can be used for distance determination, either by analysing the splitting from the lineshape [78, 186] for strongly coupled spin pairs, or more commonly, by measuring the rate of Zeeman magnetization exchange between the two sites. RR NMR has been applied to a broad range to biological systems, including the membrane bound peptide phospholamban [187, 188], prion fragments [189], the gastric proton pump [190], the β-amyloid protein of Alzheimer's disease [191] and bacteriorhodopsin [148, 180, 192]. These studies have often made use of site-specific ^{13}C labelling with a wide chemical shift range, that lead to a well dispersed NMR spectrum. Peersen *et al* established the upper limit for ^{13}C-^{13}C rotational resonance by studying the structure of an 11 amino-acid residue crystalline peptide that models the N-terminus of alamethicin, approximately 6.5Å , where the rate of exchange approaches that of the off-resonance condition [193, 194]. The accuracy can be as high as 0.1Å, enabling the investigation of protein bound ligands at a much higher resolution than can be achieved from crystallographic studies [185, 190].
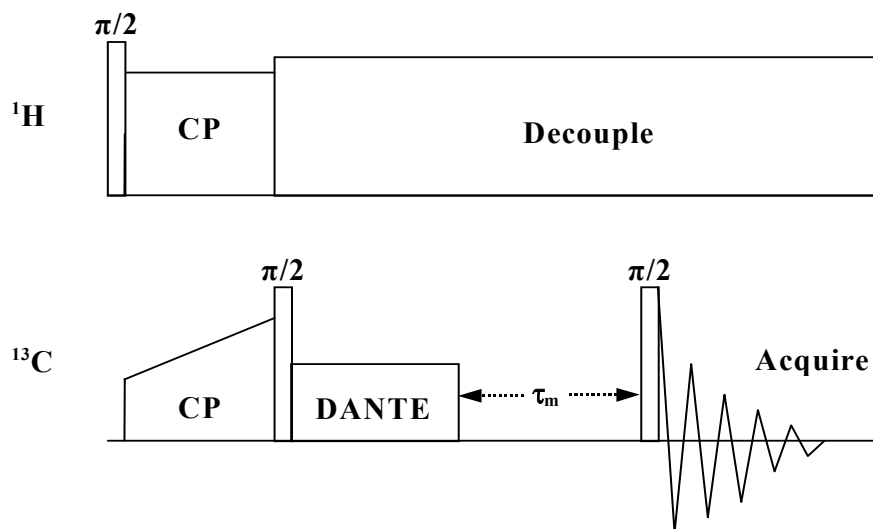
Figure 3.3 – The ^{13}C NMR rotational resonance pulse sequence.

The RR pulse sequence (Figure 3.3) begins with cross polarization from protons to generate ^{13}C magnetization in the transverse frame. A ramped CP is often used to optimise cross-polarization at high spinning speeds. This magnetization is then returned to the longitudinal axis by a non-selective $\pi/2$ pulse and one of the two ^{13}C resonances is selectively inverted using a standard DANTE pulse train. Magnetization is then allowed to exchange between the two sites for a variable mixing time (τ_m) under strong proton decoupling, and the distribution of ^{13}C signal detected with a $\pi/2$ pulse that flips the magnetization back into the transverse plane. The experiment is repeated for a set of mixing times, usually in the range of 0 to 40ms.

3.3.2 Determination of homonuclear interatomic distances – Generation and analysis of exchange curves

The intensity changes observed in the RR experiment are translated into an intermolecular distance by first generating a magnetization exchange curve. It is convenient to track the magnetization transfer by measuring the difference in Zeeman order (I_z-S_z) between non-

inverted and inverted spins, by the integral of the resonances over the varying mixing time. The interpretation and comparison of RR exchange curves require the curves to be normalised to an initial value of 1.0 before any exchange of magnetization has occurred, so it is essential to obtain an accurate intensity for each ^{13}C label at the start of the mixing period. An initial intensity is determined by averaging the signals obtained over several short mixing times (<0.1ms) before significant exchange has occurred. This reduces the effects of pulse length errors and probe ring-down artefacts associated with short mixing times.

The changes in resonance intensities as a function of the mixing time must be expressed as fractional changes of the full ^{13}C resonance intensity of the labelled nuclei only. The most straightforward approach to account for the natural-abundance background is to run the RR experiment on ^{13}C labelled and unlabelled samples and to generate a difference spectrum that contains only the signals from the ^{13}C labels.

Interpretation of the magnetization curves to obtain the dipolar coupling is made through their accurate simulation using the algorithms of Levitt [135], derived from original theory describing magnetization exchange in rotary resonance, which have been modified by Glaubitz [195].

The simulation reveals that the rate of magnetization exchange depends on several parameters in addition to the dipolar coupling (b_{IS}), these are:

- the principal values and orientations of the chemical shift tensors for the I and S spins

- the J coupling between sites

- the zero-quantum relaxation time constant (T_2^{ZQ}) which describes the coupling of

both spins with the environment.

The size of the chemical shift tensors can easily be determined from the analysis of low speed MAS spectra, using the Herzfeld-Berger method [196]. At higher orders of rotational resonance (n>1) the relative orientation of the chemical shift tensors influence magnetization exchange, however, in this study all experiments are conducted at n=1 rotational resonance, where the simulation of magnetization exchange is insensitive to the absolute and relative orientation of the chemical shift tensors [135]. The J coupling, which has only a small influence on magnetization exchange, can be estimated from solution NMR data.

The zero-quantum relaxation accounts for several processes and interactions with natural abundance spins that can disrupt and compete with the RR-driven magnetization exchange. Zero-quantum relaxation is suppressed (i.e. T_2^{ZQ} is maximised) by the use of strong decoupling fields but is a significant factor in its uncertainty, especially in situations where the dipolar couplings are weak.

Estimates for T_2^{ZQ} have previously been derived from the linewidths of the resonances [148] however, contributions to the linewidths from factors such as incompletely averaged proton coupling and magnetic field inhomogeniety generally give an underestimate of T_2^{ZQ} [180]. In this study, the single-quantum T_2 relaxation constants were measured with a Hahn spin-echo experiment to obtain an estimate of T_2^{ZQ}, taken from the combined relaxation rates for the spin pairs. An initial value for the dipolar coupling (b_{IS}) was subsequently deduced and used to obtain an improved estimate of T_2^{ZQ} through fitting T_2^{ZQ} between an upper limit described by the T_2 relaxation rate and a lower limit deduced from the linewdith. This apparent T_2^{ZQ} value accounts for off-resonance effects due to inhomogenous linebroadening

and inaccuracies in the initial T_2^{ZQ} estimate. A final value for b_{IS} was subsequently derived using the improved T_2^{ZQ} value and used to determine the internuclear distance using the relationship previously described (Equation 3.1).

3.3.3 Chemical shifts

In a uniform applied magnetic field the movement of electrons around a nucleus results in the generation of a secondary magnetic field. This secondary field is opposed to the applied field and causes a nucleus to experience a reduced net magnetic field, the exact value of which is dependent upon the degree of shielding provided by the associated electrons. The chemical shift of a nucleus is therefore a sensitive indicator of its local electronic environment and, as such, is also a potential source of structural information.

Chemical shifts are dominated by the type of atom under investigation (which defines the ground-state electron arrangement) and the nature of chemical bonding to neighbouring atoms (which determines both hybridisation of electron orbitals and the degree of electron withdrawal, donation or delocalization). For structural studies on biological samples it is the more subtle effects which are of greatest interest, such as perturbation arising from molecular conformation of intermolecular interactions.

In practise, the presence of multiple effects can make deconvolution of specific interactions difficult (including steric interactions, ring currents, electrostatics and hydrogen bonding). Solid-state NMR has an advantage over solution studies in relation to the investigation of chemical shifts due to the absence of CSA averaging. As a result, both the isotropic chemical shift and the anisotropy can be characterised, enabling a more detailed analysis of the electronic shielding distribution within a system. The principal values of the chemical shift tensor of the ^{13}C-5 resonance in retinylidene compared to that in retinal model compounds

has been used as further evidence for a *6-s-cis* conformation in rhodopsin [105].

3.3.4 NMR details

All NMR measurements were conducted at 125.8MHz for ^{13}C and 500.1MHz for protons using a Chemagnetics (Varian) Infinity spectrometer. A 4mm double resonance Chemagnetics Apex MAS probe was used at -60°C. The temperature was controlled ±1° using a Chemagnetics temperature controller. Spinning was maintained at ±3Hz through the experiments using a Chemagnetics spinning speed controller.

CP-MAS spectra of rhodopsin samples were acquired with a 30% linear ramp [197] on the output for the carbon frequency and with 63kHz proton decoupling. Field strengths for ^{13}C were around 63kHz throughout.

Rotational resonance experiments were as originally described except that the initial carbon magnetization was generated by cross-polarization using a 30% linear ramp. The inversion of the methyl ^{13}C spins was accomplished with a DANTE pulse sequence. Proton field strengths of 63kHz used for the CP were increased to 100kHz for decoupling during the rotational resonance mixing time period and signal acquisition. Field strengths for ^{13}C were around 63kHz throughout.

The data were stored in 1024 points and prior to Fourier transformation the FID arrays were zero-filled up to 8192 points. Exponential linebroadening was typically in the region of 70Hz. All NMR chemical shifts are externally referenced to the methylene resonance of adamantane which resonates at 38.6ppm downfield from TMS.

Magnetization exchange curves were simulated using the RR-FIT program developed by Prof C. Glaubitz [195].

3.4 Results

3.4.1 RR ^{13}C NMR on [1,2-^{13}C$_2$] glycine

Initial RR ^{13}C NMR experiments were conducted on a standard of [1,2-^{13}C$_2$] glycine to test the experimental and analytical methods to be used on ^{13}C labelled rhodopsin samples. The ^{13}C labelled glycine was diluted ~1:17 with unlabelled glycine to prevent intermolecular magnetization transfer between the labelled sites.

The Cross-Polarization Magic Angle Spinning (CP-MAS) ^{13}C NMR spectrum of glycine (Figure 3.4 (a)) shows the isotropic resonances from the Cα methylene group (42.4ppm) and carboxylate group (175.3ppm). In this instance of off rotational resonance, the fast magic-angle spinning (12kHz) effectively averages the dipolar coupling between the isolated ^{13}C spins. Figure 3.4 (b) shows the splitting of the isotropic Cα methylene and carboxylate ^{13}C resonances into dipolar-coupled spin-pairs, due to the recoupling of the dipolar interaction under the n=1 rotational resonance condition (16.7kHz). The dipolar coupling induces an

additional field that splits the Zeeman levels in an asymmetric pattern as described by the relatively complex theory for this effect [135]. Isotropic resonances from uncoupled natural abundance ^{13}C spins in separate glycine molecules can be observed at the isotropic shift values and do not participate in rotational resonance exchange.

The exchange of magnetization between the Cα and carboxyl spins with variable mixing time (τ_m), following DANTE selective inversion of the alkyl region resonances, is observed in Figure 3.5. Initially at τ_m=0ms (Figure 3.5 (a)) the methylene resonance is inverted and no
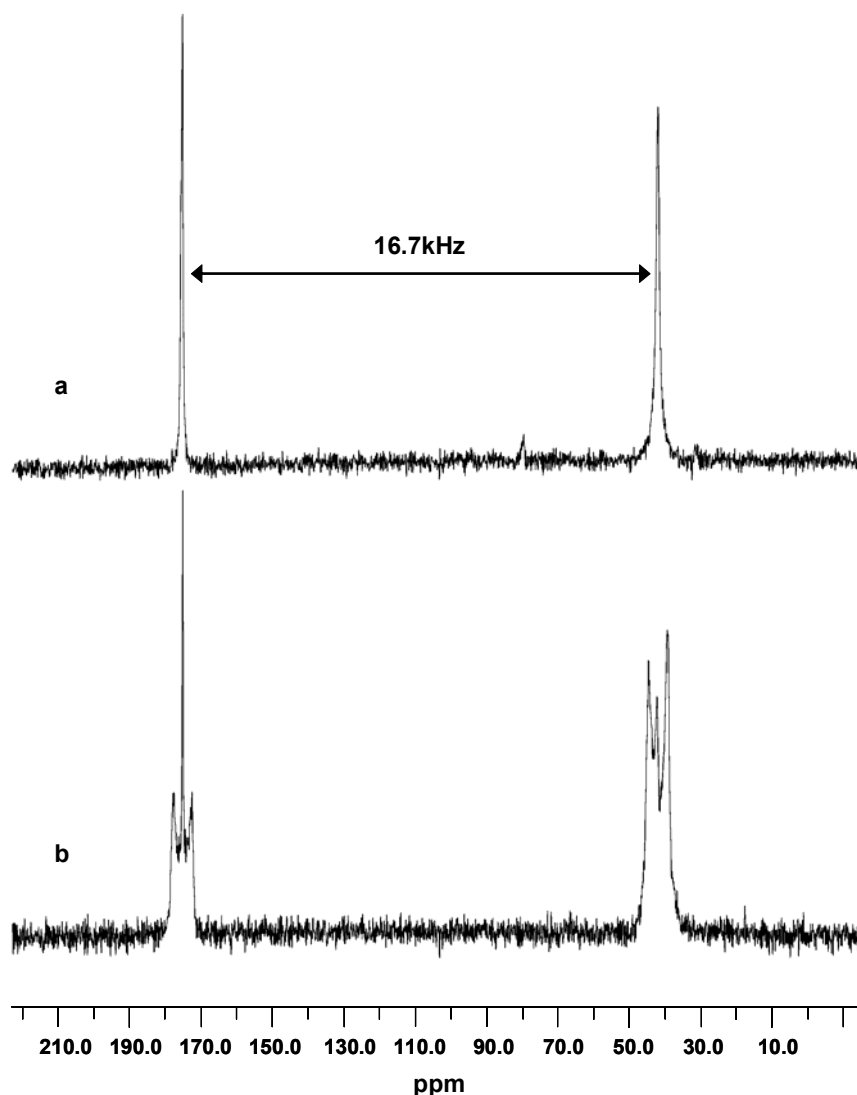
Figure 3.4 – CP-MAS NMR spectrum of [1,2-$^{13}C_2$] glycine off rotational resonance, ω_r = 12kHz (a). The separation between the isotropic chemical shifts is 16.7kHz. RR ^{13}C NMR spectrum of [1,2-$^{13}C_2$] glycine at the n=1 rotational resonance condition, ω_r = 16.7kHz (b)

exchange has occurred. As the mixing period progresses, magnetization transfer occurs with the Cα signal first decreasing in magnitude, (τ_m=0.5 ms) then proceeding to oscillate between positive and negative absorption. Concurrently, the carboxyl resonance, which is initially a positive absorption, decreases in intensity then oscillates between negative and positive values synchronously, but with depleted amplitude (τ_m=0.9 ms τ_m=1.2 ms and τ_m=1.6 ms, Figure 3.5 (c), (d) and (e), respectively). This oscillation effect is only observed when the
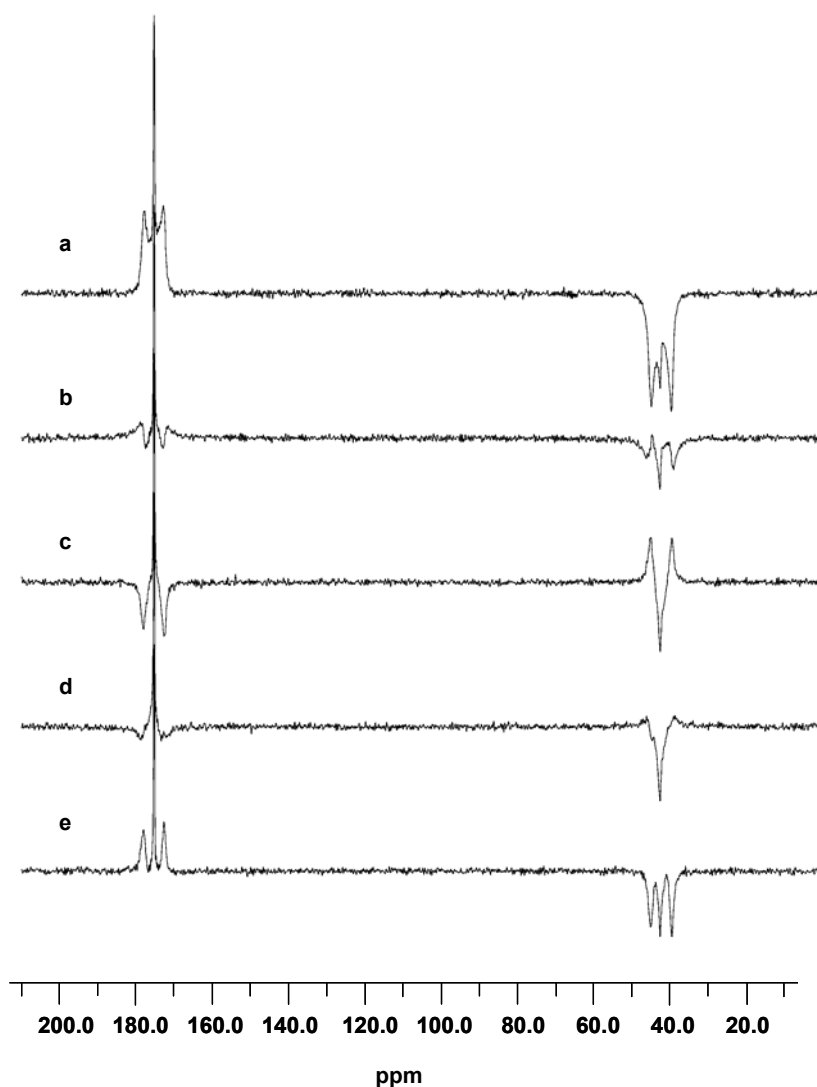
Figure 3.5 – Magnetic oscillations of [1,2-^{13}C$_2$] glycine under rotational resonance. At n=1 rotational resonance, ω_r = 16.7kHz, rotational resonaonce exchange following inversion of the ^{13}Cα peak is shown, with variable mixing times of 0, 0.5, 0.9, 1.2 and 1.6ms (a-e), respectively.

dipolar coupling is strong enough to dominate the damping effect of the T_2^{ZQ} relaxation.

Figure 3.6 shows the magnetisation exchange data from the $[1,2\text{-}^{13}C_2]$ glycine RR NMR spectra (circles). A simulation for the observed magnetisation exchange behaviour (black line) was generated using the RR-FIT software [195]. Due to the well defined oscillating profile of magnetisation transfer it was possible to create a simulated fit without the need to restrain the zero-quantum parameter, since there is likely to be a low correlation with the dipolar coupling strength [198].
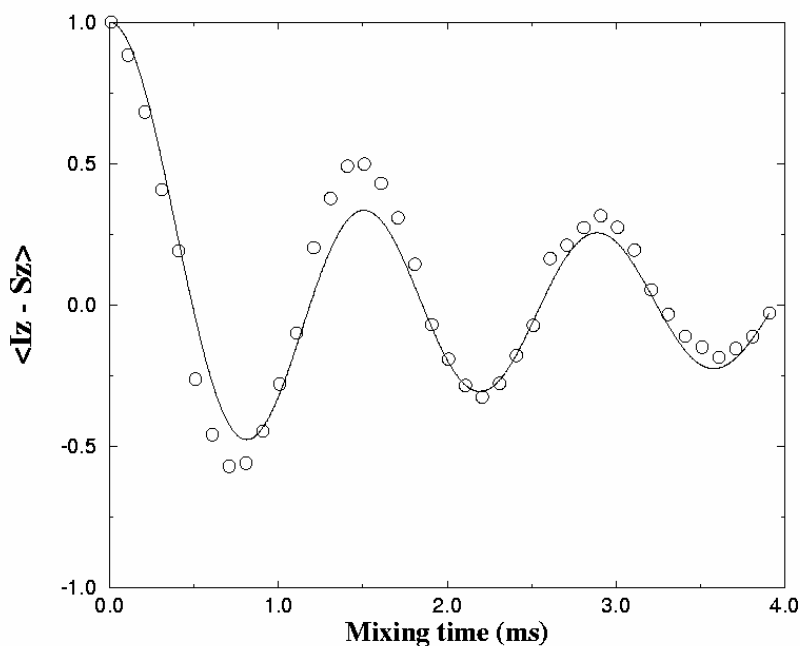
Figure 3.6 — Magnetisation exchange data taken from RR ^{13}C NMR experiments on $[1,2\text{-}^{13}C_2]$ glycine (circles) superimposed on the RR-FIT simulated magnetization exchange curve (black line). A dipolar coupling of 2171Hz was derived, corresponding to an internuclear distance of 1.52Å.

Using standard values for the chemical shift tensors, a restricted two-parameter fit was run for zero-quantum T_2 (T_2^{ZQ}) and dipolar coupling (b_{IS}). The simulation that best fitted the magnetisation exchange data corresponded to a dipolar coupling of 2171Hz. Using this value and inserting values for constants γ, μ_o and η into Equation 3.1, the $C_1\text{-}C_2$ internuclear

distance r, was calculated as 1.52Å, in good agreement with the C_1-C_2 internuclear distance measured in the X-ray [199], neutron diffraction [200] and NMR [201] derived structures of glycine (1.52Å ± 0.02Å, 1.526Å ± 0.001Å 1.543Å ± 0.008Å, respectively). The accuracy of the rotational resonance measurement is normally expected to be no better than ± 0.1Å under the optimal measuring conditions, due to errors from experimental instability and natural variations in the intensities that are measured.

3.4.2 CP-MAS ^{13}C NMR on [8,18-^{13}C$_2$]retinylidene rhodopsin and [8,16/17-^{13}C$_2$]retinylidene rhodopsin

Figure 3.7 represents the CP-MAS spectrum of control[1], prepared from regenerating opsin in ROS membranes with unlabelled 11-Z retinal (see Section **Error! Reference source not found.**) and illustrates the general features that appear in an NMR spectrum from a membrane protein embedded into a phospholipid bilayer. The region between 0 and 40ppm represents the saturated -CH$_2$ and -CH$_3$ groups from the lipid and the protein. Resonances from α-carbons in the protein backbone, as well as the amino acid side groups are observed between 40 and 70ppm. The lipid glycerol backbone also contributes to the signal observed in this region. The feature observed between 125ppm and 130ppm is attributable to unsaturated carbons in the acyl chains, while the carbonyl resonances from both the lipid and the protein result in signal between 170 and 180ppm.
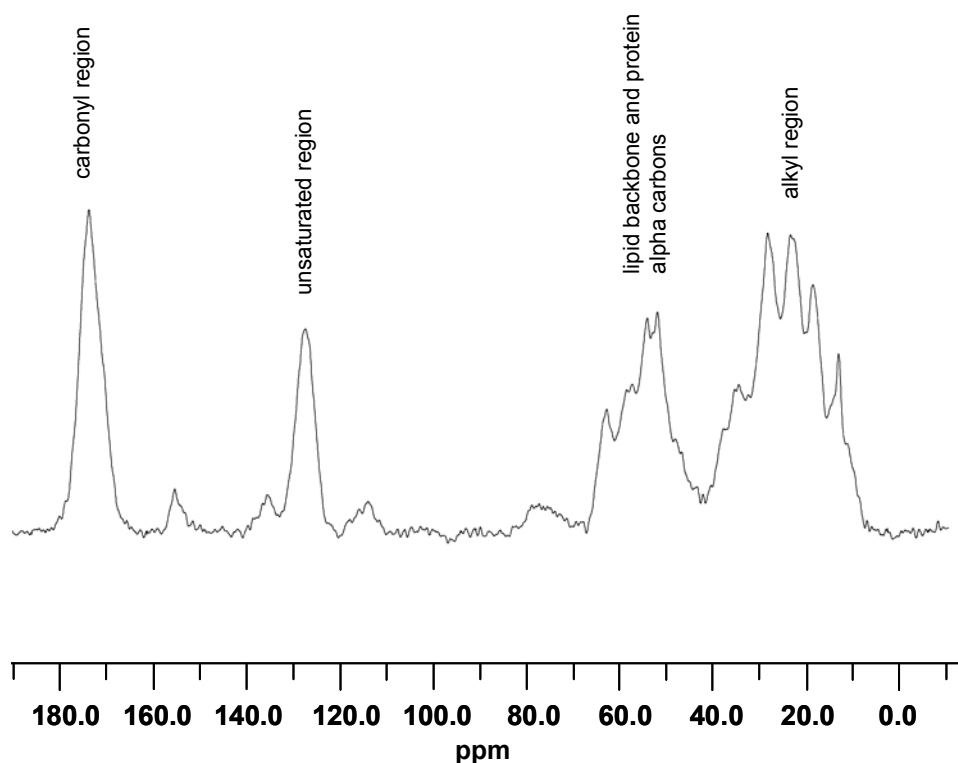
Figure 3.7 – CP-MAS ^{13}C NMR spectrum of rhodopsin (12mg) prepared from regenerating opsin in ROS membranes with unlabelled 11-Z retinal (control[1])(see Table 2.5), w_r = 12kHz

Figure 3.8 shows the RR MAS ^{13}C NMR spectrum of rhodopsin regenerated with unlabelled 11-Z retinal (a), [8,18-^{13}C$_2$] 11-Z retinal (b) and the subtracted spectrum (c), each with a selective DANTE inversion of the alkyl region resonances. At τ_m=0 no exchange of magnetization has occurred. By preparing labelled and unlabelled samples in the identical manner and recording measurements under identical conditions it was possible to subtract out effectively the natural abundance ^{13}C background contribution from the membranes to leave the NMR signals solely from the ^{13}C labelled sites in the bound retinylidene. Isotropic chemical shifts for C18 in the ring and C8 in the polyene chain were observed at 22.1ppm and 139.4ppm, respectively.
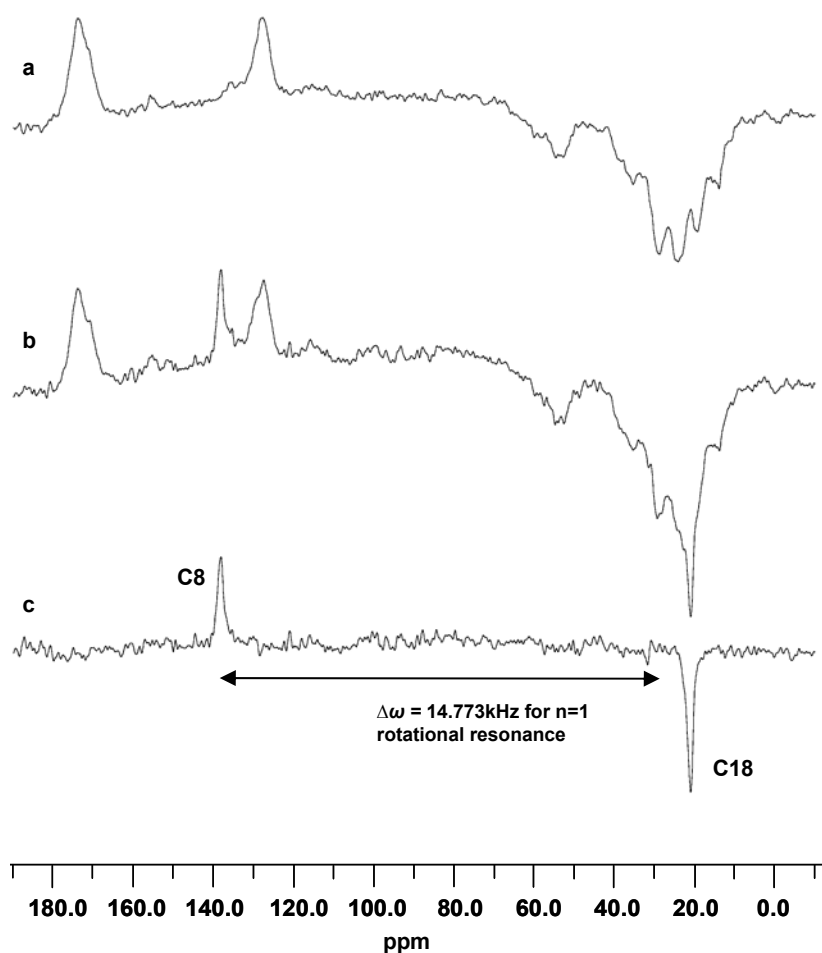
Figure 3.8 – Rotational resonance ^{13}C NMR spectrum of unlabelled rhodopsin sample, control[1] (a) and [8,18-[13]C$_2$]retinylidene rhodopsin (b) with DANTE inversion of the methyl region. The subtracted spectrum (c) shows only signal derived from the C8 (139.4ppm) and C18 (22.1ppm) ^{13}C labels. τ_m=0ms

A "clean" subtraction was also observed for the [8,16/17-[13]C$_2$]retinylidene rhodopsin sample with signal in the difference spectrum only derived from the C8 and C16/C17 resonances (Figure 3.9 (c)). The C8 chemical shift, which is highly sensitive to the orientation around the C6-C7 bond was also observed at 139.4ppm (see Section 3.4.5). The distribution of signal from C16 and C17 was more complex than expected. In the solution state ^{13}C NMR spectrum of retinal in chloroform the C16 and C17 methyl resonances are observed at one chemical shift (28.9ppm [133]) as would be expected for chemically equivalent methyl groups. However, upon regeneration into the binding pocket of rhodopsin the major

components of the C16 and C17 methyl resonances appear separated at two distinct chemical shifts. A resonance could be clearly observed at 26.4ppm, 4.3ppm from a higher frequency resonance observed at 30.7ppm.
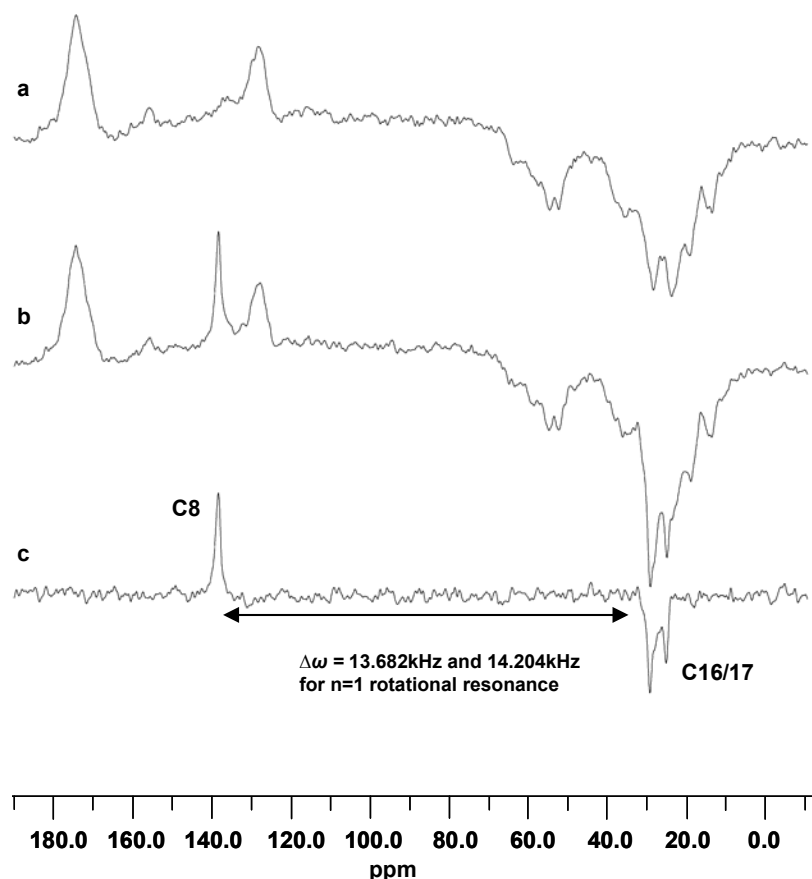
Figure 3.9 — Rotational resonance ^{13}C NMR spectrum of unlabelled rhodopsin sample, control[1] (a) and [8,16/17-^{13}C$_2$]retinylidene rhodopsin (b) with DANTE inversion of the methyl region. The subtracted spectrum (c) shows only signal derived from the C8 (139.4ppm) and C16/C17 (26.4 and 30.7ppm) ^{13}C labels. τ_m=0ms

The different intensities for the two resonances was not consistent with the equal distribution of ^{13}C label at the C16 and C17 positions in the retinal [148]. Inversion recovery NMR experiments revealed that the spin-lattice (T_1) relaxation rates for the protons providing polarization for these sites were quite short (~0.75s) and not significantly different (±0.15s) to account for the difference in intensities. To quantify the distribution of signal

from the C16 and C17 methyl resonances a high signal-to-noise CP-MAS NMR spectrum was recorded under equilibrium conditions for the labelled and unlabelled samples (Figure 3.10) (recycle time = 4s, 20000 acquisitions).
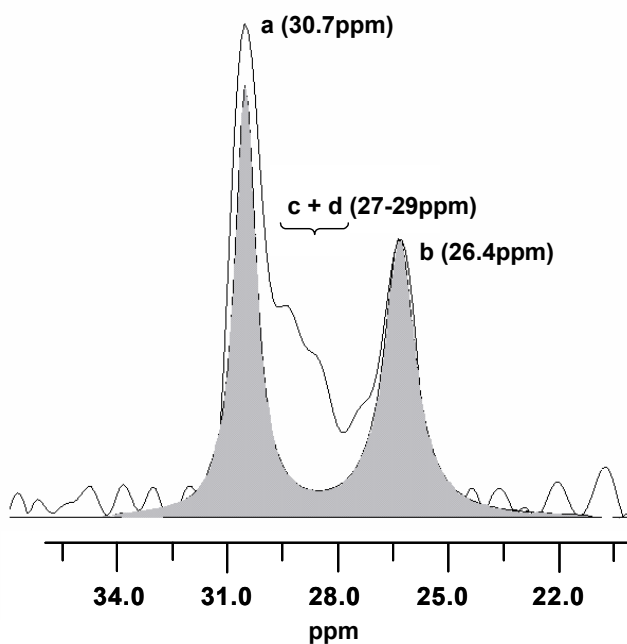
Figure 3.10 – CP-MAS ^{13}C NMR spectrum (background subtracted) of [8,16/17-^{13}C$_2$]retinylidene rhodopsin under equilibrium conditions (recycle time = 4s) showing minor components **c** + **d** (~24%) between the major C16/C17 resonances **a** and **b**. The spectral simulation of the major C16 and C17 resonances (~76%) with the minor

This enabled the resulting difference spectrum to be processed with no linebroadening and revealed the presence of additional spectral components in the 27-29ppm region merging with the 30.7ppm resonance. When the spectrum was deconvoluted two clear components could be identified (Figure 3.10 **c** and **d**), together accounting for 26% of the total intensity from the two labelled methyl groups. The remaining intensity, shown in the equilibrium spectrum was attributed as follow: 40% at 30.7ppm with a linewidth of 110Hz (Figure 3.10 **a**) and 34% at 26.4ppm with a linewidth of 155Hz (Figure 3.10 **b**). These intensities were sufficiently similar for them to be assumed to represent the two labelled methyl groups (C16 and C17) that exist within the major structural form (comprising 74%) of retinylidene in the

protein.

The presence of additional resonances could have possibly interfered with the rotational resonance exchange between C8 and resonance **a**, however this appears not to be the case. The separation of resonance **a** from the minor components exceeded 150Hz, which is beyond its linewidth (110Hz). The resolution in the rotational resonance experiment would also be better than that observed in the equilibrium spectrum due to the shorter measurement time (3hrs compared to 22hrs) and subsequently less field drift. Isolated exchange between C8 and resonance **a** is illustrated in Figure 3.11 showing the intensity of the minor component unaffected whilst the major resonance undergoes selective rotational resonance exchange with C8.
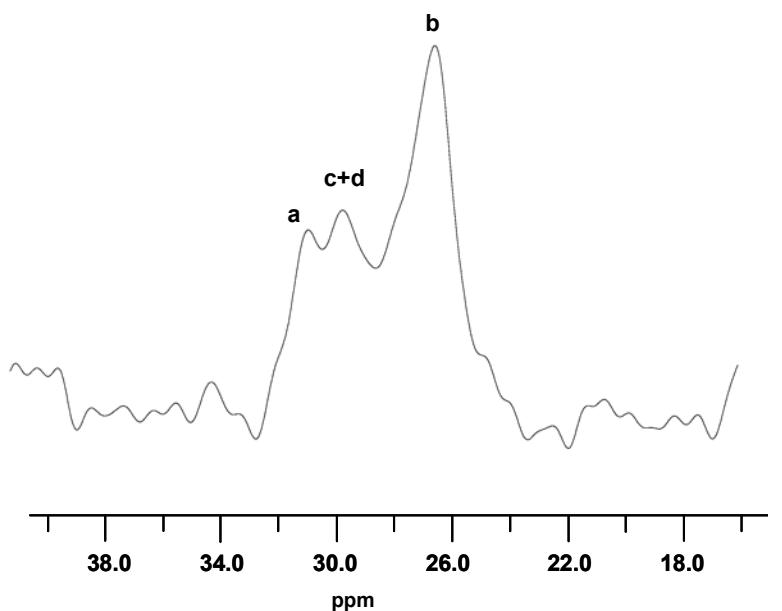
Figure 3.11 - RR ^{13}C NMR spectrum of [8,16/17-^{13}C$_2$]retinylidene rhodopsin with the major resonance **a** depleted following 15ms of n = 1 rotational resonance exchange with C8. The minor components merge as a single resonance when observed with 70Hz linebroadening.

3.4.3 C8 to C16/C17 internuclear distance determination using RR NMR

From the frequency difference between the C8 and the two major C16/C17 resonances **a**

and **b**, the spinning speed was set at 13.682kHz and 14.204kHz respectively, corresponding to the n=1 rotational resonance condition. Rotational resonance experiments were run between 0 and 40ms for each pair. The intensities of the resonance were measured through peak fitting and the exchange of Zeeman magnetization plotted as a function of mixing time. The rotational resonance exchange between C8 and both C16/C17 major signals is plotted in Figure 3.12.

The net magnetization ($<I_z-S_z>$) was corrected for the proportion of C8 undergoing

exchange with the separate methyl resonances then normalized to the initial, corrected net

magnetization averaged from a number of short mixing times (<0.1ms). The exchange rates
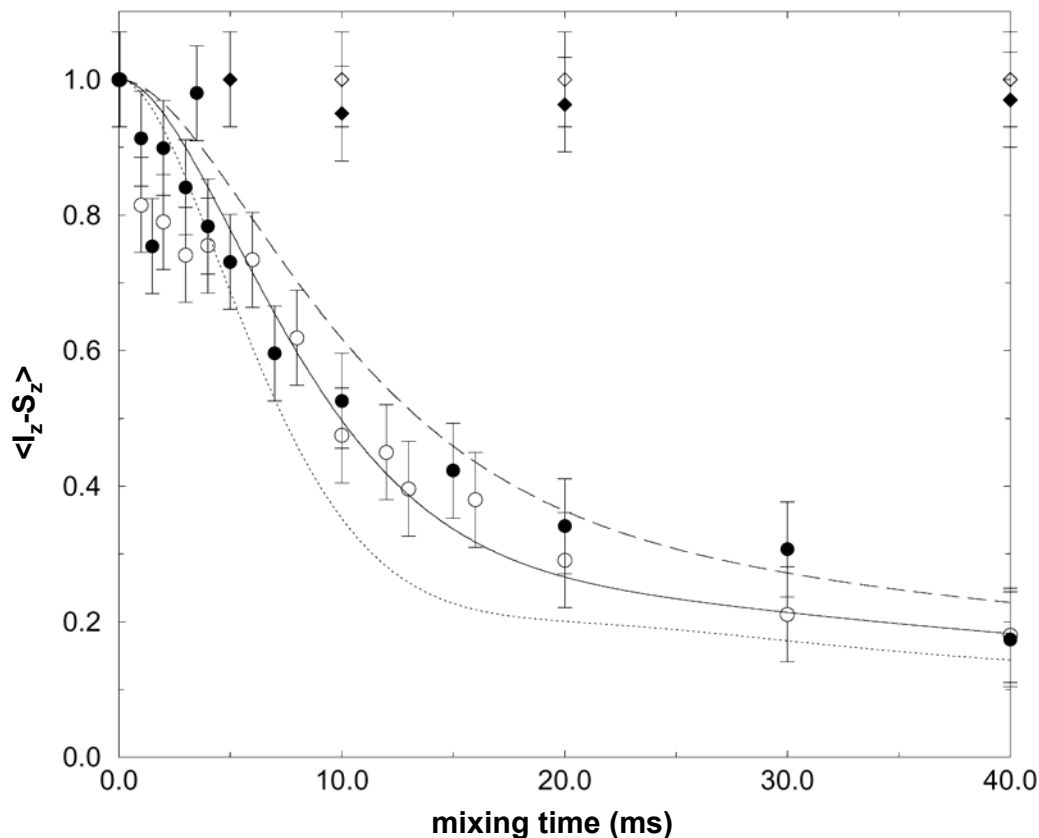
Figure 3.12 – Exchange data for n=1 rotational resonance experiment between the C8 and resonance **a** (filled circles) and C8 and resonance **b** (open circles) in [8,16/17-$^{13}C_2$]retinylidene rhodopsin showing net magnetization as a function of mixing time. Error bars for each data point were calculated from the RMSD of the noise. Net magnetization was corrected for the proportion of C8 participating in rotational resonance in each case (see text). Simulations are shown corresponding to a best-fit internuclear distance of 4.05Å (solid line) and for 4.30Å (dashed line) and 3.80Å (dotted line) representing an estimation of the upper and lower limit. Off-resonance exchange (diamonds) shows neglible change in intensity.

measured between C8 and resonance **a** (filled circles) and between C8 and resonance **b**

(open circles) were indistinguishable from each other.

To enable an interpretation of the exchange data a measurement of the T_2^{ZQ} was made for

the coupling between both the major methyl resonances and C8 using a Hahn spin-echo experiment. Despite the differences in linewidths the T_2 relaxation rates for both sites were similar, providing an initial estimate of T_2^{ZQ} of 6ms ($\pm$1ms). Therefore the additional broadening of the resonance **b** was not a result of an increased T_2 but a result of slight heterogeneity in the orientation of this methyl group. Following the procedure described previously (Section 3.3.2) the value for T_2^{ZQ} was amended to 3ms, reflecting a more accurate representation of T_2^{ZQ} damping and off resonance effects.

As the T_2^{ZQ} processes and the rotational resonance exchange were indistinguishable between both C16 and C17 methyls and C8 the exchange data was combined for the analysis. A dipolar coupling of 114Hz was derived from the best fit simulation to the data, corresponding to an internuclear distance of 4.05Å (solid curve Figure 3.12) between C8 and both C16/C17 methyl groups. In Figure 3.12, exchange curves are shown for 3.8Å (dotted line) and 4.3Å (dashed line) which encapsulates almost all of the data. Most of the variation observed arises from non-systematic errors, such as instability in the spectrometer and errors in the handling of the data from peak fitting and spectral subtraction. Error bars are diplayed on each data point which were calculated from the root mean squared deviation (RMSD) of the noise. The systematic errors for the fitting procedure arising from inaccuracies in the estimates for tensor values, tensor orientations and T_2^{ZQ} will also contribute to the error. The systematic errors in tensor value and orientation measurements will not contribute significantly to the overall error, especially as the experiments were run at n=1 rotational resonance. The effect of errors in the estimate of T_2^{ZQ} will be more influential, however it is unlikely that they will be greater than the 6% difference in intensities measured for the major C16/C17 methyl resonances **a** and **b** deconvoluted from the CP-MAS equilibrium spectrum of [8,16/17-$^{13}C_2$] retinylidene rhodopsin.

3.4.4 C8 to C18 internuclear distance determination using RR NMR

In contrast to the relatively slow exchange observed between C8 and C16/C17 a much faster

exchange was observed between C8 and C18, as seen in the stacked plot of the difference

spectra of [8,18-^{13}C$_2$] rhodopsin undergoing rotational resonance exchange (Figure 3.13).
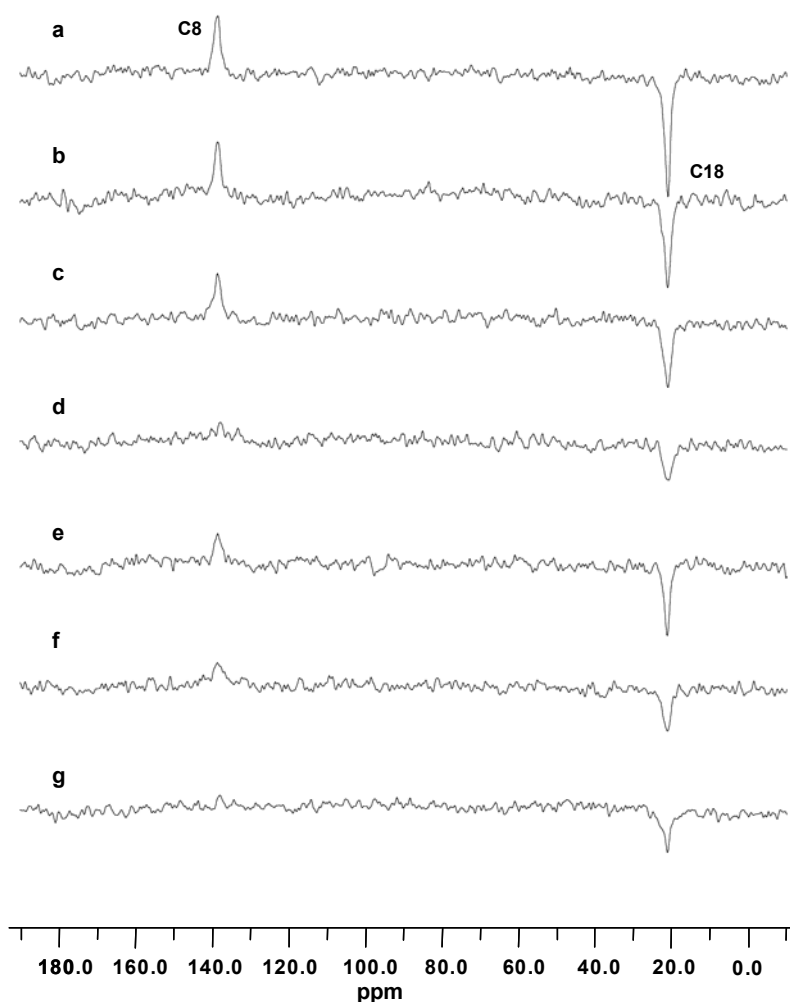
Figure 3.13 - RR ^{13}C NMR spectra of [8,18-^{13}C$_2$]retinylidene rhodopsin undergoing rotational resonance exchange between C8 and C18 (n=1 rotational resonance, ω_r = 14.773kHz) with mixing times of 0, 1, 2.5, 7.5, 10, 20 and 30 ms (a-g, respectively).

When these data were plotted as an exchange curve the experimental data described a biphasic exchange with the majority of net magnetization transferred within the first 5ms, followed by a very slow decrease over the longer mixing times (10 to 30ms)(Figure 3.14). The initial fast exchange and the oscillation observed in the exchange at 10ms are characteristic of a fast rotational resonance exchange (see glycine Figure 3.5) whilst the slow decrease at later mixing times is characteristic of a weakly coupled spin pair.
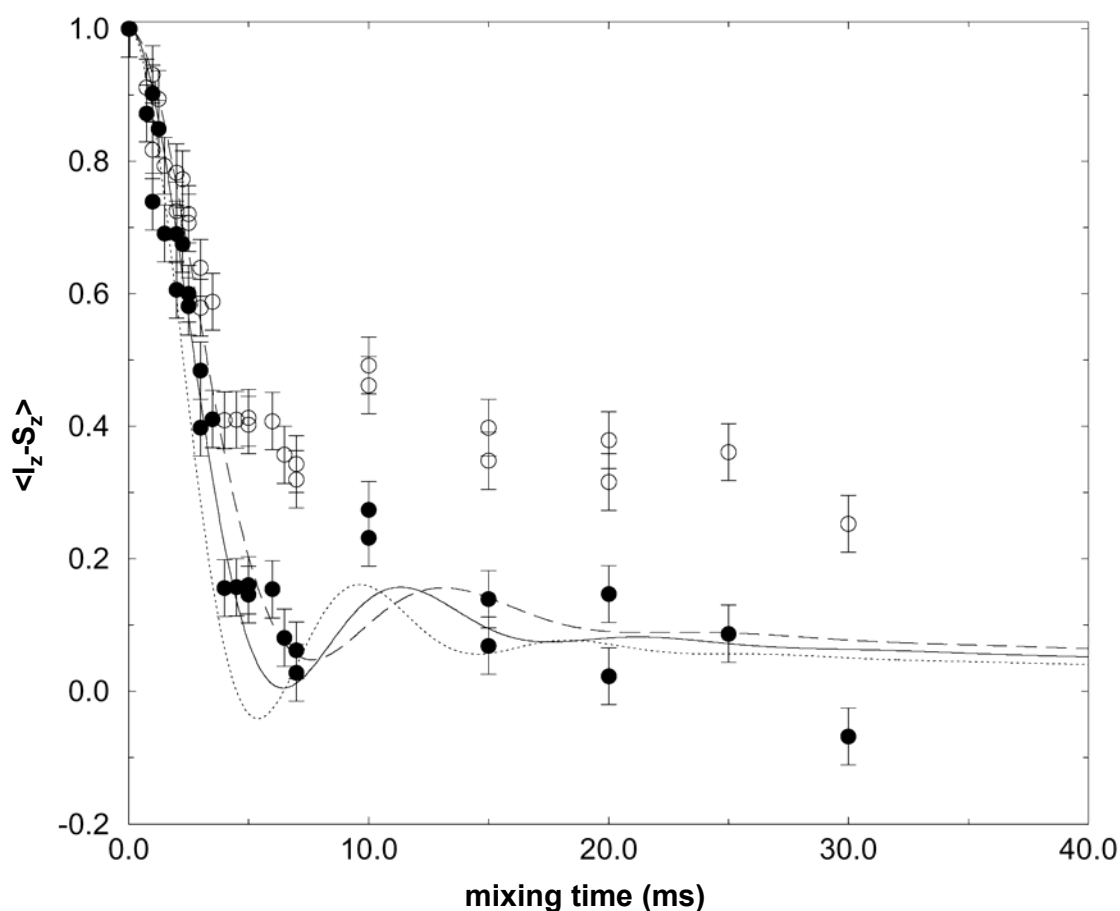
Figure 3.14 - Experimental exchange data for n=1 rotational resonance experiment between the C8 and C18 spin pair in [8,18-^{13}C$_2$]retinylidene rhodopsin showing net magnetization as a function of mixing time (open circles) and data corrected to represent the rapid phase of exchange for the major component (filled circles). Error bars for each data point were calculated from the RMSD of the noise. Net magnetization was corrected for the proportion of C8 participating in rotational resonance (see text). Simulations are

It was possible that the slow decrease in magnetisation observed after the initial oscillation was a result of "tail off" effects that are sometimes observed in rotational resonance experiments. Unstable spinning, large spectral linewidths and imperfect decoupling can sometimes lead to a gradual drop in magnetisation as observed here, however, the spinning was stable in this experiment ($\pm$ 3Hz) and the linewidths were acceptable (~100-150Hz). The [1,2-^{13}C$_2$]glycine model system in which there are strong homonuclear and heteronuclear couplings maintained efficient rotational resonance exchange at all mixing times, indicating that the experimental setup was not susceptible to these limitations. Furthermore, the slow phase of exchange does not appear to damp out the oscillation in the rapid exchange process, occurring at τ_m=10ms, providing further evidence for independent exchange processes.

The observed biphasic decay therefore indicated that this sample has minor components present, as in [8,16/17-^{13}C$_2$]retinylidene rhodopsin and the slow exchange was a result of exchange between C8 and C18 in these minor forms. Whereas the minor components appear at distinct chemical shifts for C16 and C17, the different conformations for C18 all resonate at the same frequency (22.1ppm). Consequently, two rates of exchange occur between C8 on the polyene chain and both C18 ring conformations as all structural forms are simultaneously recoupled.

To obtain a good simulated fit to the intensity remaining at longer mixing times a correction of 30% was applied for the proportion of C8 and C18 not participating in the major rapid (<5ms) phase of exchange. The slight increase over the % of minor components detected in the [8,16/17-^{13}C$_2$]retinylidene rhodopsin sample (24%) suggests that insufficient minor component intensity was deconvoluted from the C16 resonance in the equilibrium spectrum,

explaining the 6% discrepancy in intensities between C16 and C17.

The best fit simulation to the corrected data for exchange between C8 and C18 (Figure 3.14, filled circles) corresponds to an internuclear distance of 2.95Å (solid line). The accuracy of this measurement is expected to be slightly better than between C8 and C16/C17 as the experimental fit to the data, with relatively little experimental scatter, is excellent and the presence of an oscillatory feature provides a further "signature" to which the fit can be judged.

The error limits are therefore set at 2.80Å (dotted line) and 3.10Å (dashed line). As for [8,16/17-$^{13}C_2$]retinylidene rhodopsin, systematic errors in the calculation of T_2^{ZQ} and chemical shift tensors are not expected to exceed the set limits. The assumption made for subtracting out the 30% contribution of minor components is reasonable, as their contribution to the exchange profile for the major population of retinylidene over the short time period (5ms) when the majority of magnetization transfer occurs will be minimal.

3.4.5 Absolute conformation of the β-ionone ring in rhodopsin

The chemical shift and structural data for retinal in rhodopsin from this study is displayed in Table 3.1 together with data reported for bR and retinal based crystalline analogues. Chemical shift analysis has been previously used to investigate the absolute orientation of the C6-C7 conformation [32, 105, 120], mainly focusing on the chemical shift and tensor values of rhodopsin regenerated with retinal ^{13}C labelled at the C5 position, which is very sensitive to the isomeric state around C6-C7. From comparing the isotropic chemical shift and chemical shift tensor values with model compounds a twisted 6-*s-cis* conformation was determined for rhodopsin, opposite to the 6-*s-trans* observed in bacteriorhodopsin. From

measuring the chemical shift of retinal model compounds Harbison *et al* [177] noticed that the C8 chemical shift was also sensitive to the C6-C7 conformation, moving from 138.9ppm in 6-*s-cis* retinoic acid to 130.9ppm in the 6-*s-trans* isomer. The upfield shift in the *s-trans* geometry is due to the steric interaction between the C16, C17 methyl groups and the C8 hydrogen. The retinal C8 chemical shift in rhodopsin in this study (139.4ppm) is similar to that previously observed (139.2ppm) and is well within the range of chemical shifts observed for the 6-*s-cis* forms, in contrast to retinal in bacteriorhodopsin which exhibits a 6-*s-trans* shift at C8.

Table 3.1 – Summary of ^{13}C chemical shift and distance measurements for retinal in rhodopsin, including distance measurements for bR and crystalline analogues

	chemical shifts (ppm)		
	C8	C16/17	C18
bovine rhodopsin (ROS)	139.4[a]	30.7/26.4[a]	22.1[a]
6-*s-cis*			
all *trans* retinal	138.2[b]	31.7/28.9[c]	23.3[c]
retinoic acid	138.9[b]	32.5/28.7[d]	24.1[d]
6-*s-trans*			
bR	131.6, 132.7[b]	28.9[b]	22.0[b]
13-*cis*-retinal	<133[b]		
retinoic acid	130.9[d]	30.9/27.3[d]	20.8[d]
	distance from C8 (Å)		
	C16/17		C18
bovine rhodopsin	4.05 ± 0.25[a]		2.95 ± 0.15[a]
bR	3.4 ± 0.2[e]		4.1 ± 0.2[e]

The opposite absolute conformation to bR was confirmed by the internuclear distance measurements between C8 and the ring methyl groups. The distance measured between C8 and C16/C17 in rhodopsin in this study (4.05Å) is equivalent to that measured for the C8 to C18 distance in bR (4.10Å)[148]. Comparing the distances from C8 to C18 (2.95Å) and to C16 and C17 (4.05Å) shows that the major proportion of the chromophore in rhodopsin is in a 6-s-*cis* conformation. The minor forms of the chromophore were expected to adopt a 6-s-*trans* conformation if it is assumed they are responsible for the slow exchange between C8 and C18. The conformation of the minor components is discussed in more detail in Section 3.5.3.

3.5 Discussion

3.5.1 C16 and C17 methyl orientations

When retinal and retinal derivatives are in solution a single resonance is observed for both C16 and C17 methyl groups, shown by the protonated Schiff base model compound (*N*-(11-*cis*-retinylidene)-n-propyl-iminium   trifluoroacetate)   with   both   C16   and   C17   methyl
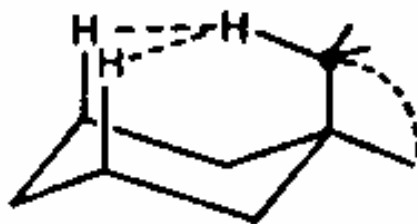
Figure 3.15 – The C1-methyl of 1,1-dimethylcyclohexane in an axial orientation results in a chemical shift of -4.2 ppm per proton interaction with the axial proton of the γ-

resonances at 28.9ppm [202]. When the retinal derivative is in a crystalline form however, a chemical shift inequivalence is often observed between the two methyls (Table 3.1) [177, 181], which can be accounted for exclusively by intramolecular steric effects within the chromophore, due to the fixed orientation of the ring methyls in an axial and equatorial conformation. Although the chemical shift difference between the two methyl groups in rhodopsin (4.3ppm) is greater than that observed for the crystalline derivatives, it is still well within the range of chemical shift differences observed for methyl groups oriented in an axial and equatorial conformation in methylated cyclohexanes, which can be as much as 6ppm [203, 204]. The chemical shift difference seen in an axial/equatorial methyl arrangement arises from the steric interaction of the axial methyl with the axial protons on the γ-carbons in the cyclohexane ring, resulting in a shielding effect and a lower chemical shift value (Figure 3.15).

The degree to which the methyl is oriented axially dictates the level of steric interaction and hence the extent of the chemical shift difference, which is predicted to be ~4.2ppm for an axial methyl with a geminal equatorial methyl per ring proton interaction [205]. This value matches the shift difference observed in rhodopsin, where the ring C16 or C17 methyl group can only interact with a single axial ring proton from just one γ-carbon (C3) in the β-ionone ring of the retinal. Although this shows that the chemical shift difference can be accounted for solely by an axial/equatorial conformation for the C16 and C17 methyls it does not deduce their precise orientations with respect to the β-ionone ring. Consequently, the distance constraints obtained from the rotational resonance measurements between C8 and C16/C17 cannot be reliably used to predict the degree of twist of the polyene chain. Nevertheless, the large chemical shift C16/C17 separation (4.3ppm) and respective axial and equatorial conformation of the C17 and C16 methyls represent a significant protein-induced

conformational restraint of the bound chromophore in this region. A chemical shift separation of 4.5ppm was recently reported for the C16 and C17 methyl groups in rhodopsin regenerated with uniformally ^{13}C labelled 11-Z retinal and attributed to an induced axial (C17) and equatorial (C16) methyl conformation [107].

3.5.2 The high-resolution structure of the β-ionone ring in rhodopsin

To estimate the extent of the twist between the polyene chain and the β-ionone ring, only the distance between C8 and C18 is used. This distance was obtained with the greatest precision, reflected in the smaller error limits (±0.15Å) and corresponds to the rigid segment of the ring, least likely to be perturbed in the protein.

Using the crystal structure of 11-Z retinal as a starting structure [175], as used in the modelling of the chromophore in other NMR studies and in the protein crystal structure [28, 78], the distance between C8 and C18 (2.95Å) predicts an out-of-plane twist of 28±7° in the chain (Figure 3.16).

To maintain the equidistant measurement made between C8 and both C16 and C17 (4.05Å) the C2-C1-C6 ring segment is tilted, bringing C17 into an axial orientation. Not only does this satisfy the rotational resonance distance constraints but also the axial/equatorial chemical shift interpretations previously made for the C16 and C17 methyls. Bringing C17 into an axial orientation, and not C16, results in far less manipulation of the starting
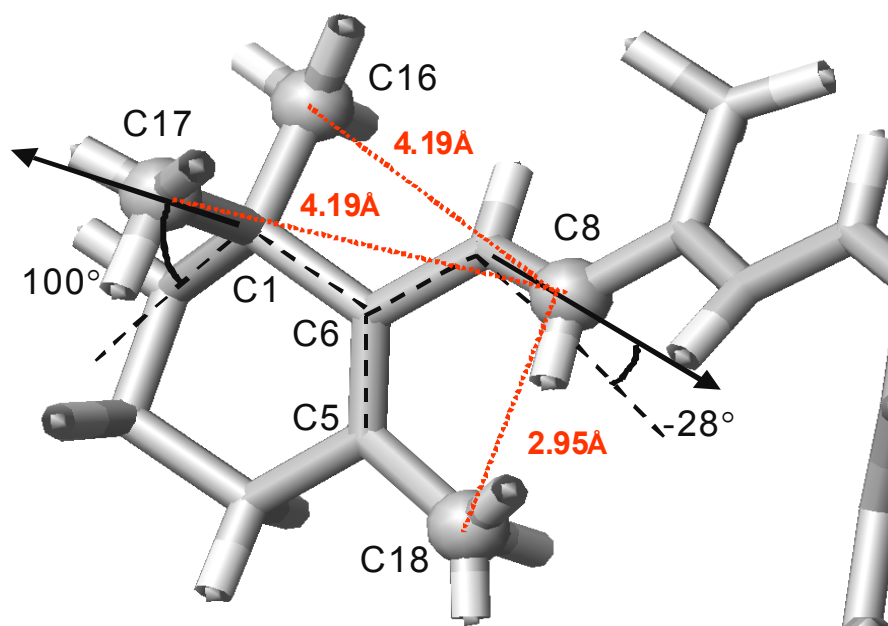
Figure 3.16 — Conformation of the β-ionone ring of retinylidene in the dark-state of rhodopsin deduced from rotational resonance ^{13}C NMR measurements. The C8-C18 internuclear distance of 2.95Å was used to predict the out-of-plane twist in the retinal chain (C5-C6-C7-C8 torsion = -28°). The axial and equatorial orientation for the C17 and C16 methyls, respectively, maintains them equidistant from C8 at 4.19Å (measured at 4.05 ±0.25Å for both groups).

structure, increasing the C5-C6-C1-C17 torsion angle by only 5° to +100°. To keep C8 equidistant from C16 and C17 the sense of the twist of the polyene chain is opposite to that used for the C17 reorientation, giving a negative twist for the C5-C6-C7-C8 torsion.

The sense of the twist has recently been confirmed in a retinal analogue binding study. Out of a positively and a negatively 6-s-*cis* locked analogue only the negatively locked retinal was found to bind to opsin (Figure 3.17) [126]. It is worth noting that in this study no 6-*s-trans*

locked retinal analogues were used as a control, which have been previously shown to bind to opsin [97].

The value of the twist determined from this study ($28\pm7^{\circ}$), is relatively modest when compared to those generally found in retinal analogues, which are normally in the range of $30\text{-}70^{\circ}$ [174] and much less than that reported in the crystal structure (-55°) [34]. Molecular modelling of the negatively twisted 6-*s-cis* analogue (Figure 3.17(a)) yielded a lowest energy conformation with a twist of -35°, close to value determined from NMR [126].

The deduced conformation of the β-ionone ring will not contribute as significantly to the opsin shift of the chromophore as would a planar 6-*s-trans* conformation. However, the modest twist between the β-ionone ring and the chain may aid delocalisation of the π-electrons relative to the PSB of 11-*Z* retinal [173-175].
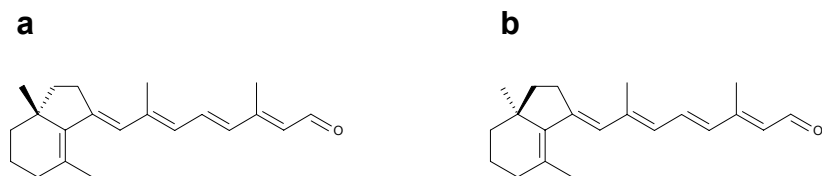
Figure 3.17 – The α and β enantiomers of 6-*s*-*cis* locked retinal. Only the α-locked analogue (a) with a negative twist around the C6-C7 bond formed a pigment (λ_{max}=539nm) upon incubation with opsin. Incubation with the positively twisted β-6-*s*-locked analogue (b) resulted in no pigment formation after 4 hours.

The range specified for the angle ($\pm 7^{\circ}$) is based on the angle obtained for the upper limits of the rotational resonance data (3.1Å) as the distance estimated for the lower limit (2.8Å) cannot be obtained by simply manipulating the C5-C6-C7-C8 torsional angle. This highlights the need to use all three C8/ring methyl distance measurements to obtain full limits on the C6-C7 torsion and specify the geometry in this region to higher resolution, which would require an accurate determination of the orientations of the C16 and C17 methyls with respect to the ring.

3.5.3 Nature of minor components

In both ^{13}C labelled rhodopsin samples minor components were observed in roughly equal proportions, although they are detected in different ways: in [8,16/17-^{13}C$_2$] retinylidene rhodopsin through their chemical shift separation from the major C16/17 resonances and in [8,18-^{13}C$_2$] retinylidene rhodopsin by the observation of biphasic exchange behaviour.

If the observation of biphasic exchange behaviour was a result of minor components, as is likely, then they would be expected to adopt an opposite 6-*s*-*trans* conformation to the major conformation of retinylidene, giving rise to the slow exchange of magnetisation observed in the exchange curve between C8 and C18.

To deduce the conformation of the β-ionone ring in the minor components, rotational resonance NMR experiments were conducted between C8 and the visible C16 and C17 minor components in the CP-MAS ^{13}C NMR spectrum of [8,16/17-^{13}C$_2$]retinylidene rhodopsin (Figure 3.18 **c** and **d**). The considerable spectral overlap in this region meant that quantifying the data in the form of exchange curves would have been ineffectual. Rotational resonance experiments were run between C8 and **c** at 13817Hz and C8 and **d** at 13905Hz, with mixing times of 0.01, 5, 10 and 20ms in each case. Selective exchange was observed to both resonances **c** and **d**, illustrating the relatively narrow "window" of resonances (~50Hz) that undergo rotational resonance exchange. The equal proportion of the major C16 and C17 components is illustrated in Figure 3.18 (c). With the minor component **c** removed through rotational resonance exchange the intensities of the remaining major peaks are similar (±2%), confirming that they represent the major methyl resonances.

Both rotational resonance experiments showed fast rotational resonance exchange between the minor components and C8, with almost all the intensity undergoing exchange by 10ms (Figure 3.18 (c) and Figure 3.19 (c)). The fast exchange observed between C8 and both C16 and C17 resonances indicates that in the minor components the ring adopts a 6-*s-trans* conformation, in accord with the biphasic exchange observed for [8,18-^{13}C$_2$]retinylidene rhodopsin and is not a consequence of equatorial/axial rearrangements around C1. The absence of any discrete resonance at a lower chemical shift (131-132ppm) as noted for 6-*s-trans* analogues would indicate that the minor form did not adopt a homogenous planar state.
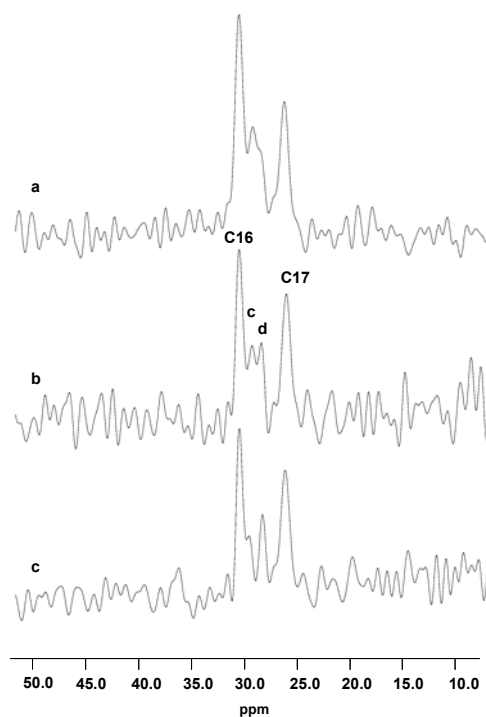
Figure 3.18 – Rotational resonance ^{13}C NMR spectra between C8 and the minor component **c** of [8,16/17-^{13}C$_2$]retinylidene rhodopsin with mixing times of 0, 5 and 10ms (a-c respectively). ω_r= 13.817kHz. By 10ms the majority of the minor component has depleted, indicating a fast exchange and a strong coupling between C8 and
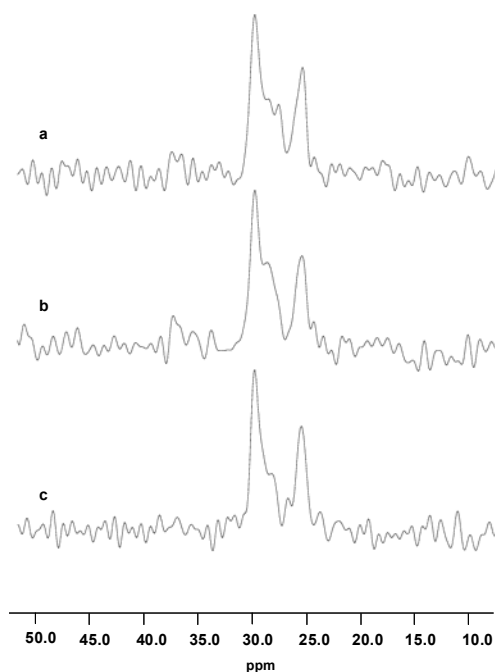
Figure 3.19 – Rotational resonance ^{13}C NMR spectra between C8 and the minor component **d** of [8,16/17-^{13}C$_2$]retinylidene rhodopsin with mixing times of 0, 5 and 10ms (a-c respectively). ω_r = 13.905kHz. A similar rapid exchange was observed for resonance **c**, supporting a 6-s-*trans* conformation for the minor components.

It has been previously shown that retinal can bind to opsin in a *6-s-trans* conformation. Ito *et al* found that both *6-s-cis* and *6-s-trans* locked bicyclic retinal analogues could bind to opsin, suggesting that the retinal cavity was non-selective with respect to the orientation of the ring moiety of retinal and it is possible for heterogeneity around the C6-C7 bond to occur in the binding pocket [97]. Density functional theory calculations have recently been used to predict the influence of the protein pocket (PDB entry: 1F88) on the structure of the bound 11-*Z* retinylidene chromophore [111]. They suggested that the binding pocket could tolerate both *6-s-cis* and *6-s-trans* conformations with the former favoured by an energy difference of 0.7kcal/mol. The *6-s-cis* chromophore model had a modest negative twist around the C6-C7 bond (-35°), in agreement with the data presented here and the *6-s-trans* chromophore had angles for the methyl bond vectors that were in close agreement (±2°) with those observed for the *6-s-trans* structure of the chromophore derived from ^{2}H NMR [80].

It was therefore of interest to investigate whether the heterogeneity of *6-s-cis* and *6-s-trans* components represented the natural equilibrium of conformations for the β-ionone ring, or were an artefact of the preparation procedure. The potential for *6-s-trans* retinal binding highlighted the possibility that the retinal may have adopted this form in the samples used for the ^{2}H NMR measurements. It was suggested that *6-s-cis*→ *6-s-trans* ring-flips could be induced as a result of reconstitution into a saturated DMPC lipid membrane, as used in the preparation of the ^{2}H NMR samples.

To investigate the source of the minor components, opsin in ROS membranes was regenerated with retinal labelled at both the C16 and C17 methyl positions ([16,17-$^{13}C_2$]retinylidene rhodopsin, see Table 2.5 for UV-VIS characterisation details) (Figure 3.20). A [16,17-$^{13}C_2$] retinylidene rhodopsin sample was also reconstituted in DMPC membranes with the same starting lipid:protein ratio as used for the ^{2}H NMR measurements (60:1

lipid:protein ratio)[1]. The actual lipid:ratio obtained in the membrane will be less than 60:1 and is likely to vary between samples, based on the degree of incorporation of the protein into the lipid bilayers.

The distinct chemical shift separation observed for the axial/equatorial C17 and C16 methyl groups of the major 6-s-*cis* component of [8,16/17-^{13}C$_2$]retinylidene rhodopsin (4.3ppm) was used as a probe for the presence of a 6-s-*cis* ring conformation.
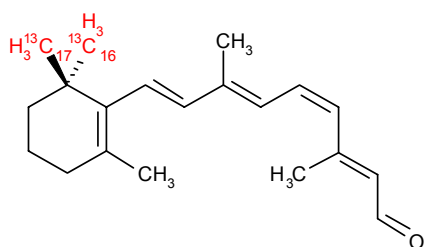
Figure 3.20 – Schematic representation of [16,17-^{13}C$_2$] 11-Z-retinal used to investigate heterogeneity around the C6-C7 bond.

The difference CP-MAS NMR spectrum of [16,17-^{13}C$_2$]retinylidene rhodopsin in ROS showed no significant minor components as had previously been observed for [8,18-^{13}C$_2$]retinylidene rhodopsin and [8,16/17-^{13}C$_2$]retinylidene rhodopsin (Figure 3.21). Deconvolution of the C16 and C17 resonances indicated the presence of a small amount of minor components (6%) with the remaining ^{13}C signal split between the major C16 (46%) and C17 (48%) resonances. A large chemical shift separation (4.7ppm) between C16 (30.7ppm) and C17 (26.0ppm), as observed for [8,16/17-^{13}C$_2$]retinylidene rhodopsin, was

characteristic of the ring binding in a *6-s-cis* conformation.
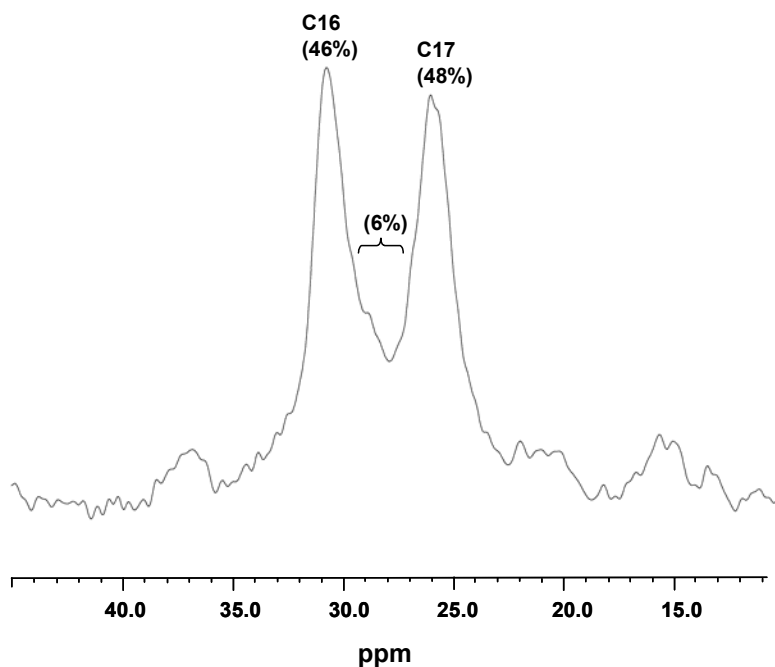
Figure 3.21 – CP-MAS ^{13}C NMR spectrum of [16,17-^{13}C$_2$]retinylidene rhodopsin in ROS showing the methyl region. $\omega_r = 10$kHz. Only a small fraction (6%) of the subtracted intensity was assigned to minor components between 27 and 29ppm, suggesting that heterogeneity around the C6-C7 bond observed in [8,16/17-^{13}C$_2$]retinylidene rhodopsin

The difference CP-MAS NMR spectrum between [16,17-^{13}C$_2$]retinylidene rhodopsin in DMPC bilayers and an unlabelled control showed a large residual lipid resonance overlaying the C16 and C17 resonances at 33.4ppm, arising from a difference in the DMPC:rhodopsin ratios between the labelled and control samples (Figure 3.22). Nevertheless, the C16 and C17 methyl resonances could be clearly observed at 30.6ppm and 26.1ppm, respectively. No 6-s-trans components could be deconvoluted between 27 and 29ppm indicating the β-ionone ring adopted a *6-s-cis* conformation and was unperturbed by the nature of the lipid bilayer.

The minimal detection of minor components suggested that the *6-s-trans* minor components previously observed were not a result of natural heterogeneity within the binding pocket and the ring adopted exclusively a *6-s-cis* conformation in rhodopsin.
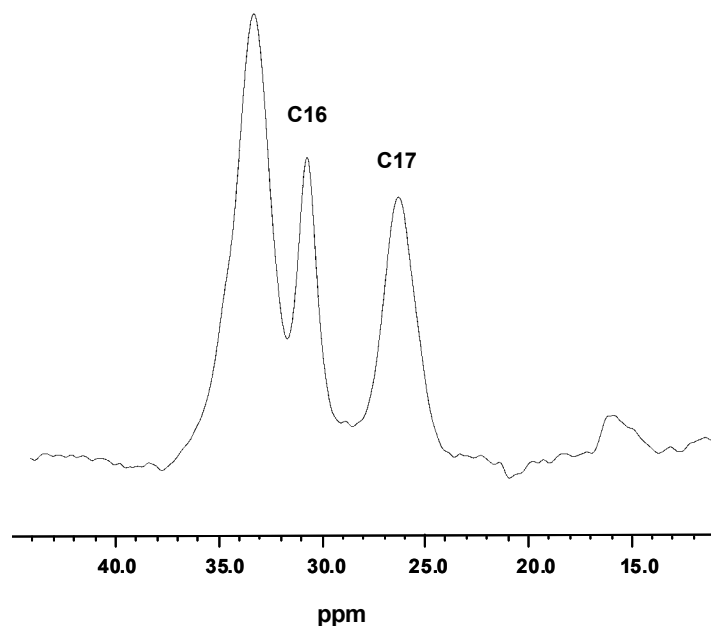
Figure 3.22 – CP-MAS ^{13}C NMR spectrum of [16,17-^{13}C$_2$]retinylidene rhodopsin in DMPC membranes (60:1 protein:lipid ratio) ω_r = 10kHz. Resonances observed at 30.6ppm and 26.1ppm correspond to the C16 and C17 resonances, respectively. A large residual resonance was observed at 33.4ppm, which was an artefact of the spectral

To identify the source of the *6-s-trans* minor components that were observed in [8,16/17-^{13}C$_2$]retinylidene rhodopsin and [8,18-^{13}C$_2$]retinylidene rhodopsin, differences in the preparation protocols between all the 11-*Z* regenerated rhodopsin samples were investigated.

Review of the UV-VIS characterisation of the regenerated rhodopsin pigments (Table 2.5) showed that some excess retinal could be remaining following regeneration of the ^{13}C labelled rhodopsin samples (see Section **Error! Reference source not found.**). A possible source of the minor components could therefore have been from ^{13}C labelled retinal-oxime associated with the membrane that had not been removed by the β-cyclodextrin washing procedure (Section **Error! Reference source not found.**). However, it would be surprising to observe an excess of non-specifically bound retinal in a *6-s-trans* conformation when 11-*Z*

retinal adopts a 6-*s-cis* conformation in solution [174]. It was also difficult to rationalise why the control sample, control[1], showed better removal of excess retinal when it was prepared in parallel with [8,18-^{13}C$_2$]retinylidene rhodopsin and [8,16/17-^{13}C$_2$]retinylidene rhodopsin. This indicated that the presence of minor components could be a result of contaminants derived from the retinal preparation.

Although it was originally thought that there were only six geometric isomers of retinal (all-*E*, 13-*Z*, 11-*Z*, 9-*Z*, 9,13-di-*Z* and 11,13-di-*Z*) [154] it was later found there were ten more sterioisomers of vitamin A [157, 179]. The binding site appears to be nonstereoselective, capable of accepting singly (7-*Z*, 9-*Z*, 11-*Z*), doubly (7,9-di-*Z*, 7,11-di-*Z*, 7,13-di-*Z*, 9,11-di-*Z*, 9,13-di-*Z*) and triply bent (7,9,11-tri-*Z*, 7,9,13-tri-*Z*) retinal isomers. The notable exceptions are the all-*E* and the 13-*Z* which fail to form stable pigment analogues.

A recent modelling study, in which two of the di-*Z* retinal isomers were modelled into the crystal structure of rhodopsin (PDB entry: 1F88) predicted that the β-ionone ring flips from a 6-*s-cis* to a 6-*s-trans* conformation upon binding of locked di-*Z* retinal isomers (11,13-di-*Z* locked retinal and 9,11-di-*Z* locked retinal) as observed for the minor components in [8,18-^{13}C$_2$]retinylidene rhodopsin and [8,16/17-^{13}C$_2$]retinylidene rhodopsin [85] (Figure 3.23).
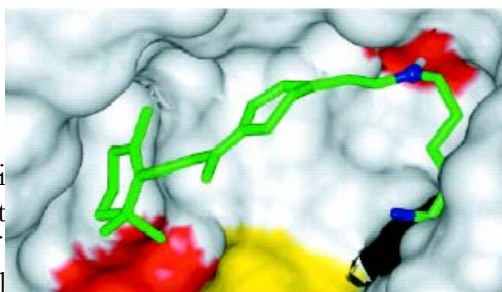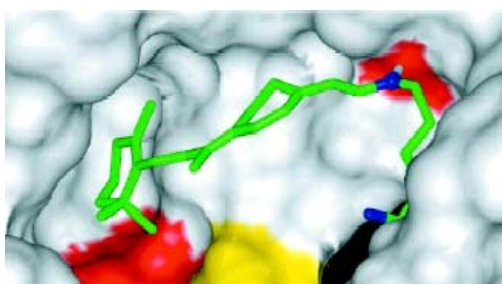
Figure 3.23 – The predi...   ) and 9,11-di-*Z* (bottom panel) locked retinal in t   ]. Nitrogen atoms of the peptide bond and Schiff   ...idues, Glu-113 and Glu-122, are shown in red. Gl...   are modelled in a 6-*s-trans*

Contaminating di-Z isomers that could represent the 6-s-*trans* minor components in [8,18-$^{13}C_2$]retinylidene rhodopsin and [8,16/17-$^{13}C_2$]retinylidene rhodopsin may have originated from the HPLC purification step of the ^{13}C labelled retinals (see Section **Error! Reference source not found.**). Analysis of an analytical HPLC trace of a mixture of retinal isomers, obtained following illumination of all-*E* retinal in acetonitrile, shows that most of the di-Z isomers (9,13-di-Z, 9,11-di-Z, 7,11-di-Z and 11,13-di-Z) have retention times similar to 11-Z retinal [150-152] (Figure 3.24 (a)). Using a lower resolution preparative HPLC to isolate the 11-Z ^{13}C labelled retinal isomers it was likely the di-Z compounds would be collected along with the 11-Z isomer (Figure 3.24 (b)). The combined amount of di-Z isomers would only have to be 2-3% of the total isomeric composition to represent 20-30% of the isomers collected with 11-Z retinal (10-15% yield [206]).
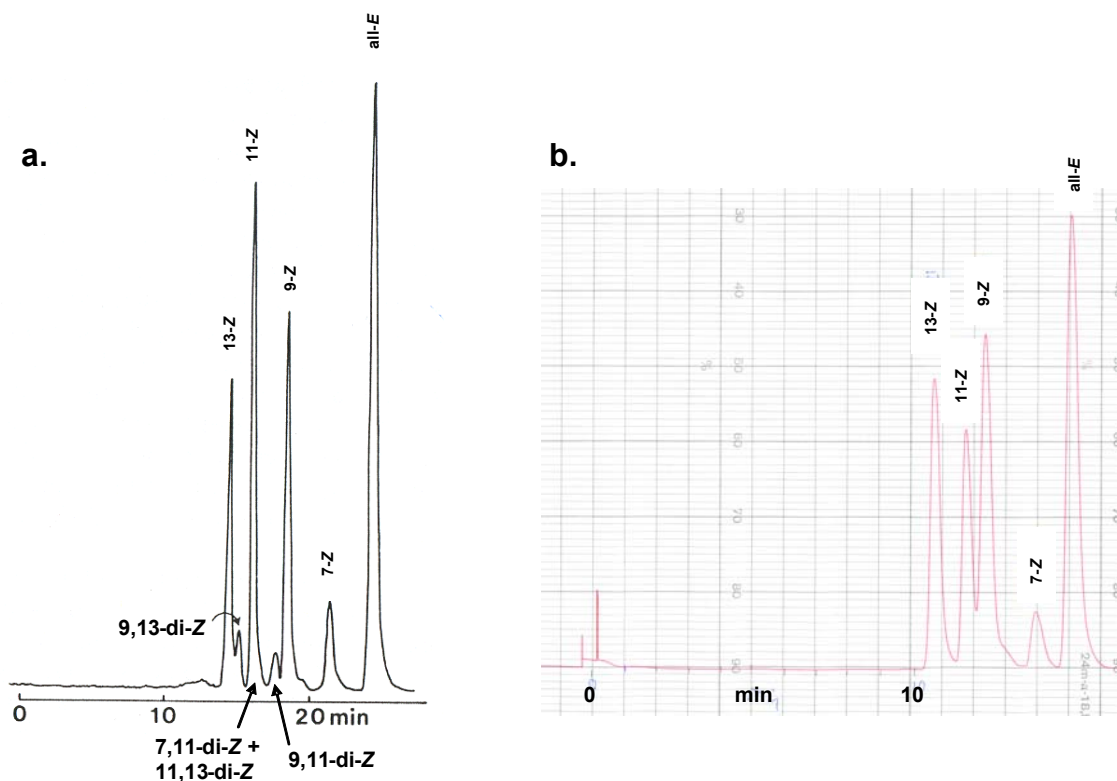
Figure 3.24 – An analytical high performance liquid chromatography (HPLC) trace of a mixture of retinal isomers obtained from irradiation of all-*E* retinal in acetonitrile (Si-60 column, 5% ether in hexane) showing the retention times of di-Z isomers (a) [151]. Preparative HPLC trace used to isolate the [16,17-$^{13}C_2$] 11-Z retinal isomer (b) (silica gel, 1.2

The UV-VIS characterisation of the ^{13}C labelled retinals suggests some di-Z contaminants could have been collected with the 11-Z isomer, particularly for those retinals that yielded rhodopsin pigments with 6-s-trans components ([8,18-[13]C₂] 11-Z retinal and [8,16/17-[13]C₂] 11-Z retinal). Di-Z retinal isomers have similar UV-VIS features to that of 11-Z retinal in hexane but slightly lower λ_{max} values (352-359nm) than 11-Z retinal, which has λ_{max} values reported between 363nm and 365nm [151, 154, 157]. The λ_{max} values recorded for [8,18-[13]C₂] 11-Z retinal and [8,16/17-[13]C₂] 11-Z retinal were 362nm, indicating some additional contaminating isomers were present (see Table 2.2). The $\lambda_{cis}/\lambda_{trans}$ ratio used to estimate the purity of 11-Z retinal after the HPLC procedure would not have been significantly effected by the presence di-Z isomers, as their molar extinction coefficients in hexane are similar to that for 11-Z retinal (26360 M^{-1} cm^{-1} for 11-Z, 18800-34000 M^{-1} cm^{-1} for di-Z isomers) [151].

The limited data on rates of pigment formation [157] show that opsin exhibits an overwhelming preference for the 11-Z and the structurally similar 9-Z isomer (11-Z k_2=5600 $M^{-1}sec^{-1}$ in ROS, 9,13-di-Z k_2=10 $M^{-1}sec^{-1}$ in ROS) so under normal regeneration conditions, when an excess of 11-Z retinal is used in the regeneration procedure, opsin will bind the 11-Z isomer preferentially over any contaminating isomers.

The amounts of [8,16/17-[13]C₂] retinal and [8,16/17-[13]C₂] retinal that were extracted from the HPLC purification were very small (<300nmol), so to obtain sufficient rhodopsin for NMR analysis these retinals were regenerated 1:1 with opsin, in contrast to the 2:1 excess generally used. This could have enabled contaminating di-Z isomers to bind slowly to the opsin once all the available 11-Z isomer had bound during the long regeneration period (~12hrs), resulting in   di-Z rhodopsin pigments that are observed as minor components in [8,16/17-[13]C₂] retinylidene rhodopsin and [8,18-[13]C₂] retinylidene rhodopsin. The rhodopsin pigments

formed by di-Z retinal isomers all have similar UV-VIS characteristics to that of wild-type rhodopsin but with lower λ_{max} values (e.g. 9,13-di-Z retinylidene rhodopsin λ_{max}= 481nm) [155, 157, 207, 208]. The slight displacement of the λ_{max} of [8,18-^{13}C$_2$]retinylidene rhodopsin and [8,16/17-^{13}C$_2$]retinylidene rhodopsin at λ_{max}=496nm is therefore as expected.

If the minor components represent di-Z rhodopsin pigments as predicted, the observation of 6-*s-trans* minor components in [8,18-^{13}C$_2$]retinylidene rhodopsin and [8,16/17-^{13}C$_2$]retinylidene rhodopsin confirms that the di-Z isomers undergo a 6-*s-cis*→ 6-*s-trans* ring-flip upon binding to opsin, as suggested by previous modelling studies [85].

3.6 β-ionone/opsin interactions

The respective axial and equatorial conformations of the C17 and C16 methyl groups deduced from the NMR studies suggest that they are in a protein-induced conformation in the binding site of rhodopsin.

It has been shown that the binding site of rhodopsin can tolerate significant modifications in the retinal structure from the wild-type 11-Z conformation and still form rhodopsin pigments, suggesting that the binding pocket is relatively unspecific regarding the initial binding of the retinal and recognition of the retinal is via a few key interactions [71, 76, 84, 98, 131, 143, 157, 209-212]. Analogue binding studies where modifications were in the region of the β-ionone ring indicated a recognition site existed in this region of the binding pocket. Crouch and Or established that there was a specific recognition site for at least one of the methyls attached to the β-ionone ring [98]. They noticed that stable pigments could be formed from 9-Z acyclic retinals which have at least one β-ionone ring methyl, indicating that it was the methyl groups that were required for forming opsin pigments and not the cyclohexane ring (Figure 3.25 (a-c)). Retinal lacking the C2-C3-C4 portion of the ring

showed almost identical binding characteristics to that of wild type retinal [212] (Figure 3.25 (d)). The cyclohexene ring however, was later shown to be required for full rhodopsin activation [131].

The formation of active rhodopsin pigments from retinal analogues lacking a methyl at C18 (18-demethyl-isorhodopsin) [213] and with an ethyl substituent at the C18 position (18-ethyl-isorhodopsin) [212] indicated this methyl does not participate significantly in an interaction with the opsin apoprotein, suggesting that the main ring/protein interaction emanates from
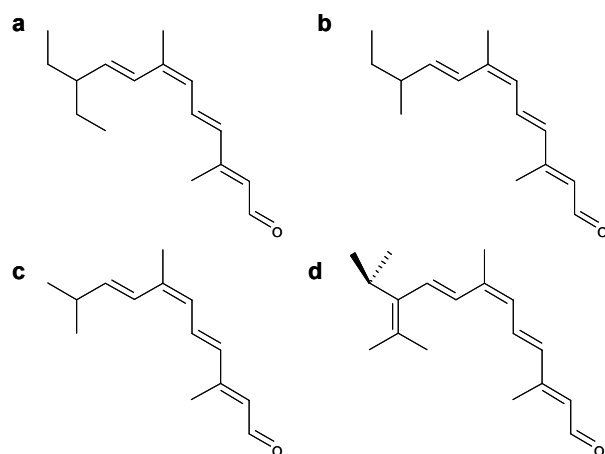
the C16/C17 methyl groups.

Inspection of the crystal structure of rhodopsin showed that the C18 methyl lies in a tight cleft formed by Gly-121, Glu-122 on helix 3 (H3) and Trp-265 and Phe-261 on helix 6 (H6), as illustrated in Figure 3.26 [42]. It is positioned within 3.7Å of both Gly-121 and Trp-265 (supporting information [34]).

Biochemical studies have identified these residues as being important for ligand binding and receptor activation. In a mutagenesis study of rhodopsin Han *et al* showed that substitutions of Gly-121 with amino acids containing progressively larger side chains caused a progressive

Figure 3.25 – 9-*Z* retinal analogue with methyl groups at the C1 and C5 positions (a and b) form rhodopsin pigments. No pigment is obtained with the unmethylated derivative (c) [98]. Removal of the C2-C4 portion of the cyclohexane ring yields a rhodopsin pigment with similar UV-VIS characteristics to the native 11-*Z* retinal (d) [212].

blue-shift in the λ_{max} value of the pigment, a decrease in thermal stability, an increase in reactivity with hydroxylamine and a relative reversal in the selectivity of opsin for 11-Z retinal over all-E retinal [113]. They also showed that the loss of function phenotypes of the Gly-121 mutants could be partially reversed by specifically replacing Phe-261 by alanine as a second site mutation. It was concluded that Gly-121 and Phe-261 formed part of the retinal binding pocket responsible for receptor activation [112].

Two cross-linking studies, using an unlocked and flexible 11-Z retinal analogue with a photoactive diazo ketone moiety at the C3 position on the β-ionone ring, identified Trp-265 exclusively as the cross-linked residue, concluding that it was directly involved in ligand binding [84, 115]. Considering the sensitivity to changes in the protein structure around the C18 methyl group and the apparent constrained nature of the binding pocket from the crystal structure, it was somewhat surprising to find that retinal with large substituents at the C18 position could be accommodated within the binding pocket.
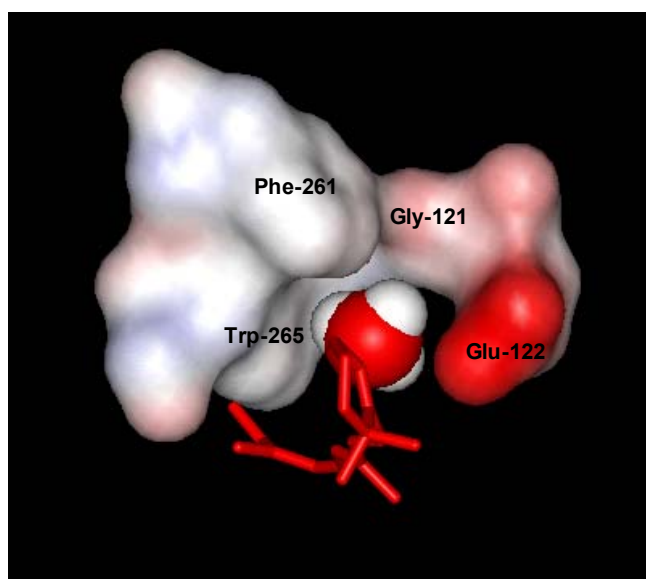
Figure 3.26 – Model of the binding region around the C18 methyl taken from the crystal structure of rhodopsin (PDB entry: 1HZX), showing the solvent accessible surface (1.4Å probe) of the residues that form a binding cleft around this methyl. Positively charged regions are shown in blue and negatively charged regions in red. The methyl

A hypothesis that satisfies this discrepancy has recently been provided by Lewis *et al* [76]. In a time-resolved UV-VIS spectroscopy study they showed that 18-demethyl-isorhodopsin displays a conventional build-up of the batho intermediate and decay to BSI intermediate. This was surprising as the steric hindrance between C18 methyl on the ring and C8 on the polyene chain is thought to serve as the primary barrier to the movement of C8 upon photoisomerisation, so stabilizing the bathorhodopsin state. They suggested that the β-ionone ring in 18-demethyl-isorhodopsin binds with a *6-s-cis*→ *6-s-trans* ring-flip, so that the C16/C17 methyls replace the C18 methyl in its interaction with the C8-hydrogen and preserves the steric barrier to batho decay. This manifests itself in a blue-shifted λ_{max} for the resulting rhodopsin pigment (474nm) with respect to isorhodopsin (490nm) as a result of the increased twist around the C6-C7 bond, which would not be expected in a sterically unhindered *6-s-cis* conformation.

Pigments formed from retinal analogues with added bulk in the place of the C18 methyl (18-ethyl and 18-propyl rhodopsin) also showed blue-shifted λ_{max} values (475nm and 458nm, respectively) [212]. In pigments modified at the C18 position, rotation around the C6-C7 bond to a 6-*s-trans* conformation could position the C16 methyl in the cleft formed by the Gly-121, Trp-265, Phe-261 triad, so that the large moieties at the C18 position may occupy the much more relaxed region of the binding site previously occupied by the C17 methyl group (see Figure 3.27).

A similar binding arrangement could enable the di-*Z* retinal isomers to bind in a 6-*s-trans* conformation. All the rhodopsin pigments formed with di-*Z* retinal isomers and C18 modified retinal analogues showed anomalously slow regeneration rates, on the order of a 100 times slower than that for unmodified 11-*Z* retinal [76, 157, 212]. This suggests the smaller chemical shift separation observed for C16 and C17 in a 6-*s-trans* β-ionone ring conformation, resulting from di-*Z*-retinylidene represent an unfavourable, less distorted axial/equatorial binding arrangement for the C16/C17 methyl groups.
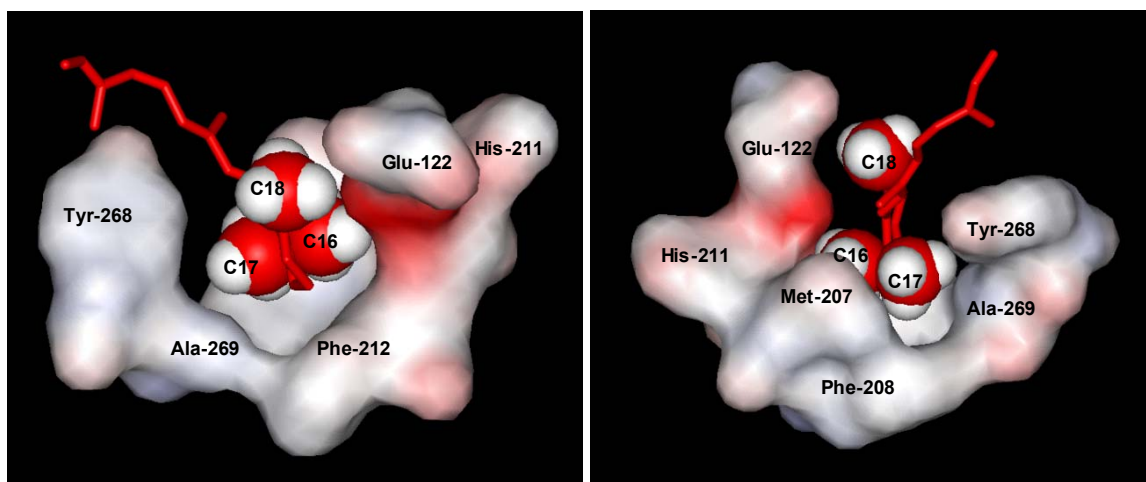
Figure 3.27 – Model of the binding region around C16 and C17 methyls from two orientations, showing the solvent accessible surface (1.4Å probe) of residues within 5Å of the C16/C17 groups. Positively charged regions are shown in blue and negatively charged regions in red. The methyl groups of the retinal are shown in space-filling CPK style to show the comparatively relaxed binding pocket around the C16 and C17 methyls.

Collectively, these results indicate that in the dark state the C18 methyl forms a key binding interaction with opsin, in the pocket formed by residues Gly-121, Glu-122, Phe-261 and Trp-265 from H3 and H6. The reduced twist (-28° ±7) of the C8-C7-C6-C5 torsion deduced in this study compared to that observed in the crystal structure (-55°) may position the C18 methyl closer towards the ring of Trp-265. The reduced twist around the C6-C7 would also position C16 in close contact with Glu-122 (~2.5Å) and Met-207. These residues are likely to form a restraint that forces C17 and C16 into their respective axial and equatorial conformations, possibly to avoid steric hindrance or possibly to position the C16 methyl so it may form an interaction with Glu-122.

Speculatively, the interactions between the C18 and the protein may include a CH···π interaction, with Trp-265. These are weak attractive forces working between CH groups and π-systems where the hydrogen is positioned above the plane of an aromatic ring or double bond [214](Figure 3.28). They have been predicted to be involved in receptor-ligand interactions [215]. A reduced torsion around C6-C7 would lead to a closer interaction with

Trp-265 and a stronger CH··· π interaction. Van der Waals interactions are also likely and have been predicted between Gly-121 and Phe-261, via the chromophore [36, 112, 113]. From the crystal structure this would appear to involve the C18 methyl group.

The β-ionone ring is ideally positioned to participate in an offset stacked π··· π interaction with the indole ring of Trp-265, approximately 4Å apart, which could yield ~1kcal/mol per interaction. The nature of the interaction between the β-ionone ring and the protein will be the focus of future work (Section 7.2).
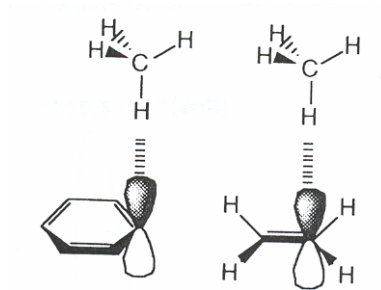
Figure 3.28 – Preferred geometries for CH··· π interactions.

3.7 Conclusions

Rotational resonance NMR internuclear distance measurements between C8 and the β-ionone ring methyls have been used to deduce *directly* a 6-*s-cis* conformation for the β-ionone in the chromophore of rhodopsin, in agreement with previous crystallographic, ^{13}C chemical shift and spectroscopic data. The geometry of the β-ionone ring region of the chromophore has been determined at atomic resolution, revealing a modest torsional twist around the C6-C7 bond (-28±7°).

The C17 and C16 methyl groups have been shown to adopt a characteristic axial and equatorial conformation respectively in the bound 6-*s-cis* chromophore, reflected in a ~4.5ppm chemical shift separation and equidistant internuclear measurement between C8

and both C16 and C17 methyl groups. The conformational distinction between these methyls represents a significant protein-induced perturbation upon chromophore binding.

Analysis of the crystal structure in the region of the β-ionone ring indicates that by adopting a negatively twisted 6-*s*-*cis* conformation the methyl groups may participate in key binding interactions with residues of the opsin binding pocket. The C18 methyl appears to form interactions with residues on H3 and H6 that may stabilise the ground state structure.

The observation of 6-*s*-*trans* minor components showed that the β-ionone ring *can* bind in a 6-*s*-*trans* conformation to enable opsin to accommodate the sterically strained di-Z isomers or ring modified retinal analogues. However, the observation of a characteristic C16/C17 methyl chemical shift separation for the native 11-Z chromophore showed the β-ionone ring binds exclusively in a 6-*s*-*cis* conformation in rhodopsin.

The atomic resolution structure of the β-ionone ring region of retinylidene should enable crucial insights into the binding of the chromophore and its role in the activation mechanism of rhodopsin.

Chapter 4   Trapping the meta-I photointermediate in rhodopsin in ROS membranes

4.1 Introduction

Once the geometry of the β-ionone ring of rhodopsin had been determined in the dark state it was intended to repeat the internuclear distance measurements in the meta-I photostate. This would require trapping the [8,18-^{13}C$_2$]retinylidene rhodopsin and [8,16/17-^{13}C$_2$]retinylidene rhodopsin samples in their respective meta-I photointermediate states in a stable form, suitable for study by NMR.

The identification of a major and minor population of retinal within these samples had already complicated the analysis of the rotational resonance (RR) NMR data in the dark state. If useful RR NMR data was to be obtained for the meta-I photostate as complete a conversion to the meta-I intermediate as possible would be required. The methods for generating the meta-I photointermediate were therefore investigated.

The meta-I photointermediate was first identified by Broda and Goodeve in 1941 [216]. An intermediate was observed which formed when rhodopsin absorbed light with an absorption maximum 5nm to the blue of that of rhodopsin, with a higher extinction coefficient. This intermediate was stable at temperatures below -50°C and was called lumi rhodopsin. Above -50°C lumi rhodopsin was converted to another intermediate with a spectral maximum of 478nm, called meta rhodopsin. It wasn't until 1963, when the meta-I/meta-II equilibrium was established by Matthews *et al*, that the meta-I photointermediate state was fully characterised [217].

The method used by Matthews *et al* to trap the meta-I photointermediate was to cool solubilized rhodopsin to -20°C in the presence of glycerol to prevent freezing, and illuminate briefly with green light (>530nm). It was noted that the product of the illumination was not just meta-I rhodopsin as previously thought [218] but a heterogeneous mixture of rhodopsin, meta-I and isorhodopsin [219]. With prolonged illumination the proportion of rhodopsin and isorhodopsin was found to increase, indicating that these components were the product of photoisomerisation in the light, so called *photoregeneration*. A steady-state equilibrium was found to form between these photoproducts upon illumination, based on the relationship illustrated in Scheme 4.1:

$$\text{rhodopsin} \underset{}{\overset{light}{\rightleftharpoons}} \text{meta-I rhodopsin} \underset{}{\overset{light}{\rightleftharpoons}} \text{isorhodopsin} \qquad \text{Scheme 4.1}$$
$$(11\text{-}Z) \qquad\qquad (\text{all-}E) \qquad\qquad (9\text{-}Z)$$
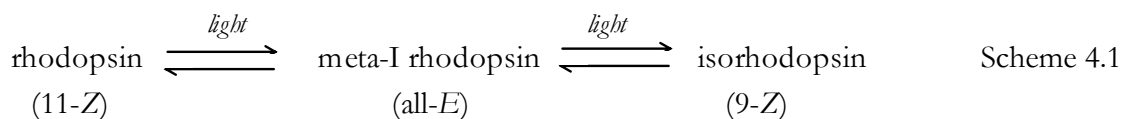
The term meta-I rhodopsin corresponds to the *labile* fraction of the mixture of stereoisomer which will pass through to meta-II upon warming above -20°C. As the absorption maxima of rhodopsin (11-*Z*) , isorhodopsin (9-*Z*) and meta-I rhodopsin (all-*E*) lie at progressively

shorter wavelengths (see Figure 4.1) it was predicted the steady-state mixture of these compounds would vary depending on the wavelength of light used to irradiate them; orange light, absorbed preferentially by rhodopsin would favour the formation of meta-I rhodopsin, whereas blue light absorbed preferentially by meta-I rhodopsin would produce more rhodopsin and isorhodopsin (Figure 4.1) [219, 220].
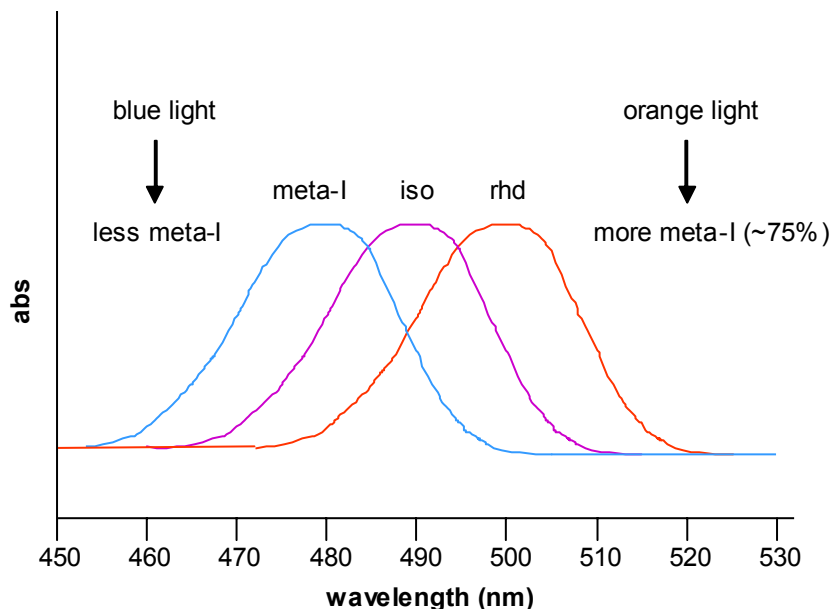
Figure 4.1 – Schematic representation of the UV-VIS spectra of meta-I, rhodopsin (λ_{max}=480nm), isorhodopsin (λ_{max}=490nm) and rhodopsin (λ_{max}=500nm), the products of the steady-state mixture formed following exhaustive irradiation of rhodopsin at -20°C. The components have different absorption coefficients, not represented here. Illumination with light at long wavelengths results in a greater proportion of meta-I, whilst illumination with shorter wavelength light results in more isorhodopsin and

Analyses of steady-state mixtures produced by irradiation at 450, 500 and 550nm confirmed this prediction [219]. Following prolonged illumination with monochromatic light at 550nm, 75% meta-I rhodopsin could be generated, compared to only 50% using the shorter wavelength filter (450nm). This method of preparing meta-I is referred to as the "direct" method in this study.

An additional method for accumulating the meta-I photointermediate was identified

following the identification of the bathorhodopsin intermediate. Yoshizawa and Kito detected a precursor to lumirhodopsin which was stable below -140°C [221]. This intermediate was named prelumirhodopsin by Yoshizawa and Wald [58] but was later named bathorhodopsin, since it has a red-shifted, or bathochromically-shifted spectrum (λ_{max}=543nm). As with meta-I rhodopsin, prolonged illumination to form bathorhodopsin resulted in the photoregeneration of isorhodopsin, along with bathorhodopsin and rhodopsin in a steady-state mixture of isomeric pigments, shown in Scheme 4.2:

rhodopsin $\underset{\longleftarrow}{\overset{\textit{light}}{\longrightarrow}}$ bathorhodopsin $\underset{\longleftarrow}{\overset{\textit{light}}{\longrightarrow}}$ isorhodopsin   Scheme 4.2

(11-*Z*)   (all-*E*)   (9-*Z*)

↓
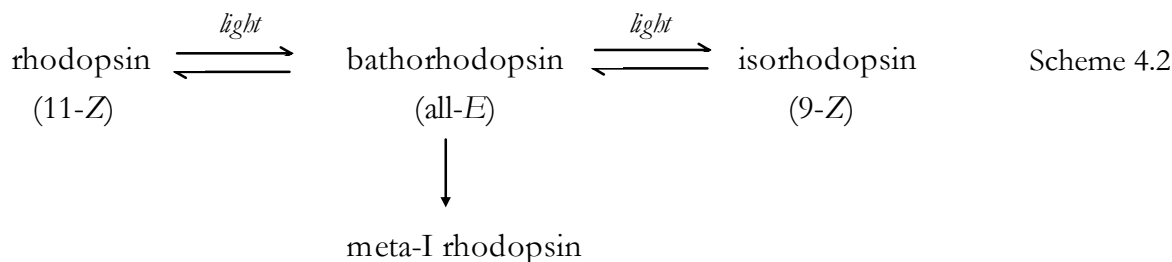
meta-I rhodopsin

In the same way that the rhodopsin/isorhodopsin/meta-I equilibrium could be manipulated by the wavelength of the incident light, the proportion of the steady-state mixture of intermediates was dominated by those isomers for which the absorptions lay furthest away from the incident wavelength. Thus, irradiation with blue light drove the mixture predominantly towards the bathorhodopsin component, whereas irradiation with orange/red light drove it towards the isorhodopsin component (Figure 4.2) [58]. It was later shown that prolonged illumination at wavelengths longer than 560nm could generate as much as 88% isorhodopsin within the steady-state mixture [222].

Various studies have involved accumulating the bathorhodopsin intermediate using blue light illumination on ROS suspensions or solubilized rhodopsin [72, 223, 224]. A study by Susuki and Callender to determine the relative quantum yields of the

rhodopsin/bathorhodopsin/ isorhodopsin photoreactions found a maximum of 59% bathorhodopsin could be achieved following illumination with light at 458nm [224]. Once trapped, the bathorhodopsin portion of the mixture could be thermally converted to meta-I rhodopsin via lumirhodopsin, by warming to between -50°C and -20°C in the dark [223]. The amount of meta-I rhodopsin generated by this method, the so-called "indirect" method, equals the amount of bathorhodopsin generated in the steady-state mixture at -190°C i.e. a maximum of ~60%.
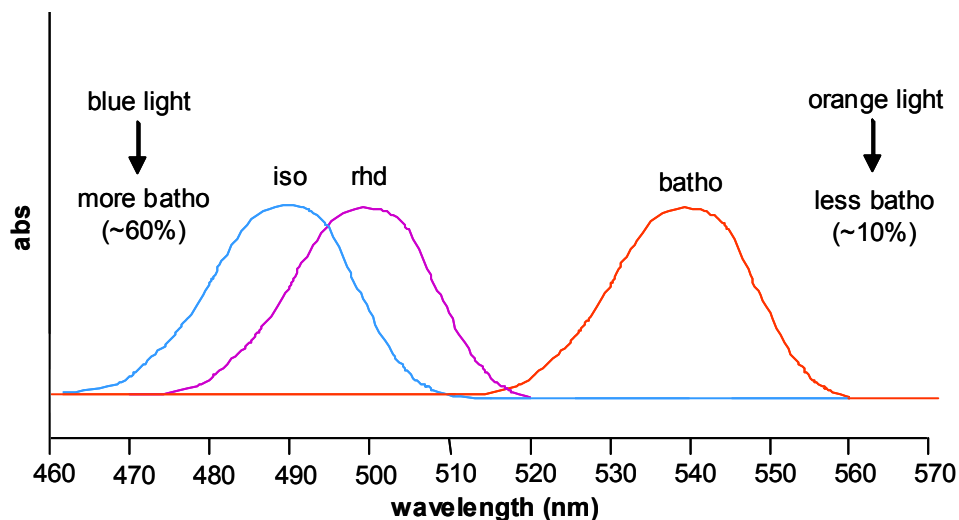
Figure 4.2 – Schematic representation of the UV-VIS spectra of bathorhodopsin (λ_{max}=540nm), rhodopsin (λ_{max}=498nm) and isorhodopsin (λ_{max}=490nm), the products of the steady-state mixture formed following exhaustive irradiation of rhodopsin at -190°C. The components have slightly different absorption coefficients, not shown here. Illumination with light at long wavelengths results in a greater proportion of isorhodopsin, whilst illumination with shorter wavelength light results in more bathorhodopsin and

From these UV-VIS studies on ROS suspensions and solubilized rhodopsin solutions the "direct" method of generating meta-I would therefore appear to be the preferable method for generating the greatest proportion of meta-I intermediate.

Despite the UV-VIS evidence favouring the "direct" method of trapping meta-I rhodopsin, NMR samples have been previously generated using the "indirect" method [78-80]. This has

involved immersing the NMR rotor in liquid nitrogen and illuminating for a prolonged period (10-20hrs) with white light, then incubating in the dark at -20°C so the labile bathorhodopsin fraction is converted to meta-I rhodopsin. In two of these studies the conversion rate to meta-I was estimated by observing a chemical shift change for the C10 ^{13}C resonance on the polyene chain of retinylidene that occurs upon the rhodopsin to meta-I transition [78, 79]. By measuring the proportion of meta-I shifted resonance using Lorenztian line-fitting, estimates of the proportion of meta-I photointermediate of ~50% [79] and ~74% [78, 133] were reported. The proportion of meta-I reported by Verdegem *et al* was greater than any previously measured by UV-VIS spectrophotometry, which is surprising considering that white incident light was used, which had been previously shown to produce less meta-I than blue light [58, 224]. It was assumed that the value measured by Verdegem *et al* was an overestimate, as a result of deconvoluting the C10 resonances in the unsubtracted CP-MAS NMR spectrum. The estimate made by Feng *et al* (~50%) was measured from the double-quantum filtered NMR spectrum of [10,11-^{13}C$_2$]retinylidene meta-I rhodopsin with visible signal derived only from the coupled ^{13}C$_2$ spin pair labels and is therefore likely to represent a more reliable value. In any of the NMR studies on meta-I rhodopsin no account was made for an isorhodopsin component, which would be expected to form following illumination.

No improvement in the proportion of trapped bathorhodopsin was observed when blue light was used to illuminate a C8 ^{13}C labelled NMR rhodopsin sample [73]. By linefitting the C8 resonance in the subtracted CP-MAS NMR spectrum of [8-^{13}C]retinylidene bathorhodopsin a 50% conversion was reported, equalling the value reported by Feng *et al*. It is likely that the lack of an improvement in the conversion rate was a result of incomplete bleaching of the rhodopsin sample, caused by illuminating the rhodopsin through the wall of

the NMR rotor.

From previous UV-VIS experiments it appeared that an approximate 75% meta-I yield could be achieved following direct production of meta-I rhodopsin at -20°C using long wavelength (>550nm) illumination. Although this method had not been attempted on frozen rhodopsin NMR samples it was expected to result in an improvement over the amount of meta-I rhodopsin produced from the "indirect" method, estimated at approximately 50% at present [79]. It also appeared that the "indirect" method for trapping meta-I in NMR samples required further characterisation. Ambiguities regarding the presence of photoregenerated isorhodopsin and variations in the proportion of trapped meta-I indicated the need for a more detailed investigation.

4.2 Aims

The primary aim of this study was to establish an optimal set of conditions for trapping the meta-I rhodopsin intermediate in frozen rhodopsin samples in ROS membranes for subsequent NMR studies. By varying the method of illumination, the wavelength of the incident light, the length and power of illumination and the temperature, the proportion of meta-I generated could hopefully be improved from current levels. Both the "direct" and "indirect" methods of meta-I trapping were intended for investigation, although initially the "direct" method would be focused on, as a result of the predictions made from UV-VIS spectrophotometry studies.

It was initially intended to use UV-VIS spectrophotometry to determine whether the meta-I conversion rates previously obtained for the "direct" method of meta-I trapping on solubilized rhodopsin could be repeated on ROS membranes [219, 220]. The optimum established light conditions would then be used as preliminary conditions for studying the

trapping of meta-I rhodopsin in frozen rhodopsin samples.

An aim of this study was to see how the photolytic behaviour of dilute ROS suspensions compared with frozen rhodopsin in ROS membranes, which are densely packed into NMR rotors. Additional factors, such as the intensity and duration of the illumination required for maximal bleaching of the rhodopsin would be investigated.

It was proposed to monitor meta-I production within the frozen rhodopsin samples using CP-MAS ^{13}C NMR on [10,20-^{13}C$_2$]retinylidene rhodopsin, as used in previous studies [78, 79]. The aim was to prepare rhodopsin ROS NMR samples regenerated with 11-Z retinal ^{13}C labelled at the C10 and C20 positions, illuminate them within the NMR rotor and use the chemical shift change observed for either the C10 or C20 methyl resonance to observe the rhodopsin to meta-I phototransition[1]. Lorenztian linefitting would be used to quantify the proportion of rhodopsin converted to meta-I, using spectral subtraction of the unlabelled membrane background to leave the NMR signal derived solely from the ^{13}C labelled resonances, in the same manner as for the RR NMR measurements on the dark state protein (see Section **Error! Reference source not found.**). As long as the sample temperature could be kept below the illumination temperature the sample could be transferred between the NMR magnet and the illumination apparatus, allowing repeated illuminations on the same sample if required.

The advantage of this method was that it provided a direct measurement of meta-I conversion rate whilst being completely non-evasive, therefore, the conditions and

---

[1] It was subsequently found that the C20 region of the NMR spectrum offered the "cleanest" and most reliable portion of the NMR spectrum for subtraction so the C20 chemical shift response was used.

conversion rates established in the study could be transferred reliably to any future samples.

Another aim of this study was to design an improved experimental setup for illuminating rhodopsin samples for NMR studies. Previous methods had involved illuminating the NMR rotor immersed in a bath of liquid nitrogen, typically from a halogen light source positioned some distance (>10cm) from the sample [78, 122].

To enable variations in the power and wavelength of the incident light, an experimental setup was required where light of precise wavelength and power could be administrated. A method of monitoring and maintaining a stable sample temperature was also required and preferentially, the illumination would be directly on the sample rather than through the wall of the NMR rotor, enabling a more efficient conversion of the rhodopsin.

Using advances in the experimental set-up and exploring variations in the trapping method, illumination power, wavelength and temperature the aim of this study was to improve the level of conversion of rhodopsin to meta-I. However, by using a non-evasive method for monitoring the generation of meta-I, it was expected to be at least possible to quantify accurately the conversion rate and so enable RR NMR distance measurements for the $[8,18-^{13}C_2]$retinylidene rhodopsin and $[8,16/17-^{13}C_2]$retinylidene rhodopsin in the meta-I state.

4.3 Material and methods

4.3.1 Apparatus for the illumination and temperature control of rhodopsin NMR samples

4.3.1.1   Temperature control

Trapping of the meta-I photointermediate in rhodopsin NMR samples using the "direct" method required illuminating the sample at approximately -30°C (see Section 4.1). As the

meta-I intermediate had not been previously trapped in NMR samples at -30°C a new method of maintaining this stable sample temperature was required. A copper block (85mm x 60mm; Workshop, Biochemistry Department, University of Oxford) was designed with a 4.1mm hole through the middle that could just fit the full length of a 4mm Chemagnetics MAS NMR rotor. A thermocouple (TC Ltd Type T mineral insulated thermocouple, 2mm x 150mm) connected to an electronic thermometer (TC Ltd) was positioned through a hole in the top of the block so that the tip rested against the NMR rotor (Chemagnetics 4mm MAS NMR rotor) in the centre of the block (Figure 4.3).

By adding solid CO_2 (dry-ice) pellets to a stirred aqueous solution of 35% w/w $CaCl_2$, a temperature of -30°C could be achieved at its melting point, which was used to cool the copper block by placing the bottom 2cm of the block in the cooled liquid. In this way the block was cooled to the temperature of the cooling solution whilst keeping the NMR sample completely clear of the salt solution. To test the temperature conductance of the block to the sample, a fine thermocouple (TC Ltd Type T mineral insulated thermocouple, 0.5mm x 150mm) was embedded in a ROS membrane sample in an NMR rotor and the assembly placed in the cooled copper block. Almost immediately (<30s) the temperature of the sample equilibrated to that of the copper block ($\pm$ 0.2°C) showing that the NMR samples could be cooled effectively to the stable temperature (-30°C) required for trapping the meta-I intermediate. A similar response was observed when the block was placed in liquid nitrogen with the sample very quickly equilibrating to almost the liquid nitrogen boiling temperature (<-188°C).

2mm x 150mm thermocouple touching the NMR rotor

fibre optic light-guide

hole for 4mm NMR rotor and light-guide (tip diameter 5mm)

cooling solution (either solid CO_2 + 35% w/w $CaCl_2$ solution or liquid N_2)

0.5mm x 150mm thermocouple embedded in a packed rhodopsin sample
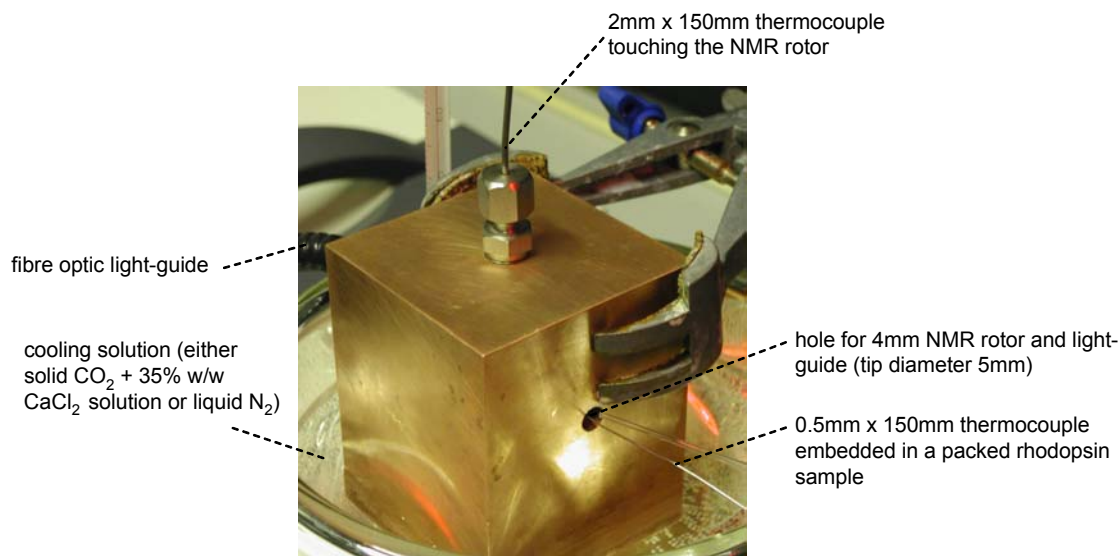
Figure 4.3 – Apparatus used for cooling the rhodopsin NMR samples packed in 4mm Chemagnetics NMR rotors, showing the setup used to test the temperature conducting properties of the system. The apparatus allowed rapid and precise temperature control of

4.3.1.2 Light administration

To illuminate the NMR sample in the block a novel approach was used. A 250W halogen lamp (Schott KL 2500 LCD) was used as a light source, fitted with an infra-red filter to give "cold light" which was focused through a pair of glass fibre optic light guides (Schott 5mm x 1000mm light guide). The copper cooling block had a wider (5.1mm) aperture at either end of the hole containing the NMR rotor so that the light guides could be positioned flush to the rotor ends. By removing the plugs and fins from the NMR rotor, the sample could be illuminated directly with homogenous light of variable intensity and, with a filter (25mm diameter; see Section 4.3.1.3) positioned in the filter wheel any specific wavelength of incident light could be chosen (shown in Figure 4.4). The light intensity was controlled using an electronic dimmer to reduce the colour temperature, and is stated in Kelvin. To test the heating effect of the lamp a fine thermocouple (TC Ltd Type T mineral insulated thermocouple 0.2mm x 150mm) was embedded directly into a rhodopsin sample packed in

an NMR rotor and the temperature recorded with varying light intensity. Even though the light was intended to be "infra-red free" a small ($<3^{\circ}$) amount of heating was measured with the lamp on full power (3300K) at -30°C. The apparatus with the light guides attached was not initially cooled to -190°C for fear of damaging the light guides, however they were later found to withstand this temperature with little heating of the sample upon illumination($<3^{\circ}$).

4.3.1.3 Filters

One aim of the study was to optimise the wavelength of the incident light used for trapping the meta-I photointermediate. Variations in the wavelength of the incident light were
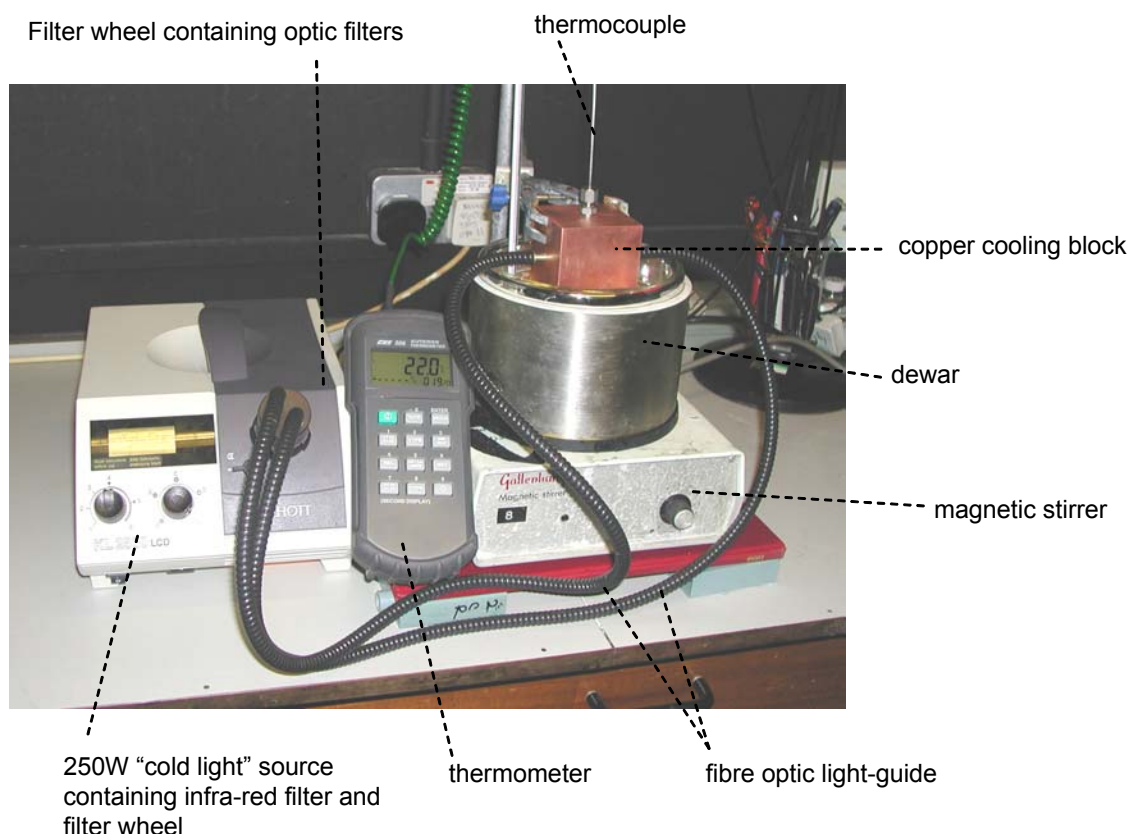
Figure 4.4 – Apparatus used for trapping rhodopsin samples in NMR rotors in the meta-I photointermediate state. Cold light of specific wavelength was passed down fibre optic light-guides to the cooled NMR sample within the copper block. The temperature of the sample could be monitored using a thermocouple touching the NMR rotor and controlled within $\pm$ 0.5°.

achieved by positioning different optical filters in a filter wheel in the light path between the halogen bulb and the fibre optic light guides. A variety of 25mm diameter filters were used (Melles Griot), falling into three different classes: short-pass (SP), long-pass (LP) and band-pass (BP).

Short-pass cut-off filters are fabricated with a wavelength-selective coating on a fused-silica substrate and transmit all wavelengths of light above a specified wavelength. They make the transition from virtually total blocking to virtually total transmission within a few nanometres.

Long-Pass cut-off filters made with coloured glass, have a similar but opposite effect to short-pass filters, permitting light to pass above a defined wavelength. Narrowband interference filters permit isolation of wavelength intervals of a few nanometres in width, without dispersion gratings or prisms. They are multilayer thin-film devices that operate on the same principles as Fabry-Perot interferometers, which rely on the interference of multiple reflected beams. The main criteria for selecting an interference filter are the peak transmission wavelength, and the full-width-half-maximum (FWHM or bandwidth) of the transmission band. For a narrowband filter, the FWHM is 10nm or less.

The UV-VIS transmission spectra of the long-pass, short-pass and interference filters used in the study are shown in Figure 4.6 (a-c), respectively, and the optical properties are recorded in Table 4.1.
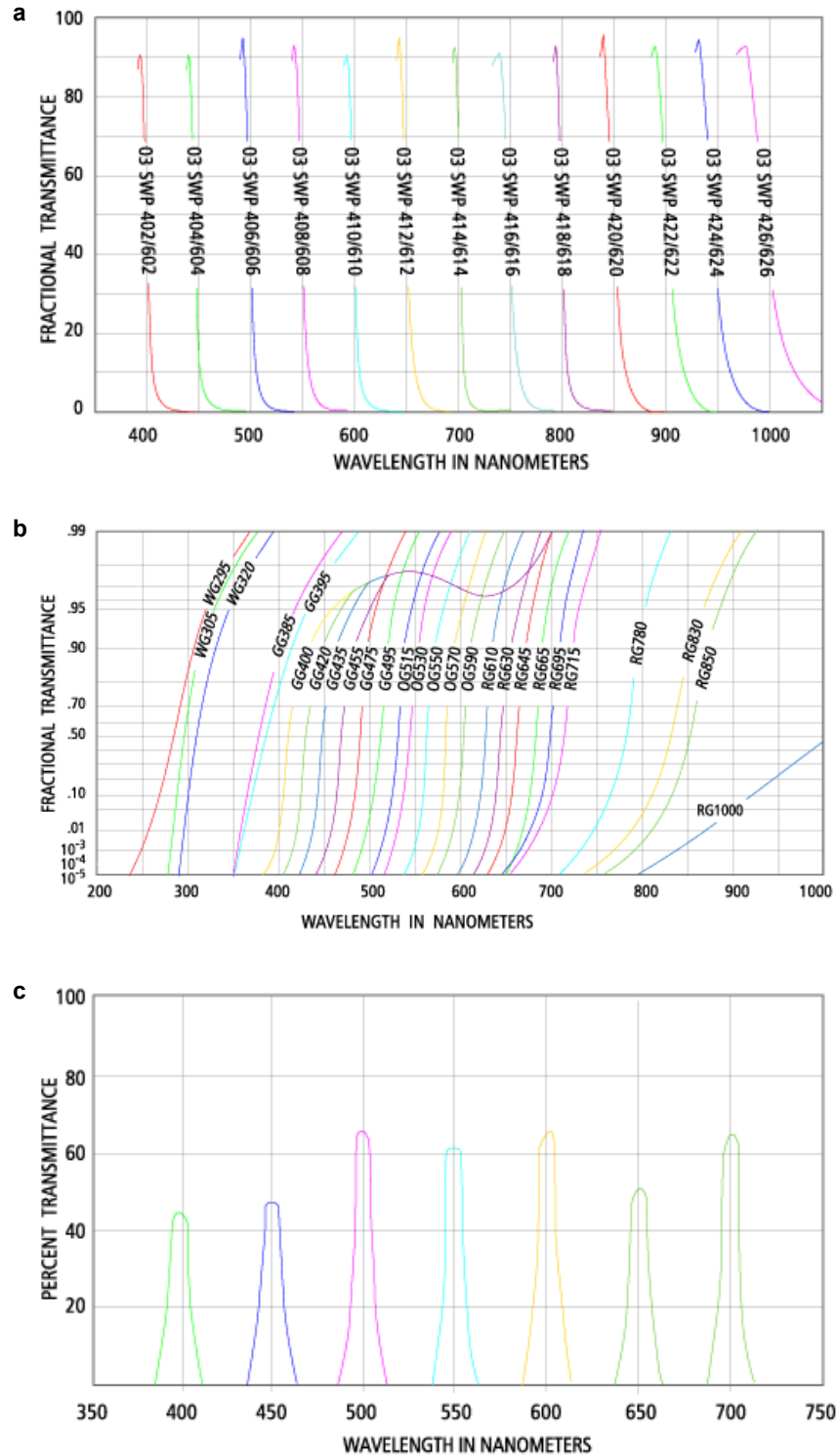
Figure 4.5 – UV-VIS transmission spectra of short-pass (a), long-pass (b) and interference filters (c) used for the illumination of rhodopsin to the meta-I photointermediate state. Filter 03 SWP 606 was used from the short-pass filter range and OG455, OG530, OG550, OG570, OG590 and RG610 out of the long-pass filters. The fractional transmittance does not correspond to the % Transmission, which was in the region of 90 ±3% throughout. FWHM of the intereference filters were ~10±2nm throughout with % Transmission of ~50%. Taken from Melles Griot product catalogue.

Table 4.1. – Summary of the UV-VIS properties of the optical filters used for trapping meta-I rhodopsin.

Filter	Type	Peak transmission/cut-off wavelength (nm)	FWHM (nm)	Peak transmission (%)
450BP	Interference	450	8 ±2	40
550BP	Interference	550	10 ±2	50
455LP	Long-pass	455	–	90
530LP	Long-pass	530	–	90
550LP	Long-pass	550	–	90
570LP	Long-pass	570	–	90
590LP	Long-pass	590	–	90
610LP	Long-pass	610	–	90
505SP	Short-pass	505	–	90

4.3.2 NMR details

All NMR measurements were conducted at 125.8MHz for ^{13}C and 500.1MHz for protons using a Chemagnetics (Varian) Infinity spectrometer. A 4mm double resonance Chemagnetics Apex MAS probe was used at -80°C. The temperature was controlled ±1° using a Chemagnetics temperature controller. Spinning was maintained at ±3Hz throughout the experiments using a Chemagnetics spinning speed controller.

CP-MAS spectra of rhodopsin samples were acquired with a 30% linear ramp [197] on the output for the carbon frequency and with 63kHz proton decoupling. Field strengths for ^{13}C were around 63kHz throughout.

All data was processed using Felix Desktop 2002 from Accelrys. The data were stored in 1024 points and prior to Fourier transformation the FIDs were zero-filled up to 8192 points. Exponential linebroadening was typically in the region of 70Hz. The background ^{13}C signal

of the rhodopsin membrane was removed by subtracting a CP-MAS spectrum acquired from an unlabelled rhodopsin ROS membrane sample, prepared under identical conditions as the ^{13}C labelled material. This resulted in signal derived only from the ^{13}C labelled nuclei within the bound retinal chromophore.

Chemical shifts were referenced to an external standard for the methylene resonance of adamantane, measured 38.6ppm downfield from TMS.

4.4 Results

4.4.1 UV-VIS spectrophotometry of meta-I rhodopsin in ROS suspensions

4.4.1.1 Introduction

The initial attempts to trap meta-I was by accumulating the meta-I intermediate "directly". It had previously been shown that 75% meta-I rhodopsin could be generated in a photosteady mixture of rhodopsin, isorhodopsin and meta-I rhodopsin at -20°C, following exhaustive illumination with filtered light (550BP filter, FWHM 11nm) that was preferentially absorbed by the rhodopsin component [219, 220]. The first aim of the study was to see whether these results, conducted on solubilized rhodopsin-digitonin preparations in the presence of glycerol (0.3% digitonin in 67% glycerol), could be repeated on rhodopsin in low-lipid ROS membranes in isotonic buffer.

During the preparation of the rhodopsin samples excess retinal bound to protein and lipid residues had been removed by consecutive extractions with heptakis-2,6-di-O-methyl-β-cyclodextrin (Section **Error! Reference source not found.**), a glycoside which produces a soluble inclusion complex upon binding with retinal and retinal-oximes [167]. These conditions are known to decrease the lipid content of the phospholipid bilayer [166]

resulting in partial blocking of the meta-I to meta-II transition in the photosequence by reducing the membrane fluidity [166, 225, 226]. FTIR measurements and UV-VIS measurements on rhodopsin samples prepared by this method indicated that the formation of the meta-I intermediate was unaffected by the reduction in membrane lipids [156].

The aim of this study was not to obtain precise kinetic data on the trapping of the meta-I intermediate in this lipid system, but to show that it was worth attempting the "direct" method of meta-I trapping on the NMR samples. Additionally, establishing the optimal wavelength of light would be preferable at this stage on unlabelled rhodopsin rather than on expensive and precious ^{13}C labelled material.

4.4.1.2 Sample preparation

A ROS sample was prepared following the procedure described in Section **Error! Reference source not found.**, yielding a sample with good UV-VIS characteristics (Abs_{500}/Abs_{280}=2.2; Abs_{400}/Abs_{500}=0.25). The ROS sample was split into three aliquots and the following samples prepared:

1. Regenerated ROS – ROS regenerated with unlabelled 11-*Z* retinal, with excess retinal removed by extraction with β-cyclodextrin, following the procedure described in Section **Error! Reference source not found.**. ~25nmol rhodopsin in buffer B (10-15μM).

2. "Low-lipid" ROS – ROS with no regeneration step, but washed with β-cyclodextrin following the procedure in Section **Error! Reference source not found.**., resulting in partial delipidation of the ROS membrane. ~20nmol rhodopsin in buffer B (10-15μM).

3. Control ROS – ROS with no regeneration step but washed with isotonic buffer B in place of β-cyclodextrin following the procedure in Section **Error! Reference source not found.**. ~20nmol rhodopsin in buffer B (10-15μM).

UV-VIS characteristics of the three samples were the same as those previously measured for the unlabelled rhodopsin NMR control samples (see Table 2.5).

ROS preparations were resuspended in Buffer B (Table 2.4) to a final concentration of 10-15µM, using freeze-thawing to give a fine homogenous suspension and measured in a 1cm^3 quartz cuvette. The temperature varied between 8 and 10°C which although above the standard meta-I trapping temperature (-18°C) was hoped to be sufficiently low enough to trap the "low-lipid" meta-I intermediate long enough to record a UV-VIS measurement.

4.4.1.3   Studying rhodopsin photolysis using UV-VIS spectrophotometry

UV-VIS spectroscopy was performed on a Perkin Elmer λ-18 UV-VIS spectrophotometer (Nijmegen, The Netherlands), modified by moving the photomultiplier close (~2mm) to the cuvette. This reduced the scattering that normally prevents the measurement of turbid membrane samples and enabled UV-VIS measurements to be made on ROS membrane suspensions without detergent solubilization. Prior to taking a UV-VIS reading the cuvette was inverted to give a uniform suspension.

To observe the photolytic behaviour of the ROS samples an initial UV-VIS spectrum was taken in the dark once the sample had equilibrated to temperature (3min) (spectrum 1). The photolytic cascade was initiated by illuminating the sample for 30s with light from the fibre optic light guides (250W "cold light" source) and three spectra taken to verify the stability of the photointermediates under the experimental conditions (spectrum 2). The wavelength of the incident light could be varied by choosing one of the following available filters in the filter wheel of the lamp: 530LP, 550LP, 570LP, 550BP, 440BP (see Table 4.1). Hydroxylamine (0.2M hydroxylamine hydrochloride in Buffer B; pH 6.5) was added to a final concentration of 100mM and incubated (45min), after which another spectrum was

taken (spectrum 3). This converts all photolysis intermediates into retinal-oxime and opsin, but leaves residual rhodopsin and photoregenerated 9-*Z* isorhodopsin intact, enabling the proportion of photointermediate generated by the illumination to be calculated [226]. A subsequent total bleach (3min; 300W tungsten lamp) followed by a final recording enabled the total amount of rhodopsin originally present to be calculated (spectrum 4).

Two calculations were conducted on the system, following established procedures [156, 226] to calculate the % of rhodopsin bleached to photointermediate and the proportion of the bleached component that was meta-I rhodopsin.

$$\% \text{ photointermediate} = \frac{(Abs_{500}^1 - Abs_{650}^1) - (Abs_{500}^3 - Abs_{650}^3)}{(Abs_{500}^1 - Abs_{650}^1) - (Abs_{500}^4 - Abs_{650}^4)}$$
                                                                                          Equation 4.1

$$\% \text{ meta-I} = \frac{(Abs_{480}^2 - Abs_{650}^2) - (Abs_{480}^3 - Abs_{650}^3)}{(Abs_{500}^1 - Abs_{650}^1) - (Abs_{500}^3 - Abs_{650}^3)}$$
                                                                                          Equation 4.2

For Abs_y^x x = spectrum no. y = wavelength (nm)

4.4.2 Trapping the meta-I photointermediate in "low-lipid" ROS membranes

The meta-I trapping effect of the low-lipid membranes was illustrated by comparing the photolytic behaviour of the control ROS (sample 3) and β-cyclodextrin washed ROS samples (sample 2)(Figure 4.6).

The photolytic behaviour of the rhodopsin in normal photoreceptor lipid membranes (lipid/protein ratio ~62:1 [226]) (sample 3) shows the conventional decay of meta-I to meta-II rhodopsin that is expected at this temperature (blue line; Figure 4.6). Upon illumination,

the meta-II intermediate (λ_{max}=380nm) was formed within the dead-time of the experiment, in a temperature dependent equilibrium with meta-I (λ_{max}=480nm). The proportion of meta-I was 57 ±3%, equalling that expected at this temperature [217]. For the partially delipidated membrane sample (sample 2) the photosequence stopped at the meta-I intermediate for long enough so that within the time of the illumination and measurement (~3min) almost all (98 ±2%) of the bleached rhodopsin was in the meta-I form. It is expected that this "blocked" portion of meta-I rhodopsin would gradually decay to meta-II [226].
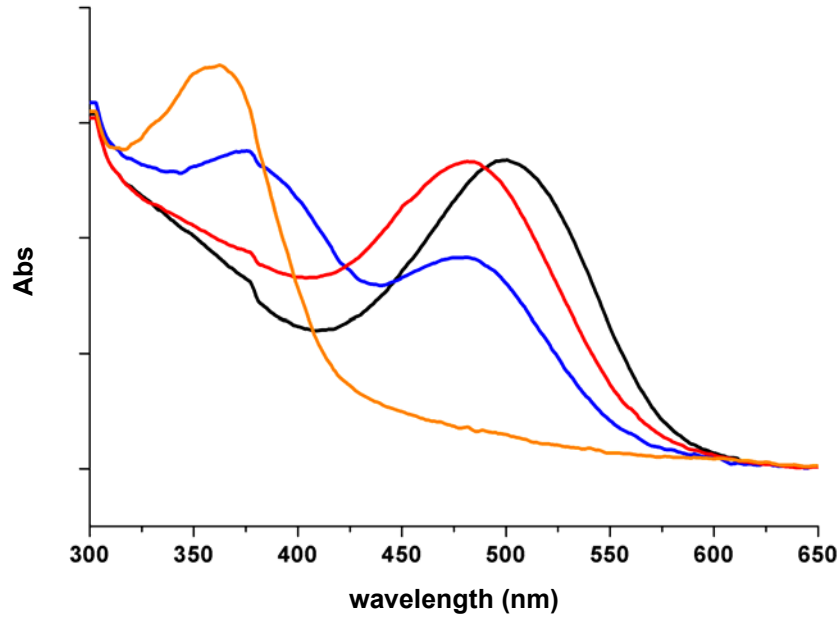
Figure 4.6 – UV-VIS spectra showing the meta-I trapping effect of rhodopsin in "low-lipid" ROS membranes at 8°C. Illumination (30s; 530LP filter; 2800K) of photoreceptor ROS membranes (sample 3)(black line; λ_{max} = 498nm) resulted in formation of an equilibrium mixture of meta-I (λ_{max}=480nm) and meta-II (blue line; λ_{max} = 380nm). Illumination of "low-lipid" photoreceptor membranes (sample 2), repeatedly washed with β-cyclodextrin (50mM), resulted in almost complete "blocking" of the meta-I photointermediate (red line; λ_{max} = 480nm). Fully bleached spectrum is shown in orange

4.4.3 Effect of wavelength on trapping the meta-I photointermediate

Using the 11-Z retinal regenerated rhodopsin sample (sample 1) the amount of trapped meta-I was calculated following illumination with incident light of varying wavelength. It could be shown that more meta-I rhodopsin could be trapped following illumination with light of progressively longer wavelength (530→ 570nm), accompanied by a reduction in the level of photoregeneration of rhodopsin and isorhodopsin (see Table 4.2). This could be explained by a gradual shift in the equilibrium between rhodopsin, isorhodopsin and meta-I rhodopsin due to the light at longer wavelengths being absorbed predominately by the rhodopsin component at 498nm. This effect is shown for the 530LP and 570LP filters in Figure 4.7. The optimum level of rhodopsin converted to photointermediate was achieved

following illumination with the 550BP and the 570LP filters (72±2% rhodopsin bleached to meta-I) and the minimum level with the 440BP (46±4% meta-I). In all cases >94% of the photointermediate was trapped in the meta-I form.
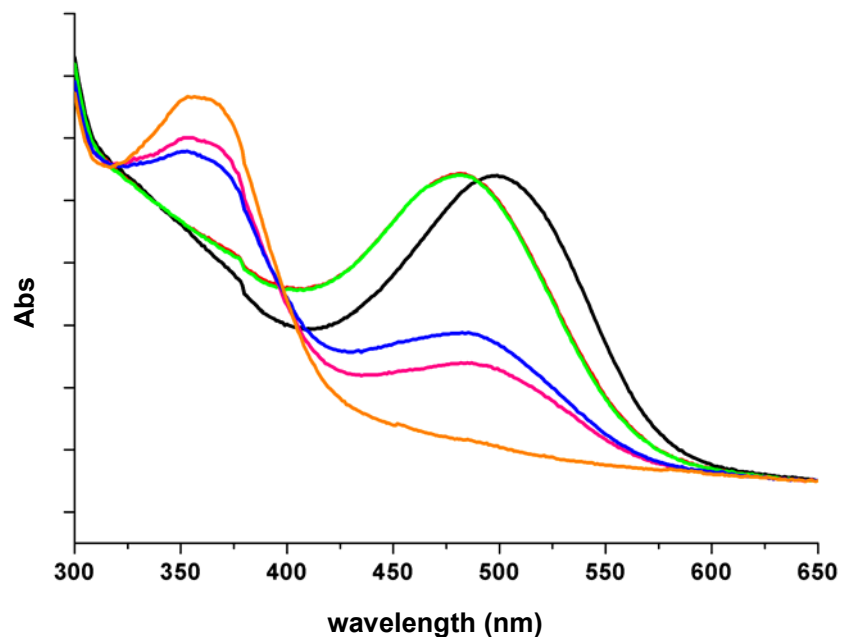
Figure 4.7 – Effects of varying the wavelength of illumination on the amount of meta-I rhodopsin trapped in regenerated ROS membranes (sample 1) at 8°C. Rhodopsin (black line) illuminated with light from a 530LP filter and 570LP filter (red and green line) resulted in trapping of the meta-I photointermediate, which could be converted into retinal-oxime (λ_{max} = 365nm) and opsin, by incubation with hydroxylamine (50mM). The remaining band derived from residual rhodopsin and isorhodopsin (λ_{max} = 490nm) was smaller for the sample illuminated with light of longer wavelength, indicating more meta-I had been trapped (pink line; 570LP, blue line 530LP). The fully bleached spectrum is shown in orange (3min; 300W tungsten lamp). All spectra were normalised at 650nm.

Table 4.2 – Products of irradiation (30s; 2800K) of rhodopsin in "low-lipid" ROS membranes at 8°C with light of various wavelengths. Errors calculated from standard deviation from three consecutive UV-VIS readings.

Filter	% photointermediate	% of trapped intermediate as meta-I
438BP	46±4	94±6
530LP	60±4	98±8
550LP	64±2	95±1
570LP	72±2	100±3

550BP	72±2	100±4

Although the maximum proportion of meta-I intermediate was slightly less than that reported by Hubbard *et al* (75%) these results showed that the "direct" method for trapping meta-I rhodopsin was a viable method for subsequent NMR investigations. It also indicated that the 530LP filter, which had been commonly used to trap the meta-I intermediate [168, 226, 227], would be better replaced by a longer wavelength filter. Although the levels of meta-I trapped following illumination with the 570LP and 550BP filters were the same (72±2) the 570LP was chosen for the initial experiments due to its higher level of light transmission (see Table 4.1).

4.4.4 "Direct" trapping of the meta-I photointermediate in [10,20-$^{13}C_2$] retinylidene rhodopsin NMR samples

4.4.4.1 Materials and methods

[10,20-$^{13}C_2$]retinylidene rhodopsin samples and an unlabelled control sample (control[2]; 12.9mg, Table 2.5) were prepared following the procedure in Section **Error! Reference source not found.**. Samples were characterized by UV-VIS spectrophotometry (see Table 2.5 and Section **Error! Reference source not found.** for characterisation details) and packed into Chemagnetics 4mm NMR rotors following the procedure described in Section **Error! Reference source not found.**. Approximately 10mg (270nmol) of [10,20-$^{13}C_2$]retinylidene rhodopsin was packed into each NMR rotor.

All of the following procedures were performed under dim red light.

Before illumination the plugs and the fins were removed from the rotor, enabling illumination of the sample from both ends of the rotor which was placed in the cooling

block, cooled to the required temperature and illuminated via both light guides (Section 4.3.1). The sample was transferred to dry-ice and the fins and plugs replaced, taking care to keep the rotor below the meta-I/meta-II transition temperature (-18°C). The sample was transferred to a pre-cooled NMR probe at -80 °C and a CP-MAS NMR spectrum acquired (8000 -12000 scans). The sample could be illuminated further if required, following the same procedure.

4.4.4.2 CP-MAS ^{13}C NMR results

Trapping meta-I rhodopsin in frozen rhodopsin NMR samples was initially attempted by the "direct" method, using the C20 chemical shift of $[10,20\text{-}^{13}C_2]$retinylidene meta-I rhodopsin as an indicator for the meta-I state [78, 133].

Initially, the optimal wavelength determined from the suspension studies was used (570LP, see Section 4.4.3). The CP-MAS NMR spectrum of dark-state $[10,20\text{-}^{13}C_2]$retinylidene rhodopsin with the natural abundance background subtracted, resulted in signal only derived from a single resonance for the C20 ^{13}C label at 16.5ppm (Resonance **1** in Figure 4.8 (a)), in agreement with previous assignments for C20 in the dark-state (16.8ppm [32], 15.8ppm [78, 133]). Upon illumination, (570LP; 10min; -30°C; 3000K) the dark-state C20 resonance reduced in intensity and two other resonances appeared at 15.5ppm (**2**) and 13.9ppm (**3**) (Figure 4.8 (b)). The observation of three C20 resonances upon illumination by the "direct" method was in contrast to Verdegem *et al*, who observed only one additional C20 ^{13}C resonance following meta-I trapping by the "indirect" method [78, 133]. Resonance **3** in Figure 4.8 (b), at 13.9ppm, was assigned as meta-I rhodopsin, based on the approximate

agreement (±0.6ppm) with the chemical shift for the meta-I C20 resonance, assigned by Verdegem *et al* at 13.3ppm [78, 133].

Resonance **2** at 15.5ppm did not appear to correspond to 9-*Z* isorhodopsin, which had previously been observed at 13.6ppm [32] and 14.5ppm [228]. This suggested that the 9-*Z* isorhodopsin component also contributed to resonance **3** at 13.9ppm. The implications of observing meta-I and isorhodopsin at the same resonance are discussed later in the chapter (Section 4.4.6.2).
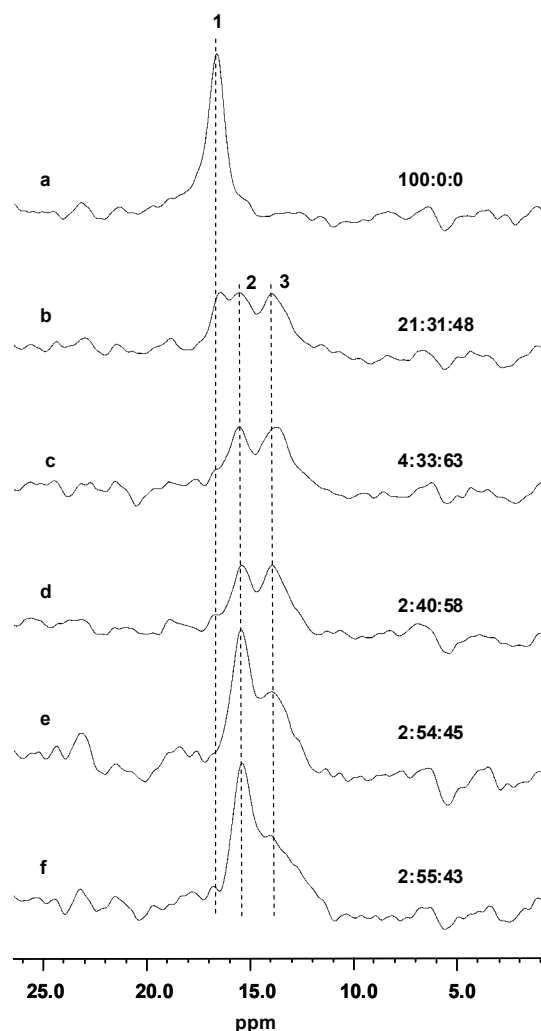
Figure 4.8 – CP-MAS ^{13}C NMR spectra of the C20 resonances of [10,20-^{13}C$_2$]retinylidene rhodopsin in the dark state (a) and following irradiation (570LP; -30°C; 3000K) for 10, 70, 240, 420 and 600mins ((b-f), respectively). The natural abundance signal of an unlabelled control (control^2, see Table 2.5) has been subtracted. A single resonance was observed for C20 in the dark state at 16.5ppm (**1**) assigned to rhodopsin, which gradually decreased upon illumination as two additional resonances appeared at 15.5ppm and 13.9ppm, (**2** and **3**). The relative intensity of resonances **1, 2** and **3** was determined by Lorenztian line

Using Lorentzian linefitting, the intensities of the resonance **1, 2** and **3**, following 10 minutes of illumination were deconvoluted at 21%, 31% and 48%, respectively (i.e. 21:31:48 as displayed in Figure 4.8 (b)). Further illumination resulted in the level of resonance **3**, containing the meta-I component reaching a maximum after 70 minutes of illumination (570LP; 70min; -30°C; 3000K), whereby almost all of the rhodopsin has been

converted to photoproducts (4:33:63 in Figure 4.8 (c)). However, prolonged illumination of the sample (570LP; 70-600min; -30°C; 3000K) led to a significant increase in the proportion of resonance **2** at the expense of resonance **3**, so that following 600 minutes of illumination there was an excess of resonance **2** (2:55:43, Figure 4.8 (f)).

These observations did not suggest that a steady-state equilibrium was forming between rhodopsin, isorhodopsin and meta-I rhodopsin, as predicted [219]. An equilibrium containing just these components would be expected to form much faster than observed and it appeared there was an additional component (resonance **2** in Figure 4.8) that was forming slowly, eventually to significant levels.

It was found that as well as photoregeneration to the 9-Z retinal isomer (isorhodopsin), the 11-Z retinylidene chromophore could also be photoregenerated to the 7-Z isomer (7-Z rhodopsin) on exposure to light at low temperatures [227]. At different points following illumination of a ROS suspension (530LP; -75°C) Maeda *et al* studied the isomeric composition of the retinal extracted from the ROS with HPLC [227].
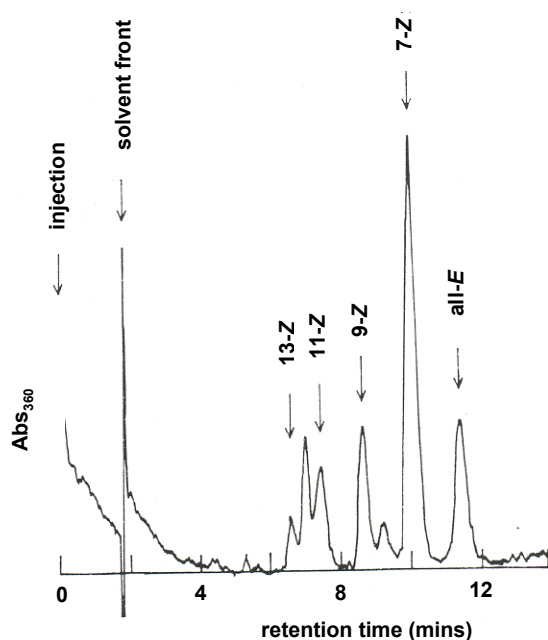
Figure 4.9 – HPLC of the retinal isomers extracted from the photosteady mixture which had been formed by irradiation of rhodopsin with light at wavelengths longer than 530nm (340mins; 530LP) at -75°C. The peaks were identified as shown by comparing with those obtained by HPLC of authentic retinal isomers. Taken from [228].

They found the initial products of the illumination were 9-Z (isorhodopsin) and all-E (lumirhodopsin) but as the photoproducts were illuminated further the 7-Z isomer (7-Z rhodopsin) began to accumulate. With extended illumination at the photostationary state (6hr), the level of the 7-Z isomer approached 50% of the total retinal isomeric mixture (Figure 4.9).

Maeda *et al* concluded that an initial quasi-photostationary state formed between rhodopsin (11-Z), isorhodopsin (9-Z) and lumirhodopsin (all-E) but with further illumination the all-E and 9-Z isomeric states were gradually converted to 7-Z retinal. Similar experiments on squid rhodopsin conducted on the meta-I photointermediate at -40°C also resulted in significant levels (46%) of regeneration of the 7-Z isomer [229].

The 7-Z isomer is not one of the energetically favoured isomers of retinal in rhodopsin, reflected in the slow rate of photoregeneration, but as the pigment formed by the 7-isomer absorbs maximally at 450nm [155, 157] it absorbs very little of the long wavelength incident light and is less likely to be converted back into 9-Z, 11-Z or all-E retinal. Over periods of prolonged illumination 7-Z rhodopsin gradually accumulates within the sample (Figure 4.10).
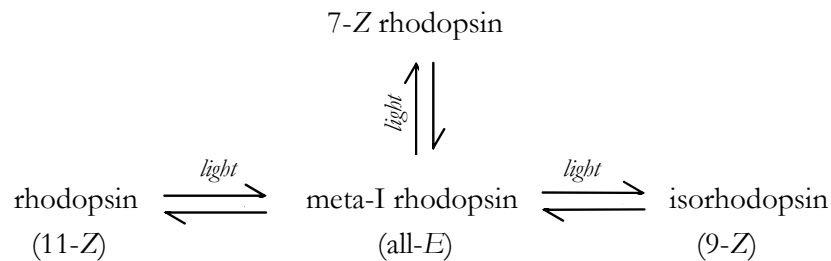
7-Z rhodopsin

Figure 4.10 – Photoscheme for the steady-state mixture formed by illuminating rhodopsin at -20°C. As well as isorhodopsin, the all-E chromophore could be

As the λ_{max} of meta-I rhodopsin (480nm) is lower than that of rhodopsin (498nm) it was

attempted to minimise the formation of photoregenerated products by illuminating with light of longer wavelength. Another $[10,20-^{13}C_2]$retinylidene rhodopsin sample was illuminated with incident light >590nm (590LP, see Table 4.1 and Figure 4.5). The series of difference CP-MAS NMR spectra recorded for $[10,20-^{13}C_2]$retinylidene rhodopsin following illumination for 10, 20, 30, 40 and 50mins are shown in Figure 4.11 (b-f), respectively (590LP; -30°C; 3000K). The optimal conversion to meta-I was recorded after 40mins of illumination where resonance **3** represented 51% of the total C20 intensity (14:35:51 in

Figure 4.11 (d)), indicating a lower proportion of meta-I than observed with the 570LP filter.

Continued illumination resulted in an increased intensity of resonance **2** at the expense of

resonance **3** (13:38:49 in Figure 4.11 (f)) as was observed in the illumination with 570LP light

(Figure 4.8).

Illumination with the longer incident wavelength of light appeared to bleach the rhodopsin

less efficiently. Considering that less light would be absorbed by the meta-I

photointermediate (λ_{max}=480nm) at this wavelength it was surprising to see that the level of
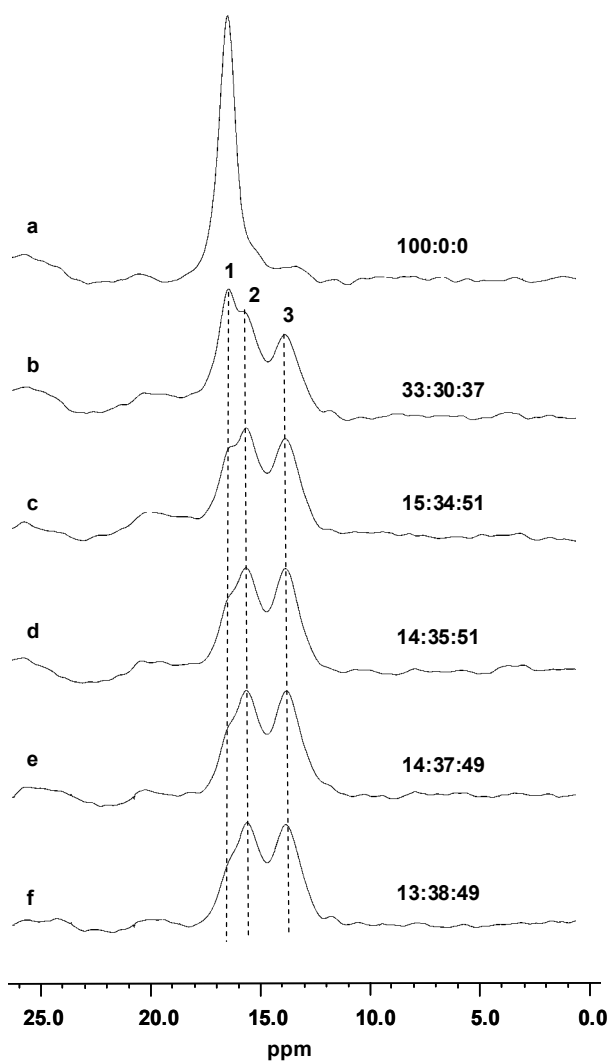
Figure 4.11 - CP-MAS NMR spectra of the C20 region of [10,20-^{13}C$_2$]retinylidene rhodopsin in the dark state (a) and after illumination (590LP; -30°C; 3000K) for 10, 20, 30, 40 and 50mins (b-f), respectively. The natural abundance signal of an unlabelled control was subtracted. The relative intensity of the resonances **1:2:3** was determined by Lorenztian line fitting for each spectrum and showed that meta-I generation was maximal after 30mins. $\omega_r/2\pi$=10000± 3Hz

photoregeneration of 7-*Z* isomers had not reduced as well.

Illumination of an additional [10,20-^{13}C$_2$]retinylidene rhodopsin sample with light >610nm (see Table 4.1 and Figure 4.5, 610LP) continued the trends previously observed with 570LP and 590LP illumination. After 315min of illumination 30% of the residual rhodopsin remained unconverted (30:40:30 in Figure 4.12) and the prolonged illumination required to bleach rhodopsin at >610nm resulted in little reduction in the level of photoregeneration of 7-*Z* rhodopsin (resonance **2** in Figure 4.12). With less efficient bleaching of rhodopsin the proportion of resonance **3**, containing the meta-I component, was lower than had been previously observed with illumination >570nm or >590nm.
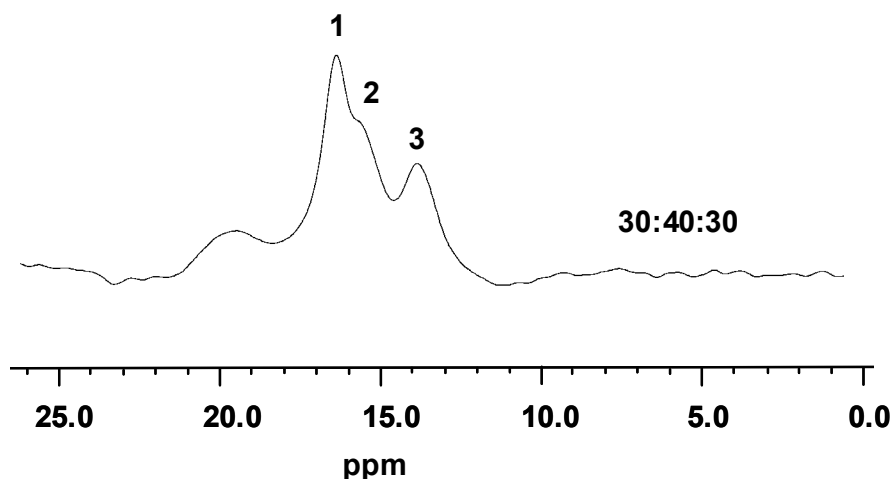
Figure 4.12 – CP-MAS NMR spectrum of the C20 region of [10,20-^{13}C$_2$]retinylidene rhodopsin following illumination at >610nm for 315mins (610LP; -30°C; 3000K). Rhodopsin (resonance **1**) was bleached inefficiently at this wavelength, hence the conversion to meta-I (in resonance **3**) was small.

4.4.5 "Direct" trapping of [10,20-^{13}C$_2$]retinylidene meta-I rhodopsin in ROS suspensions

4.4.5.1 Introduction

As the formation of the 7-*Z* isomers occurred slowly [227, 229] (see Figure 4.8), a strategy to illuminate the rhodopsin rapidly was adopted, enabling maximal amounts of the meta-I

photointermediate to be generated before the slower forming 7-*Z* rhodopsin could accumulate. It was thought that by uniformly distributing the NMR rhodopsin sample in a fine suspension the rhodopsin sample could be illuminated faster than within the NMR rotor, where longer illumination times were required to penetrate the dense sample and convert all the rhodopsin. With a shorter illumination period the prolonged irradiation of meta-I photointermediates would be minimised and so photoregeneration reduced.

4.4.5.2 Method of sample preparation

The method used to trap meta-I in ROS suspension was similar to that used in the meta-I UV-VIS spectroscopy studies (Section 4.4.1), although on a much larger scale. It required resuspending a $[10,20^{-13}C_2]$retinylidene rhodopsin sample from an NMR rotor in buffer, illuminating it to trap the meta-I intermediate and then repacking the sample back into the NMR rotor. As with the previous meta-I UV-VIS studies on the ROS suspensions, trapping the photocycle at the meta-I state would rely on the low-lipid characteristics of the ROS membranes which restrict the meta-I to meta-II transition at temperatures above the normal meta-I/meta-II transition temperature (-20°C) but do not effect the formation of earlier photointermediates (see Section 4.4.1) [156, 226].

To minimise the possibility of conversion to meta-II, the sample was kept at 0°C at all times. All equipment, including centrifuge rotors, tubes, pipette tips and glassware was stored at -20°C prior to use and each stage of the procedure performed as quickly as possible.

Approximately 250nmol (10mg) of $[10,20^{-13}C_2]$retinylidene rhodopsin, previously packed into a Chemagnetics 4mm NMR rotor following the usual procedure (Section **Error! Reference source not found.**) was emptied by removing the fins and the plugs and centrifuging into a 2.5ml Eppendorf (1min; 14000g; Beckman microfuge). The sample was

transferred to a centrifuge tube (Beckman Ti 50) and resuspended in 3ml of Buffer B by freeze-thawing to give a fine ROS suspension. The sample was cooled to 0°C in a round bottom flask (100ml) in an ice/CaCl$_2$ water bath, with stirring and the sample illuminated briefly (30s; 570LP filter; 0°C; 3000K), through the neck of the flask.

The sample was centrifuged (SW 40; 0°C; 150000g; 10min) then packed back into a 4mm NMR rotor following the procedure described in Section **Error! Reference source not found.**.

4.4.5.3 CP-MAS NMR spectrum of [10,20-^{13}C$_2$]retinylidene rhodopsin sample illuminated in suspension

The methyl region (5-30ppm) of the CP-MAS NMR spectrum of the [10,20-^{13}C$_2$]retinylidene rhodopsin sample illuminated in suspension is illustrated in Figure 4.13 (a). The subtraction of the natural abundance spectrum was not very "clean" for this sample, as can be seen by the artefact at 20ppm. The distribution of the resonances **1**, **2** and **3** was 34:24:42 respectively, indicating a reduction in the amount of 7-*Z* photoregenerated products, however, there was incomplete conversion of the rhodopsin (resonance **1** in Figure 4.13 (a)), indicating the illumination time had been too short. Consequently, no overall increase in the intensity of resonance **3**, containing the meta-I component, was observed in comparison to the optimum conversion previously observed using illumination within the NMR rotor (63% for resonance **3** in Figure 4.8 (c)).

The experiment was repeated with a longer illumination time (3min; 570LP; 0°C; 3000K) to give a more complete conversion of the rhodopsin to the meta-I intermediate. This resulted in an improvement in the amount of rhodopsin bleached but was accompanied by an increase in the level of photoregeneration of 7-*Z* isomers (17:38:45 in Figure 4.13 (b)). The level of meta-I had not improved significantly from that observed with the shorter

illumination time and both experiments generated less meta-I rhodopsin than had been generated by illuminating the rhodopsin sample within the rotor (see Section 4.4.4.2 and Figure 4.8 (c)).
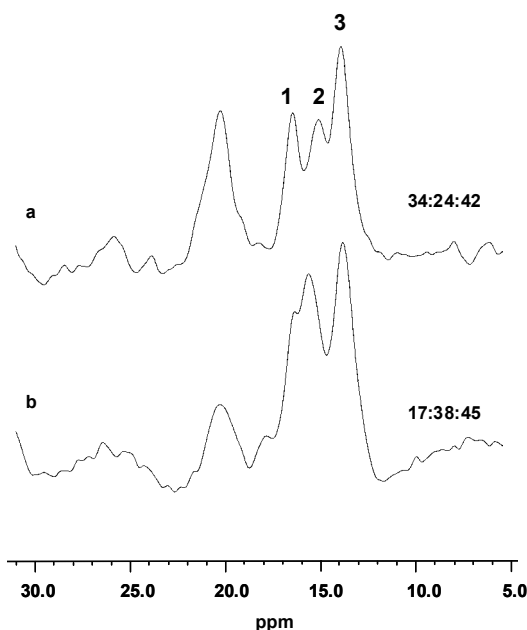
Figure 4.13 - CP-MAS NMR spectra of the C20 region (5-30ppm) of [10,20-$^{13}C_2$]retinylidene rhodopsin following illumination (570LP filter; 0°C; 3000K) for 30s (a) and 3mins (b) in ROS suspension (~3mg/ml). Illumination and packing of the samples were performed at 0°C, making use of the low-lipid characteristics of the regenerated ROS membrane to trap the meta-I photointermediate. The natural abundance signal of an unlabelled control is subtracted although not as cleanly as in other experiments, with

4.4.5.4   Discussion

Although it was previously expected that only photoregeneration to 9-*Z* isorhodopsin occurred upon illumination of rhodopsin at low temperatures, it is now apparent that trapping of meta-I via the "direct" method (-30ºC) is severly hampered by the photoregeneration of 7-*Z* rhodopsin. An initial increase was observed in the intensity of resonance **3** (13.9ppm) in the CP-MAS NMR spectra of [10,20-$^{13}C_2$]retinylidene rhodopsin as the 11-*Z* retinylidene chromophore was converted to   all-*E* meta-I rhodopsin and isorhodopsin (Figure 4.8 (b)). This intensity then dropped as the 7-*Z* isomer gradually

accumulated at 15.5ppm, eventually to significant levels (Figure 4.8 (e)). By measuring the integrated intensity of resonance **2**, which was assigned to 7-*Z* rhodopsin, the maximum level of 7-*Z* photoregeneration corresponded to ~50% of the total retinal isomeric content. The level of 7-*Z* rhodopsin measured by NMR was approximately equal to the proportion of photoregenerated 7-*Z* retinal extracted by HPLC, following prolonged illumination of dilute ROS suspensions at -40°C (46%) [227, 229].

Illumination with longer wavelengths of incident light (590LP and 610LP) slightly reduced the proportion of regenerated 7-*Z* rhodopsin as less light was absorbed by the isorhodopsin and meta-I photoproducts, but as rhodopsin absorbs less efficiently at these wavelengths the maximum amount of meta-I was also reduced (Figure 4.11 and Figure 4.12). Attempts to improve the meta-I conversion proportion by irradiating the NMR samples in ROS suspension also reduced the level of photoregeneration, but rhodopsin also bleached less efficiently by this method and no overall increase in the level of meta-I rhodopsin was observed (Figure 4.13).

UV-VIS spectrophotometry had predicted that only minimal (<20%) of photoregeneration of 9-*Z* isorhodopsin occurred and meta-I rhodopsin represented >70% of the photoproducts when meta-I rhodopsin was generated using the "direct" method, under optimal conditions [219, 220] (Section 4.4.3.).

The short illumination times (<1min) used to irradiate the rhodopsin in UV-VIS spectrophotometry studies were thought to have been sufficient to generate a steady-state mixture of photointermediates (Figure 4.7). However, this irradiation time actually represents a quasi-photosteady state, where photoregeneration of 9-*Z* retinal in isorhodopsin has occurred but the 7-*Z* isomer has yet to accumulate significantly, due to its unfavourable

formation within the opsin binding pocket [155, 157]. Additionally, 7-*Z* rhodopsin generated by the illumination procedure would not be identified by UV-VIS spectrophotometry as it is unstable in hydroxylamine [155, 157], which was added following illumination to break the meta-I retinylidene Schiff base linkage, so the amount of trapped photointermediate could be measured. This would have resulted in an overestimate of the proportion of meta-I generated by the illumination by UV-VIS spectrophotometry.

The optimal conditions observed for the trapping of the meta-I intermediate for NMR samples (70min illumination within the rotor; 570LP filter; 3000K) represented a condition where rhodopsin was almost completely bleached within the NMR rotor but the level of photoregeneration of 7-*Z* rhodopsin was minimal (Figure 4.8 (c)). Nevertheless, the photoregeneration of 7-*Z* rhodopsin under these conditions was still significant, limiting the use of the "direct" method for trapping meta-I in frozen rhodopsin NMR samples. The "indirect" method, involving accumulating the bathorhodopsin photointermediate to generate meta-I rhodopsin, was therefore investigated (Section 4.4.6).

4.4.6 "Indirect" trapping of the meta-I intermediate in [10,20-^{13}C$_2$] retinylidene rhodopsin NMR samples

4.4.6.1 Introduction

Although photoregeneration of 7-*Z* rhodopsin has been shown to occur from the lumi and meta-I rhodopsin photointermediates, analysis of the isomeric retinal composition of steady-state bathorhodopsin with HPLC showed that photoregeneration of only 9-*Z* isorhodopsin occurred at this stage in the photocycle (Scheme 4.2) [227, 229]. This suggested that the retinal binding pocket of bathorhodopsin had a conformation which formed a barrier to the conversion of all-*E* retinal to 7-*Z* retinal, which relaxed upon the conversion of bathorhodopsin to lumirhodopsin. Consequently, the build up of 7-*Z* isomers would not be

a problem when trapping meta-I via bathorhodopsin, as they had been when converting rhodopsin "directly" to meta-I (see Section 4.4.4)

4.4.6.2   CP-MAS NMR results

Following the results from the UV-VIS spectrophotometry experiments on the bathorhodopsin photointermediate it was thought that the optimum amount of bathorhodopsin, and hence meta-I rhodopsin, could be generated with blue light illumination (430-460nm) [72, 223, 224].

Using the 440BP filter (see Table 4.1), a $[10,20-^{13}C_2]$retinylidene rhodopsin sample was irradiated extensively within the NMR rotor at -188 $\pm3^{\circ}$C (600min; 3300W) then warmed to -20°C (10mins) to enable the meta-I photointermediate to be generated from the trapped batho photointermediate. CP-MAS ^{13}C NMR was then used to observe the interconversion of rhodopsin, isorhodopsin and meta-I rhodopsin.

Figure 4.14 shows the difference CP-MAS NMR spectra of $[10,20-^{13}C_2]$retinylidene rhodopsin acquired in the dark state (black line) and following "indirect" trapping of the meta-I photostate (600mins; 3300W; 440BP filter) (red line). Following illumination, a slight decrease in the amount of resonance **1** was observed at 16.5ppm (rhodopsin) and a small resonance appeared at 14.0ppm (resonance **3** in Figure 4.14), corresponding to 15% of the total C20 intensity.
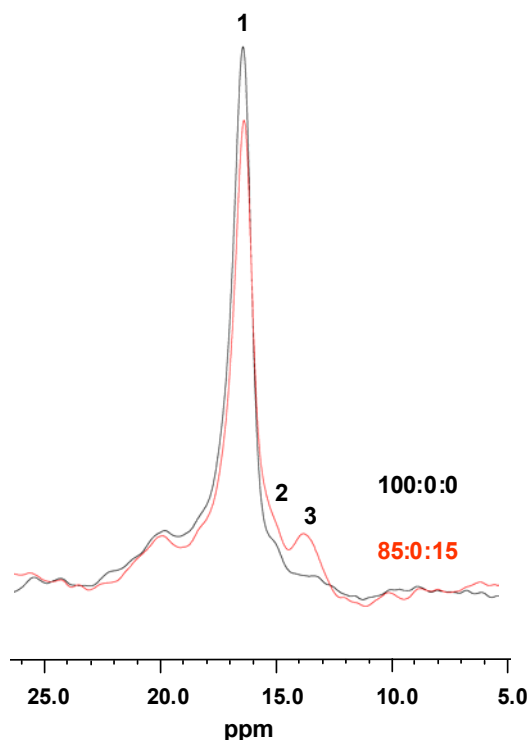
Figure 4.14 – CP-MAS NMR spectra of the C20 region of $[10,20-^{13}C_2]$retinylidene rhodopsin in the dark state (black line) and after illumination (600mins; 440BP; 3300K)(red line) with the natural abundance signal of the unlabelled control subtracted, showing minimal bleaching of rhodopsin (15%). The relative intensities of the resonances **1**, **2** and **3** were determined by Lorentzian line fitting for each spectrum and

No resonance was resolved at 15.5ppm, where resonance **2** had been previously assigned to 7-*Z* rhodopsin (Figure 4.8). This indicated that photoregeneration of 7-*Z* rhodopsin did not occur upon illumination of rhodopsin at -188°C, as predicted.

The conversion of rhodopsin was much lower than expected, based on the conversion

efficiency to the batho photointermediate previously generated by illuminating under these conditions (50-60%) [72, 73, 223, 224]. This was thought to be a result of the low transmission of the 450BP filter (40%, see Table 4.2), which had led to only partial illumination of rhodopsin in the densely packed NMR rotor.

A more efficiently transmitting bandpass filter with a narrower bandpass range was created by combining a short-pass 505 filter (505SP) with a long-pass 455 filter (455LP), giving light of the required wavelength (~475nm) and of higher intensity than with the 440BP filter (see Table 4.1). Irradiation of a $[10,20-^{13}C_2]$retinylidene rhodopsin sample using this light (505SP + 455LP; 600min; 3300K) resulted in a very small increase in the amount of trapped meta-I rhodopsin with most of the sample still in the rhodopsin state (83:0:17)(data not shown).

It was difficult to rationalise how significant levels (~50%) of bathorhodopsin had been previously generated by irradiating a solid rhodopsin NMR sample through the walls of the NMR rotor using relatively low intensity light (150W) and a 460nm interference filter [73].

As the preferable blue light had been unsuccessful in bleaching rhodopsin the filter was removed and the same $[10,20-^{13}C_2]$retinylidene rhodopsin sample illuminated at -188°C with white light (360mins; white light; 3300W). Following warming to -20°C, a large conversion of rhodopsin to resonance **3** was observed (19:0:81, Figure 4.15). The blue light illumination and subsequent warming of the sample to -20°C, before re-illuminating at -188°C, may have interfered with the conversion process. To confirm this result the irradiation was repeated on a fresh $[10,20-^{13}C_2]$retinylidene rhodopsin sample with just white light irradiation (360min; white light; 3300K; -188°C). The difference CP-MAS NMR spectrum (Figure 4.16) showed an even greater conversion of rhodopsin than previously observed (17:0:83).
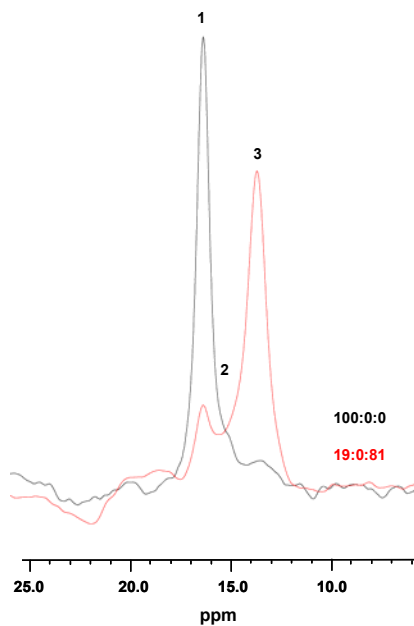
Figure 4.15 – CP-MAS NMR spectra of the C20 region of $[10,20\text{-}^{13}C_2]$retinylidene rhodopsin in the dark state (black line) and after illumination (600mins; 440BP followed by 360min; white light; 3300K)(red line). A dramatic improvement in the bleaching of rhodopsin (resonance **1**, 16.5ppm) was observed as the majority of signal shifted to 14.0ppm (81% by line fitting) containing the meta I component (resonance **3**)
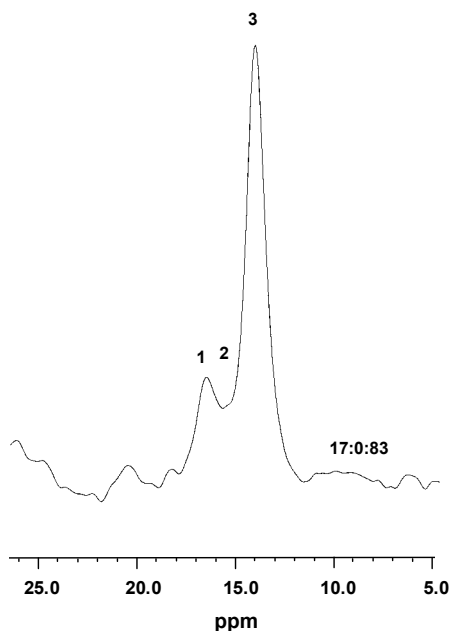
Figure 4.16 – CP-MAS NMR spectra of the C20 region of $[10,20\text{-}^{13}C_2]$retinylidene rhodopsin trapped by illumination at -188°C (360min; white light; 3300K) and incubation at -20°C, showing that the conversion of rhodopsin (resonance **1**) previously observed (Figure 4.15) could be repeated (resonance **3** = 83%). The relative proportions of resonances **1 2** and **3** were measured by Lorentzian line fitting and normalised and is

The appearance of just one additional resonance following formation of bathorhodopsin (resonance **3**) confirmed that the C20 ^{13}C resonance for isorhodopsin and meta-I rhodopsin were not independently resolved from each other (14.0ppm), as was suggested from the "direct" meta-I trapping NMR experiments (Section 4.4.4.2) and previous chemical shift assignments [32, 228].

The C10 region of the difference CP-MAS NMR spectra of $[10,20-^{13}C_2]$retinylidene rhodopsin, which had been used to quantify the conversion to meta-I in previous NMR studies [78, 79] also showed no discreet isorhodopsin resonance (Figure 4.17). Deconvolution of spectral intensity from the C10 region (127.7 to 131.3 ppm) indicated just two resonances at 127.7ppm (resonance **1**) and 131.3ppm (resonance **2**), previously assigned as rhodopsin and meta-I, respectively [78, 79]. The proportion of signal at 131.3ppm showed that the C10 resonances from the isorhodopsin and meta-I rhodopsin components were not independently resolved, in accord with the observations at C20.
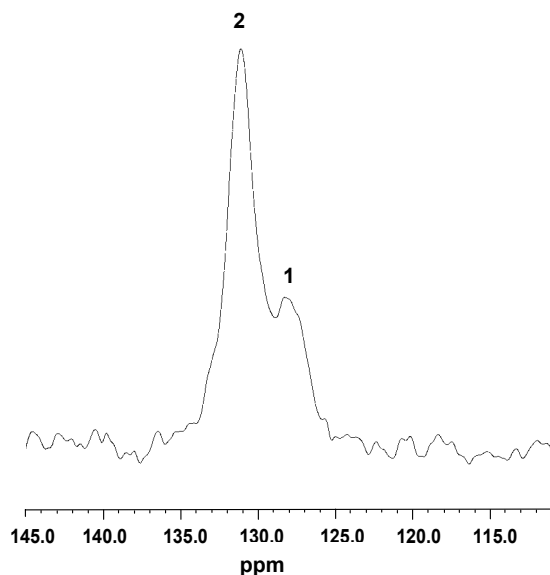
Figure 4.17 – CP-MAS NMR spectrum of the C10 region (110-145ppm) of $[10,20-^{13}C_2]$retinylidene meta-I rhodopsin trapped by illumination at -188°C (360min; white light; 3300K) and incubation at -20°C. Upon illumination, a single resonance at 127.7ppm reduced in intensity (resonance **1**) and an additional resonance was resolved at

To determine the proportion of meta-I in the $[10,20-^{13}C_2]$retinylidene rhodopsin NMR samples that have been trapped by either the "direct" or "indirect" pathways, a method for resolving the isorhodopsin and meta-I components was required.

The resolution between the isorhodopsin and meta-I components was investigated using the C8 ^{13}C nucleus, which is highly sensitive to the formation of isorhodopsin [32]. The $[8,18-^{13}C_2]$retinylidene rhodopsin sample (see Table 2.5 for UV-VIS characterisation) previously used for rotational resonance NMR measurements in Section **Error! Reference source not found.**, was irradiated under exactly the same conditions as those which had been used to generate the highest conversion of rhodopsin to meta-I and isorhodopsin (360min of white light illumination at $-188^{o}C$ followed by dark incubation at $-20^{o}C$ for 10min). A CP-MAS ^{13}C NMR spectrum was recorded under equilibrium conditions (4s recycle delay) and is displayed for the C8 region (120-150ppm) in the dark state and following meta-I trapping in Figure 4.18 (a) and (b), respectively. A broad resonance was observed at 139.2ppm, corresponding to 60% of the overall C8 signal, and a narrower resonance at 130.9ppm, corresponding to 40% of the C8 signal (60:40 in Figure 4.18 (b)).

To confirm the conversion observed with C8 the additional sample containing the C8 ^{13}C label, $[8,16/17-^{13}C_2]$retinylidene rhodopsin was illuminated following the established procedure (360min of white light illumination at $-188\ ^{o}C$ followed by dark incubation at $-20^{o}C$ for 10min). Deconvolution of the C8 resonance revealed a very similar distribution of signal (58:42, Figure 4.18 (c)) as was observed with $[8,18-^{13}C_2]$retinylidene meta-I rhodopsin.
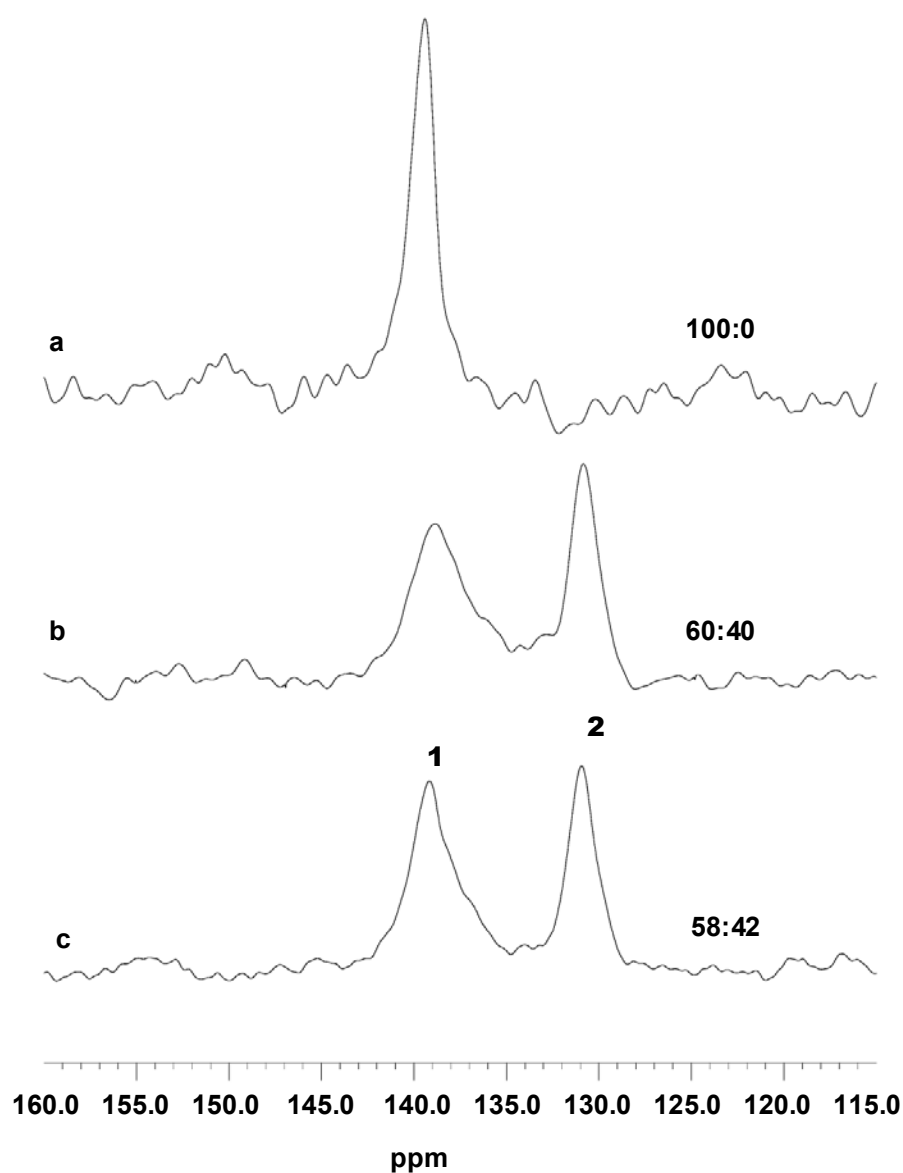
Figure 4.18 – CP-MAS NMR spectra of the C8 spectral region of [8,18-$^{13}C_2$]retinylidene rhodopsin in the dark state (a) and trapped by illumination at -188°C (360min; white light; 3300K) followed by incubation at -20°C (b). The C8 region of [8,16/17-$^{13}C_2$]retinylidene meta-I rhodopsin trapped under the same conditions (c). The relative intensity of the resonances **1** and **2** was determined by Lorenztian line fitting for each

4.5 Discussion

All the relevant chemical shift measurements for the rhodopsin (11-Z-retinal), isorhodopsin

(9-Z-retinal), 7-Z rhodopsin (7-Z-retinal) and meta-I rhodopsin (all-E-retinal) components

for the C20 and C8 ^{13}C resonances, measured by solid-state NMR are shown in Table 5.3.

Table 5.3 – Summary of C8, C10 and C20 ^{13}C chemical shifts for rhodopsin (11-Z-retinal), 7-Z rhodopsin (7-Z-retinal) isorhodopsin (9-Z-retinal) and meta-I rhodopsin (all-E-retinal) measured in different solid-state NMR studies.

Study	chemical shifts (ppm)									
	C8			C10			C20			
	11-Z	9-Z	all-E	11-Z	9-Z	all-E	11-Z	9-Z	all-E	7-Z
This study [a]	139.4	130.9	139.2	127.7	131.3	131.3	16.5	13.9	13.9	15.5
Creemers et al [b]	-	-	-	-	-	-	16.3	14.5	-	-
Verdegem et al [c]	-	-	-	127.3	130.6	130.6	15.8	13.3	13.3	-
Smith et al (1990)[d]	139.2	131.1	-	127.8	130.8	-	16.8	13.6	-	-
Smith et al (1991)[e]	139.5	130.5	-	127.4	130.8	-	-	-	-	-

[a] Measured here and referenced against adamantane methylene (38.6 ppm) [b][228] [c][78] [d][32] [e][73]

Using the distribution of the C20 signal in [10,20-^{13}C$_2$]retinylidene meta-I rhodopsin, together with the distribution of C8 signal in the [8,18-^{13}C$_2$]retinylidene meta-I rhodopsin and [8,16/17-^{13}C$_2$]retinylidene meta-I rhodopsin samples, the proportion of meta-I rhodopsin generated by the "indirect" illumination method could be calculated.

For the C8 ^{13}C nucleus, isorhodopsin was resolved as a discreet resonance (130.9ppm), corresponding to 40-42% of the photoproduct, whilst the rhodopsin and meta-I photoproducts resonated at the same chemical shift (139.2ppm for rhodopsin, 139.4ppm for meta-I rhodopsin in Figure 4.18). For the C20 ^{13}C nucleus, dark state rhodopsin was independently resolved at 16.5ppm, whilst meta-I rhodopsin and isorhodopsin were observed together at 13.9ppm, corresponding to 81-83% of the total photoproducts. Subtracting the amount of isorhodopsin (41%) from the amount of meta-I and isorhodopsin (82%) enabled the amount of meta-I generated by the "indirect" trapping to be calculated:

41%. This degree of conversion to meta-I is modest compared to the proportions of bathorhodopsin generated by illuminating at -188°C that were determined by UV-VIS spectrophotometry (50-60%) [72, 223, 224], but is as would be expected from generating bathorhodopsin with light of unspecific wavelength.

Quantifying the maximum proportion of meta-I that was generated by "directly" trapping meta-I at -30°C is not possible at present as the isorhodopsin and meta-I components (resonance **3** in Figure 4.8) cannot be separated. This would require "directly" trapping a meta-I rhodopsin sample regenerated with ^{13}C C8 labelled retinal to deduce the proportion of isorhodopsin generated by this method. The proportion of 9-Z retinal generated by "direct" meta-I trapping may be relatively small (12-25% [219, 227]) so the amount of meta-I rhodopsin generated by this procedure is likely to be similar to that formed from "indirectly" trapping meta-I rhodopsin (maximum meta-I and isorhodopsin trapped at -30°C = 63% in Figure 4.8 (c)).

Although the amount of trapped meta-I rhodopsin was less than anticipated, it was important that the proportion of the meta-I photoproduct had been quantified, especially as the C8 nuclei of rhodopsin and meta-I were observed at the same frequency. Without knowing what proportion of the C8 resonance at 139.4ppm corresponded to meta-I rhodopsin it would be very difficult to quantify the exchange of magnetization in a RR NMR experiment with C8, which is the aim of the study in Chapter 5.

The results have important consequences for the previous NMR studies that have been conducted on the meta-I photointermediate. As mentioned, the C10 chemical shifts of isorhodopsin and meta-I are observed at similar frequencies (130.6ppm for meta-I [78, 79], 130.8ppm for isorhodopsin [32]) and are observed as one resonance following "indirect"

trapping of meta-I rhodopsin (Figure 4.17). The high meta-I conversion rate reported by Verdegem *et al* (74%) that had been previously been attributed in this study to an error in the line fitting of C10 is likely to be a result of isorhodopsin within the sample that has been mistaken for meta-I rhodopsin. Photoregenerated isorhodopsin is not accounted for in any of the previous solid-state NMR studies on meta-I rhodopsin [78-80], meaning results interpreted for the meta-I state in these studies had in fact been derived from a mixed population of meta-I rhodopsin and isorhodopsin.

4.6 Conclusions

Solid state NMR has been successfully used to investigate the generation of meta-I rhodopsin from rhodopsin by both "direct" trapping of the meta-I photointermediate at -30°C and via accumulating bathorhodopsin at -188°C.

An experimental set-up has been developed that provided light of precise wavelength and power directly on the NMR sample at a designated temperature. This has resulted in a reliable and reproducible method for trapping the meta-I state.

Although directly trapping the meta-I state could prove useful for trapping the meta-I photointermediate in situations requiring short illumination times (i.e. dilute ROS suspensions), the prolonged illumination required for bleaching the dense rhodopsin NMR samples results in significant photoregeneration of 7-*Z* rhodopsin. This means careful timing is required to obtain the optimum level of meta-I, which limits the use of this method in the solid state.

The optimal method for trapping meta-I in rhodopsin NMR samples was by prolonged white light illumination (360min; 3300K) administered directly on the sample at - 188 °C followed by an incubation period in the dark at -20°C. Although this resulted in only a

modest meta-I conversion rate it could be quantified (42%), making use of a different chemical shift response for the C8 and C20 resonances upon formation of the meta-I state. In quantifying the meta-I conversion rate significant levels of photoregeneration were identified when trapping both the meta-I (9-*Z* and 7-*Z* retinal) and bathorhodopsin (9-*Z* retinal) photointermediates, previously unaccounted for in NMR studies on meta-I rhodopsin. The conversion rate represents the only properly quantified meta-I conversion rate for rhodopsin in the solid state at present.

Although unsuccessful in improving the amount of meta-I rhodopsin generated from rhodopsin it was hoped that the conversion to the meta-I intermediate established in the protocol would be sufficient to enable the RR NMR measurements on the β-ionone ring structure to be repeated in the meta-I state (Chapter 5).

Chapter 5   Determining the β-Ionone ring conformation of retinylidene in meta-I rhodopsin using RR NMR

5.1 Introduction

As $[8,18-^{13}C_2]$retinylidene rhodopsin and $[8,16/17-^{13}C_2]$retinylidene rhodopsin in ROS disk membranes had been successfully trapped in their respective meta-I photostates the structure and environment of the β-ionone ring could be investigated in this photointermediate, using solid-state ^{13}C NMR.

A number of biochemical and spectroscopic studies incorporating modified retinal analogues have indicated that the ring is directly involved in conducting changes in the retinal structure upon 11-Z→ 11-E isomerization, into changes in the opsin structure that produce the active form of the receptor [70, 85, 129, 131]. A study on the rhodopsin pigment regenerated with the modified retinal analogue illustrated in Figure 5.1, showed that substitution of the β-

ionone ring by two ethyl groups severely inhibited transducin activity, concluding that steric interactions between the β-ionone ring and the protein were essential for meta-II formation [131].
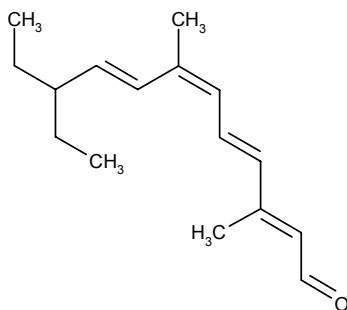
Figure 5.1 – Chemical structure of diethyl-acyclic-9-Z retinal. The rhodopsin pigment regenerated with this retinal formed very little meta-II intermediate following activation, and resulted in greatly reduced activation (18%) of transducin compared to 9-Z retinal with an unmodified β-ionone ring [131].

This hypothesis was supported by a study on rhodopsin pigments regenerated with constrained retinal analogues that had a bridge between C10 and C13, to prevent isomerization around the C11-C12 bond. These rhodopsin pigments were stabilized in their inactive conformation, even in the light [85, 230]. Photoisomerization of these retinals could still occur in the binding site, albeit not around the C11-C12 double bond, resulting in the extraction of several isomers following illumination (9-Z and/or 13-Z forms of the ring-constrained 11-Z analogue)[85]. However, transducin activation assays and FTIR spectroscopy showed that this photoisomerisation did not result in significant transducin activity, or in chromophore-induced structural changes in the opsin moiety [85, 230], suggesting that repositioning of the β-ionone ring following C11-C12 isomerization was required for rhodopsin activation.

It is well established that the formation of the primary photointermediate, bathorhodopsin, and its successive BSI intermediate is primarily restricted to changes in the chromophore structure [59]. Isomerization around the C11-C12 bond generates a twisted 11-E structure

that relaxes to the BSI intermediate, predicted to include a movement of the β-ionone ring with respect to the polyene chain [59, 76].

FTIR data [130], together with NMR [78, 79, 133] and Resonance Raman measurements [81, 124] indicated that the chromophore adopts a more relaxed structure in the lumi rhodopsin photointermediate and that this relaxation was complete by the meta-I intermediate. However, whereas the photocycle up to BSI is confined to changes in the retinal structure, the formation of the lumi rhodopsin intermediate was shown to be accompanied by a change in the protein structure. The appearance of a strong CD band upon formation of lumi rhodopsin was attributed to a new chromophore-protein interaction, whilst the ability to photoregenerate 7-Z retinal, with its highly twisted ring-chain conformation in lumi rhodopsin but not batho rhodopsin provided evidence for an expanded retinal binding pocket in the lumi rhodopsin state [227]. FTIR and UV-VIS spectroscopy studies [99, 129] also suggested the BSI to lumi transition involved a relaxation of the protein, and through the use of ring modified retinal analogues this was shown to involve the region near the β-ionone ring [71, 99].

Coupling these protein changes to a movement of the β-ionone ring was made following a photoaffinity labelling study that used a retinal analogue with two photoactive moieties (DK-Rh; Figure 5.2). Photoaffinity labelling of the dark state and batho intermediate resulted in cross-linking to Trp-265 on H6 (yellow; Figure 5.2), suggesting minimal movement of the β-ionone ring for this transition. However, in the lumi, meta-I and meta-II intermediates the cross-linked residue was Ala-169 on H4 (green; Figure 5.2) [83, 84].

It was concluded that the β-ionone ring flipped out of the binding pocket for the batho→lumi transition and the subsequent TM rearrangement of the helices resulted in the lumi and

meta-I intermediates [85]. The new position of the β-ionone ring was suggested to initiate a sequence of conformational changes that produce the activated meta-II receptor. By tracing the path of the retinal throughout the photocycle this result suggested that repositioning of the β-ionone ring was required for rhodopsin activation and significantly, that this change occurred early in the photocycle. The movement of the β-ionone ring would require a relatively large scale rearrangement of the protein structure to bring the chromophore in close proximity to H4 in lumirhodopsin.
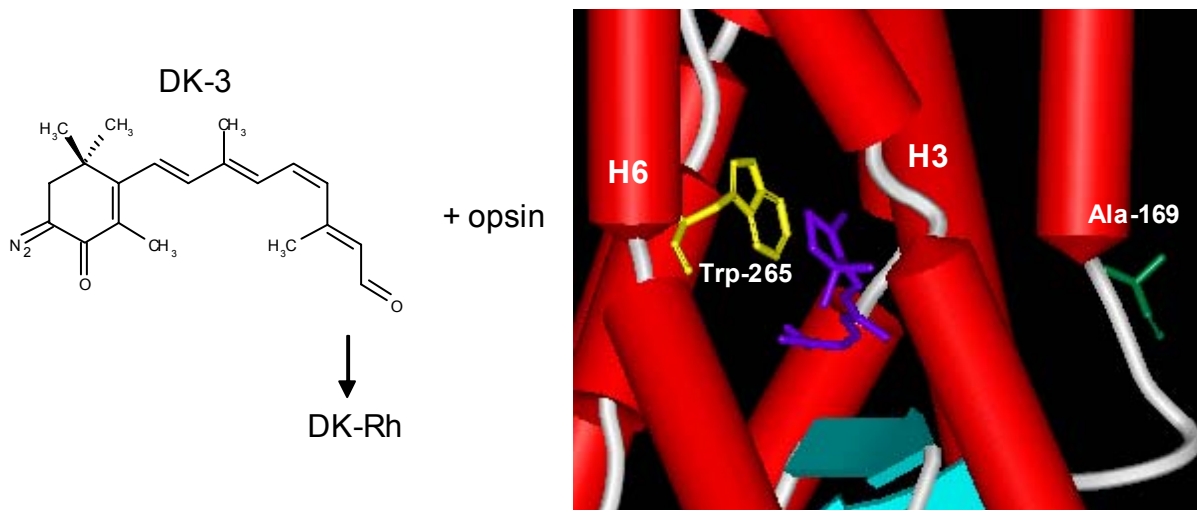
Figure 5.2 – Reaction mechanism for the regeneration of opsin with photoDK-Rh used to trace the path of the retinal during the photocycle. Photoaffinity labelling of DK-Rh resulted in cross-linking to Trp-265 in the dark (yellow). The same amino-acid was cross-linked when the pigment was photoisomerized to DK-batho-Rh, suggesting minimal movement of the chromophore during this transition. Upon forming the lumi, meta-I and meta-II intermediates the cross-linked residues was Ala-169, indicating a dramatic repositioning of the ring for the batho→ lumi transition. The model of the rhodopsin was taken from the PDB entry 1HZX for the crystal structure with the native 11-Z chromophore (purple).

The importance of this result for the activation mechanism of the protein, and for GPCRs in general, meant that further investigation of this predicted change in chromophore environment would be useful. As the experiment had been conducted using a significantly modified retinal chromophore (see Figure 5.2) it was preferable to re-examine the suggestion

using the natural chemically unmodified chromophore, unperturbed in the chromophore binding pocket and displaying conventional UV-VIS characteristics.

The availability of the rhodopsin samples with ^{13}C labels on the β-ionone ring, trapped in their respective meta-I photointermediate states enabled an investigation into β-ionone ring movements in photointermediates using solid-state NMR. The way in which the dark state NMR data had been interpreted, particularly the observation of a constrained C16/C17 methyl conformation in bound retinylidene (Section **Error! Reference source not found.**), would enable the retinals to act as a probe for the environment of the ring if flipped out of the binding pocket, as predicted in the meta-I state [83, 84].

The conformation of the ring with respect to the chain was also directly of interest as it had been predicted to adopt an all-*E* structure by solid-state ^{2}H NMR [78-80], in which steric interactions and torsional twists observed in the ground state retinal had relaxed so that the chromophore was approximately planar.

This was in contrast to a study that had shown that opsin regenerated with a 6-*s*-*cis* locked retinal analogue was capable of activating transducin (80% wild type activity) and therefore passed through the meta-I intermediate state in a 6-*s*-*cis*, 11-*E* conformation [126]. The ^{2}H NMR studies were viewed with caution as the rhodopsin samples in DMPC membranes had been estimated to be 70-80% meta-I rhodopsin [80], when in fact the proportion would have been less than 50%, the remainder being rhodopsin and isorhodopsin (see Section **Error! Reference source not found.**). However, the analogue study using 6-*s*-*cis* locked retinal [126] did not prove unequivocally that the retinal adopted a 6-*s*-*cis* conformation in meta-I rhodopsin, because a locked 6-*s*-*trans* retinal pigment was not shown to be incapable of activating transducin, as a control study [126].

5.2 Aims

The aim of this study was to use the rhodopsin samples regenerated with ^{13}C labels on the ring methyls (C16, C17 and C18) and the C8 position on the chain, as a *non-invasive* probe of the structure and environment of the chromophore in the meta-I photointermediate state.

RR NMR was used to determine the relative orientation of the β-ionone ring and the polyene chain in the meta-I intermediate, by measuring the internuclear distances in the [8,18-[13]C$_2$]retinylidene meta-I and [8,16/17-[13]C$_2$]retinylidene meta-I rhodopsin samples. These samples had been previously trapped with 42% of the rhodopsin in the meta-I intermediate, using the procedure developed and quantified in Chapter 4.

It was also intended to determine the conformation of the β-ionone ring in the isorhodopsin component by measuring the internuclear distance between C8 and C18 using RR NMR. The isorhodopsin component comprised 41% of the photoproduct in the meta-I trapped rhodopsin samples.

By observing changes in the chemical shifts and lineshapes of the individual resonances, observations on the environment of the β-ionone ring and polyene chain in the meta-I state could hopefully be made. Together with the intermolecular distances between the ring and the polyene chain, the conformation and binding characteristics of the β-ionone ring in the meta-I state could be determined, clarifying the role of the chromophore in the activation mechanism.

5.3 Materials and methods

The [8,18-[13]C$_2$] and [8,16/17-[13]C$_2$]retinylidene rhodopsin samples had been trapped in their meta-I photointermediate states following the procedure previously established. Once

trapped, the samples were kept below -70°C at all times ensuring that the photointermediate remained in the meta-I state [217].

All NMR measurements were conducted at 125.8MHz for ^{13}C and 500.1MHz for protons using a Chemagnetics (Varian) Infinity spectrometer. A 4mm double resonance Chemagnetics Apex MAS probe was used at -80°C. A lower temperature was used than for the dark state rotational resonance measurements (-60°C) ensuring the samples were kept below the meta-I transition temperature (-20°C) in the presence of possible heating effects from sample spinning. The temperature was controlled ±1° using a Chemagnetics temperature controller and the spinning was maintained at ±3Hz through the experiments using a Chemagnetics spinning speed controller.

CP-MAS spectra of rhodopsin samples were acquired with a 30% linear ramp [197] on the output for the carbon frequency and with 63kHz proton decoupling. Field strengths for ^{13}C were around 63kHz throughout.

The Rotational Resonance NMR experiments, data analysis and generation of exchange curves were as previously described (Section **Error! Reference source not found.** and **Error! Reference source not found.**). The inversion of the methyl ^{13}C spins was accomplished with a DANTE pulse train. Proton field strengths of 63kHz used for the CP were increased to 100kHz for decoupling during the rotational resonance mixing time period and signal acquisition. Field strengths for ^{13}C were around 63kHz throughout.

The data was stored in 1024 points and prior to Fourier transform the FID arrays were zero-filled up to 8192 points. Exponential linebroadening was typically in the region of 70Hz. All NMR chemical shifts were externally referenced to the methylene resonance of adamantane which resonates at 38.6ppm downfield from TMS.

Magnetization exchange curves were simulated using the RR-FIT program developed by Prof. C.Glaubitz [195].

5.4 Results

5.4.1 CP-MAS NMR on [8,18-^{13}C$_2$]retinylidene meta-I rhodopsin

The CP-MAS NMR spectrum of [8,18-^{13}C$_2$]retinylidene rhodopsin showed a single resonance for C8 at 139.4ppm in dark state rhodopsin (Figure 5.3 (a)), corresponding to a 6-*s-cis* conformation for the β-ionone ring of retinylidene (Chapter 3).

The CP-MAS NMR spectra of [8,18-^{13}C$_2$]retinylidene meta-I rhodopsin (Figure 5.3 (b)) and [8,16/17-^{13}C$_2$]retinylidene meta-I rhodopsin (Figure 5.3 (c)) had previously been used to quantify the conversion rate of rhodopsin to meta-I, together with the changes in the resonance distribution observed for the [10,20-^{13}C$_2$]retinylidene rhodopsin to meta-I transition (Section **Error! Reference source not found.**).

The C8 carbonyl region of both CP-MAS NMR spectra contained two resonances corresponding to the three components produced in meta-I trapping; isorhodopsin at 130.9ppm and rhodopsin together with meta-I rhodopsin at 139.2ppm. The proportion of isorhodopsin was measured as 40% for [8,18-^{13}C$_2$]retinylidene meta-I rhodopsin and 42% for [8,16/17-^{13}C$_2$]retinylidene meta-I rhodopsin, both trapped under identical conditions.
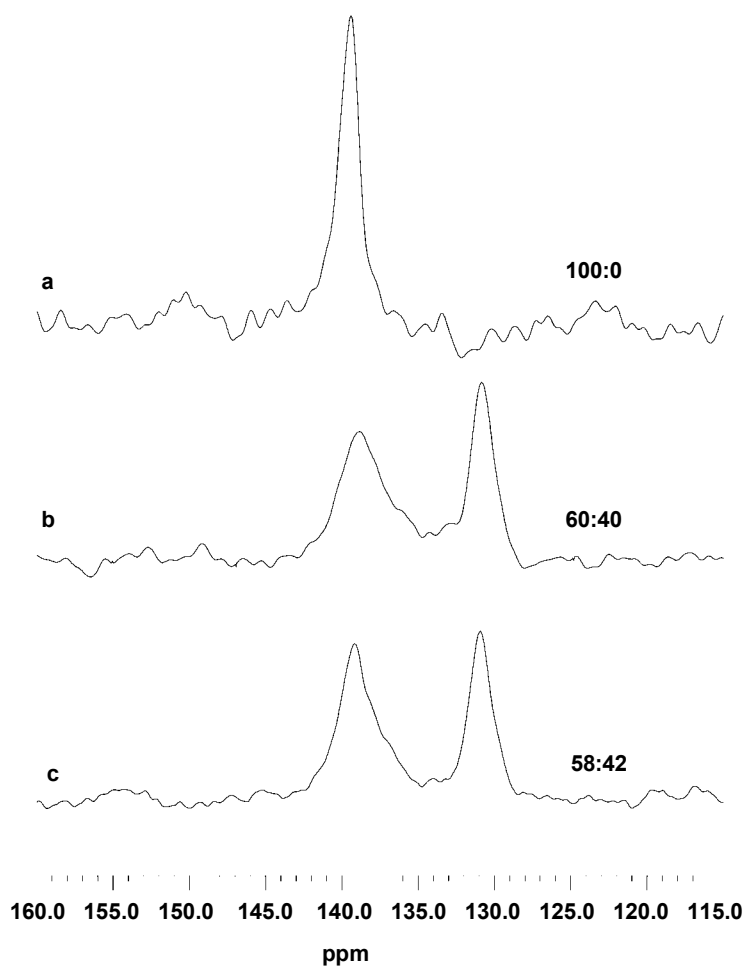
Figure 5.3 – CP-MAS NMR difference spectra of the C8 region of [8,18-$^{13}C_2$]retinylidene meta-I rhodopsin in the dark state (a) and trapped in its meta-I state by illumination at -188°C (360min; white light; 3300K) followed by incubation at -20°C (b). The C8 region of [8,16/17-$^{13}C_2$]retinylidene meta-I rhodopsin trapped under the same conditions (c). In the meta-I photointermediate state two resonances were observed: a narrow (200Hz) resonance at 130.9ppm assigned to isorhodopsin and a broad (400Hz) resonance at 139.2ppm assigned to both dark state rhodopsin and meta-I rhodopsin. The relative intensity of the resonances was determined by Lorenztian line fitting for each spectrum. $\omega_r/2\pi=10000\pm 3$Hz

The chemical shift of the C8 resonance is very sensitive to the conformation around the C6-C7 bond, due to the steric effect of the C16 and C17 methyls attached on the β-ionone ring [32]. The appearance of both rhodopsin and meta-I at the same resonance (139.2ppm) offered preliminary indications that the ring adopted a *6-s-cis* conformation in the meta-I photointermediate state, based on previous RR NMR measurements on rhodopsin (Section **Error! Reference source not found.**) and previous chemical shift assignments (Table 3.1).

Confirmation of the absolute C6-C7 conformation would require an internuclear distance measurement between C8 and C18 using an RR NMR experiment in the meta-I photostate.

In general there was an increase in the linewidths for samples in the meta-I state compared to the dark state, possibly due to a lower operating temperature (-80°C in meta-I state, -60°C in the dark state). This could not account for the pronounced increase in the linewidth of the C8 meta-I resonance (120Hz, dark state to 400Hz, meta-I; Figure 5.3 (b) and (c)), which suggested a less discreet ring conformation existed compared to dark state rhodopsin. An increase in conformational heterogeneity for C8 indicated a less constrained environment for this region of the polyene chain in the meta-I photostate.

Just one resonance was observed for the C18 resonance, which had not shifted from its dark state position (22.2ppm meta-I; 22.1ppm rhodopsin) although it had increased in linewidth by approximately 70Hz. This suggested that the C18 methyl was in a similar, but less homogenous environment to that in the dark state structure.

5.4.2 Determining the conformation of the β-ionone ring in [8,18-^{13}C$_2$]isorhodopsin using RR NMR.

Isorhodopsin is thought to adopt the same β-ionone ring environment as the natural 11-*Z* chromophore within the opsin binding pocket [32]. Accordingly, it has been postulated to have a 6-*s-cis* conformation, even though the chemical shift for C8 would at first indicate a 6-*s-trans* conformation. This is due to the steric effect of the protons on the C18 and C11 carbons that mimic the shielding of the C16 and C17 methyls in the 6-*s-trans* 11-*Z* isomeric conformation. No direct evidence was available for the absolute conformation around the C6-C7 bond for isorhodopsin.
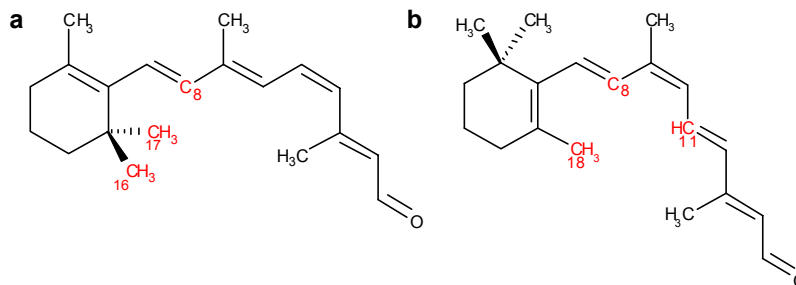
Figure 5.4 – Schematic representation of 11-*Z* retinal (a) and 9-*Z* retinal (b). The steric hindrance from the protons from the C16 and C17 methyl groups in 11-*Z* retinal creates the same shift to lower frequency for the C8 resonance (~131ppm) as the protons from C18 and C11 in 9-*Z* retinal [32, 105].

To determine the ring conformation for isorhodopsin, a RR NMR experiment was performed between the C8 resonance at 130.9ppm and C18 at 22.2ppm. From the frequency difference between the two resonances the spinning speed was set at 13660Hz, corresponding to the n=1 rotational resonance condition. The intensities of the resonances were measured through Lorentzian peak fitting and the exchange of Zeeman magnetization plotted as a function of mixing time (τ_m), which was varied between 0 and 40ms. The rotational resonance exchange between C18 and the C8 isorhodopsin resonance is plotted in Figure 5.5 as a function of time. The net magnetization ($<I_z\text{-}S_z>$) following inversion of the methyl resonance has been corrected for the proportion of C8 label participating in exchange with C18, corresponding to 41% of the overall C8 intensity (Section **Error! Reference source not found.**). The corrected intensities have then been normalised to the initial, corrected net magnetization averaged from a number of short mixing times (<0.1ms).

For the dark state rhodopsin RR NMR measurements the aim was to obtain accurate distance measurements between C8 and the ring methyls, hence the error limits on the distance measurements were indicated by showing the maximum and minimum simulated distances that covered the spread in the exchange data (±0.15Å between C8 and C18, Figure 3.14; ±0.25Å between C8 and C16/C17, Figure 3.12). Due to the mixed population of

isomers formed in trapping the meta-I intermediate, the proportion of C8 resonance participating in rotational resonance exchange for isorhodopsin and meta-I was much less than in the dark state (~40% for each). With broader lines and less data available it was unrealistic to obtain a reliable distance measurement, but instead the aim was to deduce the absolute β-ionone ring conformation by comparison with the dark state exchange data.

Errors were deduced for the maximum and minimum relative intensities for each time point, calculated from manually fitting the maximum and minimum Lorenztian to each C8 and C18 resonance. This resulted in larger errors than would be calculated through signal-to-noise calculations but it was thought this accurately represented the subjective nature of the fitting process.
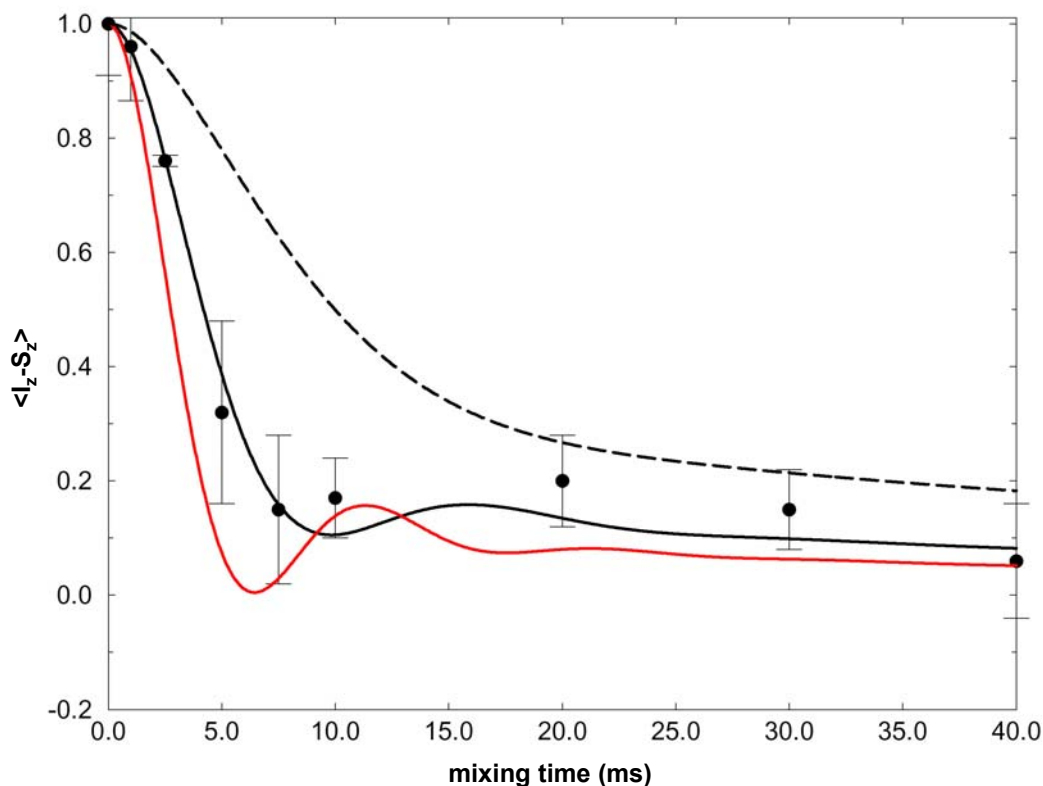
Figure 5.5 – Exchange data for the n=1 rotational resonance experiment between C18 (22.2ppm) and the C8 isorhodopsin resonance at 130.9ppm (filled circles) for [8,18-^{13}C$_2$]retinylidene meta-I rhodopsin showing net magnetization as a function of mixing time. Net magnetization was corrected for the proportion of C18 participating in RR exchange (see text for details). Simulations are shown corresponding to a best-fit internuclear distance of 3.25Å (black line) and for 2.95Å (red line) and 4.05Å (dashed line), which represent the dark state 6-s-cis and 6-s-trans distances respectively. Errors were calculated from the maximum and minimum intensities that could be fitted to the C8 and C18 resonances at each time point.

By showing errors on the exchange data, comparisons with the exchange curves previously calculated for the C8/C18 and C8/C16/C17 RR NMR exchange data in the dark state could be made (Figure 3.14 and Figure 3.12, respectively). The exchange behaviour between C18 and the isorhodopsin C8 resonance (black circles) represented the exchange observed between C8 and C18 in dark state rhodopsin (2.95Å, red line) much closer than that between C8 and C16/C17 (4.05Å, dashed line) indicating that the β-ionone ring adopted a 6-*s-cis* conformation with retinal in both 11-*Z* and 9-*Z* forms.

A best-fit simulation to the data was made using the same estimate for T_2^{ZQ} determined for the ring methyls in the dark state (3±1ms). A dipolar coupling of 217Hz was derived, corresponding to an internuclear distance of 3.25Å. Taking into account the large errors on each of the intensities a 6-*s-cis* conformation was confirmed, possibly with a nominal increase in the C6-C7-C8-C9 torsion angle from that deduced for 11-*Z* retinal in rhodopsin (-28 ±7°).

5.4.3 Determining the conformation of the β-ionone ring in [8,18-^{13}C$_2$]retinylidene meta-I rhodopsin using RR NMR

To elucidate the absolute conformation of the retinylidene β-ionone ring in the meta-I photostate a RR NMR experiment was set between the broad meta-I (and rhodopsin) C8 resonance at 139.2ppm and C18 22.2ppm, corresponding to a frequency difference of 14.7kHz. The exchange is plotted in Figure 5.6 (open circles), corrected for the proportion of the C18 resonance that undergoes rotational resonance exchange with the C8 isorhodopsin resonance (41%)(Section **Error! Reference source not found.**).

The data exhibited the same biphasic character that had been observed for the exchange between C8 and C18 in dark state rhodopsin (Section **Error! Reference source not found.**). The majority of the exchange occurred within the first 5ms, followed by a very slow decrease over the longer mixing times (10 to 40ms), indicating a mixed population of

strongly and weakly coupled spin pairs. The minor *6-s-trans* components that had previously been detected in [8,18-^{13}C$_2$]retinylidene rhodopsin appeared to also be present in the meta-I photointermediate state (Section **Error! Reference source not found.**). Accordingly, a 30% correction was applied for the proportion of C8 and C18 not participating in the major rapid (<5ms) phase of exchange, as used in the dark state measurement (Section 3.4.4). The corrected exchange data (filled circles, Figure 5.6) showed a good fit to the initial region of the rhodopsin C8/C18 exchange curve (<5ms), however less so over later mixing times (red line, Figure 5.6). This could be accounted for by off-resonance effects resulting from the difference in linewidths between the two exchanging resonances, preventing all of the broad meta-I C8 resonance participating in rotational resonance exchange with the narrower C18 resonance. Even with these complications, the distance estimated between C8 and C18

Figure 5.6 – Exchange data for the n=1 rotational resonance experiment between C18 (22.2ppm) and the C8 meta-I resonance at 139.2ppm for [8,18-^{13}C$_2$]retinylidene meta-I rhodopsin showing net magnetization as a function of mixing time (open circles). The net magnetization was corrected for the presence of *6-s-trans* minor components and the proportion of C18 participating in rotational resonance exchange (filled circles)(see text for details). Simulations are shown corresponding to a best-fit internuclear distance of 3.40Å (black line) and for 2.95Å (red line) and 4.05Å (dashed line), representing the dark

confirmed that the β-ionone ring of retinylidene in the meta-I photointermediate state adopted a 6-*s-cis* conformation, as expected from the isotropic chemical shift measurements.

A simulated exchange curve was fitted to the corrected data, corresponding to an internuclear distance of 3.40Å (black line, Figure 5.6), however this did not fit the initial fast exchange of magnetisation particularly well. Although difficult to confirm with the data, this could indicate that the ring adopts a more twisted 6-*s-cis* conformation in the meta-I photointermediate compared to dark state rhodopsin (-28 ±7°).

5.5 Binding of the β-ionone ring in [8,16/17-^{13}C$_2$] and [16/17-^{13}C$_2$] retinylidene meta-I rhodopsin

In the CP-MAS NMR spectrum of dark state rhodopsin containing [8,16/17-
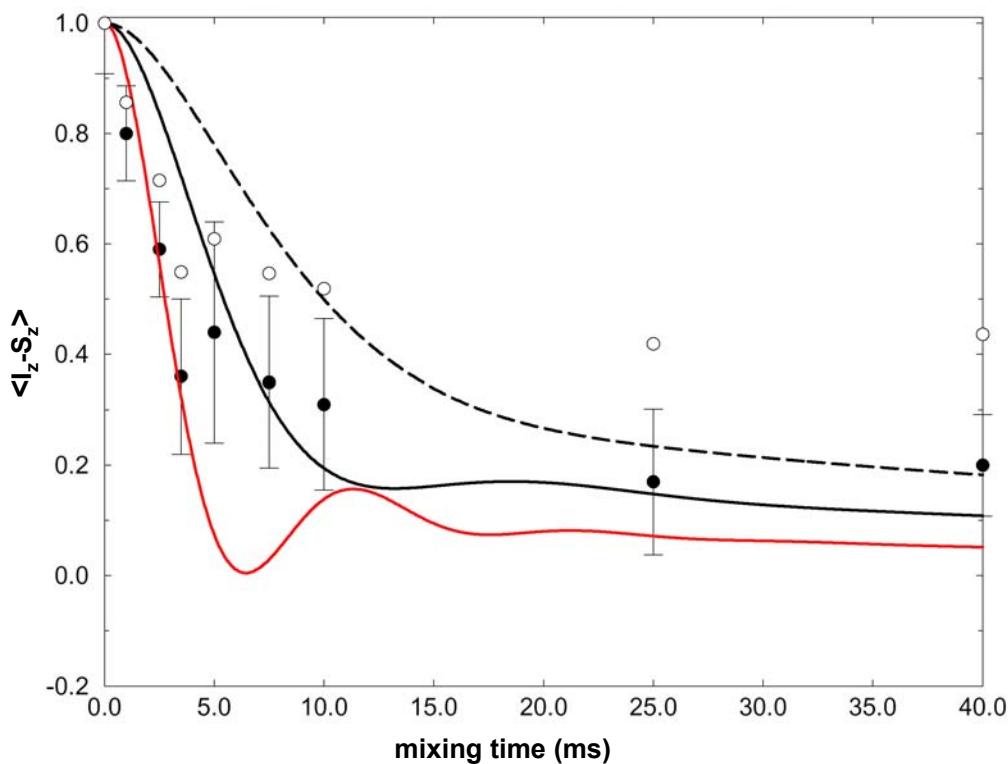
^{13}C$_2$]retinylidene a chemical shift inequivalence was observed for the C16 and C17 (30.7ppm and 26.4ppm, respectively Figure 5.7 (b)) (Section **Error! Reference source not found.**).

This had been attributed to an axial and equatorial conformation adopted by the C16 and C17 methyls when bound to the protein (both 28.9ppm in solution [133]).

The methyl region of subtracted CP-MAS spectra of $[8,16/17-^{13}C_2]$retinylidene meta-I rhodopsin (Figure 5.7 (a)) showed the same characteristics as had been observed in the dark state (Figure 5.7 (b)). Processed with the same linebroadening, (60Hz) both spectra showed a shifted C17 resonance (**1**), approximately 4.5ppm downfield from C16 (**3**), with a proportion of 6-*s-trans* minor components between the major C16 and C17 resonances (**2**).

Deconvolution of both spectra indicated a similar proportion of intensity between the major C16 and C17 components in the dark (40% C16, 34% C17) and in the meta-I (35% C16, 29% C17) photostates. The contribution from the minor components was greater in the meta-I state, possibly as a result of deconvoluting the broader meta-I resonances, however it appeared the methyls were in similar axial/equatorial conformations in both photostates.

The C17 resonance was broader in the meta-I state (230Hz) than in the dark state (200Hz) and shifted to a slightly lower chemical shift (by 0.4ppm), suggesting that the C17 methyl group was oriented slightly more towards an axial conformation in the meta-I photointermediate than in the ground state conformation.
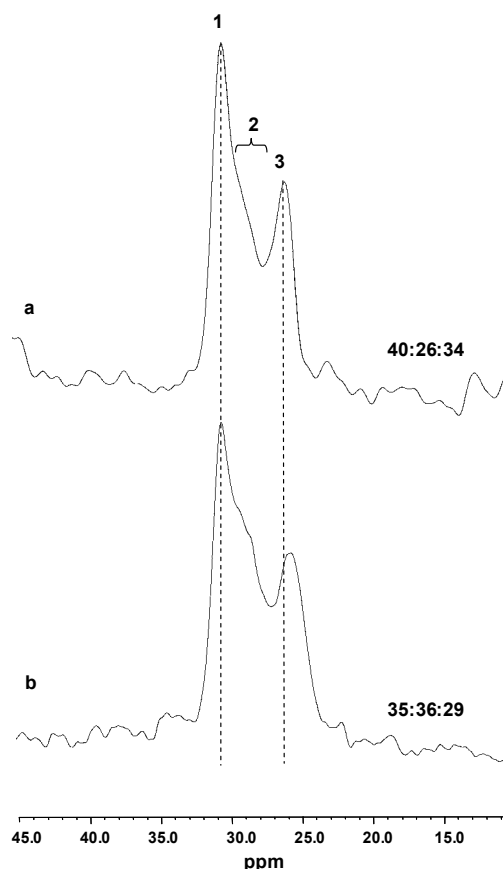
Figure 5.7 - The methyl region of the subtracted CP-MAS spectra of $[8,16/17-^{13}C_2]$retinylidene rhodopsin in the dark (a) and meta-I (b) photostates. Both spectra showed a shifted C17 resonance (**3**) at ~4.5ppm lower frequency than the C16 resonance (**1**, 130.8ppm) with a proportion of 6-*s-trans* minor components between the major C16 and C17 resonances (**2**). The relative intensity of the components **1**, **2** and **3** was determined by Lorenztian line fitting for each spectrum (displayed as **1:2:3**). Both rhodopsin and meta-I rhodopsin spectra showed the same features in approximately the same proportions. $\omega_r/2\pi=10000\pm3$ Hz.

A RR NMR experiment was attempted between the C8 and the C17 resonance in the meta-I state however with broader lines, and such a small proportion of C8 undergoing exchange (~25%), the data obtained could not be quantified reliably. Overall, the exchange observed between C8 and C17 appeared much weaker than between C8 and C18, indicating a longer internuclear distance (>~4Å) and supporting the 6-*s-cis* conformation.

To investigate the environment of the β-ionone ring in the meta-I state further, rhodopsin regenerated with retinal ^{13}C labelled at both C16 and C17 positions ($[16,17-^{13}C_2]$retinylidene rhodopsin], see Table 2.5 for UV-VIS characterisation details) was trapped in the meta-I

photointermediate state, using the established procedure (Section **Error! Reference source not found.**). This sample contained a much smaller contribution from minor components (6%) and therefore was easier to observe any changes occurring in the chemical shifts or intensities of the major C16 and C17 methyl resonances (**Error! Reference source not found.**21).

As with $[8,16/17-^{13}C_2]$retinylidene rhodopsin, nominal changes were observed between the dark and meta-I subtracted CP-MAS NMR spectra (Figure 5.8). The relative intensities of the C16 and C17 resonances were approximately equal in both states (46:6:48 rhodopsin, 44:10:46 meta-I rhodopsin), and as observed previously, the C17 resonance increased in linewidth (by 25Hz) and shifted to lower frequency (26.0ppm to 25.7ppm) in the meta-I photostate, suggesting a slight increase in the torsional axial/equatorial twist around C1. Overall, the similarity between the spectra in the dark state and the meta-I intermediate indicated that the methyls were in the same restrained conformation in both photostates.
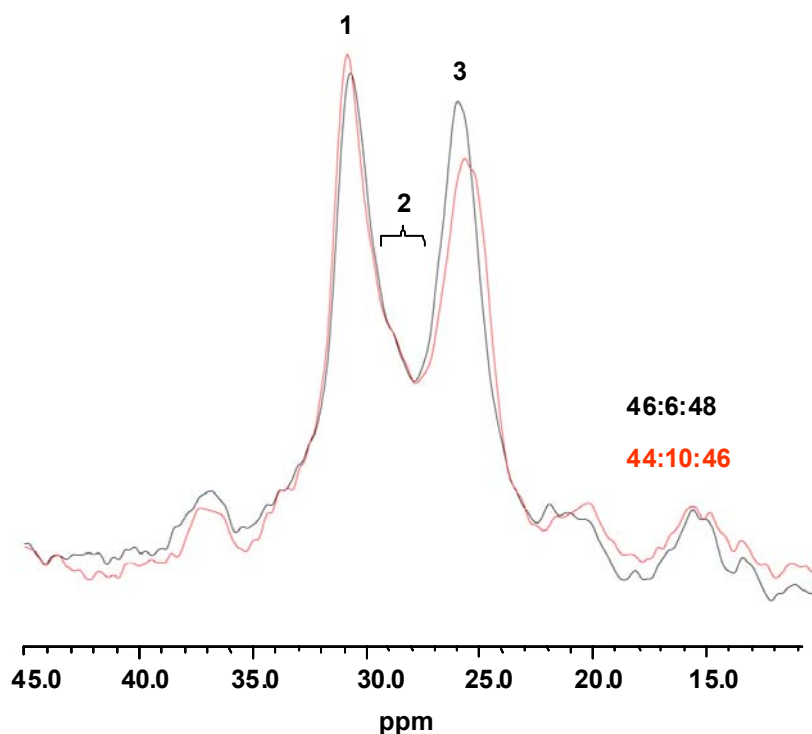
Figure 5.8 - The methyl region of the subtracted CP-MAS spectra of $[16,17-^{13}C_2]$retinylidene rhodopsin in the dark (black) and meta-I (red) photostates. The relative intensity of the components **1**, **2** and **3** was similar for each spectrum (displayed as **1:2:3**), indicating that the methyls adopted the same restricted conformation in both photostates. $\omega_r/2\pi = 10000 \pm 3Hz$.

To show that the chemical shift separation observed for the C16 and C17 methyls was a result of binding within the protein the retinal was fully bleached out of the binding pocket. Hydroxylamine (10μl 0.5M hydroxylamine hydrochloride, pH 6.5) was added to the solid rhodopsin sample and illuminated for 3min (3000K; white light; 20°C). The sample turned yellow/white indicating that the retinal had been removed from the binding site, in the all-*E* oxime form. The resulting CP-MAS NMR spectrum showed a broad single isotropic resonance for the C16 and C17 labelled nuclei at 29.4ppm resulting from a range of frozen orientations for C16 and C17, but with a single average orientation. This indicated that the characteristic chemical shift discrimination between C16 and C17 was lost outside the binding pocket, with an equivalent equatorial conformation for both methyl groups when unconstrained by the protein. The large (~4.5ppm) chemical shift separation could be considered to be highly diagnostic of the β-ionone ring when restrained by strong contacts with the opsin binding pocket, supporting a similar constrained ring 6-*s*-*cis* conformation in the dark and meta-I photostates.
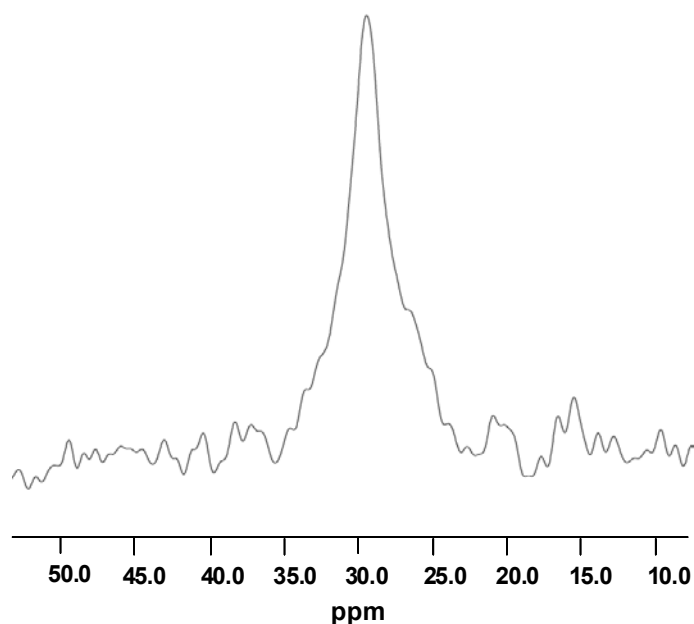
Figure 5.9 — The methyl region of the subtracted CP-MAS spectra of [16,17-$^{13}C_2$]retinylidene rhodopsin following bleaching in the presence of hydroxylamine (3min; 3000K white light; 20°C with 10μl 0.5M hydroxylamine hydrochloride added). The all-*E* retinal in its oxime form showed a single resonance for both C16 and C17 methyls when fully bleached out of the opsin binding pocket.

5.6 Discussion

The RR NMR measurement between C8 and C18 in the meta-I photostate indicated that the relative orientation between the polyene chain and β-ionone ring were similar in the dark state and meta-I intermediate state (6-*s-cis*), in contrast to the previous model of the retinylidene in rhodopsin derived from ^{2}H NMR [80]. The observation of a constrained conformation for the C16 and C17 methyls in the dark and meta-I photostates showed that the β-ionone ring had not changed its environment significantly with respect to the protein, indicating that the β-ionone ring accommodated a similar binding site in both photostates. Although it was possible that the ring could be in a 6-*s-cis* conformation if relocated within the protein, it was extremely unlikely that the C16 and C17 methyls would readopt the same constrained conformation in their new environment.

This result suggested that the ring *does not* flip out of the binding site upon forming the lumirhodopsin photointermediate as predicted by photolabelling studies [83, 84] and implied that the protein changes that accompany the BSI to lumirhodopsin transition are limited to the region adjacent to the β-ionone ring.

In a recent time-resolved UV-VIS spectroscopy study, the bleaching kinetics of an artificial visual pigment with modifications near the ring-polyene chain connection were studied [125]. It was found that the decay of the lumi intermediate could be dramatically increased by extending the C18 methyl group to an ethyl residue (Figure 5.10 (a)) and the meta-I/meta-II equilibrium could be shifted significantly towards meta-I by locking the ring in a 6-*s-trans* conformation (Figure 5.10 (b)). It was difficult to interpret these results in terms of specific details for the activation mechanism, but it demonstrated a general control of the late photocycle reactions by synthetic modifications of the chromophore near the ring.

These results support the suggestion that the β-ionone ring is not repositioned upon forming meta-I rhodopsin, because the structure of the ring would not be expected to have such a significant control over formation and decay of the meta-I and meta-II intermediates if flipped out of the binding pocket.
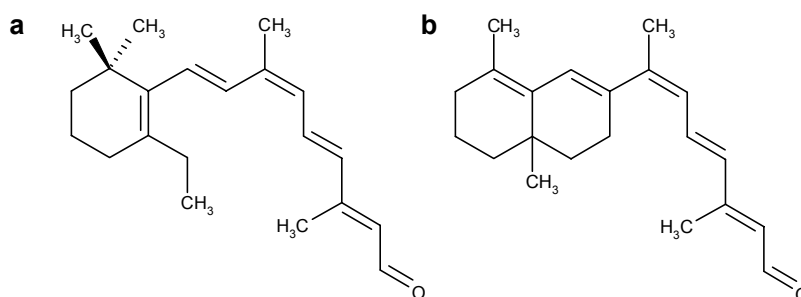
Figure 5.10 – Schematic representation of 9-*Z*-5-ethylretinal (a) and 9-*Z*-8,16-methanoretinal (b). Time-resolved UV-VIS spectrophotometry of the rhodopsin pigments regenerated with both retinals showed dramatically altered photolysis characteristics for the later photointermediates (meta-I and meta-II) (see text for details).

By observing the changes in the protein region (270-310nm) of the UV-VIS spectra of rhodopsin in the ground, meta-I and meta-II photostates, Lin and Sakmar identified perturbations in the environments of tryptophan and/or tyrosine residues that only occurred for the meta-I→ meta-II transition [231]. The absence of any large spectral feature in the rhodopsin/meta-I difference spectrum suggested that the opsin structure of rhodopsin and meta-I rhodopsin were not significantly different. Using site-directed mutagenesis to investigate the contribution of individual tryptophan residues to the observed UV-VIS changes, Trp-126 (H3) and Trp-265 (H6) were shown to move to more polar environments during receptor activation, supporting the hypothesis for rigid-body movement of H3 and H6 [86, 87] and indicating that a change in opsin structure accompanied the formation of the active meta-II conformation.

Viewing changes in the whole protein structure, FTIR difference spectra have indicated that the largest light-induced alterations of the opsin structure take place upon meta-II formation

[232], consistent with the volume increase observed to accompany meta-II formation [233]. The sensitivity of the meta-I/meta-II equilibrium to the fluidity of the membrane [226, 234], as demonstrated in this study by the trapping of the meta-I intermediate by the partially delipidated ROS membranes (Section **Error! Reference source not found.**), and the large entropy change observed for the meta-I→ meta-II transition [235] suggest a slight unfolding of the protein at this point in the photocycle.

The results from this study indicate that the chromophore of rhodopsin triggers the large-scale rearrangement of the opsin structure that is required for receptor activation, with the β-ionone ring positioned in the dark-state binding pocket. The implications of this result for the activation mechanism of rhodopsin, and for GPCRs in general are considered in Chapter 6.

5.7 Conclusions

CP-MAS and rotational resonance NMR have been successfully used to study the conformation of the β-ionone ring in $[8,18-^{13}C_2]$retinylidene rhodopsin, $[8,16/17-^{13}C_2]$retinylidene rhodopsin and $[16,17-^{13}C_2]$retinylidene rhodopsin in their respective meta-I photointermediate states.

Internuclear distance measurements between the C18 methyl group on the ring and C8 on the polyene chain have shown that the β-ionone ring adopts a 6-*s-cis* conformation in the meta-I photostate, similar to that observed for 11-*Z* retinylidene in dark state rhodopsin.

The C16 and C17 methyl groups were shown to be positioned in a similar axial/equatorial conformation in both dark and meta-I photostates, suggesting that the ring remains bound in the dark state binding pocket in the meta-I intermediate.

Using rotational resonance NMR internuclear distance measurements between C8 and C18 in isorhodopsin, it has been shown that the β-ionone ring adopts a *6-s-cis* conformation around the C6-C7 bond in bound 9-*Z* retinal, in agreement with previous NMR chemical shift predictions [32].

Chapter 6   General discussion

6.1   The helix movement model of rhodopsin activation

The light induced isomerization of the chromophore from 11-Z to the all-E geometry initiates the conversion of the chromophore-opsin complex via several spectrally distinct intermediates to the active meta-II state. During the transition from meta-I rhodopsin (λ_{max} = 480nm) to   meta-II rhodopsin (λ_{max} = 380nm) [217], the chromophore deprotonates and the protein adopts the active conformation, defined by a change in the structures of the loop domains on the cytoplasmic surface to conformations that are capable of binding and activating transducin [42, 67].

The transduction of the signal (i.e. light absorption) from the interior of the receptor to the surface loops is thought to be accomplished by modification of its transmembrane (TM) structure through the relative disposition of TM helices within the core of the receptor [86, 87]. The functional interaction of H3 and H6 (Figure 6.1) was probed in a study in which metal ion-binding sites were introduced between the cytoplasmic surfaces of TM helices, with the aim of restraining specific activation-induced conformational changes [86]. Pairs of

His residues are capable of chelating metal ions such as Zn^{2+}, if the distance and geometry between the residues are appropriate. His residues substituted for the native amino acids at the cytoplasmic ends of H3 and H6, but not H5 and H7, created mutant proteins that activated transducin in the absence, but not in the presence, of metal ions. It was concluded that specific metal ion cross-links between the His residues on H3 and H6 prevented receptor activation, indicating a direct coupling of receptor activation to a change in the spatial disposition of H3 and H6 [86]. In a similar experiment, double cysteine mutants were constructed with cysteines at various positions in H3 and H6. Magnetic dipolar interactions between spin labels attached to these residues revealed their proximity and changes in their interaction upon light activation to meta-II suggested a rigid body movement of helices relative to one another [87]. Disulphide cross-linking of the helices prevented activation of transducin, indicating the importance of this movement for the activation of rhodopsin.

Movement of α-helical domains is known to be involved in the signal transduction mechanisms of some TM receptor proteins, such as the bacterial chemoreceptors [236] and has been shown to occur during the proton-pumping cycle in bacteriorhodopsin [237, 238], the 7TM light-driven proton pump.
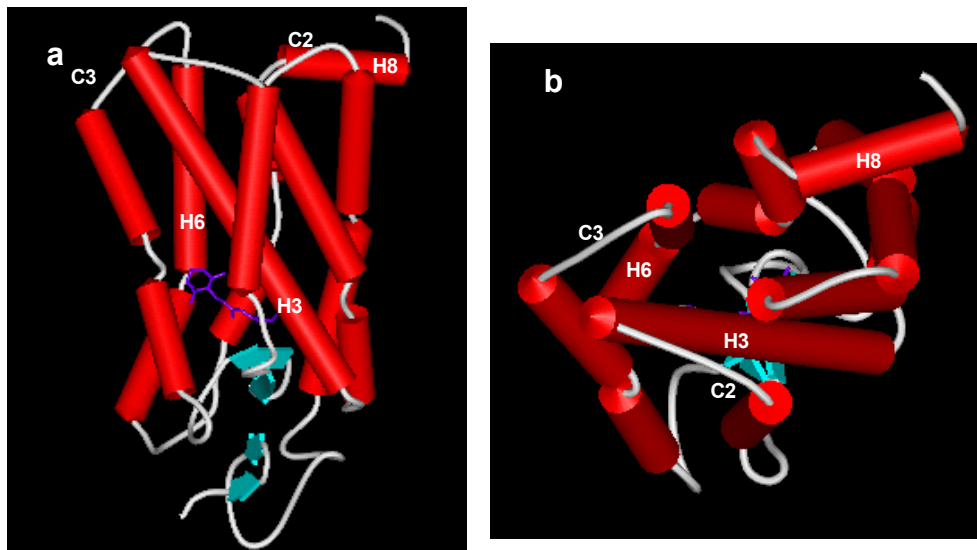
Figure 6.1 – The crystal structure of bovine rhodopsin (PDB entry: 1HZX) viewed perpendicular to the membrane normal (a) and down the membrane normal from the cytoplasmic face (b) [34]. Helix 3 (H3) and helix 6 (H6) have been shown to shift upon formation of the meta-II intermediate, resulting in a change in the structure of the domains on the cytoplasmic face. Cytoplasmic loops 2 and 3 (C2 and C3) and H8 have been

Movement of H3 and H6 results in structural reorganisation at the cytoplasmic face upon forming the meta-II state (see Section **Error! Reference source not found.** and Figure 6.1) enabling cytoplasmic loops 2 (C2, H3-H4 loop), 3 (C3, H5-H6 loop) and H8 to interact with transducin. [45, 46, 89-91]. Separation of H3 and H6 at the cytoplasmic face [86, 87] is thought to disrupt H-bond interactions within H3 (Glu-134 and Arg-135) and between H3 and H6 (Arg-135 and Glu-247) that stabilize the ground state structure [239], releasing Glu-134, that is subsequently protonated [88] and Arg-135, so it may interact with transducin [45, 55].

A recent model of the activated meta-II receptor was generated by assembling a series of overlapping peptide fragments with known structure (deduced by 2-D ^{1}H NMR) that together described the polypeptide chain of the protein [55]. Long-range distance constraints derived from a variety of independent experiments on the intact active receptor were used to define the tertiary structure of the construct. The region of the cytoplasmic face of the meta-II rhodopsin model, for which the most long-distance constraints were available, showed a separation of H3, H6 and H7 that disrupted interhelical interaction between Arg-135 and Glu-247 and formed a groove on the cytoplasmic face that could bind transducin.

6.2 The role of the β-ionone ring in the activation mechanism of rhodopsin

The use of modified retinal analogues has shown that the β-ionone ring forms the primary binding interaction with the opsin apoprotein [123]. This interaction is mediated predominately through the ring methyl moieties [98], which are essentially required for retinal binding and form a "point of anchor" within the binding pocket, the other being the Schiff base linkage to Lys-296 (see Section 3.7).

In Chapter 3 it was deduced using internuclear distance RR NMR measurements that the β-ionone ring of the bound retinylidene adopts a modest, negatively twisted 6-*s-cis* conformation around the C6-C7 bond (-28 ±7º), with C17 and C16 in respective axial and equatorial conformations. Analysis of the crystal structure of bovine rhodopsin suggested that this retinylidene conformation "fits" the approximate structure of opsin, and could enable key interactions between the ring methyl groups and the protein (Section **Error! Reference source not found.**). C18 is positioned in a cleft formed from residues from H3 (Gly-121) and H6 (Phe-261, Trp-265), all of which have been suggested to participate in hydrophobic binding interactions with the chromophore from biochemical and mutagenesis studies [113-115]. The axial/equatorial conformation for the C17 and C16 methyl that forms

upon binding of 11-*Z* retinal represents a protein induced restraint on the ring and a possible chromophore/opsin interaction. Therefore, binding of the β-ionone ring in a 6-*s-cis*

orientation provides a structural basis for coupling the chromophore to helical movements of H3 and H6 required for receptor activation.

The close proximity of C18 to residues from H3 and H6 suggests that helical movements are likely to be transmitted at least partially through contacts with the β-ionone ring. Removal of the C2-C4 ring segment of the chromophore almost abolishes formation of the active meta-II state of the receptor [131], whilst modifications to the ring methyl groups dramatically effect the formation of the later intermediates [125] (Section **Error! Reference source not found.**).

In contrast to previous models for the activation mechanism [42, 44, 53, 64, 67, 85] where the ring is ejected from the binding site upon forming lumirhodopsin, the observation of a
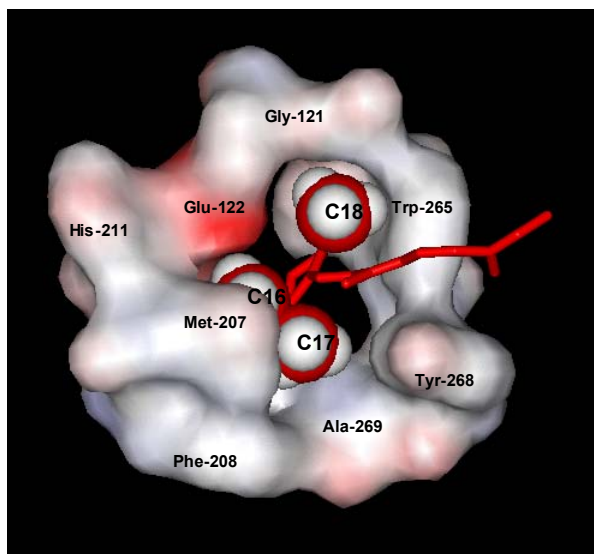
Figure 6.2 – Model of the binding pocket of the β-ionone ring of the 11-*Z* retinylidene chromophore of rhodopsin taken from the 2.8Å resolution crystal structure of bovine rhodopsin (PDB entry: 1HZX). The solvent accessible surface (1.4Å probe) of residues with contacts <5Å with the β-ionone ring is shown. Positively charged regions are shown in blue and negatively charged regions in red. The methyl group of the retinylidene, displyaed in space-filling CPK style, illustrates the binding pocket that forms around the ring in a 6-*s-cis* conformation, with a negative torsional twist around the C6-C7 bond.

6-*s-cis* ring conformation and restrained C16/C17 methyl conformation in both the dark and meta-I photo states in this study (Section **Error! Reference source not found.**) suggests

that the chromophore retains its ability to trigger receptor activation from within the dark state binding pocket. Formation of the meta-II intermediate accompanies a large shift in the absorption maximum from 478nm in meta-I to 380nm in meta-II as a result of deprotonation of the Schiff base followed by protonation of the counterion, Glu-113 [53, 217]. Proton transfer reactions are, in general, indicators of structural changes since they require the appropriate reorientation of donor and acceptor groups that form the hydrogen bonds [64]. It has been found that the C19 methyl group is essential for forming steric interactions with the protein that lead to the active meta-II intermediate [128, 132, 240] and suggested that the all-E retinal provides a scaffold for the correct adjustment of the donor/acceptor groups, which enable the structurally sensitive proton transfers [128]. This conformational change affects the environment of the protonated Schiff base such that its pK_a is lowered from 16 to about 2.5 in meta-II [241]. The resulting proton transfer destroys the salt bridge between Glu-113 and the Schiff base nitrogen, which is one of the stabilizing elements of the ground state structure [241].

The large increase in the linewidth of the C8 resonance in [8,18-$^{13}C_2$]retinylidene meta-I rhodopsin and [8,16/17-$^{13}C_2$]retinylidene meta-I rhodopsin suggests a more heterogeneous conformation and hence a less constrained binding pocket for this region of the polyene chain on forming the meta-I photointermediate. It is possible that relaxation of the polyene chain in forming the lumi and meta-I photointermediates allows a realignment of the residues adjacent to the C19 methyl group on H3 [34] until Glu-113 is positioned to facilitate charge transfer with the Schiff base. Charge transfer could lead to a reordering of residues around the Schiff base, destabilizing interhelical contacts and enabling the predicted helix movements that form the active receptor.

The β-ionone ring, participating in important chromophore/opsin contacts, would assist in

maintaining the overall conformation of the protein up until the point of activation. As this study investigates the structure and environment of the β-ionone ring up until the meta-I photointermediate it is not possible to predict the position of the β-ionone ring in the active meta-II state at present.

Displacement of H6 and H3 could be achieved by disrupting the interactions between the β-ionone ring, H3 and H6 through repositioning of β-ionone ring upon forming meta-II rhodopsin. Disrupting the hydrophobic contacts between H3 (Gly-121) and H6 (Phe-261) with the C18 methyl group by site-directed mutagenesis has been shown to result in partial agonist activity of the 11-Z chromophore [112, 113]. Additionally, a UV-VIS study observed a change in the environment of Trp-265 upon formation of the meta-II intermediate, which forms a boundary to the β-ionone ring and appears to interact closely with C18 from the rhodopsin crystal structure [34] and cross-linking studies [115].

Conversely, the "scaffold" that the β-ionone ring provides for the protein up to the meta-I photostate could be maintained in forming the active meta-II state. Movements of H3 and H6 were observed to be inhibited by cross-linking the helices at sites on the *cytoplasmic* face of the protein [86, 87]. As the β-ionone ring is positioned towards the *extracellular* face of the membrane it could act as pivot, maintaining its overall position within the binding pocket upon activation but enabling an altered configuration of the side chains of the residues around the β-ionone ring. Helix 6 is the most bent helix in rhodopsin (36°) because of the presence of Pro-267, which is one of the most conserved residues among GPCRs [34]. The proximity of Pro-267 to the β-ionone ring (~8Å) means it could act as a flexible hinge around which helical rearrangements could occur, resulting in the outwards movement of H6 at the cytoplasmic face. This mechanism is supported by a number of studies that propose that the extent of Pro-kink bending is associated with receptor activation within

GPCRs [242-244].

To investigate these hypotheses the environment for the β-ionone ring in the meta-II state could be studied by observing [16,17-$^{13}C_2$]retinylidene rhodopsin trapped in its meta-II photointermediate state (see Section **Error! Reference source not found.**, Future Work). Unfortunately the "low-lipid" composition of the ROS membranes used in this study meant that the photoactivated rhodopsin samples did not pass freely beyond the meta-I intermediate, so the structure and environment of the β-ionone ring could not be investigated in the active meta-II photostate. This would require studying the protein trapped in the meta-II state, in membranes that were fully relipidated following removal of excess 11-*Z*-retinal with β-cyclodextrin [166, 226].

6.3   The helix movement model of 7TM$_A$ GPCR activation

Family A (7TM$_A$) GPCRs are the largest of the three families of GPCRs and share structural homology with rhodopsin. As previously discussed, sequence analysis of GPCRs has revealed that 7TM$_A$ GPCRs are characterized by a set of conserved residues distributed amongst the seven helical domains that maintain a common overall fold (Section **Error! Reference source not found.** and Figure 1.15) [95, 245].

As the arrangement of 7TM segments appears to be evolutionarily conserved throughout 7TM$_A$ GPCRs the helix movement model of rhodopsin activation is also likely to be conserved [53, 54]. The introduction of an environmentally sensitive fluorophore into the β-adrenergic receptor suggested an outward movement of H6 occurs upon activation, whilst restricting the motion of H6 relative to H3 by engineering a Zn^{2+} binding site to link these helices inhibited the activation of the receptor, as observed in rhodopsin [246, 247]. Linking H3 and H6 was also found to inhibit the activation of the class B parathyroid hormone

receptor, suggesting a similar mechanism of activation in this region of all three proteins [247].

Similarities are also likely in the nature of the intramolecular contact networks which are disrupted by helical rearrangements. Recent mutagenesis studies have provided evidence for an ionic lock at the cytoplasmic end of H3 (Arg-3.50 and Asp-3.49) and H6 (Glu-6.30) in the β_2-adrenergic receptor that stabilizes the inactive form of the receptor, as part of the highly conserved Asp(Glu)/Arg/Tyr motif in H3 [243]. This is analogous to the interhelical contact observed between Arg-3.50 and Glu-6.30 in rhodopsin and as for rhodopsin, charge-neutralizing mutations of Glu-6.30 and Asp-3.50 residues were found to increase the basal activity of the receptor [239].
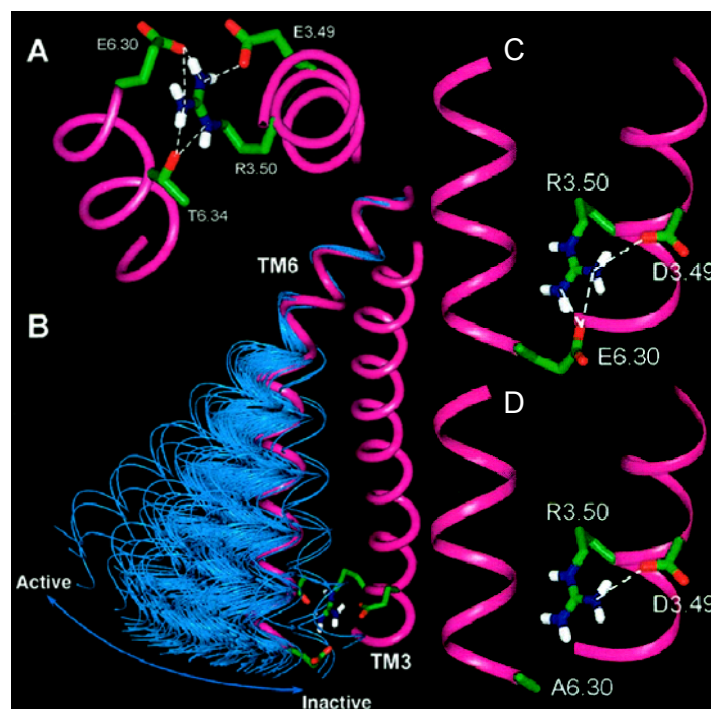
Figure 6.3 – Molecular 3-D representation of the interaction of H3 and H6 at their cytoplasmic ends. An extracellular view of the interaction between residues at the cytoplasmic ends of H3 and H6 of rhodopsin (A). The Cα ribbons of H3 and H6 are shown in pink. Simulations of a 31 amino acid α-helix with Pro at position 21 and Ala at the other positions were generated to show the conformational space that could be adopted as a result of the Pro kink (blue arrow). The resulting structures were superimposed from positions 1 to 17 from the start of H6 at the cytoplasmic face, showing the possible change that could result from disruption of ionic contacts between H3 and H6 (B)(see text for details). A 3-D model of the β_2-adrenergic receptor based on the backbone structure of rhodopsin with residues of the β_2-adrenergic receptor substituted for rhodopsin at aligned positions (C). The wild type interactions are shown with ionic

In the muscarinic M_1 receptor, mutation of the Asp residue on H3 does not activate the receptor as in rhodopsin, but mutation of a Glu residue at the end of H6 causes receptor activation, consistent with the postulated charge-reinforced H-bond to Arg-3.50 [66]. This suggests a common mechanism where a network of stabilizing ionic interactions within H3 and between H3 and H6 are disrupted following movement of H3, H6 and H7 upon activation. Glu-6.30 on H6 is not universally conserved in $7TM_A$ GPCRs although it is nearly 100% conserved amongst the neurotransmitter receptors, the glycoprotein hormone receptors and the opsins [243].

Disruption of the Asp(Glu)/Arg/Tyr contacts probably results in protonation of the conserved Asp(Glu) residue on H3 in rhodopsin (Glu-134), yielding a high-affinity conformation (meta-II_b) of the receptor for transducin. Analogous proton translocation reactions have been proposed for other GPCRs, including the α_{1B}-adrenergic receptor, the β_2-adrenergic and the thrombin receptor at this site [248-250]. There is therefore an analogy of the meta-I and meta-II states of rhodopsin to the low and high-affinity binding conformations (R' and R^*, respectively) of ligand-activated GPCRs (L) (Scheme 6.1 and 6.2).

For rhodopsin (light-induced pathway):

$$\text{meta-I} + G \rightleftharpoons \text{meta-II}_a + G \rightleftharpoons \text{meta-II}_b \cdot G \qquad \text{Scheme 6.1}$$

For GPCRs (in general):

$$L + R + G \rightleftharpoons LR' + G \rightleftharpoons LR^* + G \rightleftharpoons LR^* \cdot G \qquad \text{Scheme 6.2}$$
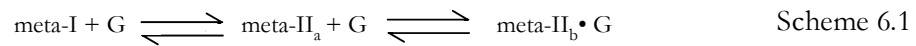
6.4   Binding site similarities between 7TM$_A$ GPCR receptors

The 11-Z retinylidene chromophore is the natural ligand of rhodopsin acting as an antagonist until it undergoes *cis/trans* isomerization upon absorption of a photon, where it becomes an agonist. The binding site for retinal can be viewed as representative of the binding mode of an antagonist in other GPCRs even though the ligand is covalently bound, unlike conventional GPCRs. Indeed, in a rhodopsin mutant lacking Lys-296, to which the retinal normally binds, is inactivated by a noncovalently bound 11-Z retinal analogue [252]. In the rhodopsin family of GPCRs, biogenic amine ligands are analogs of the retinal structure with cationic ammonium groups at one end and a ring-like structure at the other
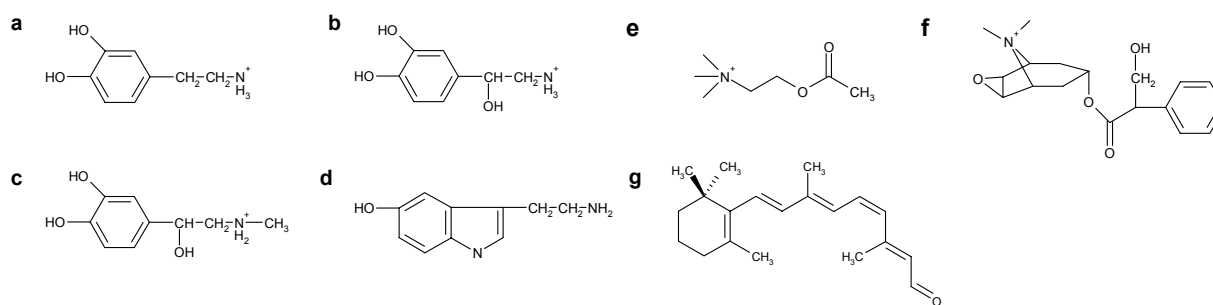
Figure 6.4 – Chemical structures of the neurotransmitter receptor ligands: dopamine (a), noradrenaline (b), adrenaline (c), serotonin (d), acetylcholine (e) N-methyl scopolamine (NMS) (f) which share a similar structure to the natural ligand of rhodopsin, 11-Z retinal (g) [66, 251]. The biogenic amine have a cationic amine group at one that is similar to the protontaed Schiff base of bound retinylidene in rhodopsin, and either a catechol or indole ring at the other end, that is similar to the β-ionone ring of retinal.

[66, 94] (Figure 6.4).

From extensive mutagenesis studies the residues that are important for the binding of amine ligands, such as the agonist acetylcholine (Figure 6.4 (e)) and the antagonist N-methyl scopolamine (NMS) (Figure 6.4 (f)) in the M$_1$ receptor, have been pinpointed [253-255]. It was found that the positions of the ligand contact points were highly homologous between

the rhodopsin and the M_1 receptor but the side-chains are specialized, reflecting the difference in the chemical nature of the ligands [66].

In the model of the muscarinic receptor the antagonist ligand NMS can be docked along a trajectory equivalent to that of 11-Z retinal in rhodopsin [66]. The quaternary ammonium group of NMS is positioned by contacts with H7 (equivalent to the retinal attachment Lys-296 residue in rhodopsin), H3 (an Asp residue that mimics the retinal Schiff base counterion, Glu-113) and H6. The tropic acid side-chain follows H3 as in rhodopsin and the phenyl ring of NMS, like the β-ionone ring of retinal, is positioned in a pocket of aromatic residues formed by residues from H3, H5 and H6 The phenyl ring of NMS and the ionone ring of retinal could both stabilise the "hydrophobic latch" between these helices, explaining how the antagonist activity of both of these ligands suppress the residual activity of the unliganded protein. Notably, acetylcholine, an agonist for the M_1 muscarinic receptor binds in the very similar way to NMS although it has a compact acetoxy side chain and therefore cannot replicate the stabilizing inter-helical interactions provided by NMS and retinal [66]. Binding of this ligand has been suggested to "pull" the aromatic residues at the top of H6 and H7 closer to H3.

Residues Phe-261 (Phe-6.44) and Trp-265 (Trp-6.48) in rhodopsin that form contacts with the β-ionone ring of retinal belong to a sequence of highly conserved aromatic residues Phe/XXX/Trp/X/Pro/Tyr(Phe) amongst $7TM_A$ GPCRs [245, 256]. A similar pattern of aromatic residues was observed in the docking of epinephrine in the $β_1$-adrenergic receptor [95] and for dopamine in the D_2 receptor [257], where they form critical interactions with the aromatic ring of catecholamine ligands [258].

The binding sites of rhodopsin, $β_1$-adrenergic receptor, and the rat and mouse 17 olfactory

receptors (OR) were recently predicted from docking their respective ligands into a modelled 3-D structure of the receptor. All three receptors were found to use H3 and H6 for binding of their ligands at a similar position in the centre of the transmembrane helices (Figure 6.5) [94], suggesting there could be conservation in the mechanism by which helix movement is initiated.
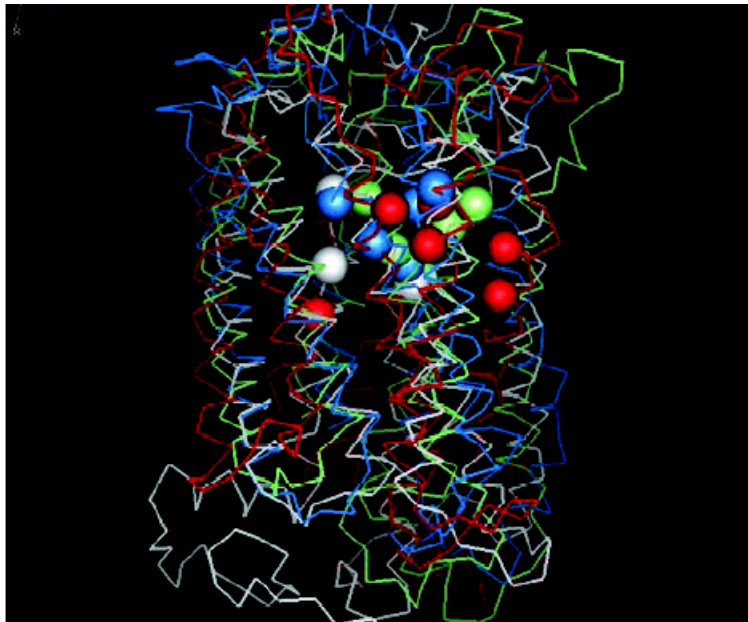
Figure 6.5 – Comparison of the predicted binding sites for four GPCRs: Key residues that form the binding site of bovine rhodopsin (white), β_1-adrenergic receptor (red), rat 17 OR (green), and mouse 17 OR (blue) were predicted using the HeirDock program in 3-D models of GPCRs generated from the amino acid sequence (using the MembStruck program). From [94].

The examples given for the cationic amine receptors oversimplify the binding of ligands in $7TM_A$ receptors. There is convincing evidence that peptide ligands bind to extracellular loops, although in some cases the peptide may contact some of the ligand contact points identified in the amine GPCRs [259]. Unlike rhodopsin where retinal is retained by the $\beta 4$-sheet that caps the binding site, no such contacts are observed in other $7TM_A$ receptors. This could reflect the diffusible nature of ligands in GPCRs that require an access channel from the extracellular face into the binding site. Peripheral binding sites have been postulated in

cationic amine receptors, where the ligand docks before transit to the central binding site [260]. The difference in sequences detected for $7TM_A$ GPCRs will be required to generate a large diversity of binding site conformations required for a wide variety of ligands.

Chapter 7   Conclusions and future work

7.1   General Conclusions

Solid state NMR has been successfully applied to determine the high-resolution structure of the β-ionone ring of the retinylidene chromophore of rhodopsin and investigate its role in the activation mechanism.

Three ^{13}C labelled 11-*Z* retinals [8,18-^{13}C$_2$] 11-*Z* retinal, [8,16/17-^{13}C$_2$] 11-*Z* retinal and [16,17-^{13}C$_2$] 11-*Z* retinal, were regenerated into opsin samples in ROS disk membranes and the resulting rhodopsin pigments characterised by UV-VIS spectrophotometry (Chapter 2).

Rotational resonance NMR internuclear distance measurements between C8, on the polyene chain and the three β-ionone ring methyl groups (C16, C17 and C18) showed directly that the β-ionone ring of retinylidene adopts a 6-*s-cis* conformation, with a modest torsional twist around the C6-C7 bond (-28±7°). The C17 and C16 methyl groups were observed in a distinct axial and equatorial conformation, reflected in a significant chemical shift separation (~4.5ppm) and an equidistant internuclear measurement with C8, in a bound 6-*s-cis* ring

conformation. The conformational distinction between the C16 and C17 represents a significant protein-induced perturbation of 11-*Z* retinal upon chromophore binding [107].

A negatively twisted, 6-*s-cis* ring conformation enables the methyl groups to participate in key binding interactions with residues of the opsin binding pocket, identified from biochemical studies [112, 113], retinal analogue binding studies [98, 212] and analysis of the crystal structure [34]. Interactions between C18 and the side-chains of residues on H3 and H6 could stabilise rhodopsin with the antagonist, 11-*Z* retinylidene, bound in the ground state structure.

6-*s-trans* minor components were observed in the rotational resonance NMR rhodopsin samples, confirming that the β-ionone ring *can* bind to opsin in a 6-*s-trans* conformation, as suggested by modelling [111, 178] and analogue binding studies [85, 97]. However, by using the distinct chemical shift separation between the C16 and C17 methyl groups as a diagnostic indicator of a 6-*s-cis* ring conformation, the β-ionone ring of the native 11-*Z* chromophore was shown to bind exclusively in a 6-*s-cis* conformation in $[16,17-^{13}C_2]$ retinylidene rhodopsin, in both DMPC and ROS disk membranes. The minor components could be the product of sterically strained di-*Z* isomers that bind to opsin in a 6-*s-trans* conformation, as previously suggested [59, 85].

To investigate the role of the chromophore in the activation mechanism of rhodopsin the conformation of the β-ionone ring was investigated in the meta-I photointermediate state, which is the precursor to the active meta-II photostate. UV-VIS spectrophotometry has shown that trapping of rhodopsin in its photointermediate states, by illumination at low temperatures, results in a steady-state equilibrium of rhodopsin (11-*Z* retinal), photointermediate (all-*E* retinal) and isorhodopsin (9-*Z* retinal) [58, 219]. To enable the

optimum conversion of the rotational resonance NMR samples to their respective meta-I intermediates, different methods for trapping meta-I rhodopsin in frozen NMR samples were investigated (Chapter 4). By using the chemical shift responses of the C20 and C8 ^{13}C nuclei as probes for the various photoproducts of rhodopsin, the proportion of meta-I intermediate trapped in frozen rhodopsin NMR samples was studied. It was found that prolonged illumination at -30°C ("direct" method) results in significant levels of photoregenerated 7-Z rhodopsin (~50% of the photoproduct), limiting the use of this method in trapping the meta-I intermediate in frozen NMR samples [227, 229]. Generating the meta-I intermediate "indirectly", by first accumulating the batho intermediate and then warming so the labile fraction forms meta-I rhodopsin is a preferable method, as only photoregeneration of 9-Z isorhodopsin occurs when trapping batho rhodopsin [227, 229]. However, the levels of photoregeneration are still significant, accounting for ~40% of the steady-state equilibrium mixture following prolonged illumination with white light, which results in moderate levels of the meta-I photointermediate (42%). The proportion of trapped meta-I rhodopsin was less than estimated from previous solid state NMR studies on meta-I rhodopsin [78-80], as in these studies the isorhodopsin component was unaccounted for. Accurate quantification of the meta-I trapping procedure was essential for quantifying the rotational resonance NMR exchange in the meta-I photostate and should prove useful for any future studies that require trapping meta-I rhodopsin at low temperatures.

CP-MAS and rotational resonance NMR studies on [8,18-^{13}C$_2$]retinylidene rhodopsin, [8,16/17-^{13}C$_2$]retinylidene rhodopsin and [16,17-^{13}C$_2$]retinylidene rhodopsin in their respective meta-I photointermediate states, suggest that the conformation and position of the β-ionone ring is largely unchanged between the dark and meta-I photointermediates, in contrast to previous models of rhodopsin activation (Chapter 5) [42, 44, 53, 64, 67, 80, 83-

85].

The short internuclear distance (<3.4Å) between the C18 methyl group on the ring and C8 on the polyene chain indicated that the β-ionone ring adopts a 6-*s-cis* conformation in the meta-I photostate, similar to that observed for 11-*Z* retinylidene in dark state rhodopsin. The C16 and C17 methyl groups were observed in a similar axial/equatorial conformation in both dark and meta-I photostates, suggesting that the β-ionone ring remains bound amongst largely aromatic residues from H3, H5 and H6 in the meta-I photointermediate.

The observation that interactions between H3 and H6 of rhodopsin are mediated through the hydrophobic contacts with the β-ionone ring of retinal suggests the binding of the β-ionone in a 6-*s-cis* conformation is central to the helix movement model of rhodopsin activation. Whether or not the β-ionone ring remains bound upon forming the active meta-II intermediate will indicate how the rearrangement of helices upon rhodopsin activation is propagated, either directly through displacement of the ligand or by acting as an anchor point that induces reordering of residues and disruption of interhelical contacts.

In the light of the structural and mechanistic similarities between 7TM$_A$ GPCRs [54, 66, 67, 94, 95, 257] the results on rhodopsin presented here, indicate that the ring moieties of amine GPRC ligands could have similar functional roles in the mechanistic pathways of 7TM$_A$ GPCR receptors.

7.2 Future Work

Following the observation that the β-ionone ring remains bound in the dark state conformation in meta-I photointermediate, the environment of the β-ionone ring in the active meta-II receptor is especially of interest. To investigate the environment of the ring in the active receptor it should be attempted to observe the conformation of the C16 and C17

methyls in [16,17-$^{13}C_2$]retinylidene rhodopsin in ROS disk membranes, trapped in the meta-II photostate.

In this study, the meta-I→ meta-II transition of the rhodopsin NMR samples was partially blocked due to the reduced lipid content of the ROS membranes, following the removal of excess ^{13}C labeled retinylidene with β-cyclodextrin [226]. However, the formation of the meta-I intermediate was not effected (Figure 4.6). To obtain the conventional meta-I/meta-II equilibrium kinetics it would be necessary to increase the fluidity of the membrane by restoring the native lipid/protein ratio. Initially, ^{13}C labeled [16,17-$^{13}C_2$] 11-Z retinal could be regenerated into opsin in ROS, following the procedure previously described. Following regeneration, [16,17-$^{13}C_2$]retinylidene rhodopsin would be solubilized (20mM nonylglucose), mixed with a 60 fold molar excess of retinal lipids and reconstituted in proteoliposomes by stepwise dilution [226].

The meta-I/meta-II equilibrium has been studied extensively by UV-VIS and FTIR spectroscopy [74, 217, 226, 261, 262], although not by solid state NMR. Methods for stably trapping and observing the meta-II intermediate in rhodopsin NMR samples would need to be investigated. The stable trapping of the meta-II photointermediate is complicated by the fact it is in a temperature dependant equilibrium with the meta-I photointermediate [217, 261]. The slow rate at which the meta-I/meta-II equilibrium is established at low temperatures ($t_{1/2}$ ~100min at -9°C [217]) means it may be possible to generate the meta-II intermediate via the batho intermediate (prolonged irradiation at -190°C followed by incubation at 10°C), then snap freeze the sample without the meta-II component reverting to meta-I rhodopsin.

If the meta-II intermediate can be stably trapped, the appearance of C16 and C17 resonances

in the CP-MAS NMR spectra should reveal whether or not the β-ionone ring of the chromophore remains bound upon rhodopsin activation. From this it should be possible to make predictions for the role of the aromatic ring moieties of the analogous 7TM$_A$ GPCR ligands, in the activation mechanism of their respective GPCR receptors.

The nature of the interactions between the β-ionone ring and the residues of the opsin binding pocket also requires further investigation. The aromatic residues that form the binding pocket around the β-ionone ring are likely to form key interactions with the β-ionone ring, highlighted by their conservation amongst 7TM$_A$ GPCRs. A computer program (CHPI) [263] has been used to search for short contacts between CH groups and π-systems in protein structures and could be used to highlight stabilizing CH···π contacts between the β-ionone ring and opsin. Similar searches for possible CH···O interactions [264] and π ··· π interactions [265, 266] between the β-ionone ring and the protein would also be of interest.

The rotational resonance exchange between C8 and C18 in the meta-I photostate was sufficient to confirm a 6-*s-cis* ring conformation. However, obtaining precise distance information between the polyene chain and the ring methyls would require taking explicit account of the off-resonance effects for exchange between the broad resonances in the meta-I photostate (C8 ~400Hz). Quantification of the exchange between C8 and C18 using the standard rotational resonance NMR method was limited by the effects of instrumental instabilities and poor signal-to-noise. Obtaining reliable quantification would therefore require exploring additional NMR methods for measuring the ^{13}C-^{13}C dipolar coupling.

Bibliography

1.   Yeagle, P.L., Cell membrane features. 2003, Encyclopedia of life sciences
        /http://www.els.net.

2.   Mathews, C.K. and Van Holde, K.E., Biochemistry. 1st ed, ed. T.B.C.P.C. Inc. 1990.

3.   Singer, S.J. and Nicolson, G.L. (1972) The fluid mosaic model of the structure of
        membranes. *Science*, **175**: 720-731.

4.   Simons, K. and Ikonene, E. (1997) Functional rafts in cell membranes. *Nature*, **387**:
        569-570.

5.   Watts, A., Burnett, I.J., Glaubitz, C., Grobner, G., Middleton, D.A., Spooner, P.J.R.,
        Watts, J.A., and Williamson, P.T.F. (1999) Membrane protein structure determination
        by solid state NMR. *Nat. Prod. Rep.*, **16**(4): 419-423.

6.   Kholodenko, B.N., Hoek, J.B., and Westerhoff, H.V. (2000) Why cytoplasmic
        signalling proteins should be recruited to cell membranes. *Trends. Cell. Biol.*, **10**(5): 173-
        178.

7.   Adam, G. and Delbruck, M. (1968) Reduction of dimensionality in biological diffusion
        processes. *Struct. Chem. Mol. Biol.*: 198-215.

8.   Bockaert, J. and Pin, J.P. (1999) Molecular tinkering of G protein-coupled receptors: an
        evolutionary success. *Embo J.*, **18**(7): 1723-1729.

9.   Bargmann, C.I. (1998) Neurobiology of the Caenorhabditis elegans genome. *Science*,
        282(5396): 2028-2033.

10.   Woodmac PharmaView2001 at http:/www.woodmacresearch.com/phwiew.

11.   Drews, J. (2000) Drug discovery: a historical perspective. *Science*, **287**: 1960-1964.

12.   Lander, E.S., Linton, L.M., Birren, B., Nusbaum, C., Zody, M.C., Baldwin, J., Devon,
        K., Dewar, K., Doyle, M., Fitzhugh, W., Funke, R., Gage, D., Harris, K., Heaford, A.,
        Howland, J., Kann, L., Lehoczky, J., Levine, R., Mcewan, P., Mckernan, K., Meldrim,
        J., Mesirov, J.P., Miranda, C., Morris, W., Naylor, J., Raymond, C., Rosetti, M., Santos,
        R., Sheridan, A., Sougnez, C., Stange-Thomann, N., Stojanovic, N., Subramanian, A.,
        Wyman, D., Rogers, J., Sulston, J., Ainscough, R., Beck, S., Bentley, D., Burton, J.,
        Clee, C., Carter, N., Coulson, A., Deadman, R., Deloukas, P., Dunham, A., Dunham,
        I., Durbin, R., French, L., Grafham, D., Gregory, S., Hubbard, T., Humphray, S., Hunt,
        A., Jones, M., Lloyd, C., Mcmurray, A., Matthews, L., Mercer, S., Milne, S., Mullikin,
        J.C., Mungall, A., Plumb, R., Ross, M., Shownkeen, R., Sims, S., Waterston, R.H.,
        Wilson, R.K., Hillier, L.W., Mcpherson, J.D., Marra, M.A., Mardis, E.R., Fulton, L.A.,
        Chinwalla, A.T., Pepin, K.H., Gish, W.R., Chissoe, S.L., Wendl, M.C., Delehaunty,
        K.D., Miner, T.L., Delehaunty, A., Kramer, J.B., Cook, L.L., Fulton, R.S., Johnson,
        D.L., Minx, P.J., Clifton, S.W., Hawkins, T., Branscomb, E., Predki, P., Richardson, P.,
        Wenning, S., Slezak, T., Doggett, N., Cheng, J.F., Olsen, A., Lucas, S., Elkin, C.,
        Uberbacher, E., Frazier, M., Gibbs, R.A., Muzny, D.M., Scherer, S.E., Bouck, J.B.,
        Sodergren, E.J., Worley, K.C., Rives, C.M., Gorrell, J.H., Metzker, M.L., Naylor, S.L.,

Kucherlapati, R.S., Nelson, D.L., Weinstock, G.M., Sakaki, Y., Fujiyama, A., Hattori, M., Yada, T., Toyoda, A., Itoh, T., Kawagoe, C., Watanabe, H., Totoki, Y., Taylor, T., Weissenbach, J., Heilig, R., Saurin, W., Artiguenave, F., Brottier, P., Bruls, T., Pelletier, E., Robert, C., Wincker, P., Rosenthal, A., Platzer, M., Nyakatura, G., Taudien, S., Rump, A., Yang, H.M., Yu, J., Wang, J., Huang, G.Y., Gu, J., Hood, L., Rowen, L., Madan, A., Qin, S.Z., Davis, R.W., Federspiel, N.A., Abola, A.P., Proctor, M.J., Myers, R.M., Schmutz, J., Dickson, M., Grimwood, J., Cox, D.R., Olson, M.V., Kaul, R., Shimizu, N., Kawasaki, K., Minoshima, S., Evans, G.A., Athanasiou, M., Schultz, R., Roe, B.A., Chen, F., Pan, H.Q., Ramser, J., Lehrach, H., Reinhardt, R., Mccombie, W.R., De La Bastide, M., Dedhia, N., Blocker, H., Hornischer, K., Nordsiek, G., Agarwala, R., Aravind, L., Bailey, J.A., Bateman, A., Batzoglou, S., Birney, E., Bork, P., Brown, D.G., Burge, C.B., Cerutti, L., Chen, H.C., Church, D., Clamp, M., Copley, R.R., Doerks, T., Eddy, S.R., Eichler, E.E., Furey, T.S., Galagan, J., Gilbert, J.G.R., Harmon, C., Hayashizaki, Y., Haussler, D., Hermjakob, H., Hokamp, K., Jang, W.H., Johnson, L.S., Jones, T.A., Kasif, S., Kaspryzk, A., Kennedy, S., Kent, W.J., Kitts, P., Koonin, E.V., Korf, I., Kulp, D., Lancet, D., Lowe, T.M., Mclysaght, A., Mikkelsen, T., Moran, J.V., Mulder, N., Pollara, V.J., Ponting, C.P., Schuler, G., Schultz, J.R., Slater, G., Smit, A.F.A., Stupka, E., Szustakowski, J., Thierry-Mieg, D., Thierry-Mieg, J., Wagner, L., Wallis, J., Wheeler, R., Williams, A., Wolf, Y.I., Wolfe, K.H., Yang, S.P., Yeh, R.F., Collins, F., Guyer, M.S., Peterson, J., Felsenfeld, A., Wetterstrand, K.A., Patrinos, A. and Morgan, M.J. (2001) Initial sequencing and analysis of the human genome. *Nature*, **409**(6822): 860-921.

13.   Venter, J.C., Adams, M.D., Myers, E.W., Li, P.W., Mural, R.J., Sutton, G.G., Smith, H.O., Yandell, M., Evans, C.A., Holt, R.A., Gocayne, J.D., Amanatides, P., Ballew, R.M., Huson, D.H., Wortman, J.R., Zhang, Q., Kodira, C.D., Zheng, X.Q.H., Chen, L., Skupski, M., Subramanian, G., Thomas, P.D., Zhang, J.H., Miklos, G.L.G., Nelson, C., Broder, S., Clark, A.G., Nadeau, C., Mckusick, V.A., Zinder, N., Levine, A.J., Roberts, R.J., Simon, M., Slayman, C., Hunkapiller, M., Bolanos, R., Delcher, A., Dew, I., Fasulo, D., Flanigan, M., Florea, L., Halpern, A., Hannenhalli, S., Kravitz, S., Levy, S., Mobarry, C., Reinert, K., Remington, K., Abu-Threideh, J., Beasley, E., Biddick, K., Bonazzi, V., Brandon, R., Cargill, M., Chandramouliswaran, I., Charlab, R., Chaturvedi, K., Deng, Z.M., Di Francesco, V., Dunn, P., Eilbeck, K., Evangelista, C., Gabrielian, A.E., Gan, W., Ge, W.M., Gong, F.C., Gu, Z.P., Guan, P., Heiman, T.J., Higgins, M.E., Ji, R.R., Ke, Z.X., Ketchum, K.A., Lai, Z.W., Lei, Y.D., Li, Z.Y., Li, J.Y., Liang, Y., Lin, X.Y., Lu, F., Merkulov, G.V., Milshina, N., Moore, H.M., Naik, A.K., Narayan, V.A., Neelam, B., Nusskern, D., Rusch, D.B., Salzberg, S., Shao, W., Shue, B.X., Sun, J.T., Wang, Z.Y., Wang, A.H., Wang, X., Wang, J., Wei, M.H., Wides, R., Xiao, C.L., Yan, C.H., Yao, A., Ye, J., Zhan, M., Zhang, W.Q., Zhang, H.Y., Zhao, Q., Zheng, L.S., Zhong, F., Zhong, W.Y., Zhu, S.P.C., Zhao, S.Y., Gilbert, D., Baumhueter, S., Spier, G., Carter, C., Cravchik, A., Woodage, T., Ali, F., An, H.J., Awe, A., Baldwin, D., Baden, H., Barnstead, M., Barrow, I., Beeson, K., Busam, D., Carver, A., Center, A., Cheng, M.L., Curry, L., Danaher, S., Davenport, L., Desilets, R., Dietz, S., Dodson, K., Doup, L., Ferriera, S., Garg, N., Gluecksmann, A., Hart, B., Haynes, J., Haynes, C., Heiner, C., Hladun, S., Hostin, D., Houck, J., Howland, T., Ibegwam, C., Johnson, J., Kalush, F., Kline, L., Koduru, S., Love, A., Mann, F., May, D., Mccawley, S., Mcintosh, T., Mcmullen, I., Moy, M., Moy, L., Murphy, B., Nelson, K., Pfannkoch, C., Pratts, E., Puri, V., Qureshi, H., Reardon, M., Rodriguez, R., Rogers, Y.H., Romblad, D., Ruhfel, B., Scott, R., Sitter, C., Smallwood, M., Stewart, E., Strong, R., Suh, E., Thomas, R., Tint, N.N., Tse, S., Vech, C., Wang, G., Wetter, J., Williams, S., Williams, M., Windsor, S., Winn-Deen, E., Wolfe, K., Zaveri, J., Zaveri, K., Abril, J.F., Guigo, R., Campbell, M.J., Sjolander, K.V., Karlak, B., Kejariwal, A., Mi, H.Y., Lazareva, B., Hatton, T.,

Narechania, A., Diemer, K., Muruganujan, A., Guo, N., Sato, S., Bafna, V., Istrail, S., Lippert, R., Schwartz, R., Walenz, B., Yooseph, S., Allen, D., Basu, A., Baxendale, J., Blick, L., Caminha, M., Carnes-Stine, J., Caulk, P., Chiang, Y.H., Coyne, M., Dahlke, C., Mays, A.D., Dombroski, M., Donnelly, M., Ely, D., Esparham, S., Fosler, C., Gire, H., Glanowski, S., Glasser, K., Glodek, A., Gorokhov, M., Graham, K., Gropman, B., Harris, M., Heil, J., Henderson, S., Hoover, J., Jennings, D., Jordan, C., Jordan, J., Kasha, J., Kagan, L., Kraft, C., Levitsky, A., Lewis, M., Liu, X.J., Lopez, J., Ma, D., Majoros, W., Mcdaniel, J., Murphy, S., Newman, M., Nguyen, T., Nguyen, N., Nodell, M., Pan, S., Peck, J., Peterson, M., Rowe, W., Sanders, R., Scott, J., Simpson, M., Smith, T., Sprague, A., Stockwell, T., Turner, R., Venter, E., Wang, M., Wen, M.Y., Wu, D., Wu, M., Xia, A., Zandieh, A. and Zhu, X.H. (2001) The sequence of the human genome. *Science*, **291**(5507): 1304-1351.

14.   Takeda, S., Kadowaki, S., Haga, T., Takaesu, H., and Mitaku, S. (2002) Identification of G protein-coupled receptor genes from the human genome sequence. *FEBS Lett.*, **520**(1-3): 97-101.

15.   Coglab online laboratory http://coglab.wadsworth.com/experiments/images/individual/eyeball.gif. 2003.

16.   Stryer, L.L., Biochemistry. 1995, New York: W.H.Freeman and Company.

17.   Hecht, S., Shlaer, S., and Pirenne, M.H. (1941) Energy, quanta and vision. *J. Gen. Physiol.*, **25**: 819-827.

18.   Heck, M. and Hofmann, K.P. (2001) Maximal rate and nucleotide dependence of rhodopsin-catalyzed transducin activation - Initial rate analysis based on a double displacement mechanism. *J. Biol. Chem.*, **276**(13): 10000-10009.

19.   Leskov, I.B., Klenchin, V.A., Handy, J.W., Whitlock, G.G., Govardovskii, V.I., Bownds, M.D., Lamb, T.D., Pugh, E.N., and Arshavsky, V.Y. (2000) The gain of rod phototransduction: Reconciliation of biochemical and electrophysiological measurements. *Neuron*, **27**(3): 525-537.

20.   Baylor, D.A. (1987) Photoreceptor signals and vision. Protor lecture. *Invest. Ophthalmol. Vis. Sci.*, **28**: 34-49.

21.   Mcbee, J.K., Palczewski, K., Baehr, W., and Pepperberg, D.R. (2001) Confronting complexity: the interlink of phototransduction and retinoid metabolism in the vertebrate retina. *Prog. Retin. Eye Res.*, **20**(4): 469-529.

22.   Ripps, H. and Weale, R.A. (1969) Rhodopsin regeneration in man. *Nature*, **222**: 775-777.

23.   Weale, R.A. (1972) Cone pigment regeneration, retinitis pigmentosa and light deprivation. *Vision. Res.*, **12**: 747-752.

24.   Ovchinnikov, Y.A. (1982) Rhodopsin and Bacteriorhodopsin - Structure-Function-Relationships. *FEBS Lett.*, **148**(2): 179-191.

25.   Nathans, J. and Hogness, D.S. (1984) Isolation and nucleotide-sequence of the gene encoding human rhodopsin. *Proc. Natl. Acad. Sci. U. S. A.*, **81**(15): 4851-4855.

26.   Nathans, J. and Hogness, D.S. (1983) Isolation, sequence-analysis, and intron exon arrangement of the gene encoding bovine rhodopsin. *Cell*, **34**(3): 807-814.

27.   Okada, T., Le Trong, I., Fox, B.A., Behnke, C.A., Stenkamp, R.E., and Palczewski, K. (2000) X-ray diffraction analysis of three-dimensional crystals of bovine rhodopsin obtained from mixed micelles. *J. Struct. Biol.*, **130**(1): 73-80.

28.   Palczewski, K., Kumasaka, T., Hori, T., Behnke, C.A., Motoshima, H., Fox, B.A., Le Trong, I., Teller, D.C., Okada, T., Stenkamp, R.E., Yamamoto, M., and Miyano, M. (2000) Crystal structure of rhodopsin: A G protein-coupled receptor. *Science*, **289**(5480): 739-745.

29.   Kuhne, Ueber den Sehpurpur Vol. 1., in *Undersuchungen aus dem Physiologischen Intitut der Universitaet Heidelberg*. 1878: Heidelberg.

30.   Okada, T., Takeda, K., and Kouyama, T. (1998) Highly selective separation of rhodopsin from bovine rod outer segment membranes using combination of bivalent cation and alkyl(thio)glucoside. *Photochem. Photobiol.*, **67**(5): 495-499.

31.   Wald, G. (1968) Molecular basis of visual excitation. *Science*, **162**: 230-239.

32.   Smith, S.O., Palings, I., Miley, M.E., Courtin, J., Degroot, H., Lugtenburg, J., Mathies, R.A., and Griffin, R.G. (1990) Solid-State Nmr-Studies of the Mechanism of the Opsin Shift in the Visual Pigment Rhodopsin. *Biochemistry*, **29**(35): 8158-8164.

33.   Merbs, S.L. and Nathans, J. (1992) Absorption-spectra of human cone pigments. *Nature*, **356**(6368): 433-435.

34.   Teller, D.C., Okada, T., Behnke, C.A., Palczewski, K., and Stenkamp, R.E. (2001) Advances in determination of a high-resolution three-dimensional structure of rhodopsin, a model of G-protein-coupled receptors (GPCRs). *Biochemistry*, **40(26)**: 7761-7772.

35.   Baldwin, J.M., Schertler, G.F.X., and Unger, V.M. (1997) An alpha-carbon template for the transmembrane helices in the rhodopsin family of G-protein-coupled receptors. *J. Mol. Biol.*, **272**(1): 144-164.

36.   Shieh, T., Han, M., Sakmar, T.P., and Smith, S.O. (1997) The steric trigger in rhodopsin activation. *J. Mol. Biol.*, **269**(3): 373-384.

37.   Hargrave, P.A. (1977) The amino-terminal tryptic peptide of bovine rhodopsin. A glycopeptide containing two sites of oligosaccharide attachment. *Biochim. Biophys. Acta*, **492**: 83-94.

38.   Morrison, D.F., Obrien, P.J., and Pepperberg, D.R. (1991) Depalmitylation with hydroxylamine alters the functional- properties of rhodopsin. *J. Biol. Chem.*, **266**(30): 20118-20123.

39.   Karnik, S.S., Sakmar, T.P., Chen, H.B., and Khorana, H.G. (1988) Cysteine residue-110 and residue-187 Are essential for the formation of correct structure in bovine rhodopsin. *Proc. Natl. Acad. Sci. U. S. A.*, **85**(22): 8459-8463.

40.   Ohguro, H., Rudnicka-Nawrot, M., Bulczylko, J., Zhao, X., Taylor, J., Walsh, K.A., and Palczewski, K. (1996) Structural and enzymatic aspects of rhodopsin phosphorylation. *J. Biol. Chem.*, **271**(9): 5215-5224.

41.   Benovic, J.L., Mayor, F., Somers, R.L., Caron, M.G., and Lefkowitz, R.J. (1986) Light-dependent phosphorylation of rhodopsin by beta-adrenergic receptor kinase. *Nature*, **321**: 869-872.

42.   Sakmar, T.P.M., S.T. Marin, E.P. And Awad, E.S. (2002) Rhodopsin:Insights from recent structural studies. *Annu. Rev. Bioph. Biom.*, **31**: 443-484.

43.   Okada, T. and Palczewski, K. (2001) Crystal structure of rhodopsin: implications for vision and beyond. *Curr. Opin. Struct. Biol.*, **11**(4): 420-426.

44.   Stenkamp, R.E., Teller, D.C., and Palczewski, K. (2002) Crystal structure of rhodopsin: A G-protein coupled receptor. *Chembiochem*, **3**: 963-967.

45.   Franke, R.R., Konig, B., Sakmar, T.P., Khorana, H.G., and Hofmann, K.P. (1990) Rhodopsin mutants that bind but fail to activate transducin. *Science*, **250**(4977): 123-125.

46.   Franke, R.R., Sakmar, T.P., Graham, R.M., and Khorana, H.G. (1992) Structure and function in rhodopsin - Studies of the interaction between the rhodopsin cytoplasmic domain and transducin. *J. Biol. Chem.*, **267**(21): 14767-14774.

47.   Ernst, O.P., Meyer, C.K., Marin, E.P., Henklein, P., Fu, W.Y., Sakmar, T.P., and Hofmann, K.P. (2000) Mutation of the fourth cytoplasmic loop of rhodopsin affects binding of transducin and peptides derived from the carboxyl- terminal sequences of transducin alpha and gamma subunits. *J. Biol. Chem.*, **275**(3): 1937-1943.

48.   Beck, M., Siebert, F., and Sakmar, T.P. (1998) Evidence for the specific interaction of a lipid molecule with rhodopsin which is altered in the transition to the active state metarhodopsin II. *FEBS Lett.*, **436**(3): 304-308.

49.   Carravetta, M., Zhao, X., Johannessen, O.G., Luthman, H., Verhoeven, M.A., Verdegem, P.J., Kihhne, S., De Groot, H.J.M., Lugtenburg, J., and Levitt, M.H. (2003) Picometre structural resolution of a membrane protein ligand: Double-quantum solid-state NMR of bovine rhodopsin. *Nature (in press)*.

50.   Holst, B., Zoffmann, S., Elling, C.E., Hjorth, S.A., and Schwartz, T.W. (1998) Steric hindrance mutagenesis vs. alanine specific scan-in mapping of ligand binding sites in the tachykinin NK1 receptor. *Mol. Pharmacol.*, **53**: 166-175.

51.   Perlman, J.H., Colson, A.O., Jain, R., Czyzewski, B., Cohen, L.A., Osman, R., and Gershengorn, M.C. (1997) Role of the extracellular loops of the thyrotropin-releasing hormone receptor: evidence for an initial interaction with thyrotropin-releasing hormone. *Biochemistry*, **36**: 15670-15676.

52.   Probst, W.C., Snyder, L.A., Schuster, D.I., Brosius, J., and Sealfon, S.C. (1992) Sequence alignment of the G-protein coupled receptor superfamily. *DNA. Cell. Biol.*, **11**: 1-20.

53.   Menon, S.T., Han, M., and Sakmar, T.P. (2001) Rhodopsin: structural basis of molecular physiology. *Physiol. Rev.*, **81**(4): 1659-1688.

54.   Sakmar, T.P. (2002) Structure of rhodopsin and the superfamily of seven-helical receptors: the same and not the same. *Curr. Opin. Cell Biol.*, **14**(2): 189-195.

55.   Choi, G., Landin, J., Galan, J.F., Birge, R.R., Albert, A.D., and Yeagle, P.L. (2002) Structural studies of metarhodopsin II, the activated form of the G-protein coupled receptor, rhodopsin. *Biochemistry*, **41**(23): 7318-7324.

56.   Okada, T., Fujiyoshi, Y., Silow, M., Navarro, J., Landau, E.M., and Shichida, Y. (2002) Functional role of internal water molecules in rhodopsin revealed by x-ray crystallography. *Proc. Natl. Acad. Sci. U. S. A.*, **99**(9): 5982-5987.

57.   Ebrey, T.G. and Koutalos, Y. (2001) Vertebrate photoreceptors. *Prog. Retin. Eye Res.*, **20**: 49-94.

58.   Yoshizawa, T. and Wald, G. (1963) Prelumirhodopsin and the bleaching of visual pigments. *Nature*, **197**: 1279-1285.

59.   Kliger, D.S. and Lewis, J.W. (1995) Spectral and kinetic characterization of visual pigment photointermediates. *Isr. J. Chem.*, **35**(3-4): 289-307.

60.   Yoshizawa, T., Shichida, Y., and Matuoka, S. (1984) Primary intermediates of rhodopsin studied by low temperature spectrophotometry and laser photolysis. Bathorhodopsin, hypsorhodopsin and photorhodopsin. *Vision. Res.*, **24**(11): 1455-1463.

61.   Thorgeirsson, T.E., Lewis, J.W., Wallacewilliams, S.E., and Kliger, D.S. (1992) Photolysis of Rhodopsin Results in Deprotonation of Its Retinal Schiff-Base Prior to Formation of Metarhodopsin-Ii. *Photochem. Photobiol.*, **56**(6): 1135-1144.

62.   Thorgeirsson, T.E., Lewis, J.W., Wallacewilliams, S.E., and Kliger, D.S. (1993) Effects of Temperature on Rhodopsin Photointermediates from Lumirhodopsin to Metarhodopsin-Ii. *Biochemistry*, **32**(50): 13861-13872.

63.   Lewis, J.W., Winterle, J.S., Powers, M.A., Kliger, D.S., and Dratz, E.A. (1981) Kinetics of rhodopsin photolysis intermediates in retinal rod disk membranes .1. Temperature-dependence of lumirhodopsin and metarhodopsin I. *Photochem. Photobiol.*, **34**(3): 375-384.

64.   Ernst, O.P. and Bartl, F.J. (2002) Active states of rhodopsin. *Chembiochem*, **3**: 968-974.

65.   Meng, E.C. and Bourne, H.R. (2001) Receptor activation: what does the rhodopsin structure tell us? *Trends Pharmacol. Sci.*, **22**(11): 587-593.

66.   Lu, Z.L., Saldanha, J.W., and Hulme, E.C. (2002) Seven-transmembrane receptors: crystals clarify. *Trends Pharmacol. Sci.*, **23**(3): 140-146.

67.   Okada, T., Ernst, O.P., Palczewski, K., and Hofmann, K.P. (2001) Activation of rhodopsin: new insights from structural and biochemical studies. *Trends Biochem.Sci.*, **26**(5): 318-324.

68.   Kim, J.E., Mccamant, D.W., Zhu, L.Y., and Mathies, R.A. (2001) Resonance Raman

structural evidence that the cis-to-trans isomerization in rhodopsin occurs in femtoseconds. *J. Phys. Chem. B*, **105**(6): 1240-1249.

69.   Cooper, A. (1979) Energy uptake in the first step of visual excitation. *Nature*, **282**: 531-533.

70.   Albeck, A., Friedman, N., Ottolenghi, M., Sheves, M., Einterz, C.M., Hug, S.J., Lewis, J.W., and Kliger, D.S. (1989) Photolysis intermediates of the artificial visual pigment cis- 5,6-dihydro-isorhodopsin. *Biophys. J.*, **55**(2): 233-241.

71.   Imamoto, Y., Sakai, M., Katsuta, Y., Wada, A., Ito, M., and Shichida, Y. (1996) Structure around C-6-C-7 bond of the chromophore in bathorhodopsin: Low-temperature spectroscopy of 6s-cis-locked bicyclic rhodopsin analogs. *Biochemistry*, **35**(20): 6257-6262.

72.   Palings, I., Pardoen, J.A., Vandenberg, E., Winkel, C., Lugtenburg, J., and Mathies, R.A. (1987) Assignment of Fingerprint Vibrations in the Resonance Raman- Spectra of Rhodopsin, Isorhodopsin, and Bathorhodopsin - Implications for Chromophore Structure and Environment. *Biochemistry*, **26**(9): 2544-2556.

73.   Smith, S.O., Courtin, J., Degroot, H., Gebhard, R., and Lugtenburg, J. (1991) C-13 Magic-Angle Spinning Nmr-Studies of Bathorhodopsin, the Primary Photoproduct of Rhodopsin. *Biochemistry*, **30**(30): 7409-7415.

74.   Siebert, F. (1995) Application of FTIR spectroscopy to the investigation of dark structures and photoreactions of visual pigments. *Isr. J. Chem.*, **35**(3-4): 309-323.

75.   Lewis, J.W., Pinkas, I., Sheves, M., Ottolenghi, M., and Kliger, D.S. (1995) Structural-changes in early photolysis intermediates of rhodopsin from time-resolved spectral measurements of artificial pigments sterically hindered along the chromophore chain. *J. Am. Chem. Soc.*, **117**(3): 918-923.

76.   Lewis, J.W., Fan, G.B., Sheves, M., Szundi, I., and Kliger, D.S. (2001) Steric barrier to bathorhodopsin decay in 5-demethyl and mesityl analogues of rhodopsin. *J. Am. Chem. Soc.*, **123**(41): 10024-10029.

77.   Shichida, Y. (1986) Primary Intermediates of Photobleaching of Rhodopsin. *Photobioch. Photobiop.*, **13**(3-4): 287-307.

78.   Verdegem, P.J., Bovee-Geurts, P.H., De-Grip, W.J., Lugtenburg, J., and De-Groot, H.J. (1999) Retinylidene ligand structure in bovine rhodopsin, metarhodopsin-I, and 10-methylrhodopsin from internuclear distance measurements using 13C-labeling and 1-D rotational resonance MAS NMR. *Biochemistry*, **38**(35): 11316-11324.

79.   Feng, X., Verdegem, P.J.E., Eden, M., Sandstrom, D., Lee, Y.K., Bovee-Geurts, P.H.M., De Grip, W.J., Lugtenburg, J., De Groot, H.J.M., and Levitt, M.H. (2000) Determination of a molecular torsional angle in the metarhodopsin-I photointermediate of rhodopsin by double- quantum solid-state NMR. *J. Biomol. NMR*, **16**(1): 1-8.

80.   Grobner, G., Burnett, I.J., Glaubitz, C., Choi, G., Mason, A.J., and Watts, A. (2000) Observations of light-induced structural changes of retinal within rhodopsin. *Nature*, **405**(6788): 810-813.

81.   Pan, D.H. and Mathies, R.A. (2001) Chromophore structure in lumirhodopsin and metarhodopsin I by time-resolved resonance Raman microchip spectroscopy. *Biochemistry*, **40**(26): 7929-7936.

82.   Doukas, A.G., Aton, B., Callender, R.H., and Ebrey, T.G. (1978) Resonance Raman studies of bovine metarhodopsin I and metarhodopsin II. *Biochemistry*, **17**(13): 2430-2435.

83.   Souto, M.L., Um, J., Borhan, B., and Nakanishi, K. (2000) Synthesis of a photoaffinity-labeled (11Z)-retinal: Identification of retinal/rhodopsin cross-linked sites along the visual-transduction path. *Helv. Chim. Acta*, **83**(9): 2617-2628.

84.   Borhan, B., Souto, M.L., Imai, H., Shichida, Y., and Nakanishi, K. (2000) Movement of retinal along the visual transduction path. *Science*, **288**(5474): 2209-2212.

85.   Jang, G.F., Kuksa, V., Filipek, S., Bartl, F., Ritter, E., Gelb, M.H., Hofmann, K.P., and Palczewski, K. (2001) Mechanism of rhodopsin activation as examined with ring-constrained retinal analogs and the crystal structure of the ground state protein. *J. Biol. Chem.*, **276**(28): 26148-26153.

86.   Sheikh, S.P., Zvyaga, T.A., Lichtarge, O., Sakmar, T.P., and Bourne, H.R. (1996) Rhodopsin activation blocked by metal-ion-binding sites linking transmembrane helices C and F. *Nature*, **383**(26): 347-350.

87.   Farrens, D.L., Altenbach, C., Yang, K., Hubbell, W.L., and Khorana, H.G. (1996) Requirement of rigid-body motion of transmembrane helices for light activation of rhodopsin. *Science*, **274**(5288): 768-770.

88.   Fahmy, K., Sakmar, T.P., and Siebert, F. (2000) Transducin-dependent protonation of glutamic acid 134 in rhodopsin. *Biochemistry*, **39**: 10607-10612.

89.   Ernst, O.P., Hofmann, K.P., and Sakmar, T.P. (1995) Characterization of rhodopsin mutants that bind transducin but fail to induce Gtp nucleotide uptake - Classification of mutant pigments by fluorescence, nucleotide release, and flash-induced light-scattering assays. *J. Biol. Chem.*, **270**(18): 10580-10586.

90.   Hamm, H.E., Deretic, D., Arendt, A., Hargrave, P.A., Koenig, B., and Hofmann, K.P. (1988) Site of G-Protein binding to rhodopsin mapped with synthetic peptides from the alpha-subunit. *Science*, **241**(4867): 832-835.

91.   Yamashita, T., Terakita, A., and Shichida, Y. (2000) Distinct roles of the second and third cytoplasmic loops of bovine rhodopsin in G protein activation. *J. Biol. Chem.*, **275**(44): 34272-34279.

92.   Abdulaev, N.G. and Ridge, K.D. (1998) Light-induced exposure of the cytoplasmic end of the transmembrane helix seven in rhodopsin. *Proc. Natl. Acad. Sci. U. S. A.*, **95**: 12854-12859.

93.   Phillips, W.J. and Cerione, R.A. (1992) Rhodopsin/transducin interactions: characterization of the binding of the transducin-βγ subunit complex to rhodopsin using fluorescence spectroscopy. *J. Biol. Chem.*, **267**: 17032-17039.

94.   Vaidehi, N., Floriano, W.B., Trabanino, R., Hall, S.E., Freddolino, P., Choi, E.J., Zamanakos, G., and Goddard, W.A. (2002) Prediction of structure and function of G protein-coupled receptors. *Proc. Natl. Acad. Sci. U. S. A.*, **99**(20): 12622-12627.

95.   Ballesteros, J.A., Shi, L., and Javitch, J.A. (2001) Structural mimicry in G protein-couples receptors: Implications of the high-resolution structure of rhodopsin for structure-function analysis of rhodopsin-like receptors. *Mol. Pharmacol.*, **60**(1): 1-19.

96.   Archer, E., Maigret, B., Escrieut, C., Pradayrol, L., and Fourmy, D. (2003) Rhodopsin crystal: new template yielding realistic models of G- protein-coupled receptors? *Trends Pharmacol. Sci.*, **24**(1): 36-40.

97.   Ito, M., Katsuta, Y., Imamoto, Y., Shichida, Y., and Yoshizawa, T. (1992) Conformational-analysis of the rhodopsin chromophore using bicyclic retinal analogs. *Photochem. Photobiol.*, **56**(6): 915-919.

98.   Crouch, R. and Or, Y.S. (1983) Opsin pigments formed with acyclic analogues. *FEBS Lett.*, **158**(1): p139-142.

99.   Degrip, W.J., Gray, D., Gillespie, J., Bovee, P.H.M., Vandenberg, E.M.M., Lugtenburg, J., and Rothschild, K.J. (1988) Photoexcitation of rhodopsin - conformation changes in the chromophore, protein and associated lipids as determined by Ftir difference spectroscopy. *Photochem. Photobiol.*, **48**(4): 497-504.

100.   Ganter, U.M., Kashima, T., Sheves, M., and Siebert, F. (1991) Ftir evidence of an altered chromophore-protein-interaction in the artificial visual pigment Cis-5,6-Dihydroisorhodopsin and Its photoproducts Bsi, lumirhodopsin, and metarhodopsin-I. *J. Am. Chem. Soc.*, **113**(11): 4087-4092.

101.   Fujimoto, Y., Fishkin, N., Pescitelli, G., Decatur, J., Berova, N., and Nakanishi, K. (2002) Solution and biologically relevant conformations of enantiomeric 11-cis-locked cyclopropyl retinals. *J. Am. Chem. Soc.*, **124**(25): 7294-7302.

102.   Wada, A., Sakai, M., Imamoto, Y., Shichida, Y., Yoshizawa, T., and Ito, M. (1993) A New Rhodopsin Analog Involving 11z-8,18-Ethanoretinal as a Chromophore. *Chem. Pharm. Bull.*, **41**(4): 793-795.

103.   Wada, A., Sakai, M., Imamoto, Y., Shichida, Y., Yamauchi, M., and Ito, M. (1997) Retinoids and related compounds .20. Synthesis of (11Z)-8,18- ethanoretinal and a conformational study of the rhodopsin chromophore. *J. Chem. Soc.-Perkin Trans. 1*, **12**: 1773-1777.

104.   Wada, A., Tsutsumi, M., Inatomi, Y., Imai, H., Shichida, Y., and Ito, M. (2001) Retinoids and related compounds. Part 26. Synthesis of (11 Z)- 8,18-propano- and methano-retinals and conformational study of the rhodopsin chromophore. *J. Chem.*

Soc.-Perkin Trans. 1, **19**: 2430-2439.

105.   Smith, S.O., Palings, I., Copie, V., Raleigh, D.P., Courtin, J., Pardoen, J.A., Lugtenburg, J., Mathies, R.A., and Griffin, R.G. (1987) Low-Temperature Solid-State C-13 Nmr-Studies of the Retinal Chromophore in Rhodopsin. *Biochemistry*, **26**(6): 1606-1611.

106.   Verhoeven, M.A., Creemers, A.F.L., Bovee-Geurts, P.H.M., De Grip, W.J., Lugtenburg, J., and De Groot, H.J.M. (2001) Ultra-high-field MAS NMR assay of a multispin labeled ligand bound to its G-protein receptor target in the natural membrane environment: Electronic structure of the retinylidene chromophore in rhodopsin. *Biochemistry*, **40**(11): 3282-3288.

107.   Creemers, A.F.L., Kiihne, S., Bovee-Geurts, P.H.M., Degrip, W.J., Lugtenburg, J., and De Groot, H.J.M. (2002) H-1 and C-13 MAS NMR evidence for pronounced ligand-protein interactions involving the ionone ring of the retinylidene chromophore in rhodopsin. *Proc. Natl. Acad. Sci. U. S. A.*, **99**(14): 9101-9106.

108.   Creemers, A.F.L., Klaassen, C.H.W., Bovee-Geurts, P.H.M., Kelle, R., Kragl, U., Raap, J., De Grip, W.J., Lugtenburg, J., and De Groot, H.J.M. (1999) Solid state N-15 NMR evidence for a complex Schiff base counterion in the visual G-protein-coupled receptor rhodopsin. *Biochemistry*, **38**(22): 7195-7199.

109.   Buss, V., Kolster, K., Terstegen, F., and Vahrenhorst, R. (1998) Absolute sense of twist of the C12-C13 bond of the retinal chromophore in rhodopsin-semiempirical and nonempirical calculations of chiroptical data. *Angew. Chem.-Int. Edit.*, **37**(13-14): 1893-1895.

110.   Buss, V. (2001) Inherent chirality of the retinal chromophore in rhodopsin - A nonempirical theoretical analysis of chiroptical data. *Chirality*, **13**(1): 13-23.

111.   Sugihara, M., Buss, V., Entel, P., Elstner, M., and Frauenheim, T. (2002) 11-cis-retinal protonated Schiff base: Influence of the protein environment on the geometry of the rhodopsin chromophore. *Biochemistry*, **41**(51): 15259-15266.

112.   Han, M., Lin, S.W., Minkova, M., Smith, S.O., and Sakmar, T.P. (1996) Functional interaction of transmembrane helices 3 and 6 in rhodopsin - Replacement of phenylalanine 261 by alanine causes reversion of phenotype of a glycine 121 replacement mutant. *J. Biol. Chem.*, **271**(50): 32337-32342.

113.   Han, M., Lin, S.W., Smith, S.O., and Sakmar, T.P. (1996) The effects of amino acid replacements of glycine 121 on transmembrane helix 3 of rhodopsin. *J. Biol. Chem.*, **271**(50): 32330-32336.

114.   Han, M., Lou, J.H., Nakanishi, K., Sakmar, T.P., and Smith, S.O. (1997) Partial agonist activity of 11-cis-retinal in rhodopsin mutants. *J. Biol. Chem.*, **272**(37): 23081-23085.

115.   Zhang, H.Z., Lerro, K.A., Yamamoto, T., Lien, T.H., Sastry, L., Gawinowicz, M.A., and Nakanishi, K. (1994) The Location of the Chromophore in Rhodopsin - a Photoaffinity Study. *J. Am. Chem. Soc.*, **116**(22): 10165-10173.

116.   Nakayama, T.A. and Khorana, H.G. (1990) Orientation of retinal in bovine rhodopsin

determined by cross- linking using a photoactivatable analog of 11-cis-retinal. *J. Biol. Chem.*, **265**(26): 15762-15769.

117. Eilers, M., Reeves, P.J., Ying, W.W., Khorana, H.G., and Smith, S.O. (1999) Magic angle spinning NMR of the protonated retinylidene Schiff base nitrogen in rhodopsin: Expression of N-15-lysine- and C- 13-glycine-labeled opsin in a stable cell line. *Proc. Natl. Acad. Sci. U. S. A.*, **96**(2): 487-492.

118. Thompson, L.K. (2002) Solid-state NMR studies of the structure and mechanisms of proteins. *Curr. Opin. Struct. Biol.*, **12**(5): 661-669.

119. Pauli, J., Baldus, M., Van Rossum, B., De Groot, H., and Oschkinat, H. (2001) Backbone and side-chain C-13 and N-15 signal assignments of the alpha-spectrin SH3 domain by magic angle spinning solid-state NMR at 17.6 tesla. *Chembiochem*, **2**(4): 272-281.

120. Mollevanger, L., Kentgens, A.P.M., Pardoen, J.A., Courtin, J.M.L., Veeman, W.S., Lugtenburg, J., and Degrip, W.J. (1987) High-Resolution solid-state C-13-Nmr study of carbons C-5 and C-12 of the chromophore of bovine rhodopsin - Evidence for a 6- s-cis conformation with negative-charge perturbation near C-12. *Eur. J. Biochem.*, **163**(1): 9-14.

121. Feng, X., Verdegem, P.J.E., Lee, Y.K., Sandstrom, D., Eden, M., Boveegeurts, P., Degrip, W.J., Lugtenburg, J., Degroot, H.J.M., and Levitt, M.H. (1997) Direct determination of a molecular torsional angle in the membrane protein rhodopsin by solid-state NMR. *J. Am. Chem. Soc.*, **119**(29): 6853-6857.

122. Grobner, G., Choi, G., Burnett, I.J., Glaubitz, C., Verdegem, P.J.E., Lugtenburg, J., and Watts, A. (1998) Photoreceptor rhodopsin: structural and conformational study of its chromophore 11-cis retinal in oriented membranes by deuterium solid state NMR. *FEBS Lett.*, **422**(2): 201-204.

123. Matsumoto, H.Y., T. (1975) Existence of a Beta-Ionone ring binding site in the rhodopsin molecule. *Nature*, **258**: 523-526.

124. Pan, D.H., Ganim, Z., Kim, J.E., Verhoeven, M.A., Lugtenburg, J., and Mathies, R.A. (2002) Time-resolved resonance Raman analysis of chromophore structural changes in the formation and decay of rhodopsin's BSI intermediate. *J. Am. Chem. Soc.*, **124**(17): 4857-4864.

125. Szundi, I., De Lera, A.R., Pazos, Y., Alvarez, R., Oliana, M., Sheves, M., Lewis, J.W., and Kliger, D.S. (2002) Bleaching kinetics of artificial visual pigments with modifications near the ring-polyene chain connection. *Biochemistry*, **41**(6): 2028-2035.

126. Fujimoto, Y., Ishihara, J., Maki, S., Fujioka, N., Wang, T., Furuta, T., Fishkin, N., Borhan, B., Berova, N., and Nakanishi, K. (2001) On the bioactive conformation of the rhodopsin chromophore: Absolute sense of twist around the 6-s-cis bond. *Chem.-Eur. J.*, **7**(19): 4198-4204.

127. Koch, D. and Gartner, W. (1997) Steric hindrance between chromophore substituents as the driving force of rhodopsin photoisomerization: 10-methyl-13- demethyl retinal containing rhodopsin. *Photochem. Photobiol.*, **65**(1): 181-184.

128.   Meyer, C.K., Bohme, M., Ockenfels, A., Gartner, W., Hofmann, K.P., and Ernst, O.P.
        (2000) Signaling states of rhodopsin - Retinal provides a scaffold for activating proton
        transfer switches. *J. Biol. Chem.*, **275**(26): 19713-19718.

129.   Okada, T., Kandori, H., Shichida, Y., Yoshizawa, T., Denny, M., Zhang, B.W., Asato,
        A.E., and Liu, R.S.H. (1991) Spectroscopic study of the batho-to-lumi transition during
        the photobleaching of rhodopsin using ring-modified retinal analogs. *Biochemistry*,
        30(19): 4796-4802.

130.   Ganter, U.M., Gartner, W., and Siebert, F. (1988) Rhodopsin-lumirhodopsin
        phototransition of bovine rhodopsin investigated by Fourier transform infrared
        difference spectroscopy. *Biochemistry*, **27**(19): 7480-7488.

131.   Jager, F., Jager, S., Krautle, O., Friedman, N., Sheves, M., Hofmann, K.P., and Siebert,
        F. (1994) Interactions of the beta-Ionone ring with the protein in the visual pigment
        rhodopsin control the activation mechanism - an Ftir and fluorescence study on
        artificial vertebrate rhodopsins. *Biochemistry*, **33**(23): 7389-7397.

132.   Vogel, R., Fan, G.B., Sheves, M., and Siebert, F. (2000) The molecular origin of the
        inhibition of transducin activation in rhodopsin lacking the 9-methyl group of the
        retinal chromophore: A UV-Vis and FTIR spectroscopic study. *Biochemistry*, **39**(30):
        8895-8908.

133.   Verdegem, P.J.E., Structure, function and dynamics of the chromophore of bovine
        rhodopsin. 1998, University of Leiden, The Netherlands: Leiden.

134.   Griffin, R.G. (1998) Dipolar recoupling in MAS spectra of biological solids. *Nat. Struct.
        Biol.*, **5**: 508-512.

135.   Levitt, M.H., Raleigh, D.P., Creuzet, F., and Griffin, R.G. (1990) Theory and
        simulations of homonuclear spin pair systems in rotating solids. *J. Chem. Phys.*, **92**(11):
        6347-6364.

136.   Pines, A., Gibby, M.G., and Waugh, J.S. (1973) Proton-enhanced NMR of dilute spinds
        in solids. *J. Chem. Phys.*, **59**(2): 569-590.

137.   Hartmann, S.R. and Hahn, E.L. (1962) Nuclear double resonance in the rotating frame.
        Physiol. Rev., **128**(5): 2042-2053.

138.   Evans, J.N.S., Biomolecular NMR spectroscopy. 1995, Oxford: Oxford University
        Press.

139.   Stejskal, E.O., Schaefer, J., and Waugh, J.S. (1977) Magic-angle spinning and
        polarization transfer in proton-enhanced NMR. *J. Magn. Reson. Ser. A*, **28**: 105-112.

140.   Metz, G., Wu, X., and Smith, S.O. (1994) Ramped-amplitude cross polarization in
        magic-ange spinning NMR. *J. Magn. Reson. Ser. A*, **110**: 219-227.

141.   Peersen, O.B. and Smith, S.O. (1993) Rotational resonance NMR of biological
        membranes. *Concept. Magnetic. Res.*, **5**: 303-317.

142.   Spooner, P.J.R., Sharples, J.M., Verhoeven, M.A., Lugtenburg, J., Glaubitz, C., and
       Watts, A. (2002) Relative orientation between the beta-ionone ring and the polyene
       chain for the chromophore of rhodopsin in native membranes. *Biochemistry*, **41**(24):
       7549-7555.

143.   Colmenares, L.U. and Liu, R.S.H. (1992) F-19 NMR evidence for restricted rotation of
       the retinyl chromophore in doubly labeled visual pigment analogs. *J. Am. Chem. Soc.*,
       114(17): 6933-6934.

144.   Hohwy, M., Jakobsen, H.J., Eden, M., Levitt, M.H., and Nielsen, N.C. (1998)
       Broadband dipolar recoupling in the nuclear magnetic resonance of rotating solids: A
       compensated C7 pulse sequence. *J. Chem. Phys.*, **108**(7): 2686-2694.

145.   Carravetta, M., Eden, M., Johannessen, O.G., Luthman, H., Verdegem, P.J.E.,
       Lugtenburg, J., Sebald, A., and Levitt, M.H. (2001) Estimation of carbon-carbon bond
       lengths and medium-range internuclear: Distances by solid-state nuclear magnetic
       resonance. *J. Am. Chem. Soc.*, **123**(43): 10628-10638.

146.   Brinkmann, A., Eden, M., and Levitt, M.H. (2000) Synchronous helical pulse sequences
       in magic-angle spinning nuclear magnetic resonance: Double quantum recoupling of
       multiple-spin systems. *J. Chem. Phys.*, **112**(19): 8539-8554.

147.   Gebhard, R., Courtin, J., Shadid, J.B., Van Haveren, J., Haeringen, C.J., and
       Lugtenburg, J. (1989) Synthesis of retinals labelled with ^{13}C in the cyclohexene ring.
       Recl. Trav. Chim. Pay-B, **108**: 207-214.

148.   Mcdermott, A.E., Creuzet, F., Gebhard, R., Vanderhoef, K., Levitt, M.H., Herzfeld, J.,
       Lugtenburg, J., and Griffin, R.G. (1994) Determination of internuclear distances and
       the orientation of functional-groups by solid-state Nmr - rotational resonance study of
       the conformation of retinal in bacteriorhodopsin. *Biochemistry*, **33**(20): 6129-6136.

149.   Still, W.C., Kahn, M., and Mitra, A. (1978) Rapid chromatographic technique for
       preparative seperations with moderate resolution. *J. Org. Chem.*, **43**(14): 63-66.

150.   Liu, R.S.H. and Asato, A.E. (1984) Photochemistry and synthesis of sterioisomers of
       vitamin A. *Tetrahedron*, **40**(11): 1931-1969.

151.   Blatchly, R.A. and Nakanishi, K. (1982) Use of high-performance liquid
       chromatography to seperate and identify retinals. *Methods. Enzymol.*, **88**: 491-516.

152.   Lugtenburg, J. (1985) The synthesis of 13C-labelled retinals. *Pure. Appl. Chem*, **57**(5):
       753-762.

153.   Jaffe, H.H. and Orchin, M., Theory and applications of ultraviolet spectroscopy. 1962,
       New York: Wiley & Sons.

154.   Wald, G., Brown, P.K., Hubbard, R., and W, O. (1955) Hindered cic isomers of
       vitamin A and retinene: The structure of the neo-b isomer. *Proc. Natl. Acad. Sci. U. S.
       A.*, **41**: 438-451.

155.   Degrip, W.J., Liu, R.S.H., Ramamurthy, V., and Asato, A.E. (1976) Rhodopsin
       analogues from highly hindered 7-*cis* isomers of retinal. *Nature*, **262**(5567): 416-418.

156.   Degrip, W.J., personal communication. 2002.

157.   Liu, R.S.H., Matsumoto, H., Kini, A., Asato, A.E., Denny, M., Kropf, A., and Degrip, W.J. (1984) Seven new hindered ssomeric rhodopsins - a reexamination of the stereospecificity of the binding-site of bovine opsin. *Tetrahedron*, **40**(3): 473-482.

158.   Daemen, F.J., De Grip, W.J., and Jansen, P.A. (1972) Biochemical aspects of the visual process. The molecular weight of rhodopsin. *Biochim. Biophys. Acta*, **271**(2): 419-428.

159.   Daemen, F.J. (1973) Vertebrate rod outer segment membranes. *Biochim. Biophys. Acta*, **300**(3): 255-288.

160.   Papermaster, D.S. and Dreyer, W.J. (1974) Rhodopsin content in the outer segment membranes of bovine and frog retinal rods. *Biochemistry*, **13**(11): 2438-44.

161.   Young, R.W. (1976) Visual cells and the concept of renewal. *Invest. Ophthalmol. Vis. Sci.*, **15**(9): 700-725.

162.   De-Grip, W.J., Daemen, F.J., and Bonting, S.L. (1980) Isolation and purification of bovine rhodopsin. *Methods Enzymology*, **67**.

163.   Futterman, S. (1974) Rhodopsin from bovine retinas. *Methods. Enzymol.*, **32**(B): 306-309.

164.   Hubbard, R., Brown, D.G., and Bownds, M.D. (1971) Methodology of vitamin A and visual pigments. *Methods. Enzymol.*, **18**(C): 615-653.

165.   Schnetkamp, P.P., Klompmakers, A.A., and Daemen, F.J. (1979) The isolation of stable cattle rod outer segments with an intact plasma membrane. *Biochim. Biophys. Acta*, **552**(3): 379-389.

166.   Delange, F., Bovee-Geurts, P.H.M., Vanoostrum, J., Portier, M.D., Verdegem, P.J.E., Lugtenburg, J., and Degrip, W.J. (1998) An additional methyl group at the 10-position of retinal dramatically slows down the kinetics of the rhodopsin photocascade. *Biochemistry*, **37**(5): 1411-1420.

167.   Saenger, W. (1980) Cyclodextrin inclusion compounds in research and industry. *Angew. Chem.-Int. Edit.*, **19**: 344-362.

168.   Delange, F., Merkx, M., Bovee-Geurts, P.H., Pistorius, A.M., and Degrip, W.J. (1997) Modulation of the metarhodopsin I/metarhodopsin II equilibrium of bovine rhodopsin by ionic strength--evidence for a surface-charge effect. *Eur. J. Biochem.*, **243**(1-2): 174-80.

169.   Nakanishi, K. (1985) Bioorganic studies with rhodopsin. *Pure. Appl. Chem*, **57**(5): 769-776.

170.   Blatz, P.E., Mohler, J.H., and Navangul, H.V. (1972) *Biochemistry*, **11**: 848-855.

171.   Honig, B., Greenberg, A., Dinur, U., and Ebrey, T.G. (1976) *Biochemistry*, **15**: 4593-4599.

172.   Kakitani, H., Kakitani, T., Rodman, H., and Honig, B. (1985) *Photochem. Photobiol.*, **41**: 471-479.

173.   Simmons, C.J., Liu, R.S.H., Denny, M., and Seff, K. (1981) The Crystal-Structure of 13-Cis-Retinal - the Molecular- Structures of Its 6-S-Cis and 6-S-Trans Conformers. *Acta Crystallogr. Sect. B-Struct. Commun.*, **37**(DEC): 2197-2205.

174.   Honig, B.H., B. Sykes, B.D. And Karplus, M. (1971) Ring Orientation in Beta-ionone and retinals. *Proc. Natl. Acad. Sci. U. S. A.*, **68**(6): 1289-1293.

175.   Gilardi, R.D.K., I.L. And Karle, J. (1972) The crystal and molecular structure of 11-cis-retinal. *Acta Crystallogr.*, **B28**(8): 2605-2612.

176.   Van Der Steen, R., Biesheuvel, P.L., Mathies, R., and Lugtenburg, J. (1986) Retinal analogues with locked 6-7 conformations show that bacteriorhodopsin reuires the 6-s-trans conformation of the chromophore. *J. Am. Chem. Soc*, **108**: 6410-6411.

177.   Harbison, G.S., Smith, S.O., Pardoen, J.A., Courtin, J.M.L., Lugtenburg, J., Herzfeld, J., Mathies, R.A., and Griffin, R.G. (1985) Solid-State C-13 Nmr detection of a perturbed 6-s-trans chromophore in Bacteriorhodopsin. *Biochemistry*, **24**(24): 6955-6962.

178.   Singh, D., Hudson, B.S., Middleton, C., and Birge, R.R. (2001) Conformation and orientation of the retinyl chromophore in rhodopsin: A critical evaluation of recent NMR data on the basis of theoretical calculations results in a minimum energy structure consistent with all experimental data. *Biochemistry*, **40**(14): 4201-4204.

179.   Liu, R.S.H. and Mirzadegan, T. (1988) The shape of a three-dimensional binding site of rhodopsin based on molecular modeling analyses of isomeric and other visual pigment analogues. *J. Am. Chem. Soc*, **110**: 8617-8623.

180.   Creuzet, F., Mcdermott, A., Gebhard, R., Vanderhoef, K., Spijkerassink, M.B., Herzfeld, J., Lugtenburg, J., Levitt, M.H., and Griffin, R.G. (1991) Determination of Membrane-Protein Structure by Rotational Resonance Nmr - Bacteriorhodopsin. *Science*, **251**(4995): 783-786.

181.   Harbison, G.S., Mulder, P.P.J., Pardoen, H., Lugtenburg, J., Herzfeld, J., and Griffin, R.G. (1985) High-resolution C-13 Nmr of retinal derivatives in the solid- state. *J. Am. Chem. Soc.*, **107**(17): 4810-4816.

182.   Harbison, G.S., Raleigh, D.P., Smith, S.O., Roberts, J.E., Pardoen, J.A., Lugtenburg, J., Herzfeld, J., Mathies, R.A., and Griffin, R.G. (1986) Solid-state C-13-Nmr and N-15 Nmr-studies of retinal and tyrosine in Bacteriorhodopsin. *Biophys. J.*, **49**(2): A476-A476.

183.   Andrew, E.R., Bradbury, A., Eades, R.G., and Wynn, V.T. (1963) Nuclear cross-relaxatioon induced by specimen rotation. *Phys. Lett.*, **4**(2): 99-100.

184.   Andrew, E.R., Clough, S., Farnell, L.F., Gledhill, T.D., and Roberts, I. (1966) Resonant rotational broadening of nuclear magnetic resonance spectra. *Phys. Lett.*, **21**(5): 505-506.

185.   Raleigh, D.P., Levitt, M.H., and Griffin, R.G. (1988) Rotational Resonance in Solid-State Nmr. *Chem. Phys. Lett.*, **146**(1-2): 71-76.

186.   Verdegem, P.J.E., Helmle, M., Lugtenburg, J., and Degroot, H.J.M. (1997) Internuclear distance measurements up to 0.44 nm for retinals in the solid state with 1-D rotational

resonance C-13 MAS NMR spectroscopy. *J. Am. Chem. Soc.*, **119**(1): 169-174.

187.   Ahmed, Z., Middleton, D., Glaubitz, C., and Watts, A. (1998) Studies on the transmembrane domain of phospholamban using rotational resonance and Magic angle oriented sample spinning (MAOSS) NMR spectroscopy. *Biochem. Soc. Trans.*, **26**(3): S194-S194.

188.   Ahmed, Z., Reid, D.G., Watts, A., and Middleton, D.A. (2000) A solid-state NMR study of the phospholamban transmembrane domain: local structure and interactions with Ca2+-ATPase. *Biochim. Biophys. Acta-Biomembr.*, **1468**(1-2): 187-198.

189.   Heller, J., Kolbert, A.C., Larsen, R., Ernst, M., Bekker, T., Baldwin, M., Prusiner, S.B., Pines, A., and Wemmer, D.E. (1996) Solid-state NMR studies of the prion protein H1 fragment. *Protein Sci.*, **5**(8): 1655-1661.

190.   Middleton, D.A., Robins, R., Feng, X.L., Levitt, M.H., Spiers, I.D., Schwalbe, C.H., Reid, D.G., and Watts, A. (1997) The conformation of an inhibitor bound to the gastric proton pump. *FEBS Lett.*, **410**(2-3): 269-274.

191.   Spencer, R.G.S., Halverson, K.J., Auger, M., Mcdermott, A.E., Griffin, R.G., and Lansbury, P.T. (1991) An Unusual Peptide Conformation May Precipitate Amyloid Formation in Alzheimers-Disease - Application of Solid-State Nmr to the Determination of Protein Secondary Structure. *Biochemistry*, **30**(43): 10382-10387.

192.   Thompson, L.K., Mcdermott, A.E., Raap, J., Vanderwielen, C.M., Lugtenburg, J., Herzfeld, J., and Griffin, R.G. (1992) Rotational Resonance Nmr-Study of the Active-Site Structure in Bacteriorhodopsin - Conformation of the Schiff-Base Linkage. *Biochemistry*, **31**(34): 7931-7938.

193.   Peersen, O.B., Groesbeek, M., Aimoto, S., and Smith, S.O. (1995) Analysis of Rotational Resonance Magnetization Exchange Curves from Crystalline Peptides. *J. Am. Chem. Soc.*, **117**(27): 7228-7237.

194.   Peersen, O.B., Yoshimura, S., Hojo, H., Aimoto, S., and Smith, S.O. (1992) Rotational Resonance Nmr Measurements of Internuclear Distances in an Alpha-Helical Peptide. *J. Am. Chem. Soc.*, **114**(11): 4332-4335.

195.   Glaubitz, C. (1998) D.Phil Thesis. Oxford, U.K.

196.   Herzfeld, J. and Berger, A.E. (1980) Sideband Intensities in NMR-Spectra of samples spinning at the magic angle. *J. Chem. Phys.*, **73**(12): 6021-6030.

197.   Metz, G., Wu, X.L., and Smith, S.O. (1994) Ramped-amplitude cross-polarization in magic-angle-spinning Nmr. *J. Magn. Reson. Ser. A*, **110**(2): 219-227.

198.   Heller, J., Larsen, R., Ernst, M., Kolbert, A.C., Baldwin, D., Prusiner, S.B., Wemmer, D.E., and Pines, A. (1996) Application of rotational resonance to inhomogeneously broadened systems. *Chem. Phys. Lett*, **251**: 223-229.

199.   Albrecht, G. and Corey, R.B. (1939) The crystal structure of glycine. *Science*, **61**: 1087-1103.

200.   Jonsson, P.G. and Kvick, A. (1972) Precision neutron diffraction structure

determination of protein and nucleic acid components. III The crystal and molecular structure of the amino acid α-glycine. *Acta Crystallogr.*, **B28**: 1827-1833.

201. Haberkorn, R.A., Stark, R.E., Willigen, H.V., and Griffin, R.G. (1981) Determination bond distances and bond angles by solid-state nuclear magnetic resonance. ^{13}C and ^{14}N NMR study of glycine. *J. Am. Chem. Soc*, **103**: 2534-2539.

202. Shriver, J.W., Mateescu, G.D., and Abrahamson, E.W. (1979) A proton and carbon-13 Nuclear Magnetic Resonance Spectroscopy study of the conformation of a protonated 11-*cis*-retinal Schiff base. *Biochemistry*, **18**(22): 4785-4792.

203. Kalinski, H.O., Berger, S., and Braun, S., Carbon-13 NMR Spectroscopy. 1988, Chichester: John Wiley and Sons.

204. Abraham, R.J. and Loftus, P., Proton and carbon-13 NMR spectroscopy. 1978, London: Heydon and Son.

205. Dalling, D.K. and Grant, D.M. (1972) Carbon-13 magnetic resonance. Steric Interactions in the methylcycohexanes. *J. Am. Chem. Soc*, **94**(15): 5318-5324.

206. Verhoeven, M.A., Personal Communication. 2001.

207. Crouch, R., Purvin, V., Nakanishi, K., and Ebrey, T.G. (1975) Isorhodopsin II: Artificial photosensitive pigment formed from 9,13-*dicis*-retinal. *Proc. Natl. Acad. Sci. U. S. A.*, **72**(4): 1538-1542.

208. Kini, A., Matsumoto, H., and Liu, R.S.H. (1979) Doubly hindered 7,11-di-cis isomers of retinal. Synthesis, properties and interaction with cattle opsin. *J. Am. Chem. Soc*, **101**(17): 5078-5079.

209. Asato, A.E., Zhang, B.W., Denny, M., Mirzadegan, T., Seff, K., and Liu, R.S.H. (1989) A study of the binding-site requirements of rhodopsin using isomers of alpha-retinal and 5-substituted alpha-retinal analogs. *Bioorganic Chem.*, **17**(4): 410-421.

210. Blatz, P.E., Lin, M.L., Balasubramaniyan, P., Balasubramaniyan, V., and Dewhurst, P.B. (1969) A new series of synthetic visual pigments from cattle opsin and homologs of retinal. *J. Am. Chem. Soc*, **91**(21): 5930-5931.

211. Crouch, R.K., Kefalov, V., Gartner, W., and Cornwall, M.C., Use of retinal analogues for the study of visual pigment function, in *G Protein Pathways, Pt a, Receptors*. 2002. p. 29-48.

212. Liu, R.S.H. and Asato, A.E., Chemistry and biology of synthetic retinoids. 1990, Boca Raton, Florida: CRC press. 51-75.

213. Kropf, A. (1976) Is proton transfer the initial photochemical process in vision? *Nature*, **264**: 92-94.

214. Nishio, M., Hirota, M., and Umezawa, Y., The CH/pi interaction. Evidence, nature and consequences. 1998, New York: Wiley-VCH.

215. Umezawa, Y. and Nishio, M. (1998) CH/pi interactions as demonstrated in the crystal structure of guanine-nucleotide binding proteins, Src homology-2 domains and human

growth hormone in complex with their specific ligands. *Bioorg. Med. Chem.*, **6**(4): 493-504.

216.   Broda, E.E. and Goodeve, C.F. (1941) The behaviour of visual purple at low temperatures. *Proc. Roy. Soc. A.*, **179**: 151-159.

217.   Matthews, R.G., Hubbard, R., Brown, P.K., and Wald, G. (1963) Tautomeric forms of metarhodopsin. *J. Gen. Physiol.*, **47**: 215-240.

218.   Wald, G., Durell, J., and St George, R.C.C. (1950) The light reaction in the bleaching of rhodopsin. *Science*, **111**: 179-181.

219.   Hubbard, R. and Kropf, A. (1958) The action of light on rhodopsin. *Proc. Natl. Acad. Sci. U. S. A.*, **44**: 130-139.

220.   Kropf, A. and Hubbard, R. (1958) The mechanism of bleaching rhodopsin. *Ann. NY. Acad. Sci*, **74**: 266-280.

221.   Yoshizawa, T. and Kito, Y. (1958) Chemistry of the rhodopsin cycle. *Nature*, **182**: 1605-1606.

222.   Kamamura, S., Wakabayashi, S., Maeda, A., and Yoshizawa, T. (1978) Isorhodopsin: Conformation and orientation of its chromophore in frog disk membranes. *Vision. Res.*, **18**: 457-462.

223.   Sasaki, N., Tokunaga, F., and Yoshizawa, T. (1980) The formation of two forms of bathorhodopsin and their optical properties. *Photochem. Photobiol.*, **32**: 433-441.

224.   Suzuki, T. and Callender, R.H. (1981) Primary photochemistry and photoisomerization of retinal at 77K in cattle and squid rhodopsin. *Biophys. J.*, **34**: 261-265.

225.   Brown, M.F. (1994) Modulation of rhodopsin function by properties of the membrane bilayer. *Chem. Phys. Lipids*, **73**: 159-180.

226.   De Grip, W.J., Olive, J., and Bovee-Geurts, P.H. (1983) Reversible modulation of rhodopsin photolysis in pure phosphatidylserine membranes. *Biochimica Et Biophysica Acta*, **734**: 168-179.

227.   Maeda, A., Ogurusu, T., Shichida, Y., Tokunaga, F., and Yoshizawa, T. (1978) Formation of a 7-cis retinal pigment by irradiating cattle rhodopsin at low temperatures. *FEBS Lett.*, **92**(1): 77-80.

228.   Creemers, A.F.L., Personal Communication. 2001.

229.   Maeda, A., Shichida, Y., and Yoshizawa, T. (1979) Formation of 7-cis and 13-cis retinal pigments by irradiating squid rhodopsin. *Biochemistry*, **18**(8): 1449-1453.

230.   Zankel, T., Ok, H., Johnson, R., Chang, C.W., Sekiya, N., Naoki, H., Yoshihara, K., and Nakanishi, K. (1990) Bovine Rhodopsin with 11-Cis-Locked Retinal Chromophore Neither Activates Rhodopsin Kinase nor Undergoes Conformational Change Upon Irradiation. *J. Am. Chem. Soc.*, **112**(13): 5387-5388.

231.   Lin, S.W. and Sakmar, T.P. (1996) Specific tryptophan UV-absorbance changes are

probes of the transition of rhodopsin to its active state. *Biochemistry*, **35**(34): 11149-11159.

232.   Siebert, F., Mantele, W., and Gerwert, K. (1983) Fourier-Transform Infrared-Spectroscopy Applied to Rhodopsin - the Problem of the Protonation State of the Retinylidene Schiff-Base Re-Investigated. *Eur. J. Biochem.*, **136**(1): 119-127.

233.   Lamola, A.A., Yamane, T., and Zipp, A. (1974) Effects of detergents and high pressures upon the metarhodopsin I--metarhodopsin II equilibrium. *Biochemistry*, **13**: 738-743.

234.   Mitchell, D.C., Straume, M., Miller, J.L., and Litman, B.J. (1990) Modulation of metarhodopsin formation by cholesterol-induced ordering of bilayer lipids. *Biochemistry*, **29**(39): 9143-9149.

235.   Straume, M., Mitchell, D.C., Miller, J.L., and Litman, B.J. (1990) Interconversion of metarhodopsins I and II: a branched photointermediate decay model. *Biochemistry*, **29**(39): 9135-9142.

236.   Milburn, M.V., Prive, G.G., Milligan, D.L., Scott, W.G., Yeh, J., Jancarik, J., Koshland, D.E., and Kim, S.H. (1991) 3-Dimensional structures of the ligand-binding domain of the bacterial aspartate receptor with and without a Ligand. *Science*, **254**(5036): 1342-1347.

237.   Subramaniam, S., Lindahl, I., Bullough, P., Faruqi, A.R., Tittor, J., Oesterhelt, D., Brown, L., Lanyi, J., and Henderson, R. (1999) Protein conformational changes in the bacteriorhodopsin photocycle. *J. Mol. Biol.*, **287**(1): 145-161.

238.   Subramaniam, S. and Henderson, R. (2000) Molecular mechanism of vectorial proton translocation by bacteriorhodopsin. *Nature*, **406**(6796): 653-657.

239.   Kim, J.M., Altenbach, C., Thurmond, R.L., Khorana, H.G., and Hubbell, W.L. (1997) Structure and function in rhodopsin: Rhodopsin mutants with a neutral amino acid at E134 have a partially activated conformation in the dark state. *Proc. Natl. Acad. Sci. U. S. A.*, **94**(26): 14273-14278.

240.   Ganter, U.M., Schmid, E.D., Perezsala, D., Rando, R.R., and Siebert, F. (1989) Removal of the 9-Methyl group of retinal inhibits signal transduction in the visual process - a Fourier-Transform Infrared and biochemical investigation. *Biochemistry*, **28**(14): 5954-5962.

241.   Vogel, R., Fan, G.B., Siebert, F., and Sheves, M. (2001) Anions stabilize a metarhodopsin II-like photoproduct with a protonated Schiff base. *Biochemistry*, **40**(44): 13342-13352.

242.   Sansom, M.S.P. and Weinstein, H. (2000) Hinges, swivels and switches: the role of prolines in signalling via transmembrane alpha-helices. *Trends Pharmacol. Sci.*, **21**(11): 445-451.

243.   Ballesteros, J.A., Jensen, A.D., Liapakis, G., Rasmussen, S.G.F., Shi, L., Gether, U., and Javitch, J.A. (2001) Activation of the beta(2)-adrenergic receptor involves disruption of an ionic lock between the cytoplasmic ends of transmembrane segments 3 and 6. *J. Biol. Chem.*, **276**(31): 29171-29177.

244.   Shi, L., Liapakis, G., Xu, R., Guarnieri, F., Ballesteros, J.A., and Javitch, J.A. (2002) Beta-2 Adrenergic Receptor Activation. Modulation of the proline kink in transmembrane 6 by a rotamer toggle switch. *J. Biol. Chem.*, **277**(43): 40989-40996.

245.   Mirzadegan, T., Benko, G., Filipek, S., and Palczewski, K. (2003) Sequence analyses of G-protein-coupled receptors: Similarities to rhodopsin. *Biochemistry*, **42**(10): 2659-2767.

246.   Jensen, A.D., Guarnieri, F., Rasmussen, S.G.F., Asmar, F., Ballesteros, J.A., and Gether, U. (2001) Agonist-induced conformational changes at the cytoplasmic side of transmembrane segment 6 in the beta(2) adrenergic receptor mapped by site-selective fluorescent labeling. *J. Biol. Chem.*, **276**(12): 9279-9290.

247.   Sheikh, S.P., Vilardarga, J.P., Baranski, T.J., Lichtarge, O., Iiri, T., Meng, E.C., Nissenson, R.A., and Bourne, H.R. (1999) Similar structures and shared switch mechanisms of the beta(2)- adrenoceptor and the parathyroid hormone receptor - Zn(II) bridges between helices III and VI block activation. *J. Biol. Chem.*, **274**(24): 17033-17041.

248.   Scheer, A., Fanelli, F., Costa, T., De Benedetti, P.G., and Cotecchia, S. (1997) The activation process of the α-adrenergic receptor: potential role of protonation and hydrophobicity of a highly conserved aspartate. *Proc. Natl. Acad. Sci. U. S. A.*, **94**: 808-813.

249.   Seibert, C., Harteneck, C., Ernst, O.P., Schultz, G., and Hofmann, K.P. (1999) Activation of the rod G-protein G(t) by the thrombin receptor (PAR1) expressed in Sf9 cells. *Eur. J. Biochem.*, **266**(3): 911-916.

250.   Rasmussen, S.G.F., Jensen, A.D., Liapakis, G., Ghanouni, P., Javitch, J.A., and Gether, U. (1999) Mutation of a highly conserved aspartic acid in the beta(2) adrenergic receptor: Constitutive activation, structural instability, and conformational rearrangement of transmembrane segment 6. *Mol. Pharmacol.*, **56**(1): 175-184.

251.   Pearl, S.M. and Zigmond, M.J., Amine neurotransmitters. 2002, Encyclopedia of life sciences /http://www.els.net.

252.   Zhukovsky, E.A., Robinson, P.R., and Oprian, D.D. (1991) Transducin activation by rhodopsin without a covalent bond to the 11-cis-retinal chromophore. *Science*, **251**(4993): 558-560.

253.   Lu, Z.L., Saldanha, J.W., and Hulme, E.C. (2001) Transmembrane domains 4 and 7 of the M-1 muscarinic acetylcholine receptor are critical for ligand binding and the receptor activation switch. *J. Biol. Chem.*, **276**(36): 34098-34104.

254.   Ward, S.D.C., Curtis, C.A.M., and Hulme, E.C. (1999) Alanine-scanning mutagenesis of transmembrane domain 6 of the M-1 muscarinic acetylcholine receptor suggests that Tyr381 plays key roles in receptor function. *Mol. Pharmacol.*, **56**(5): 1031-1041.

255.   Lu, Z.L. and Hulme, E.C. (1999) The functional topography of transmembrane domain 3 of the M-1 muscarinic acetylcholine receptor, revealed by scanning

mutagenesis. *J. Biol. Chem.*, **274**(11): 7309-7315.

256.   Oliveira, L., Paiva, A.C.M., Sander, C., and Vriend, G. (1994) A common step for signal transduction in G protein-coupled receptors. *Trends Pharmacol. Sci.*, **15**(6): 170-172.

257.   Javitch, J.A., Ballesteros, J.A., Weinstein, H., and Chen, J.Y. (1998) A cluster of aromatic residues in the sixth membrane-spanning segment of the dopamine D2 receptor is accessible in the binding-site crevice. *Biochemistry*, **37**(4): 998-1006.

258.   Javitch, J.A., Ballesteros, J.A., Weinstein, H., and Chen, J. (1998) A cluster of aromatic residues in the sixth membrane-spanning segments of the dopamine D2 receptor: contributions of the second membrane-spanning segment. *Biochemistry*, **38**: 7961-7968.

259.   Gerber, B.O., Meng, E.C., Dotsch, V., Baranski, T.J., and Bourne, H.R. (2001) An activation switch in the ligand binding pocket of teh C5a receptor. *J. Biol. Chem.*, **276**: 3394-3400.

260.   Jakubik, J., El-Fakahany, E.E., and Tucek, S. (2000) Evidence for a tandem two-site model of ligand binding to muscarinic acetylcholine receptors. *J. Biol. Chem.*, **275**(25): 18836-18844.

261.   Parkes, J.H. and Liebman, P.A. (1984) Temperature and pH dependence of the metarhodopsin I-metarhodopsin II kinetics and equilibria in bovine rod disk membrane suspensions. *Biochemistry*, **23**: 5054-5061.

262.   Delange, F., Merkx, M., Boveegeurts, P.H.M., Pistorius, A.M.A., and Degrip, W. (1997) Modulation of the metarhodopsin I/metarhodopsin II equilibrium of bovine rhodopsin by ionic strength - Evidence for a surface- charge effect. *Eur. J. Biochem.*, **243**(1-2): 174-180.

263.   Nishio, M., Umezawa, Y., Hirota, M., and Takeuchi, Y. (1995) Tetrahedron report number-378 - the Ch/Pi Interaction - significance in molecular recognition. *Tetrahedron*, **51**(32): 8665-8701.

264.   Derewenda, Z.S., Lee, L., and Derewenda, U. (1995) The occurence of CH-O hydrogen bonds in proteins. *J. Mol. Biol.*, **252**: 248-262.

265.   Burley, S.K. and Petsko, G.A. (1986) Amino-aromatic interactions in proteins. *FEBS Lett.*, **203**(2): 139-143.

266.   Hunter, C.A., Singh, J., and Thornton, J.M. (1991) Pi-Pi-Interactions - the geometry and energetics of phenylalanine phenylalanine interactions in proteins. *J. Mol. Biol.*, **218**(4): 837-846.